MOUNTAIN-PLAINS CONSORTIUM

MPC 21-442 | J. Seo and I. Amatya

OPTIMIZED ADHESIVE PERFORMANCE IN ELECTRONIC TRANSPORTATION SIGN CONSTRUCTION

MOUNTAIN-PLAINS CONSORTIUM REGION 8

A University Transportation Center sponsored by the U.S. Department of Transportation serving the Mountain-Plains Region. Consortium members:

Colorado State University
North Dakota State University
South Dakota State University
University of Colorado Denver
University of Denver
University of Utah
Utah State University
University of Wyoming

Technical Report Documentation Page

1. Report No.	2. Government Accession No.	3. Recipient's Catalog No.
MPC-563		

4. Title and Subtitle	5. Report Date
Optimized Adhesive Performance in Electronic Transportation Sign Construction	November 2021
	6. Performing Organization Code

7. Author(s)	8. Performing Organization Report No.
Junwon Seo Ibin Amatya	MPC 21-442

9. Performing Organization Name and Address	10. Work Unit No. (TRAIS)
South Dakota State University Dept. of Civil and Environmental Engineering SCEH 120, Box 2219 Brookings, SD 57007	11. Contract or Grant No.

12. Sponsoring Agency Name and Address	13. Type of Report and Period Covered
Mountain-Plains Consortium North Dakota State University PO Box 6050, Fargo, ND 58108	Final Report
	14. Sponsoring Agency Code

15. Supplementary Notes

Supported by a grant from the US DOT, University Transportation Centers Program

16. Abstract

The ultimate objective of this project was to determine the structural performance of the Dynamic Message Sign (DMS) bonded with chemical adhesive in terms of ultimate strength and fatigue strength. To achieve this objective, this project first investigated the effects of various parameters (i.e., conditioning humidity and conditioning temperature) on tensile, shear, peel, and cleavage strength through small-scale tests of adhesive specimens with variation in specimen width. Numerous data resulting from the tests were analyzed through graphical comparisons and statistical analysis to explore the effect of the considered parameters on each of the strengths. It was found that conditioning humidity and width were the most significant parameters negatively affecting the tensile and peel strength, respectively. Four full-scale DMS tests were also performed to examine their structural performance. Specifically, the ultimate strength testing was carried out on one DMS with adhesive joints and one with typically welded connections, and the fatigue testing was also conducted for one DMS system with adhesive joints and one with welded connections. The ultimate strength testing demonstrated that the adhesive DMS failed at 125 kN, while the weld DMS failed at 146 kN. During the fatigue test, stress ranges observed in the panel were much below the threshold of the aluminum panel of the DMS. No sign of damage was observed in both adhesive and welded DMSs from the fatigue tests. The results indicated that DMS with adhesively bonded connections is relatively better than welded DMS with respect to the stress induced in the panel.

17. Key Word	18. Distribution Statement
adhesion, adhesives, fatigue strength, joints (engineering), optimization, structural analysis, variable message signs	Public distribution

19. Security Classif. (of this report)	20. Security Classif. (of this page)	21. No. of Pages	22. Price
Unclassified	Unclassified	172	n/a

Form DOT F 1700.7 (8-72) Reproduction of completed page authorized

Optimized Adhesive Performance in Electronic Transportation Sign Construction

Junwon Seo, PhD, PE
Ibin Amatya, GRA

Department of Civil and Environmental Engineering
South Dakota State University
Brookings, South Dakota

November 2021

Acknowledgements

The authors thank the Daktronics and United States DOT through Mountain-Plains Consortium (MPC) – University Transportation Center (UTC) for providing the funding for this project. The authors wish to acknowledge the Project Committee: Dan Bierschbach, Toby Pulscher, Jeff Haliburton, John Syrstad, and Eric Johns at Daktronics for their invaluable comments and support for this work. The authors are grateful to Dr. Todd Letcher for his help with the small-scale testing and to Mr. Gutzmer for his guidance over the full-scale testing of dynamic message signs (DMS).

Disclaimer

ABSTRACT

The ultimate objective of this project was to determine the structural performance of the dynamic message sign (DMS) bonded with chemical adhesive in terms of ultimate strength and fatigue strength. To achieve this objective, this project first investigated the effects of various parameters (i.e., conditioning humidity and conditioning temperature) on tensile, shear, peel, and cleavage strength through small-scale tests of adhesive specimens with variations in specimen width. Numerous data resulting from the tests were analyzed through graphical comparisons and statistical analysis to explore the effect of the considered parameters on each of the strengths. It was found that conditioning humidity and width were the most significant parameters negatively affecting the tensile and peel strength, respectively. Four full-scale DMS tests were also performed to examine their structural performance. Specifically, the ultimate strength testing was carried out on one DMS with adhesive joints and one with typically welded connections, and the fatigue testing was also conducted for one DMS system with adhesive joints and one with welded connections. The ultimate strength testing demonstrated that the adhesive DMS failed at 125 kN, while the weld DMS failed at 146 kN. During the fatigue test, stress ranges observed in the panel were much below the threshold of the DMS' aluminum panel. No sign of damage was observed in either adhesive or welded DMSs from the fatigue tests. The results indicated that a DMS with adhesively bonded connections is relatively better than welded DMS with respect to the stress induced in the panel.

EXECUTIVE SUMMARY

A dynamic message sign (DMS), an electronic sign that provides drivers with traffic information, is made up of a display, cabinet sheet aluminum skin, and internal structure along with electrical components. The aluminum skin is connected to the internal structure usually with a welded connection; however, adhesive or chemical bonding can be used instead for the connection between these components due to several benefits of adhesives, such as low labor cost, uniform load distribution, and fabrication efficiency. Despite having such high potential, studies have been limited for the structural performance evaluation of the adhesive bonded DMSs.

The goal of this project is to examine the mechanical properties of adhesives used in a DMS under varying environmental and geometrical conditions and to investigate the structural performance of full-sized DMSs with adhesive and welded connections. Adhesive tensile, shear, peel, and cleavage specimens with different widths were tested according to the American Society for Testing and Materials (ASTM) standards after conditioning them in different temperature and humidity conditions. The average tensile stress of 16.94 MPa with a standard deviation of 0.87 MPa was found from the tensile testing data. For the shear tests, the average shear stress of 16.40 MPa with a standard deviation of 1.37 MPa was observed. From peel testing data, the average peel strength was found to be 6.63 N/mm with a standard deviation of 2.49 N/mm, while the average cleavage strength of 196.61 N/mm with a standard deviation of 30.14 N/mm was observed from the cleavage testing data. The tensile, shear, and peel testing data were also found to be in agreement with the LORD technical data sheet (LORD Corporation 2020). Numerous data resulting from the tests were analyzed through graphical comparisons and statistical analysis, so as to explore the effect of the considered parameters on tensile, shear, peel, and cleavage strengths. As a part of the statistical analysis, multiple linear regression (MLR) and response surface metamodels (RSM) were utilized not only to determine statistically significant parameters affecting the strengths, but also to develop separate regression models for the tensile, shear, peel, and cleavage strengths. The MLR and RSM model-based analysis also found conditioning humidity to be the most significant parameter negatively affecting the tensile stress as the probability values of 0.427% and 2.529% were observed from MLR and RSM models, respectively. The statistical analysis also indicated that the width was a significant parameter affecting the peel strength. 3-D surfaces were also generated from the RSM regression model to observe the effect of different parameters on each strength type of adhesive joint.

Furthermore, additional adhesive specimens were tested to examine the effect of the extreme conditioning temperature ranging from -56.67°C to 93.33°C on each strength type. Four different strengths, including tensile, shear, peel, and cleavage strength, were studied for both of the adhesive and welded connections. The effects of temperature and width on each of the strengths were evaluated by analyzing the testing data in a graphical manner. It should be noted that the adhesive and welded specimens with same specimen width were tested after conditioning at the identical temperature to make comparison between the strength of adhesive and welded specimens for each test type. As expected, the welded specimens were found to have significantly higher strength compared with the adhesive specimens in tensile, shear, and peel loadings. The majority of welded cleavage specimens observed higher strength than the adhesive specimens.

Ultimate strength and fatigue tests were also conducted on four full-sized DMSs to determine the structural performance of adhesive and welded DMSs. Specifically, the ultimate strength testing was carried out on one DMS with adhesive joints and one with typical welded connections, and the fatigue testing was also conducted on one DMS with adhesive joints and one with welded connections. For the ultimate testing, monotonic loadings were applied to each of the DMSs by a hydraulic actuator under the displacement-based control until failure. For the fatigue testing, each of the DMSs was loaded up to 500,000 cycles with a constant force of 0.818 kN equivalent to design the natural wind gust pressure

based on a yearly mean speed of 18.02 km/hr according to the American Association of State Highway and Transportation Officials (AASHTO) specifications for structural supports for highway signs, luminaires, and traffic signals. During each test, strain, deflection, and load data along with visual inspection imagery were collected to gain a better understanding of structural behaviors and failure modes of each of the individually tested DMSs. The ultimate testing demonstrated that the adhesive DMS failed at 123.41 kN with the peak deflection of 133.35 mm, while the welded DMS observed a maximum load of 153.46 kN at a deflection of 158.57 mm. During the fatigue load testing, all the stress ranges observed in each of the tested DMSs were found to be considerably below the threshold of the aluminum DMS panel. No damage was observed in either the adhesive or welded DMSs subjected to the fatigue loading. The structural behavior of the adhesive DMS was found to be analogous to that of welded DMS, indicating equivalent performance of adhesive DMS to the welded DMS in terms of fatigue loading. Finally, this work found adhesive or chemical bonding to be a possible substitute to welding for assembly of the DMS.

TABLE OF CONTENTS

LIST OF TABLES

LIST OF FIGURES

1. INTRODUCTION

An adhesive has the potential to increase the production of dynamic message signs (DMSs) due to its efficient applications, less labor, and the ability to join different metals. The majority of clients, such as state departments of transportation prefer welded connections for connecting the aluminum back-skin with the DMS frame. The adhesive is a decent alternative to join lightweight metals with different melting points. In adhesive joints, loads are more homogeneously distributed than in welded joints. Different complexities, such as difficulties in joining irregular seams and panel distortion (Tsai et al. 1999), have been observed in the course of manufacturing of welded connections. Further, the probability of noticing residual stresses and distortion is also high in welded connections. Even with such high potential of adhesive joints, limited experimental studies (Çolak et al. 2009, Agarwal et al. 2014, Savvilotidou et al. 2017, Kim et al. 2012, Goglio and Rezaei 2014, Silva et al. 2016, Sousa et al. 2018, Moussa et al. 2012, Da Silva et al. 2009, and Neto et al. 2012) have been carried out to study the adhesive joint performance of DMSs.

To further examine the structural performance of a DMS with adhesive joints, this project conducted small- and full-scale testings. For the small-scale testing, an experimental program was initially designed to examine the tensile, shear, peel, and cleavage strength of the adhesive and welded specimens at different conditioning temperatures and conditioning humidity conditions. All the specimens with different specimen widths were tested according to American Society for Testing and Materials (ASTM) after conditioning them in different temperature and humidity conditions. Note, the welded specimens were fabricated following American Welding Society (AWS) guidelines. Numerous data resulting from each of the small-scale tests were analyzed through graphical comparisons and statistical analysis, so as to investigate the effect of the conditioning temperature, conditioning humidity, and width on the tensile, shear, peel, and cleavage strengths. As part of the statistical analysis, multiple linear regression (MLR) and response surface metamodels (RSM) for adhesive specimens were utilized not only to determine statistically significant parameters (i.e., conditioning temperature, conditioning humidity, and width) affecting the strengths, but also to develop separate regression models for each of the strengths. Figure 1.1a through d show sample photographs for the successfully conducted small-scale tests for adhesive specimens.

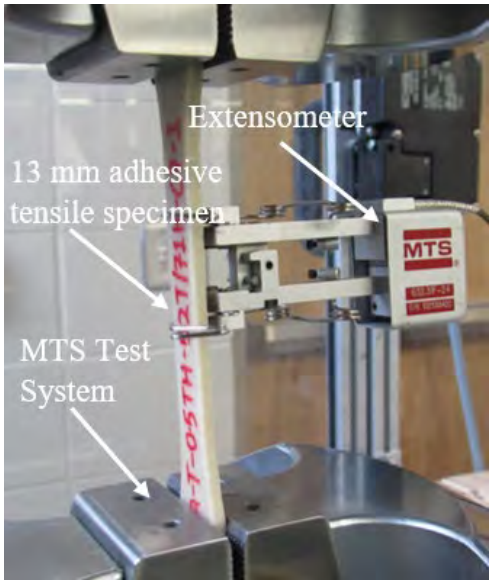

(a)

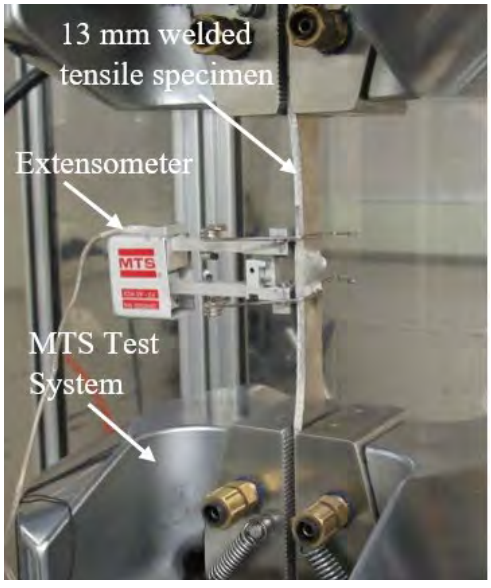

(b)

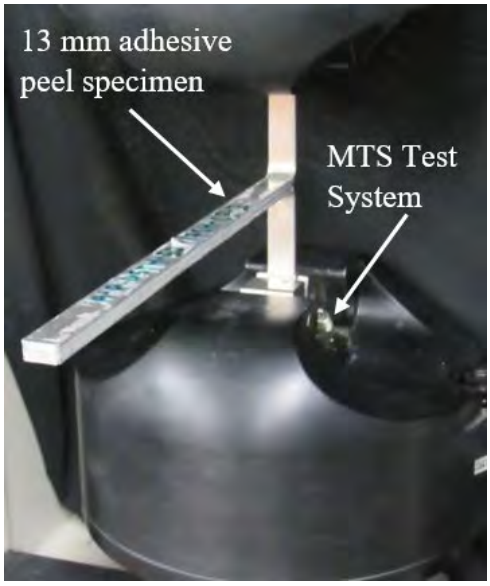

(c)

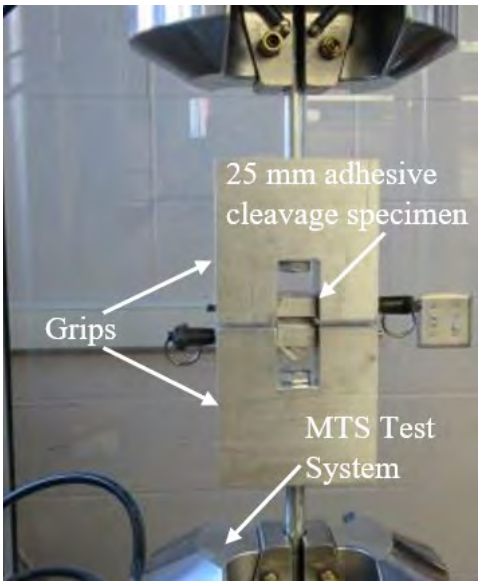

(d)

Figure 1.1 Sample photographs of small scale testing for the adhesive specimens (a) tensile, (b) shear, (c) peel, and (d) cleavage

Figure 1.2a through d.

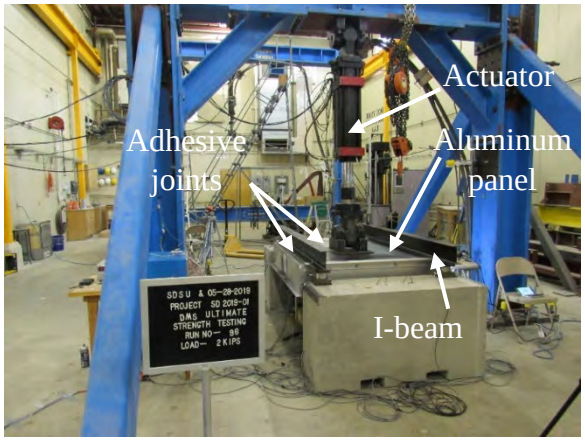

(a)

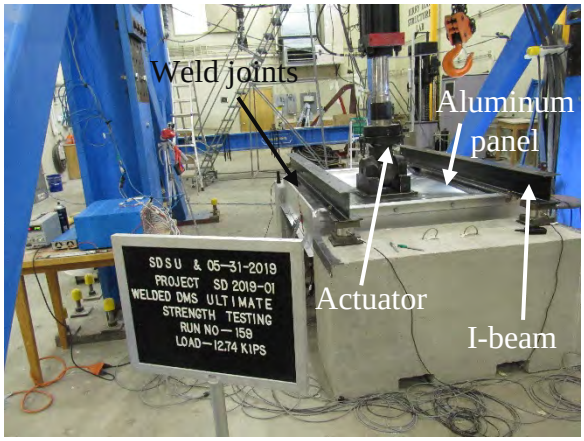

(b)

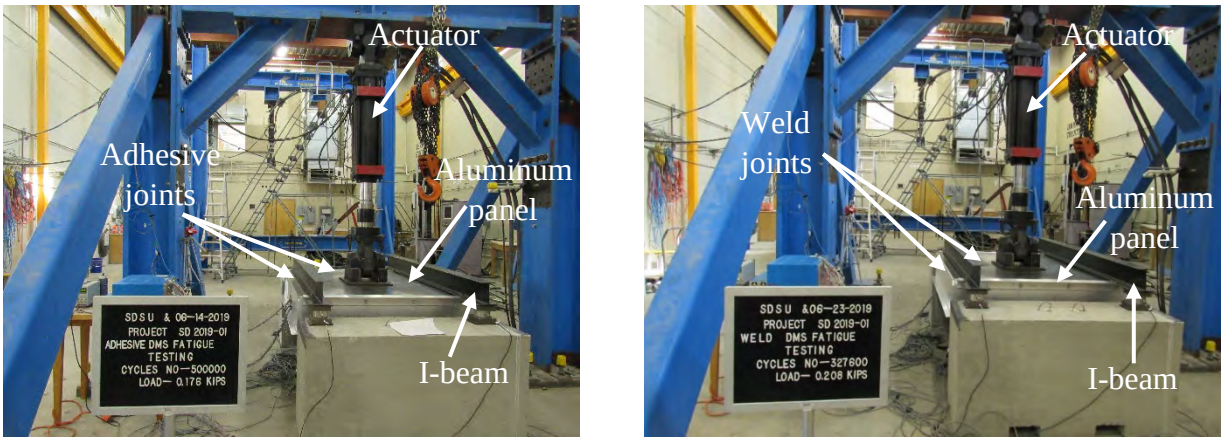

(c) (d)

Figure 1.2 Sample photographs obtained during full-scale tests in this project: (a) ultimate strength test of adhesive DMS, (b) ultimate strength test of welded DMS, (c) fatigue load test of adhesive DMS, and (d) fatigue load test of welded DMS

1.1 Background and Problem Statement

DMSs are used in intelligent transportation system applications along road networks to improve traffic control and mobility. The DMS consists of cabinet sheet metal skin, internal structure frame, sign controller, inter-connect cable, and traffic cabinet enclosure. Typically, welded connections with appropriate design strength are used in the DMSs.

In spite of the ubiquity of welded connections in the system, adhesive connections between the cabinet sheet metal skin and internal structure frame have gained popularity in many fields due to their cost-effectiveness and fabrication efficiency (Mclean et al. 2004, Močibob and Crisinel 2008). Unlike the welded connections that see residual stresses and distortion that develop during the welding process, the adhesive joints can facilitate a more uniform load transfer mechanism between cabinet skin-frames that may reduce these issues. The adhesive connections also provide a better water seal than welded connections. For these reasons, some transportation sign manufacturing companies are pursuing adhesive connections in DMSs. However, a comprehensive knowledge of the mechanical properties and structural behavior of the adhesive to be used in the DMS is still needed.

Some studies (Çolak et al. 2009, Agarwal et al. 2014, Savvilotidou et al. 2017, Kim et al. 2012, Goglio and Rezaei 2014, Silva et al. 2016, Sousa et al. 2018, and Moussa et al. 2012) have shown that temperature and moisture affected the strength and durability of adhesives; however, the severity of the effects due to these parameters has not been conclusive. Although the tensile and shear strength of the adhesive joints have been studied considering temperature and moisture variability, these effects on the peel and cleavage strength of the adhesive have not been investigated. Most DMS applications would rarely be immersed in water, especially for extended periods, and high humidity conditions are generally intermittent. Therefore, the effects of practical exposure to moisture and temperature should be researched at or slightly above expected service conditions for adhesives to measure their performance. Tensile, shear, peel, and cleavage tests of the adhesive joints exposed to different environmental conditions need to be completed to provide an insight for the prospect of adhesive use in DMS connections. It is also required that the tensile, shear, peel, and cleavage strength of the adhesive be compared with the respective strength of weld connections used in DMS.

In addition to the mechanical properties of the connections used in the DMS, a detailed study of the structural behavior of DMSs with adhesive joints is also required and can be achieved from the ultimate strength and fatigue testings. Even though some studies (Constantinescu et al. 2007, Huckelbridges and Metzger 2007) have assessed the structural integrity of welded connected DMS supporting structures, very limited substantiated test data exist to investigate structural performance of DMSs with adhesive joints. Specifically, there is a lack of detailed ultimate and fatigue load testing data on cabinet skin-frame joints made with adhesive joints. Therefore, extensive research to study the structural performance of DMSs with adhesive joints subjected to ultimate and fatigue loads is needed. The structural performance of DMSs with conventional welded connections subjected to ultimate and fatigue loads needs to be examined as well to have a better comparison of the adhesively bonded DMS performance.

1.2 Research Objectives

The goal of this project is to provide comprehensive knowledge of the structural behavior of DMSs with adhesive joints and welded connections subjected to ultimate and fatigue loads. The following objectives are designed to achieve this goal.

1) Study the effects of environmental and geometrical characteristics on joint performance of adhesive and welded small-scale specimens.
2) Examine the ultimate strength and fatigue performance of DMSs with adhesive connections.
3) Compare the structural performance between adhesive bonded DMSs and welded DMSs.

1.3 Project Scope and Organization

To achieve the aforementioned objectives, the following tasks were undertaken in this project:

1) Literature review of the state of the art and practice on adhesive joints
2) Small-scale testing and data investigation for adhesive specimens
3) Comparison with small-scale testing data of welding specimens
4) Ultimate load and fatigue testing of full-scale DMS systems
5) Full-scale testing data analysis
6) Final report

This project is divided into six sections. Section 2 deals with the research findings from the literature review in small-scale tests of adhesive joints and full-scale tests of DMSs. Section 3 provides results and discussion on the small-scale tests of the adhesive specimens. Section 4 is dedicated to the comparison of small-scale testing data between the adhesive and welded specimens. Section 5 presents the results and discussion on the ultimate strength tests and fatigue load tests conducted for adhesive and welded DMSs. Finally, Section 6 encompasses the conclusions obtained from this project and future work.

2. LITERATURE REVIEW

2.1 Small-Scale Tests

A significant amount of work (Çolak et al. 2009, Savvilotidou et al. 2017, Goglio and Rezaei 2014, Silva et al. 2016, Moussa et al. 2012, Agarwal et al. 2014, Kim et al. 2012, Ferreira et al. 2002, Sugiman et al. 2013, Sousa et al. 2018, Da Silva et al. 2009, Neto et al. 2012, Kim and Aravas 1988, De Freitas and Sinke 2014, Broughton et al. 1999, Noori et al. 2016, Shahid and Hashim 2000, 2002, and Zheng et al. 2007) in relation to small-scale tests of adhesive specimens has been conducted, but inconsistent research results on adhesives have restricted their potential in DMSs.

Numerous studies (Çolak et al. 2009, Savvilotidou et al. 2017, Goglio and Rezaei 2014, Silva et al. 2016, Zhang et al. 2007, and Moussa et al. 2012) to study tensile strength of the adhesives have been performed. Colak et al. (2009) indicated that the strength of the adhesive was reduced the most during the formation of the bond under saturated conditions. A directly proportional relationship was found between strength reduction and the amount of moisture absorbed. Savvilotidou et al. (2017) investigated the adhesives to observe the effects of moisture on the elastic modulus and tensile strength. The results found a reduction in elastic modulus and tensile strength due to humidity after saturation when submerged in water. Goglio and Rezaei (2014) conditioned the specimens at 100% relative humidity and 50°C for five weeks to study the effects of warm temperatures and moisture on the mechanical properties of adhesives. It was reported that the tensile strength and strain were reduced by 75% and 100% before failure, while the modulus of elasticity and shear modulus was reduced by 20%. Silva et al. (2016) studied the effects of thermal cycles (-15°C to 60°C) and immersion in water on adhesives. The thermal cycles resulted in an increase in tensile strength and modulus of elasticity, but the exposure to water resulted in decreases in tensile strength and modulus of elasticity due to plasticization. Zhang et al. (2007) studied the effects of temperatures ranging between -35°C and 60°C on the tensile strength of adhesive connecting pultruded glass fiber-reinforced polymer laminates. It was found that the tensile strength and stiffness of the adhesive connection was decreased when the temperature was increased above the glass transition temperature range from 40°C to 50°C. Moussa et al. (2012) studied a structural adhesive to temperatures above the glass transition temperature and found that a slight increase in tensile stiffness and strength was observed.

Shear strength of the adhesives have also been studied (Agarwal et al. 2014, Kim et al. 2012, Ferreira et al. 2002, Sugiman et al. 2013, Sousa et al. 2018, Da Silva et al. 2009, and Neto et al. 2012) to some extent. Agarwal et al. (2014) studied the effects of freeze-thaw cycles on the adhesive connection of steel-carbon fiber reinforced polymer joints. The single-lap shear specimens were tested and a reduction in shear strength between 12% and 18% was found after freeze-thaw cycles. The adhesives were studied by Kim et al. (2012) for the shear strength using double-lap joint specimens after repeated freeze-thaw cycles. A slight increase in shear strength was found due to further curing of the adhesive as a result of moisture. Ferreira et al. (2002) studied the effects of immersion of water, elevated temperatures, and joint length on the static and fatigue shear strength of adhesives. The results indicated that shorter bond lengths had higher static and fatigue strength, while the effects of water were dependent on the water temperature. Sugiman et al. (2013a, b) tested single-lap joints specimens at a temperature of 50°C. The exposure to the temperature decreased the number of cycles for the failure of the lap-joints. Sousa et al. (2018) studied the effects of moisture and temperature on the durability of adhesives, demonstrating that the shear modulus decreased by 43%, but the shear strength increased by nearly 25% due to immersion in water. Da Silva et al. (2009) found that lap shear strength was improved with the increase in overlap length, and Neto et al. (2012) demonstrated that the increase in overlap length increased the failure load in the ductile adhesive.

Some studies on peel strength tests have been conducted by Kim and Aravas (1988), De Freitas and Sinke (2014), Broughton et al. (1999), and Noori et al. (2016) for adhesively bonded substrates to understand their strength when subjected to peel loading. For peel strength, previous research accomplished by Kim and Aravas (1988) showed that the peel strength was significant to the yield strength, Young's modulus, ductility, and thickness of flexible adherend. De Freitas and Sinke (2014) determined the adhesive properties using peel tests for bonded composite-to-aluminum joints, demonstrating that the peel load decreased when composite adherend was used instead of flexible adherend. Broughton et al. (1999) conducted T-peel tests of the adhesively bonded specimens subjected to temperature, humidity, and load to determine their peel strength. It was reported that average peeling force was observed to be higher for smaller specimens due to higher and more uniform clamping forces being applied during curing. Noori et al. (2016) conducted the peel test of polymer laminated sheet metal specimens. It was found that the interfacial peel strength was greatly influenced by residual stress in the polymer adherend.

There are a few studies pertaining to investigation of the effects of environmental and geometrical factors on the cleavage strength of adhesives. Some studies led by Shahid and Hashim (2000, 2002) and Zheng et al. (2007) have been completed to better understand the cleavage strength of small-scale adhesive specimens. Shahid and Hashim (2000) tested adhesively bonded cleavage specimens to determine their cleavage strengths with different adhesive thicknesses. The adhesive thickness was found to be highly insignificant to the measured cleavage strengths. Shahid and Hashim (2002) further investigated the effect of surface roughness on the cleavage strength of specimens through experimental testing. It was observed that the increase in roughness and surface area of adherend increased the cleavage strength. Zheng et al. (2007) demonstrated that the hardness of the adhesively bonded area increased the cleavage strength slightly.

Although some of the aforementioned past studies have reported that temperature and moisture can affect the strength and durability of adhesives, the severity of the effects due to these parameters has not been conclusive. A comprehensive small-scale study to examine tensile, shear, peel, and cleavage strength necessary for demonstrating the use of adhesive bonded DMSs exposed to varying environmental and geometrical conditions has not been done to date.

2.2 Full-Scale Tests

Full-scale testing can provide a wealth of information about the behavior of the entire DMS system with adhesive connections; however, only a few studies (Connor and Altstadt 2013, Huckelbridge and Metzger 2009) have been conducted on frame structures supporting DMSs using welded connections. For example, Connor and Altstadt (2013) investigated the after-fracture reserve strength of two four-chord aluminum trusses that support the DMS with destructive testing. Truss members were cut to replicate the fractures in chords and simulated DMS dead load and wind load were applied on the truss. It was found that the truss member possessed significant reserve strength even in its severe condition. Huckelbridge and Metzger (2009) conducted a detailed field monitoring of an aluminum sign support truss that was fractured in two truss members near one truss support. It was revealed that the truss failed due to excessive fatigue of the chord-web diagonal welded connection. As far as the authors are aware, an ultimate strength test of a DMS with adhesive connections has not been conducted to date.

Several studies (Puckett et al. 2010, Arabi et al. 2018, Chang et al. 2014, Park and Stallings 2006) have been conducted in terms of fatigue load tests. However, all the studies have been limited to investigating the performance of the DMS supporting structures. For instance, Puckett et al. (2010) delved into the fatigue resistance of the DMS supporting structure with welded specimens in accordance with the American Association of State Highway and Transportation Officials (AASHTO) Standard Specifications for Structural Supports for Highway Signs, Luminaires and Traffic Signals (AASHTO 2015). It was demonstrated that the fatigue resistance of a ring-stiffened box connection was better than the standard

box connection. Arabi et al. (2018) also performed a complete field test to study the damage due to fatigue loads in the DMS support structures during transportation, indicating that the failure damage of 0.01% in the most vital member of the support structure was observed. Chang et al. (2014) studied the overhead truss structures supporting the DMS to determine the impact of wind loads resulting from truck-induced wind gusts and thermal-induced loads, and found that the wind loads generated unnoticeable stresses and minimal damage on the DMS support structures. Park and Stallings (2006) performed field testing for fatigue evaluation of DMS support structures due to natural and truck-induced wind gusts, signifying that natural wind gusts caused the highest critical stress cycles in the structures.

While all the past studies have been researched to investigate the strength and/or fatigue performance of the structure to support the DMS, the structural adequacy of any DMS with adhesive connections have not been examined in a satisfactory manner until now. Therefore, an extensive body of research on the structural performance of DMSs with adhesive connections is needed.

3. SMALL-SCALE TESTING

This section discusses the testing matrix and conditioning, specimens, and testing necessary for the determination of the tensile strength, shear strength, peel strength, and cleavage strength and other mechanical properties.

3.1 Testing Matrix and Conditioning

To study the performance of the adhesive connection, 16 different combinations comprising different parameters were developed using Plackett-Burman Design designated as PBD (Seo 2013, Chandorkar et al. 2008, Seo and Linzell 2010, 2012, 2013a, b) through JMP, commercially available statistical software (SAS Institute 2008). Note, PBD was used to develop statistical models in an efficient manner. Included in the parameters were conditioning temperature, conditioning humidity, and width of the specimens. These parameters were considered inputs for statistical analysis. The combinations consisted of a low, medium, and high value for each of the considered input parameters. Three different widths of 13 mm, 25 mm, and 38 mm were used to account for variation in geometry of the specimens, while three conditioning temperature values of 20°C, 52.5°C, and 85°C and three conditioning humidity values of 48%, 71.5%, and 95% were considered for the PBD development. The developed 16 combinations with three different values for each parameter can be seen in Table 3.1. It consists of five combinations with 13-mm width, six combinations with 25-mm width, and five combinations with 38-mm width specimens. Note, each combination consisted of two tensile, two shear, two peel, and two cleavage specimens; thus, the total number of specimens was 132, including 32 tensile, 32 shear, 32 peel, and 32 cleavage specimens.

Table 3.1 Matrix for the sixteen combinations

Combination	Conditioning Temperature (°C)	Conditioning Humidity (%)	Width (mm)
C1	20	48	13
C2	20	48	38
C3	20	71.5	25
C4	20	95	13
C5	20	95	38
C6	52.5	48	25
C7	52.5	71.5	13
C8	52.5	71.5	25
C9	52.5	71.5	25
C10	52.5	71.5	38
C11	52.5	95	25
C12	85	48	13
C13	85	48	38
C14	85	71.5	25
C15	85	95	13
C16	85	95	38

The specimens per combination were conditioned in a temperature and humidity-controlled chamber as seen in Figure 3.1a. Specifically, the specimens were grouped with the same conditioning humidity, yet different conditioning temperatures were first conditioned at the lowest conditioning temperature of the group for 96 hours for its moisture saturation. Then, the combinations conditioned at the lowest conditioning temperature among the group were first taken out of the chamber for the test, and the conditioning temperature was increased up to the next lower conditioning temperature to condition the remaining specimens for additional 24 hours. For example, the specimens for the combinations C1, C2, C6, C12, and C13 were placed inside the chamber at 20°C and 48% conditioning humidity. The specimens for combinations C1 and C2 were taken out for test after conditioning for 96 hours and the conditioning temperature of the chamber was increased to 52.5°C for the remaining specimens. The specimens for combination C6 were taken out of the chamber for testing after conditioning for additional 24 hours, and the conditioning temperature of the chamber was again increased to 85°C for the specimens with combination C12 and C13. The conditioning humidity was kept constant at 48% throughout this period. To observe the change in moisture, the specimens were weighed prior to conditioning, after conditioning, after transporting to the lab, and after testing. Mylar bags were used to minimize any loss of humidity during transportation of the specimens from the conditioning lab to the testing lab. The specimens were transported in a thick Styrofoam (see Figure 3.1b) cooler to prevent the loss of heat after taking the specimens out of the chamber. Temperatures were recorded after transporting the specimens to the lab and after the test for each of the specimens. The conditioning time of the specimens for different temperatures and humidity is shown graphically in a bar chart in Figure 3.2a and Figure 3.2b, respectively.

(a) (b)

Figure 3.1 Conditioning of the specimens (a) temperature-humidity controlled chamber and (b) Styrofoam cooler

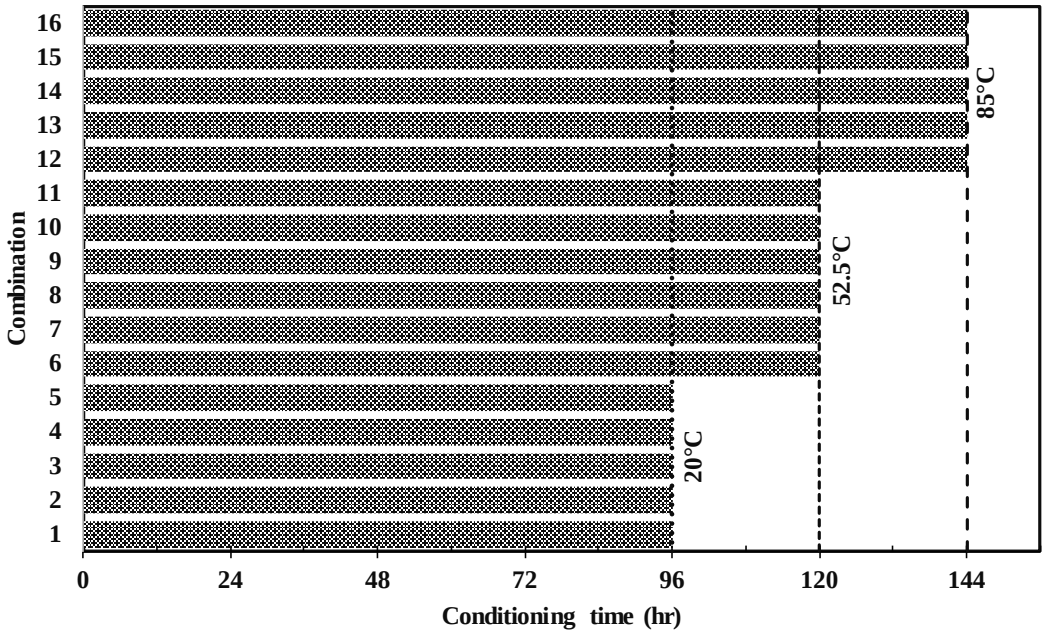

(a)

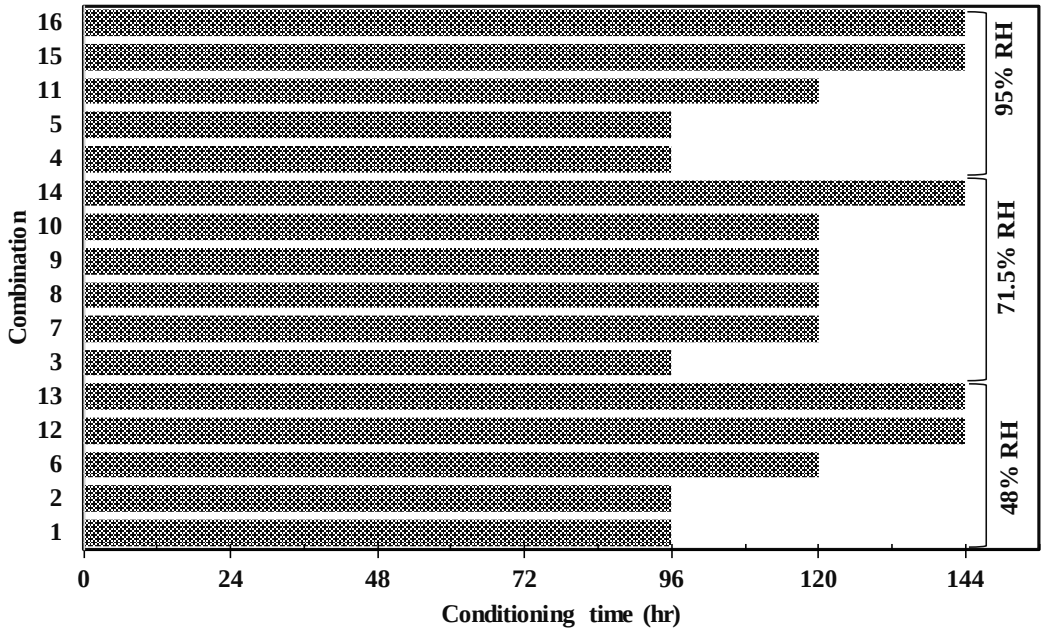

(b)

Figure 3.2 Conditioning time of the specimens for (a) temperature and (b) humidity

To increase the efficiency and accuracy during conditioning and testing, every specimen was designated as a specimen ID, such as A-T-13TH-20T/48H-C1. The first letter represents the type of specimen (A-adhesive), and the second letter symbolizes the type of test (T-tensile/S-shear/P-peel/C-cleavage). 13TH, 25TH, or 38TH suggest whether the width of the specimen is 13 mm, 25 mm, or 38 mm. T/H represents the conditioning temperature and conditioning humidity of the chamber during conditioning. C is the combination number generated from the PBD. Change in moisture and temperature for both tensile and shear specimens is shown in Table 3.2, whereas Table 3.3 represents the change in moisture and temperature for both peel and cleavage specimens. It should be noted that two specimens for each combination were considered for this study; thus, the values shown in this table correspond to the average value. Note, all changes in moisture between before and after conditioning phases named "moisture change after chamber (%)," between after conditioning and after transporting phases titled "moisture change after transportation (%)," and after transporting and after the testing phases called "moisture change after test (%)" are listed in these tables. In these tables, the positive value of moisture change indicates moisture absorption, whereas negative value represents the loss in moisture. It appears that there is insignificant change in moisture for the majority of the specimens during each of the three phases. Change in temperature after transportation and test was calculated by comparing the temperature measured after the specimens were transported to the lab and after the tests were completed. Positive temperature change indicates a rise in temperature while negative temperature change represents temperature loss. Specimens conditioned at higher temperatures showed a greater loss in temperature than those conditioned at lower temperatures due to the difference in ambient conditions during the testing. Performing the tests at the same temperature as conditioning temperature was not feasible in this study, as it required special testing apparatus with an in-built chamber. The specimens were tested as soon as possible after transporting them to the SDSU lab. The aim of this study was to analyze the effect of conditioning temperature and conditioning humidity in the mechanical properties. Additionally, numerous studies (Goglio and Rezaei 2014, Hu et al. 2012, Agarwal et al. 2014, Çolak et al. 2009, Kim et al. 2012, Lettieri and Frigione 2011) suggested that specimens be tested at room temperature and humidity. Therefore, the effect of change in temperature and humidity on the test results during testing was not evaluated in this study as it was not the main objective of this study.

Table 3.2 Moisture and temperature change in tensile and shear specimens

Specimen type	Combination	Specimen ID	Moisture change after chamber (%)	Moisture change after transportation (%)	Moisture change after test (%)	Temperature change after transportation and test (%)
Tensile	C1	A-T-13TH-20T/48H-C1	-0.853	+0.811	-0.003	-2.2
	C2	A-T-38TH-20T/48H-C2	-0.062	+0.006	-0.002	+4.5
	C3	A-T-25TH-20T/71H-C3	+0.025	-0.001	-0.008	-4.2
	C4	A-T-13TH-20T/95H-C4	+0.341	-0.007	-0.168	-8.0
	C5	A-T-38TH-20T/95H-C5	+0.154	-0.005	-0.074	-9.6
	C6	A-T-25TH-52T/48H-C6	-0.247	-0.001	0.006	-34.7
	C7	A-T-13TH-52T/71H-C7	+0.145	-0.170	-0.017	-8.0
	C8	A-T-25TH-52T/71H-C8	+0.142	-0.042	-0.019	-4.0
	C9	A-T-25TH-52T/71H-C9	+0.066	-0.022	-0.028	-7.7
	C10	A-T-38TH-52T/71H-C10	+0.036	-0.011	-0.007	-41.5
	C11	A-T-25TH-52T/95H-C11	+0.538	-0.029	-0.070	-30.3
	C12	A-T-13TH-85T/48H-C12	-0.512	-0.038	-0.005	-43.0
	C13	A-T-38TH-85T/48H-C13	-0.462	+0.035	-0.034	-39.2
	C14	A-T-25TH-85T/71H-C14	+0.063	-0.032	-0.015	+2.0
	C15	A-T-13TH-85T/95H-C15	+1.015	-0.051	-0.094	-21.0
	C16	A-T-38TH-85T/95H-C16	+0.982	-0.030	-0.067	-22.6
Shear	C1	A-S-13TH-20T/48H-C1	-0.072	+0.005	-0.002	+12.0
	C2	A-S-38TH-20T/48H-C2	-0.039	+0.003	-0.019	+8.0
	C3	A-S-25TH-20T/71H-C3	-0.002	0.000	-0.010	-4.2
	C4	A-S-13TH-20T/95H-C4	-0.001	-0.007	-0.020	+2.1
	C5	A-S-38TH-20T/95H-C5	+0.009	-0.006	-0.012	+6.5
	C6	A-S-25TH-52T/48H-C6	-0.012	-0.002	-0.007	-30.0
	C7	A-S-13TH-52T/71H-C7	-0.018	-0.003	-0.007	0.0
	C8	A-S-25TH-52T/71H-C8	-0.015	-0.001	-0.004	-7.4
	C9	A-S-25TH-52T/71H-C9	-0.008	-0.001	-0.002	-5.6
	C10	A-S-38TH-52T/71H-C10	-0.009	0.000	-0.029	-27.8
	C11	A-S-25TH-52T/95H-C11	+0.009	-0.008	-0.016	-21.9
	C12	A-S-13TH-85T/48H-C12	-0.039	+0.011	+0.003	-39.3
	C13	A-S-38TH-85T/48H-C13	-0.028	+0.010	-0.002	-48.3
	C14	A-S-25TH-85T/71H-C14	-0.003	-0.009	-2.086	-35.9
	C15	A-S-13TH-85T/95H-C15	+0.011	+0.001	-0.013	-13.3
	C16	A-S-38TH-85T/95H-C16	-1.390	0.000	-0.010	-20.0

Table 3.3 Moisture and temperature change in peel and cleavage specimens

Specimen type	Combination	Specimen ID	Moisture change after chamber (%)	Moisture change after transportation (%)	Moisture change after test (%)	Temperature change after transportation and test (%)
Peel	C1	A-P-13TH-20T/48H-C1	-0.013	0.000	-0.011	+9.1
	C2	A-P-38TH-20T/48H-C2	+0.003	-0.011	-0.005	+9.1
	C3	A-P-25TH-20T/71H-C3	-0.001	-0.003	-0.007	+6.8
	C4	A-P-13TH-20T/95H-C4	+0.001	-0.003	-0.015	0.0
	C5	A-P-38TH-20T/95H-C5	+0.011	+0.009	-0.023	+9.1
	C6	A-P-25TH-52T/48H-C6	-0.011	-0.001	-0.004	-23.8
	C7	A-P-13TH-52T/71H-C7	-0.009	-0.003	-0.009	-26.5
	C8	A-P-25TH-52T/71H-C8	-0.006	-0.002	-0.004	-10.7
	C9	A-P-25TH-52T/71H-C9	-0.006	-0.003	-0.004	-10.7
	C10	A-P-38TH-52T/71H-C10	+0.007	-0.012	0.000	-9.1
	C11	A-P-25TH-52T/95H-C11	0.000	-0.004	-0.008	-25.0
	C12	A-P-13TH-85T/48H-C12	-0.029	-0.001	-0.006	0.0
	C13	A-P-38TH-85T/48H-C13	-0.002	-0.013	0.000	-35.8
	C14	A-P-25TH-85T/71H-C14	-0.011	0.000	-0.004	-26.7
	C15	A-P-13TH-85T/95H-C15	-0.001	-0.005	-0.013	-20.0
	C16	A-P-38TH-85T/95H-C16	+0.015	-0.015	0.000	-12.1
Cleavage	C1	A-C-13TH-20T/48H-C1	-0.001	0.000	+1.566	+4.5
	C2	A-C-38TH-20T/48H-C2	-0.002	+0.001	-0.003	+4.5
	C3	A-C-25TH-20T/71H-C3	+0.001	0.000	-0.001	0.0
	C4	A-C-13TH-20T/95H-C4	+0.003	-0.004	-0.003	6.4
	C5	A-C-38TH-20T/95H-C5	+0.001	-0.002	-0.003	+4.3
	C6	A-C-25TH-52T/48H-C6	-0.007	+0.002	-0.001	-27.0
	C7	A-C-13TH-52T/71H-C7	-0.002	0.000	0.000	-8.9
	C8	A-C-25TH-52T/71H-C8	-0.003	0.000	-0.001	-10.7
	C9	A-C-25TH-52T/71H-C9	-0.001	0.000	0.000	-12.5
	C10	A-C-38TH-52T/71H-C10	-0.002	0.000	0.000	-12.5
	C11	A-C-25TH-52T/95H-C11	0.000	-0.002	-0.002	-28.1
	C12	A-C-13TH-85T/48H-C12	-0.007	0.000	+0.002	-43.3
	C13	A-C-38TH-85T/48H-C13	-0.006	-0.001	+0.001	-40.5
	C14	A-C-25TH-85T/71H-C14	-0.002	-0.001	0.000	-37.7
	C15	A-C-13TH-85T/95H-C15	+0.004	-0.003	-0.003	-21.8
	C16	A-C-38TH-85T/95H-C16	0.000	-0.002	-0.003	-24.2

3.2 Adhesive Specimens

This section focuses on the fabrication and geometry of tensile, shear, peel, and cleavage specimens for small-scale adhesive strength testings.

The adhesive tensile, shear, peel, and cleavage specimens were fabricated based on ASTM D638 (2010), ASTM D1002 (2010), ASTM D1876 (2008), and ASTM D1062 (2008), respectively. The bone-shaped tensile specimens were entirely made up of LORD 406-19GB (LORD Corporation 2018) acrylic adhesive with a glass transition temperature of 72°C. The shear specimens were built with two 5052 aluminum metal bars bonded with the same LORD acrylic adhesive at the overlap in the middle of each specimen. An extra aluminum piece was added to each of the shear specimens to facilitate efficient installation of an extensometer. For the fabrication of peel specimens, two 5052 aluminum metal bars were bent 90° to 76 mm from the end. The bent aluminum bars are adhesively bonded with LORD 406-19GB acrylic adhesive. Cleavage specimens were fabricated with two metal blocks adhesively bonded with LORD 406-19GB acrylic adhesive in the middle of each specimen. The specimens were left for two weeks to ensure proper curing of the adhesive after conditioning. The geometry of representative tensile, shear, peel, and cleavage specimens with a width of 13 mm is shown in Figure 3.3a through Figure 3.3h, correspondingly.

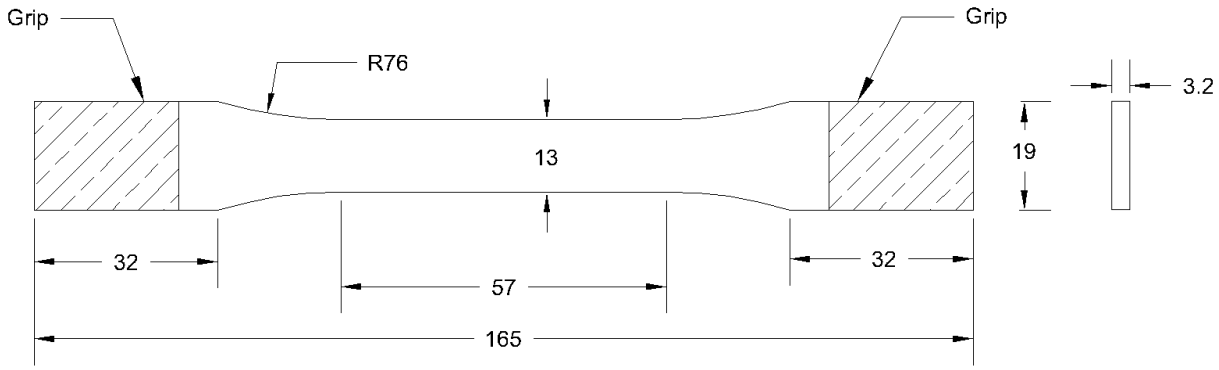

(a) (b)

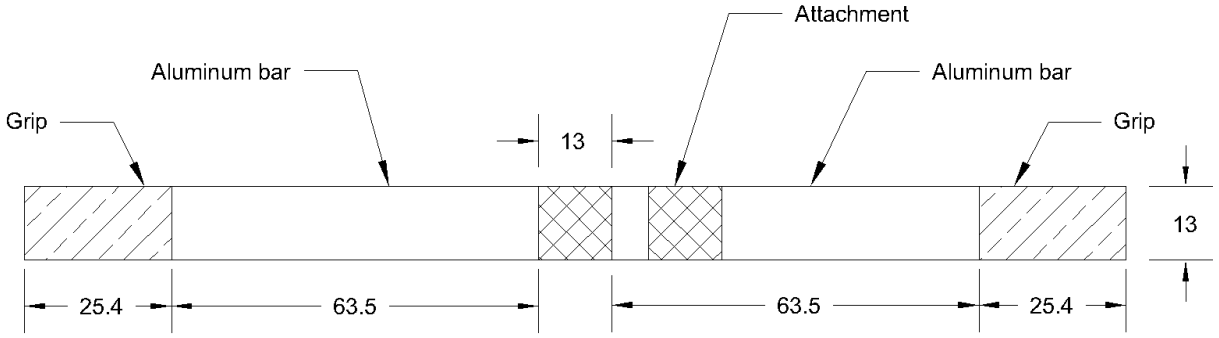

(c)

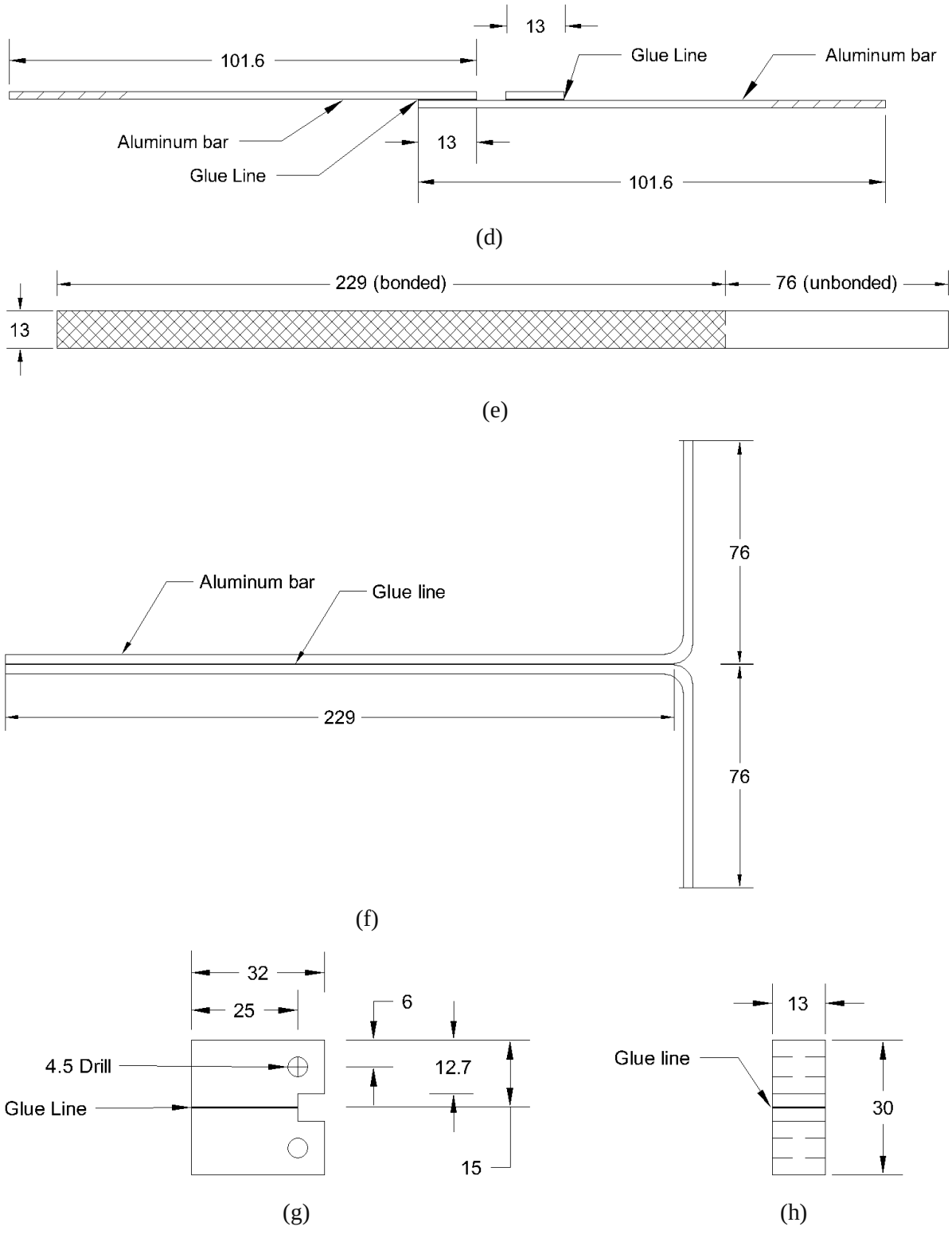

Figure 3.3 Geometry of adhesive test specimens (a) top view of tensile dogbone; (b) cross-section of tensile dogbone; (c) top view of single-lap shear and (d) side view of single-lap shear (e) top view of peel; (f) side view of peel; (g) side view of cleavage and (h) front view of cleavage (All dimensions are in mm)

3.3 Testing

All the specimens were tested to failure using two different types of MTS (material testing system) universal testing systems. It should be noted that all the tests were performed at room temperature. Each specimen was mounted and aligned in the grips of the MTS. In detail, the tensile, shear, peel, and cleavage specimens were tested using an MTS 370 Landmark (MTS Systems Corporation 2018) 100-kN servo-hydraulic load unit calibrated to 20% of its load capacity; whereas, the peel tests were performed using MTS Insight 5 (MTS Systems Corporation 2019) . The longitudinal strains of the tensile and shear specimens were calculated by measuring the extension recorded from an MTS 634.31F-24 clip-on extensometer with a gauge length of 20 mm mounted to each specimen during the test. The extensometer was a class B2 calibrated with an accuracy of ±0.25% of measured strain. The tests were conducted by applying a loading with a free crosshead speed of 5 mm/min for the tensile specimens, 1.3 mm/min for the shear specimens, 254 mm/min for the peel specimens, and 1.27 mm/min for the cleavage specimens. The testing procedures for the tensile, shear, peel, and cleavage tests are specified by ASTM D638 (2010), ASTM D1002 (2010), ASTM D1876 (2008), and ASTM D1062 (2008), respectively. The testing setups for the tensile, shear, peel, and cleavage specimens are shown in Figure 3.4.

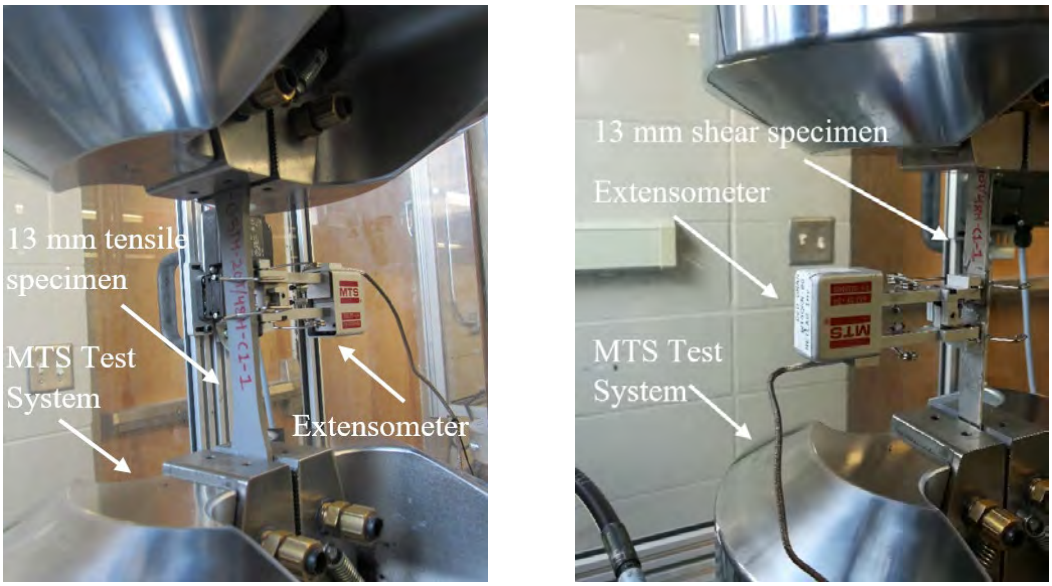

(a) (b)

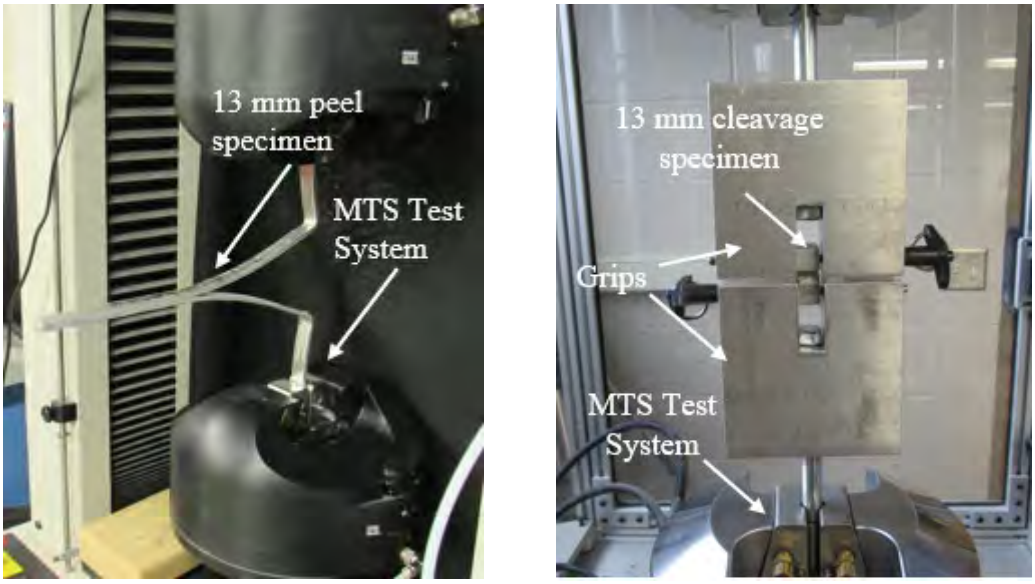

(c) (d)

Figure 3.4 Installation of the adhesive specimens in the testing machine (a) tensile, (b) shear, (c) peel, and (d) cleavage

3.4 Results and Discussion

Results from the tensile, shear, peel, and cleavage tests are presented and discussed in this section. Load-displacement and stress-strain curves were plotted for each of the tests along with the determination of various mechanical properties such as strength. The influence of conditioning temperature, conditioning humidity, and width on the strength of adhesive specimens is graphically explained.

3.4.1 Tensile Test

Representative load-displacement and stress-strain curves for the tensile specimens of combination C1 are presented in Figure 3.5. The ultimate tensile load and stiffness of the specimens are determined by analyzing the data used for the load-displacement curve; whereas, mechanical properties, encompassing ultimate stress, yield stress, Young's modulus of elasticity and ductility are determined from the stress-strain curve. The ultimate tensile stress, along with relevant mechanical properties for all the combinations, is summarized in Table 3.4. An average ultimate tensile stress of 16.94 MPa with a standard deviation of 0.87 MPa was found from the tensile testing data. The ultimate tensile stress data was found to be in agreement with Lord technical data sheet (LORD Corporation 2020).

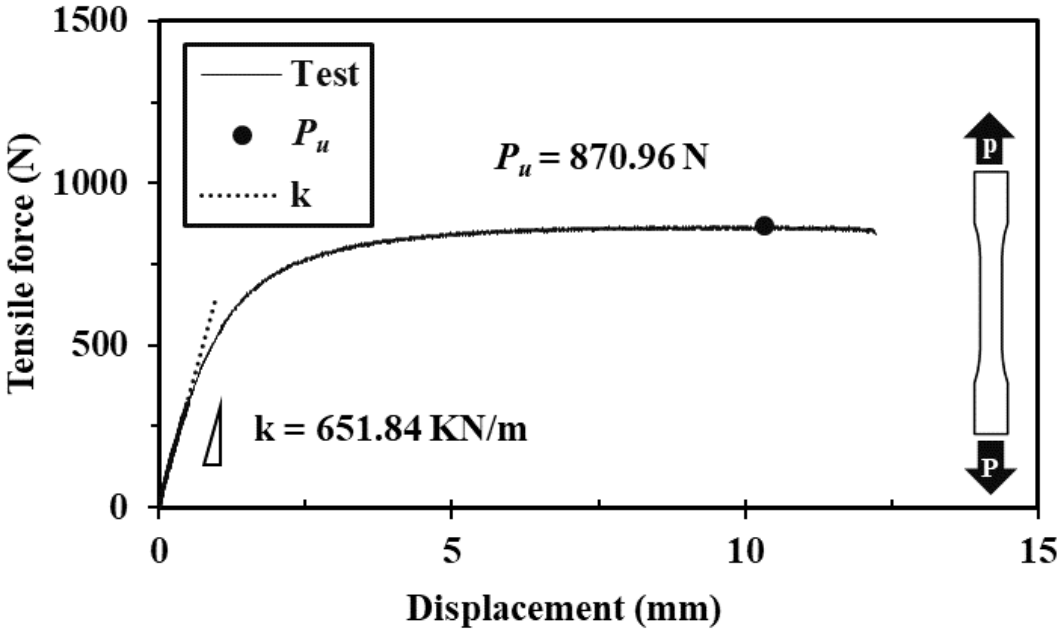

(a)

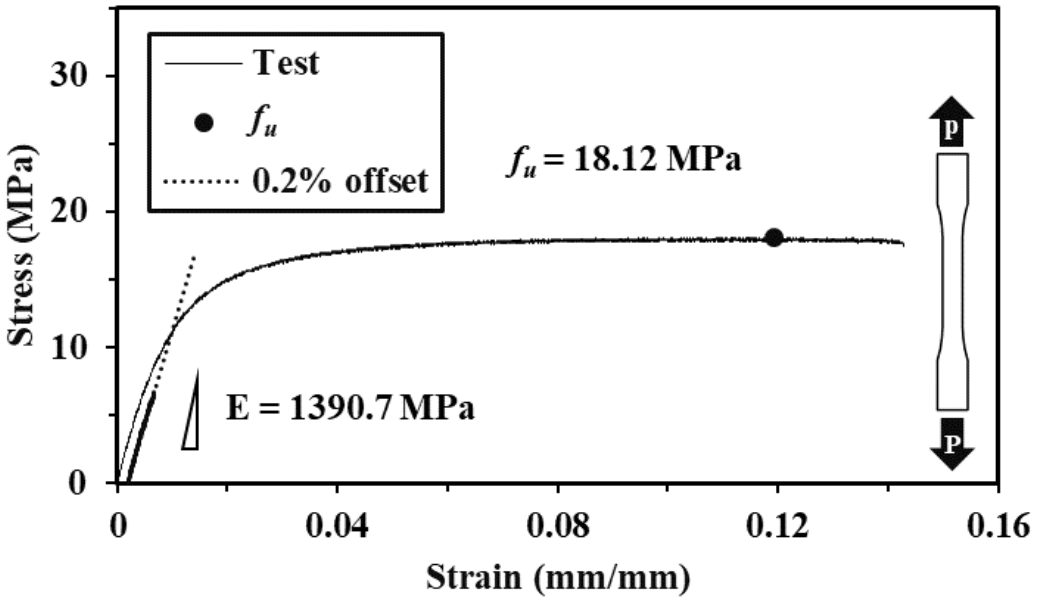

(b)

Figure 3.5 Curves for tensile specimen (a) load displacement and (b) stress-strain

Table 3.4 Mechanical properties from the tensile tests

Combination	Specimen	Young's modulus, E (MPa)	Stiffness, k (KN/m)	Ultimate tensile stress, f_u(MPa)	Ultimate tensile load, P_u(N)	Strain at ultimate load, (mm/mm)	Yield stress, f_y (MPa)	Load at yield point, P_y (N)	Strain at yield point, (mm/mm)	Ductility, e (%)
C1	A-T-13TH-20T/48H-C1	1339.49	671.3	17.87	923.65	0.124	10.36	534.97	0.009	14.81
C2	A-T-38TH-20T/48H-C2	1303.06	2044.6	17.63	2879.69	0.126	9.86	1613.19	0.009	13.02
C3	A-T-25TH-20T/71H-C3	1289.87	1351.3	17.61	1819.57	0.128	10.47	1082.45	0.010	14.86
C4	A-T-13TH-20T-95H-C4	1227.73	440.0	16.21	643.15	0.171	9.05	359.04	0.009	18.34
C5	A-T-38TH-20T-95H-C5	1227.02	1867.9	17.24	2834.96	0.171	9.28	1525.75	0.009	17.55
C6	A-T-25TH-52T/48H-C6	1025.97	1061.8	17.14	1784.29	0.182	8.44	879.66	0.010	18.79
C7	A-T-13TH-52T/71H-C7	971.62	447.0	17.30	714.27	0.168	9.42	388.75	0.012	17.74
C8	A-T-25TH-52T/71H-C8	1075.74	1149.4	17.10	1805.13	0.159	9.27	980.50	0.011	16.45
C9	A-T-25TH-52T/71H-C9	1081.75	1149.3	16.95	1794.52	0.142	9.17	970.69	0.010	14.91
C10	A-T-38TH-52T/71H-C10	888.87	1590.0	15.75	2591.00	0.168	7.66	1259.71	0.011	17.08
C11	A-T-25TH-52T-95H-C11	1279.08	1117.0	16.89	1625.04	0.154	9.58	922.83	0.010	16.29
C12	A-T-13TH-85T/48H-C12	896.23	546.1	17.80	974.00	0.116	8.71	476.63	0.012	11.75
C13	A-T-38TH-85T/48H-C13	1261.39	1619.1	17.76	2773.96	0.118	8.65	1350.30	0.009	11.93
C14	A-T-25TH-85T/71H-C14	932.76	1013.9	16.13	1692.97	0.112	8.25	864.85	0.011	11.31
C15	A-T-13TH-85T-95H-C15	1029.21	418.6	15.68	656.46	0.152	8.08	337.39	0.010	15.79
C16	A-T-38TH-85T-95H-C16	1010.92	1663.5	16.00	2688.01	0.130	8.55	1436.56	0.010	13.19

3.4.1.1 Effect of Conditioning Temperature

An effort has been made to understand the effect of conditioning temperature on the ultimate tensile stress as shown in the graphical representation in Figure 3.6. In Figure 3.6a, the ultimate tensile stress for 13-mm width specimens decreases for both 48% and 95% conditioning humidity when the conditioning temperature increases from 20°C to 8°C. In Figure 3.6b, the ultimate tensile stress is also observed to be dropped off for 25-mm width specimens at 71.5% conditioning humidity when the conditioning temperature is increased from 20°C to 52.5°C and then to 85°C. For 38-mm width specimens, the ultimate tensile stress is increased at 48% conditioning humidity, whereas it decreases at 95% conditioning humidity (see Figure 3.6c).

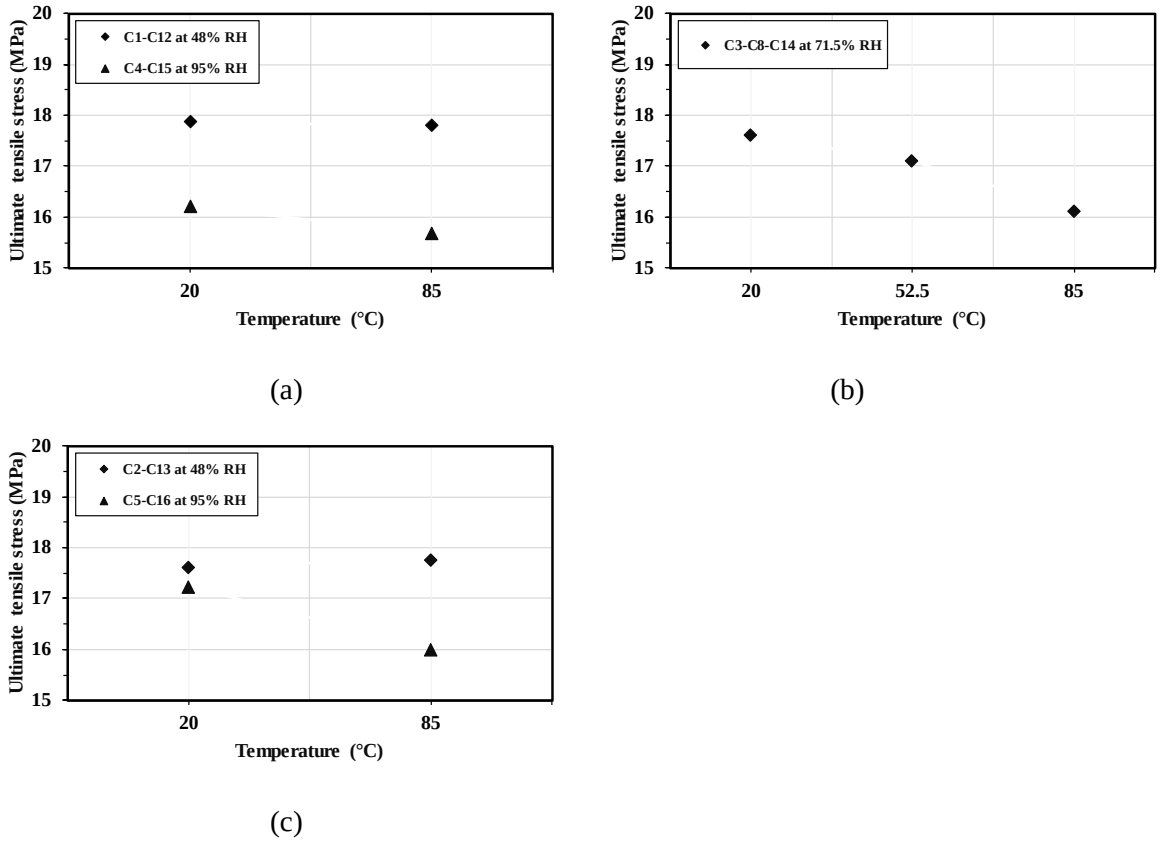

Figure 3.6 Effect of conditioning temperature on ultimate stress for tensile specimens with different widths (a) 13 mm (b) 25 mm and (c) 38 mm

The effect of conditioning temperature on the ultimate tensile stress in terms of the percent difference between combination pairs is further examined using a bar chart as seen in Figure 3.7. For specimens of 13-mm width, the stress is reduced by 0.4% at 48% conditioning humidity and 3.3% at 95% conditioning humidity, respectively, when the conditioning temperature is increased from 20°C to 85°C as shown in pairs C1-C12 and C4-C15 in this figure. At 71.5 % conditioning humidity, when the conditioning temperature is increased from 20°C to 52.5°C, the stress declines by 2.9% for 25-mm specimens. The stress decreases by 5.7 % after the conditioning temperature rises from 52.°C to 85°C as displayed in pairs C3-C8 and C8-C14 in this figure. The stress is increased by 0.8% at 48% conditioning humidity; however, it decreased by 7.2% at 95% conditioning humidity for specimens of 38-mm width after the elevation of conditioning temperature to 85°C from 20°C as depicted in pairs C2-C13 and C5-C16.

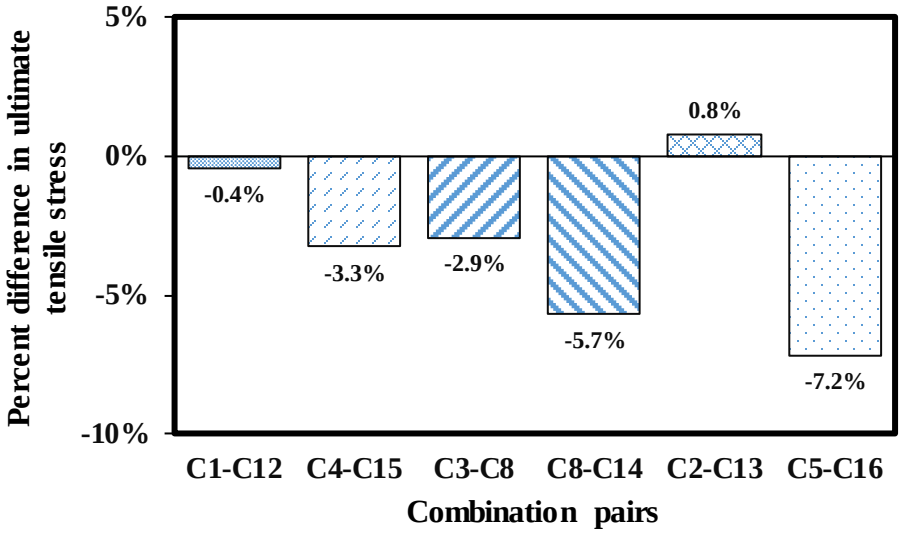

Figure 3.7 Percent difference in ultimate tensile stress due to the variation in conditioning temperature with a fixed conditioning humidity and width

In addition to the tensile stress examination, the other mechanical properties focusing on ductility were investigated. Ductility is a crucial property of the adhesive in the structural system of DMS under lateral forces such as wind. A graphical representation of the effect of conditioning temperature on ductility showing percent difference between combination pairs is presented in the bar chart (see Figure 3.8). For 13mm-wide specimens, ductility declines by 20.7% at 48% conditioning humidity and 13.9% at 95% conditioning humidity, respectively, when the conditioning temperature is increased from 20°C to 85°C as presented in pairs C1-C12 and C4-C15. When the conditioning temperature is increased from 20°C to 52.5°C, ductility increases by 10.7% for 25-mm specimens at 71.5% conditioning humidity. Ductility is reduced by 31.2% after the conditioning temperature is elevated to 85°C from 52.5°C as depicted in pairs C3-C8 and C8-C14 in this figure. Ductility is decreased by 8.3% at 48% conditioning humidity and 24.8% at 95% conditioning humidity for 38-mm specimens when the conditioning temperature is increased from 20°C to 85°C as presented in pairs C2-C13 and C5-C16.

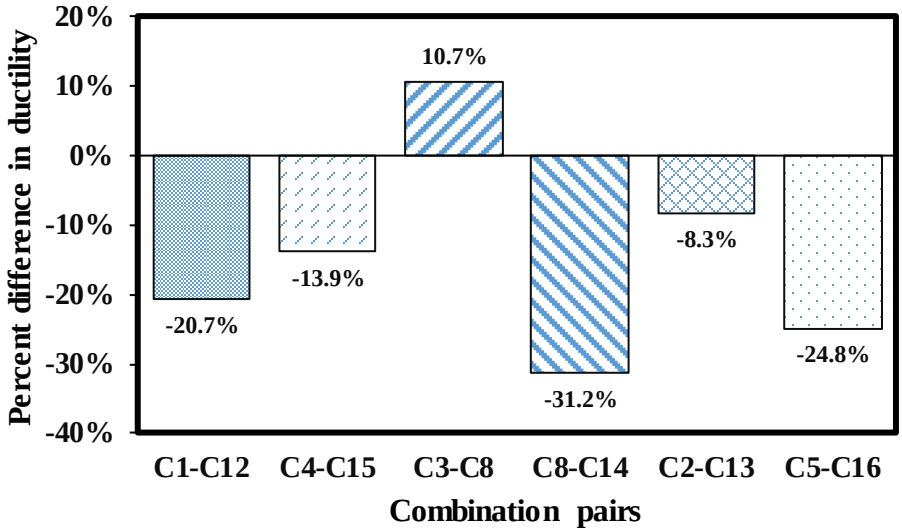

Figure 3.8 Percent difference in ductility for tensile specimens due to variation in conditioning temperature with a fixed conditioning humidity and width

3.4.1.2 Effect of Conditioning Humidity

Figure 3.9 shows the graphical representation of the effect of conditioning humidity on the ultimate tensile stress. The stress is observed to decline at both 20°C and 85°C with the increase in conditioning humidity from 48% to 95% for 13-mm width specimens (see Figure 3.9a). The stress of 25-mm specimens also decreased at 52.5°C when conditioning humidity was raised from 48% to 71.5% and from 71.5% to 95% (see Figure 3.9b). Specimens of 38-mm width are observed to increase the stress at 20°C; however, it decreased at 85 °C with the increase in conditioning humidity from 48% to 95% as displayed in Figure 3.9c.

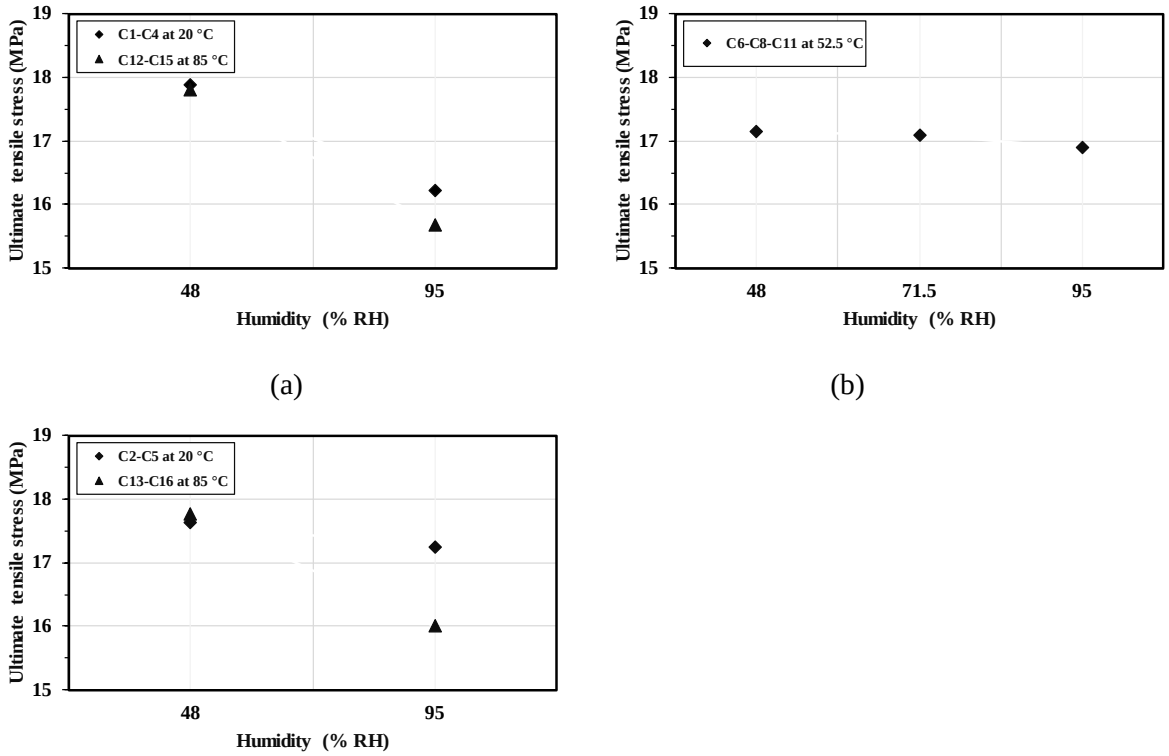

Figure 3.9 Effect of conditioning humidity on ultimate stress for tensile specimens with different widths (a) 13 mm (b) 25 mm and (c) 38 mm

Figure 3.10 shows a bar chart to further illustrate the effect of conditioning humidity in ultimate tensile stress in terms of percent difference among combination pairs. For specimens of 13-mm width, the stress is reduced by 9.3% at 20°C and 11.9% at 85°C, respectively, when the conditioning humidity is increased from 48% to 95 % as depicted in pairs C1-C4 and C12-C15 in this figure. At 52.5°C, when the conditioning humidity was increased from 48% to 95%, the stress decreases by 0.3% for 25-mm specimens. The stress is decreased by 1.2% after the conditioning humidity is elevated to 95% from 48% as shown in pairs C6-C8 and C8-C11. The stress is decreased by 2.2% at 20°C and 9.9% at 95% conditioning humidity for specimens of 38-mm width after the conditioning humidity is increased from 48% to 95%, which is shown in pairs C2-C5 and C13-C16.

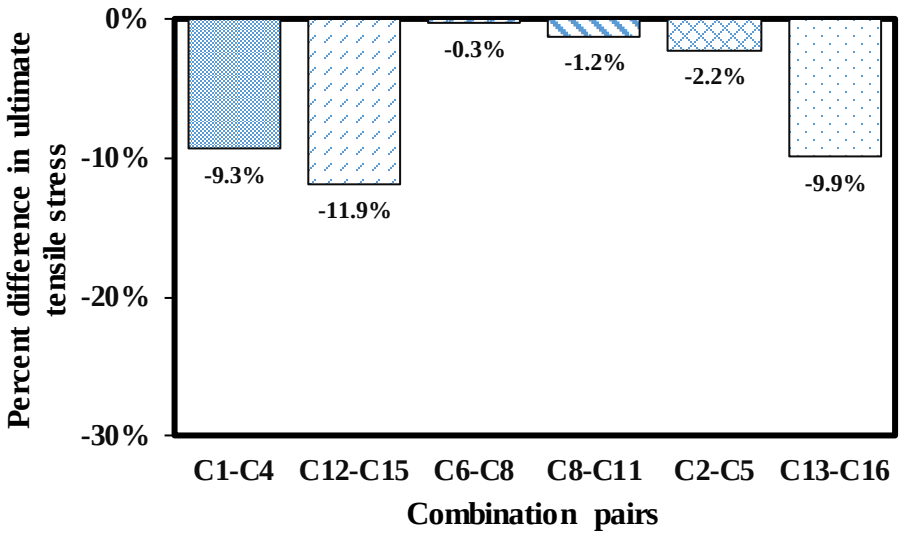

Figure 3.10 Percent difference in ultimate tensile stress due to the variation in conditioning humidity with a fixed conditioning temperature and width

Furthermore, the effect of conditioning humidity in ductility is shown in Figure 3.11. For a specimen of 13-mm width, ductility increased by 23.9% at 20°C and 34.5% at 85°C, respectively, when conditioning humidity is increased from 48% to 95% (see C1-C4 and C12-C15). At 52.5°C conditioning temperature, when conditioning humidity was increased from 48% to 71.5%, ductility declined by 12.5% for 25-mm specimens. Ductility was slightly decreased by 0.9 % after the elevation of conditioning humidity to 95% from 71.5% (see C6-C8 and C8-C11). Ductility, however, increased by 34.8% at 20°C with an increment of 10.6% at 85°C for a specimen of 38 mm after the elevation of conditioning humidity to 95% from 48% (see C2-C5 and C13-C16).

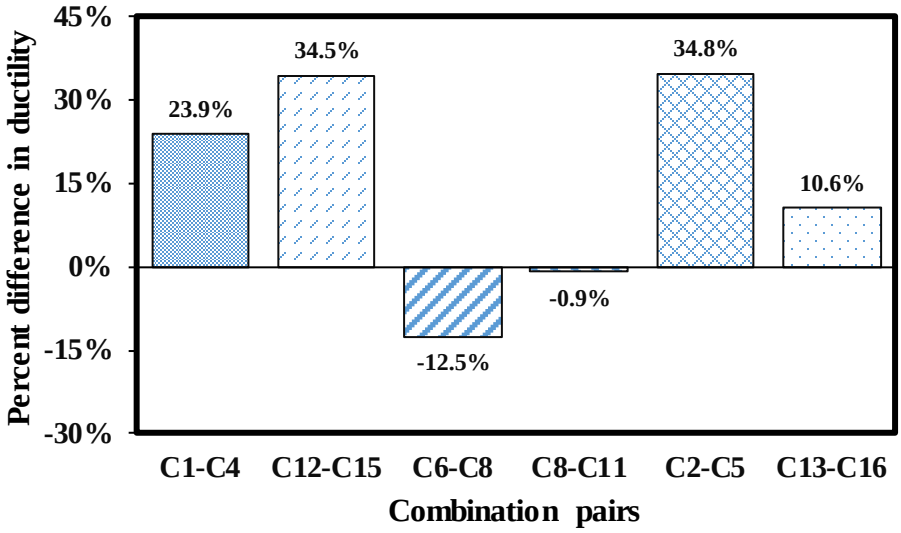

Figure 3.11 Percent difference in ductility for tensile specimens due to the variation in conditioning humidity with a fixed conditioning temperature and width

3.4.1.3 Effect of Width

The trend of the effect of width in ultimate tensile stress can be seen in Figure 3.12. As shown in Figure 3.12a, at 20°C, the stress decreased for specimens conditioned at 48% conditioning humidity and increased for specimens conditioned at 95% conditioning humidity with the increment of specimen width from 13 mm to 38 mm. The stress at 52.5°C is decreased when the width of the specimen is increased from 13 mm to 25 mm and 25 mm to 38 mm simultaneously for specimens conditioned at 71.5% conditioning humidity (see Figure 3.12b). For specimens conditioned at 85°C, the stress is decreased at 48% conditioning humidity and increased at 95% conditioning humidity when the specimen width is increased from 13 mm to 38 mm (see Figure 3.12c).

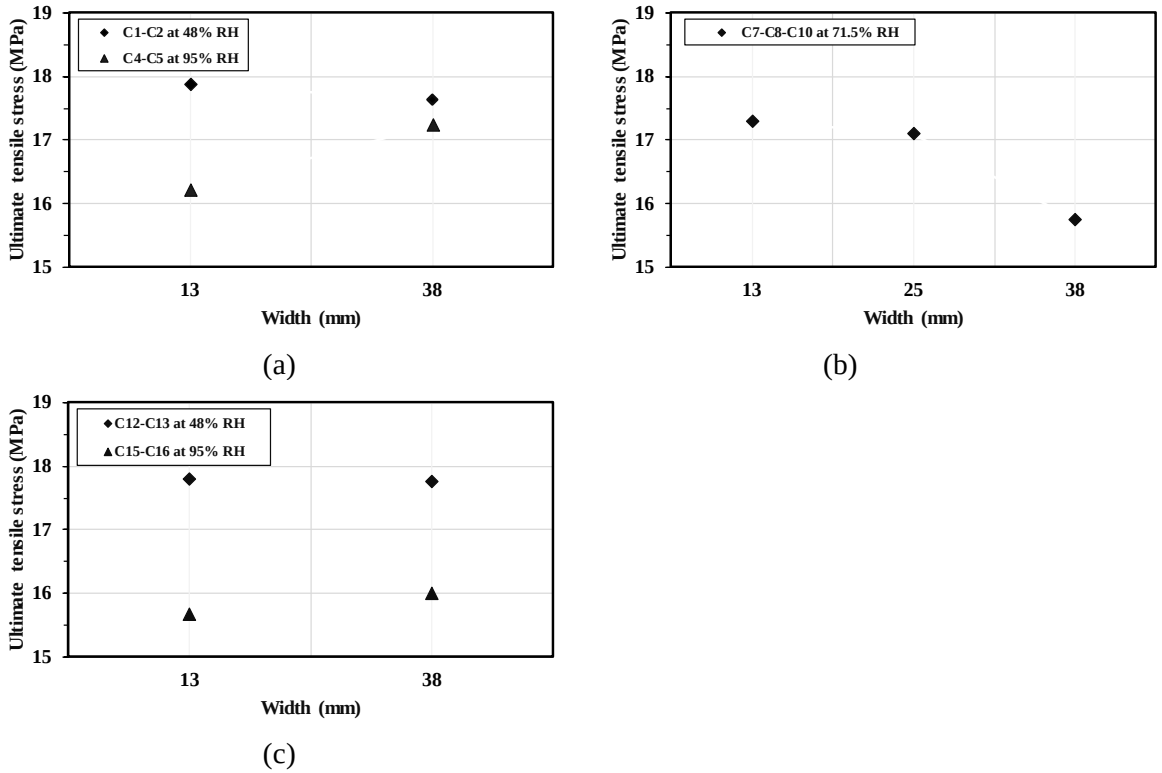

Figure 3.12 Width effect on ultimate stress for tensile specimens at different conditioning temperatures (a) 20°C (b) 52.5°C and (c) 85°C

Figure 3.13 shows the bar chart depicting the percent difference in ultimate tensile stress due to the effect of width at different conditioning. For specimens at 20°C, the ultimate tensile stress is reduced by 1.4% at 48% conditioning humidity and increased by 6.3% at 95% conditioning humidity, respectively, when the width of the specimen is increased from 13mm to 38mm (see C1-C2 and C4-C5). At 52.5°C, when the specimen width was increased from 13 mm to 25 mm, the stress declined by 1.2% at 71.5% conditioning humidity (see C7-C8). The stress was further decreased by 7.9% after the increment of width to 38 mm from 25 mm (see C8-C10). The stress is decreased by 0.2% at 48% conditioning humidity and increased by 2% at 95% conditioning humidity for specimens conditioned at 85°C with an increment of specimen width from 13mm to 38mm (see C12-C13 and C15-C16).

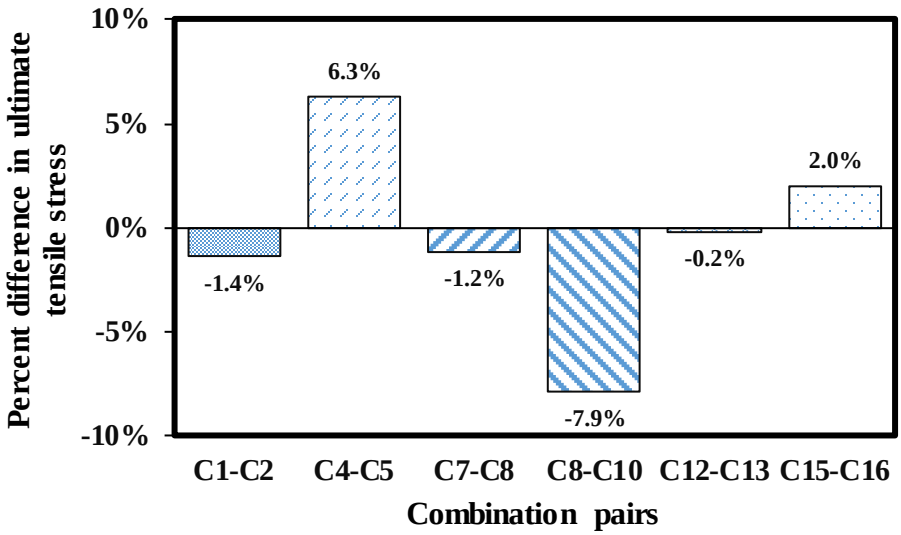

Figure 3.13 Percent difference in ultimate tensile stress due to the variation in width with a fixed conditioning temperature and conditioning humidity

Figure 3.14 shows a bar chart of the effect of width on ductility with percent difference for different combination pairs in tensile specimens. For specimens at 20°C, ductility declined by 12.1% at 48% conditioning humidity and 4.3% at 95% conditioning humidity respectively when specimen width is increased from 13mm to 38mm as portrayed in pairs C1-C2 and C4-C5. For specimens conditioned at 52.5°C, when the width is increased from 13mm to 25mm, ductility is reduced by 7.2% at 71.5% conditioning humidity. Ductility, however, increased by 3.8% with the further increment of specimens width from 25mm to 38 mm as presented in C7-C8 and C8-C10. The ductility is increased by 1.6% at 48% conditioning humidity, though decreased by 16.5% at 95% conditioning humidity for the specimens conditioned at 85°C with the increment of width from 13mm to 38mm as shown in pairs C2-C13 and C5-C16.

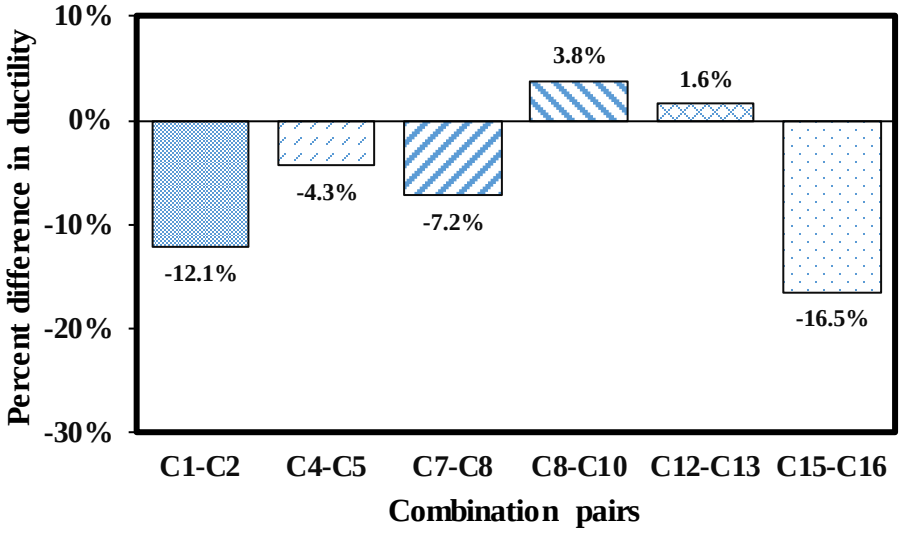

Figure 3.14 Percent difference in ductility due to the variation in width with a fixed conditioning temperature and conditioning humidity

3.4.1.4 Summary of Tensile Testing Results

The results of tensile tests were investigated for various ranges of conditioning temperature, conditioning humidity, and width. When the conditioning temperature was increased, the ultimate tensile stress reduced significantly for all the pairs at different conditioning humidity and width, except for pair C2-C13 when the conditioning temperature was increased from 20°C to 85°C for 38-mm specimens at 48% conditioning humidity. The increase in conditioning temperature reduced the ductility of tensile specimens for all the pairs, excluding pair C3-C8 where 25-mm specimens at 71.5% conditioning humidity were tested for a conditioning temperature change from 20°C to 52.5°C. The effect of increasing conditioning humidity showed that the stress decreased for all the pairs at various conditioning temperature and width. Ductility was increased for four pairs (C1-C4, C12-C15, C2-C5, and C13-C16) when conditioning humidity was increased from 48% to 95% and decreased for the other two pairs (C6-C8 and C8-C11) when conditioning humidity was increased from 48% to 71.5% and 71.5% to 95%, respectively. When the width of the specimens was increased, the stress reduced for four pairs (C1-C2, C7-C8, C8-C10, and C12-C13) at 48% and 71.5% conditioning humidity and decreased for two pairs (C4-C5 and C15-C16) at 95% conditioning humidity. Ductility was significantly decreased for four pairs (C1-C2, C4-C5, C7-C8, and C15-C16), whereas it decreased for two pairs (C8-C10 at 52.5°C and 71.5% conditioning humidity and C12-C13 at 85°C and 48% conditioning humidity).

3.4.2 Shear Test

Sample load-displacement and stress-strain curves for the shear specimens are shown in Figure 3.15 for C1. The ultimate shear load and stiffness of the specimens are determined from the load-displacement curve while the mechanical properties, including ultimate stress, yield stress, and Young’s modulus of elasticity and ductility, are determined from the stress-strain curve. The ultimate shear stress and other mechanical properties at different conditions are shown in Table 3.5. An average ultimate shear stress of 16.40 MPa with a standard deviation of 1.37 MPa was observed from the shear tests, which was consistent with the Lord technical data sheet (LORD Corporation 2020).

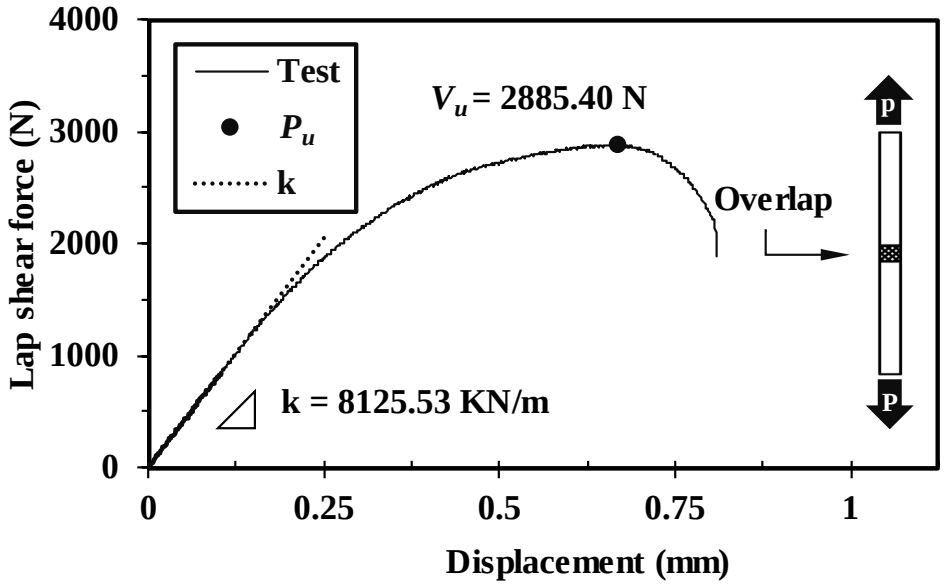

(a)

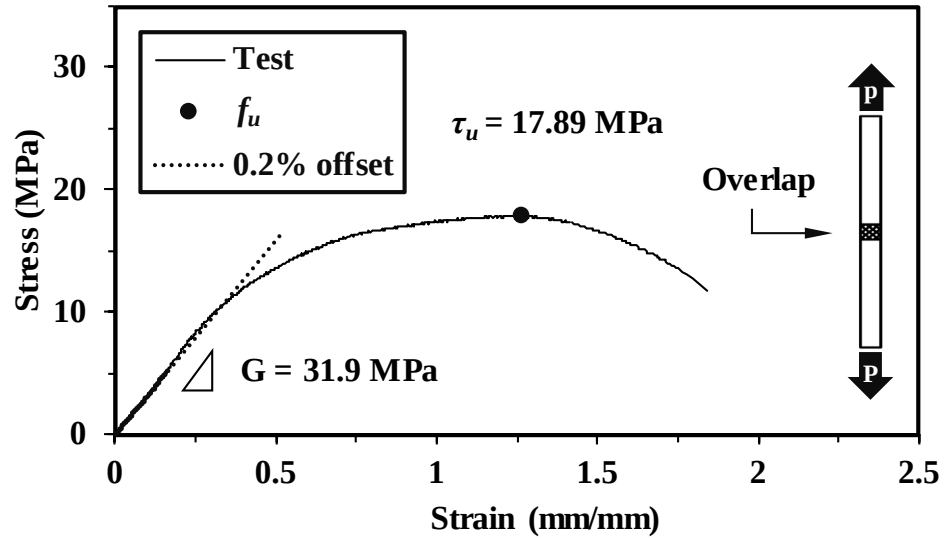

(b)

Figure 3.15 Curves for shear specimen (a) load displacement and (b) stress-strain

Table 3.5 Mechanical properties from the shear tests

Combination	Specimen ID	Shear modulus, G (MPa)	Stiffness, k (KN/m)	Ultimate shear stress, τ_u (MPa)	Ultimate shear load, V_u (N)	Strain at ultimate load, (mm/mm)	Yield stress, τ_y (MPa)	Load at yield point, V_y (N)	Strain at yield point, (mm/mm)	Ductility, e (%)
C1	A-S-13TH-20T/48H-C1	26.11	7993.8	17.48	2819.77	1.623	11.12	1793.01	0.462	4.17
C2	A-S-38TH-20T/48H-C2	43.45	19406.9	16.06	7770.98	1.265	6.91	3343.26	0.160	4.45
C3	A-S-25TH-20T/71H-C3	35.72	14084.6	17.97	5796.92	1.148	11.09	3576.10	0.322	4.66
C4	A-S-13TH-20T-95H-C4	34.89	7952.2	15.85	2556.14	1.081	10.07	1623.92	0.294	3.40
C5	A-S-38TH-20T-95H-C5	27.32	19059.0	16.39	7930.42	1.318	10.99	5319.12	0.424	3.49
C6	A-S-25TH-52T/48H-C6	27.76	14520.2	17.75	5726.20	1.270	11.03	3558.60	0.407	4.00
C7	A-S-13TH-52T/71H-C7	32.23	7944.1	16.00	2580.46	1.149	7.96	1284.40	0.255	3.64
C8	A-S-25TH-52T/71H-C8	37.23	14780.4	14.96	4824.39	1.035	8.84	2852.29	0.252	3.66
C9	A-S-25TH-52T/71H-C9	27.28	14560.6	14.89	4804.15	1.342	9.27	2989.18	0.354	3.20
C10	A-S-38TH-52T/71H-C10	33.48	21015.0	17.84	8634.64	1.382	9.54	4615.67	0.300	3.42
C11	A-S-25TH-52T-95H-C11	26.45	12435.0	16.00	5161.99	1.370	9.79	3159.17	0.378	3.70
C12	A-S-13TH-85T/48H-C12	29.58	8331.4	17.05	2749.49	1.326	9.70	1564.62	0.340	3.53
C13	A-S-38TH-85T/48H-C13	32.73	21270.4	17.66	8547.41	1.514	8.54	4133.67	0.273	3.20
C14	A-S-25TH-85T/71H-C14	29.11	12496.2	15.47	4989.15	1.208	9.76	3149.59	0.348	3.76
C15	A-S-13TH-85T-95H-C15	34.59	6279.8	15.63	2521.27	1.115	8.89	1433.57	0.271	3.50
C16	A-S-38TH-85T-95H-C16	28.85	17481.8	15.41	7458.04	1.193	10.78	5216.78	0.399	3.47

3.4.2.1 Effect of Conditioning Temperature

Figure 3.16 shows the graphical illustration of the effect of conditioning temperature on the ultimate shear stress. In Figure 3.16a, the shear stress is decreased for specimens having 13-mm width at both 48% and 95% conditioning humidity when conditioning temperature increased from 20°C to 85°C. For 25-mm specimens at 71.5% conditioning humidity, the shear stress is observed to be reduced when the conditioning temperature is increased from 20°C to 52.5°C; however, the shear stress increased with an increment of conditioning temperature from 52.5°C to 85°C as displayed in Figure 3.16b. The shear stress increased for specimens having 38-mm width at 48% conditioning humidity but decreased at 95% conditioning humidity when the conditioning temperature increased from 20°C to 85°C (see Figure 3.16c).

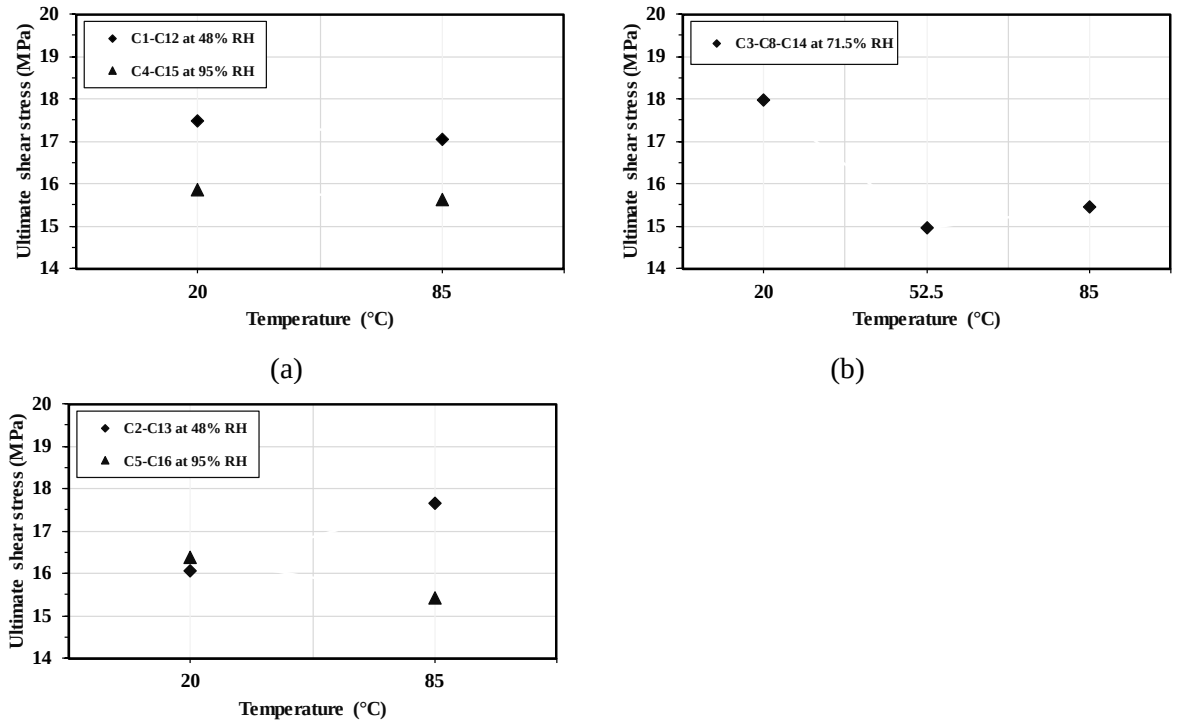

Figure 3.16 Effect of conditioning temperature on ultimate stress for shear specimens with different widths (a) 13 mm (b) 25 mm and (c) 38 mm

A figure showing the change in ultimate shear stress in terms of percent difference due to effect of conditioning temperature is further shown in Figure 3.17. For specimens of 13-mm width, the shear stress is reduced by 2.5% at 48% conditioning humidity and 1.4% at 95% conditioning humidity, respectively, when the conditioning temperature is increased from 20°C to 85°C as presented in pairs C1-C12 and C4-C15. At 71.5 % conditioning humidity, when the conditioning temperature is increased from 20°C to 52.5°C, the shear stress is significantly declined by 16.8% for 25-mm specimens. The shear stress, on the contrary, is increased by 3.4 % after the elevation of conditioning temperature to 85°C from 52.5°C as displayed in pairs C3-C8 and C8-C14. The shear stress is increased by 10% at 48% conditioning humidity; however, it decreased by 6% at 95% conditioning humidity for specimens of 38 mm after the elevation of conditioning temperature to 85°C from 20°C as shown in pairs C2-C13 and C5-C16.

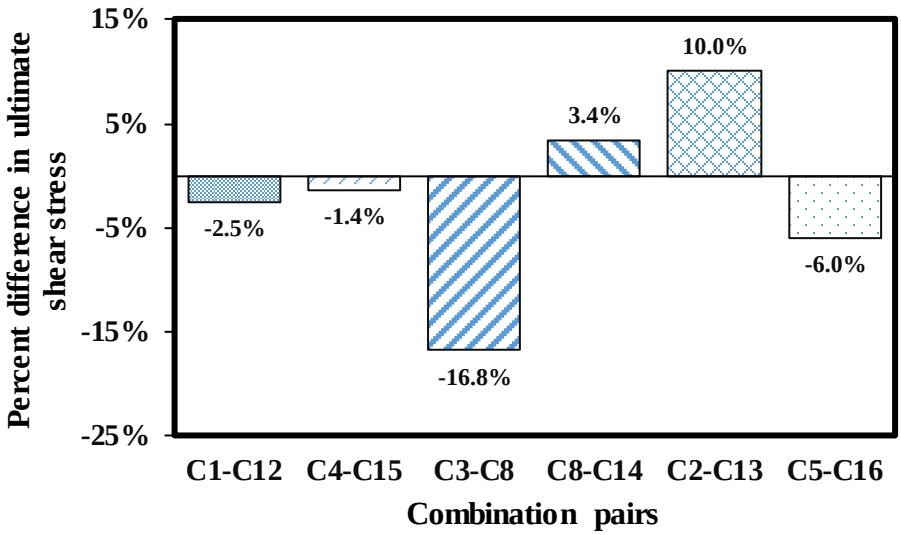

Figure 3.17 Percent difference in ultimate shear stress due to the variation in conditioning temperature with a fixed conditioning humidity and width

As discussed previously, the effect of conditioning temperature on ductility of tested shear specimens was examined through a relevant bar chart (see Figure 3.18). For specimens of 13-mm width, the ductility declined by 15.2% at 48% conditioning humidity, yet increased by 2.8% at 95% conditioning humidity, respectively, when the conditioning temperature increased from 20°C to 85°C as shown in pairs C1-C12 and C4-C15. At 71.5% conditioning humidity, when the conditioning temperature is increased from 20°C to 52.5°C, ductility is lowered by 21.6% for 25-mm specimens. The ductility is increased by 2.7% after an additional increase of conditioning temperature to 85°C from 52.5°C as shown in pairs C3-C8 and C8-C14. The ductility is reduced by 28.1% at 48% conditioning humidity and 0.6% at 95% conditioning humidity for specimens of 38-mm width after the elevation of conditioning temperature to 85°C from 20°C as presented in pairs C2-C13 and C5-C16.

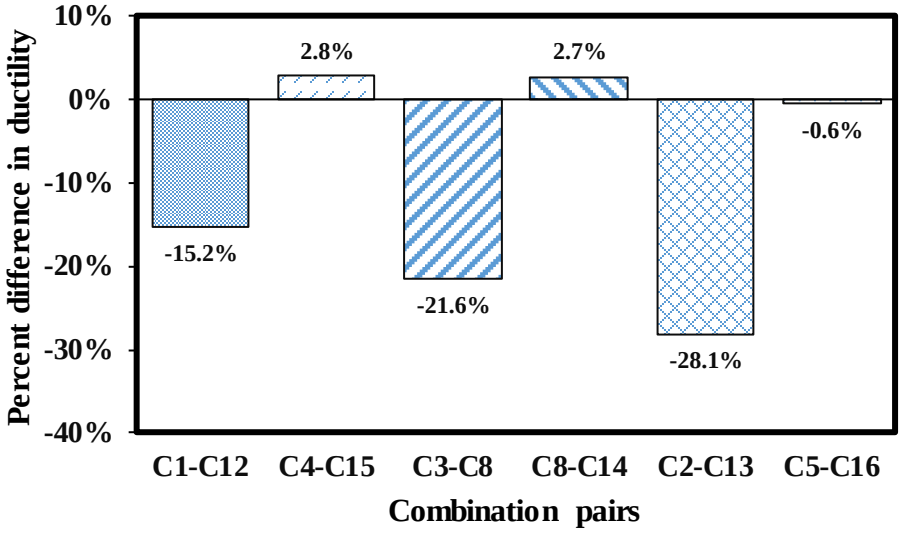

Figure 3.18 Percent difference in ductility for shear specimens due to the variation in conditioning temperature with a fixed conditioning humidity and width

3.4.2.2 Effect of Conditioning Humidity

Figure 3.19 shows the graphs representing the effect of conditioning humidity in the ultimate shear stress. The shear stress is reduced in shear specimens having 13-mm width at both 20°C and 85°C when conditioning humidity is increased from 48% to 95% (see Figure 3.19a). The shear stress declines at 52.5°C for 25-mm specimens when the conditioning humidity is increased from 48% to 71.5%; however, the ultimate shear stress is increased with the further increment of conditioning humidity from 71.5% to 95% (see Figure 3.19b). For 38-mm width specimens, the shear stress is dropped for specimens conditioned at both 20°C and 85°C when the conditioning humidity is increased from 48% to 95% as shown in Figure 3.19c.

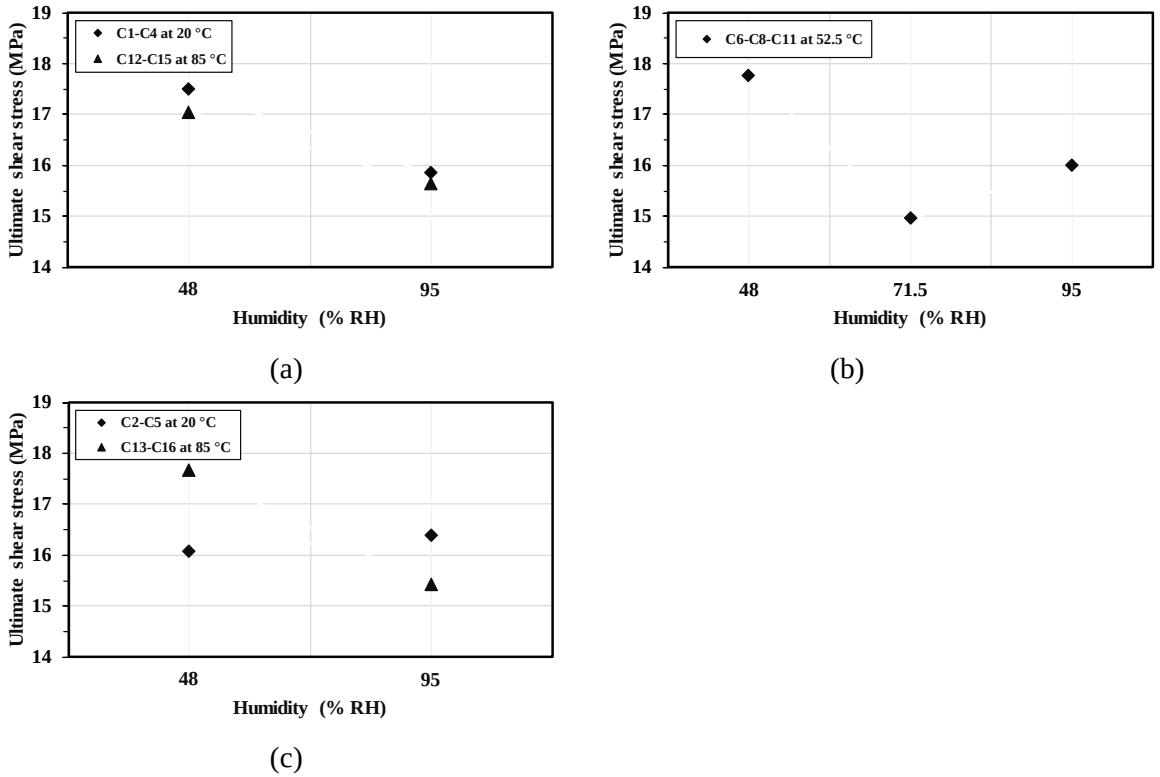

Figure 3.19 Effect of conditioning humidity on ultimate stress for shear specimens with different widths (a) 13 mm (b) 25 mm and (c) 38 mm

The effect of conditioning humidity in ultimate shear stress is further depicted in Figure 3.20 for different conditioning. For specimens of 13-mm width, the shear stress is reduced by 9.3% at 20°C and 8.3% at 85°C, respectively, when conditioning humidity is increased from 48% to 95% (see comparison C1-C4 and C12-C15). At 52.5°C, when conditioning humidity is increased from 48% to 95%, ultimate shear stress is declined by 15.7% for 25-mm specimens. The shear stress, however, increases by 7% after the elevation of conditioning humidity to 95% from 48% (see comparison C6-C8 and C8-C11). The shear stress is increased by 2.1% at 20°C but decreased by 12.7% at 95% conditioning humidity for specimens of 38 mm after the elevation of conditioning humidity from 48% to 95% (see comparison C2-C5 and C13-C16).

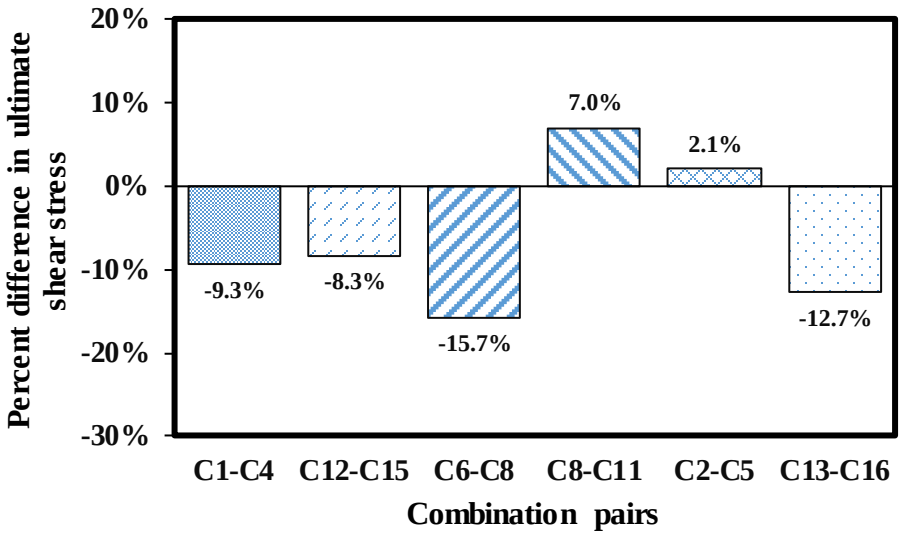

Figure 3.20 Percent difference in ultimate shear stress due to the variation in conditioning humidity with a fixed conditioning temperature and width

In addition to the shear stress comparison, the effect of conditioning humidity on ductility in terms of percent difference is shown in the bar chart (see Figure 3.21). For specimens of 13-mm width, ductility is declined by 18.3% at 20°C and 0.9% at 85°C, respectively, when the conditioning humidity is increased from 48% to 95% as illustrated in pairs C1-C4 and C12-C15. At 52.5°C, when the conditioning humidity is increased from 48% to 71.5%, the ductility reduces by 8.6% for 25-mm specimens (see pair C6-C8). The ductility, however, increases by 1.3 % after the elevation of conditioning humidity from 71.5% to 95% as shown in pair C8-C11 in this figure. The ductility decreases by 21.5% at 20°C and increases by 8.6% at 85°C for specimens of 38-mm width when conditioning humidity is increased from 48% to 95% as presented in pairs C2-C5 and C13-C16 in this figure.

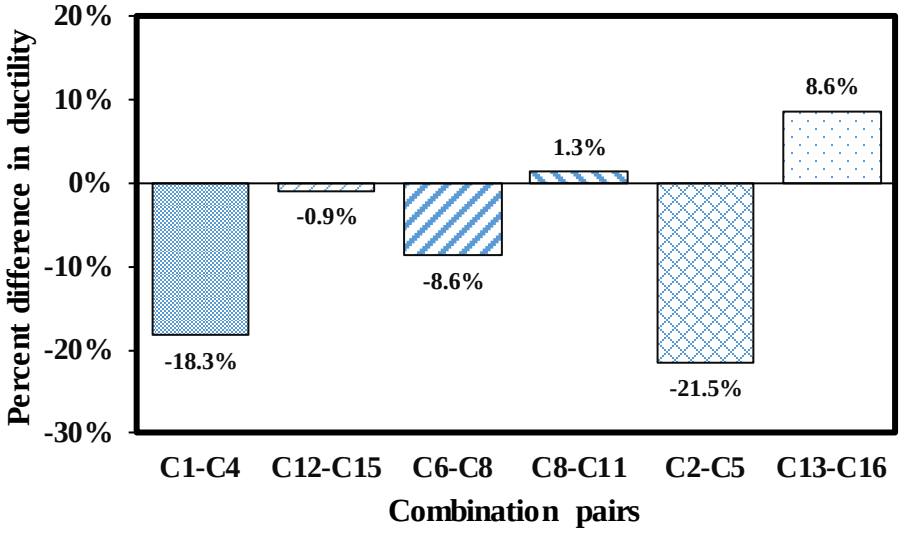

Figure 3.21 Percent difference in ductility for shear specimens due to the variation in conditioning humidity with a fixed conditioning temperature and width

3.4.2.3 Effect of Width

The effect of width on the ultimate shear stress is graphically explored in Figure 3.22. For specimens at 20°C, the ultimate shear stress decreases at 48% conditioning humidity but increases at 95% conditioning humidity when the specimen width increases from 13 mm to 38 mm (see Figure 3.22a). At 52.5°C and 71.5% conditioning humidity, the ultimate shear stress is reduced when the specimen width is increased from 13 mm to 25 mm; however, the ultimate shear stress increases with the increment of width from 25 mm to 38 mm as depicted in Figure 3.22b. At 85°C, the ultimate shear stress increases for the specimens conditioned at 48% conditioning humidity, yet decreases for specimens conditioned at 95% conditioning humidity when the specimen width is increased from 13 mm to 38 mm (see Figure 3.22c).

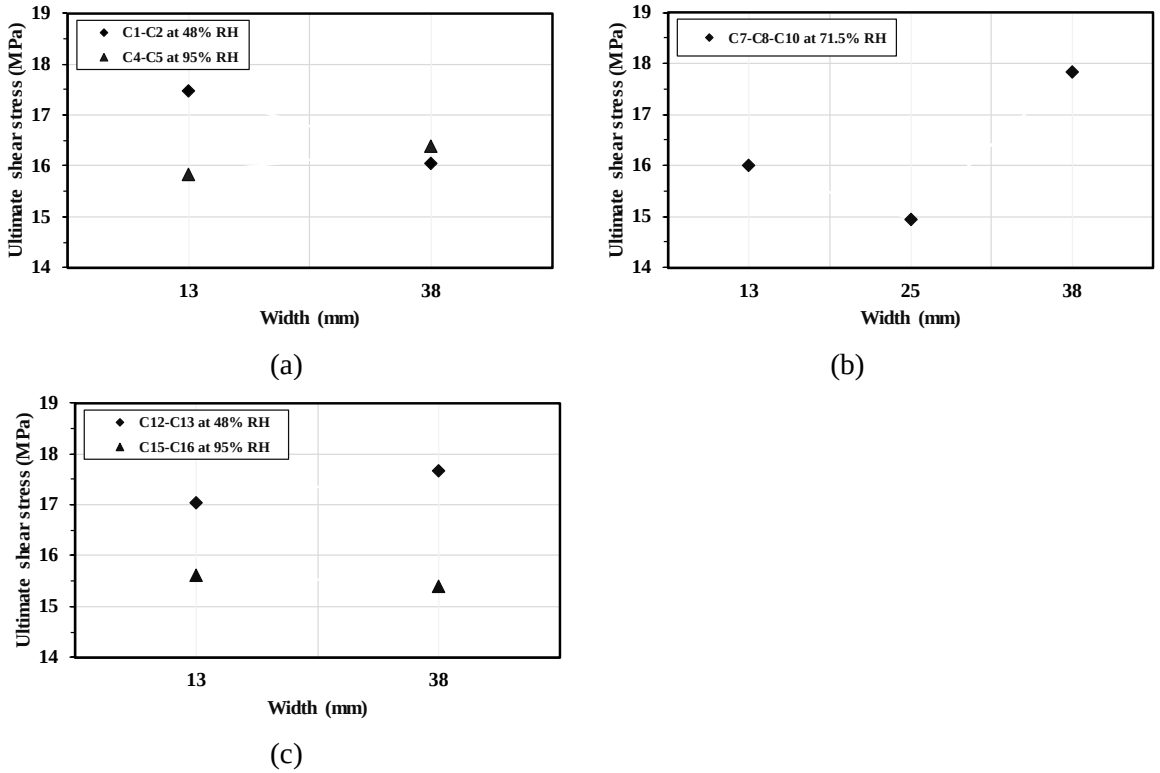

Figure 3.22 Width effect on ultimate stress for shear specimens at different conditioning temperatures (a) 20°C (b) 52.5°C and (c) 85°C

The effect of width on the ultimate shear stress in percentage is further illustrated in a bar chart as shown in Figure 3.23. For specimens at 20°C, the shear stress is reduced by 8.1% at 48% conditioning humidity and increased by 3.4% at 95% conditioning humidity, respectively, when the width of the specimens is increased from 13mm to 38mm as shown in pairs C1-C2 and C4-C5. At 52.5°C, when the specimen width is increased from 13 mm to 25 mm, the shear stress declines by 6.5% at 71.5% conditioning humidity. The shear stress, however, increases by 19.3% after the increment of width to 38 mm from 25 mm as presented in pairs C7-C8 and C8-C10. The shear stress increases by 3.6% at 48% conditioning humidity and decreases by 1.4% at 95% conditioning humidity for specimens at 85°C when the specimen width is increased from 13mm to 38mm as displayed in pairs C12-C13 and C15-C16.

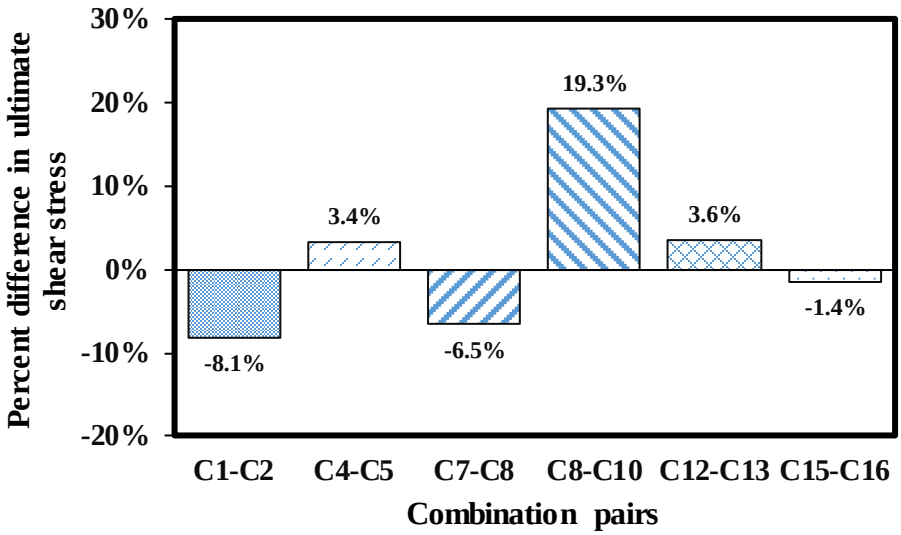

Figure 3.23 Percent difference in ultimate shear stress due to the variation in width with a fixed conditioning temperature and conditioning humidity

Figure 3.24 shows a bar chart for the effect of width on ductility in the shear specimens. For specimens at 20°C, the ductility is increased by 6.7% at 48% conditioning humidity and 2.5% at 95% conditioning humidity while at an increase in width from 13mm to 38mm as displayed in pairs C1-C2 and C4-C5 in this figure. For specimens conditioned at 52.5°C, when the width changes from 13mm to 25mm, ductility increases by 0.4% at 71.5% conditioning humidity (see pair C7-C8). Ductility, however, dropped off by 6.4% with a further increment of specimen width from 25mm to 38mm as depicted in pair C8-C10. As shown in pairs C12-C13 and C15-C16, the ductility decreases by 9.5% at 48% conditioning humidity and 0.8% at 95% conditioning humidity for the specimens conditioned at 85°C with the increase of specimen width from 13mm to 38mm.

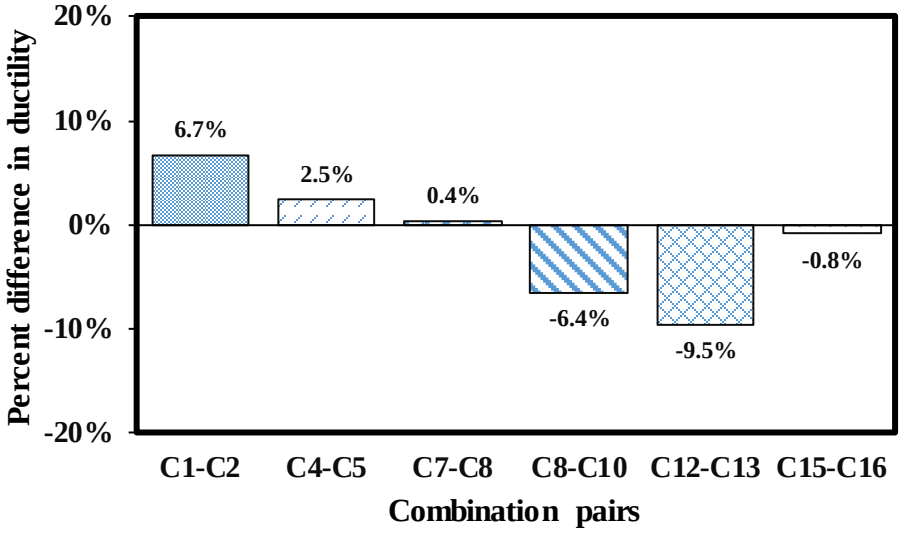

Figure 3.24 Percent difference in ductility for shear specimens due to the variation in width with a fixed conditioning temperature and conditioning humidity

3.4.2.4 Summary of Shear Testing Results

The ultimate shear stress and ductility of shear specimens were examined within a certain range of conditioning temperature, conditioning humidity, and width. When the conditioning temperature was increased, the ultimate shear stress decreased for four pairs (C1-C12, C4-C15, C3-C8, and C5-C16) out of six pairs. This includes the change in conditioning temperature from 20°C to 85°C for pairs C1-C12, C4-C15, and C5-C16 and 20°C to 52.5°C for pair C3-C8. The ductility is also reduced for four pairs (C1-C12, C3-C8, C2-C13, and C5-C16) and increased for the other two combinations (C4-C15 for change in conditioning temperature from 20°C to 85°C and C8-C14 for conditioning temperature change from 52.5°C to 85°C). With the increase in conditioning humidity, the shear stress also reduced for the four pairs (C1-C4, C12-C15, C6-C8, and C13-C16) and increased for the pairs C8-C11 (25-mm specimens at 52.5°C) and C2-C5 (38-mm specimens at 20°C). The ductility was decreased for four pairs (C1-C4, C12-C15, C6-C8, and C2-C5) and increased for the other two pairs (C8-C11 for 25-mm specimens at 52.5°C and C13-C16 for 38-mm specimens at 20°C). When the specimen width was increased, the shear stress decreased for three pairs (C1-C2, C7-C8, and C15-C16) and increased for the other three pairs (C4-C5, C8-C10, and C12-C13). The ductility also increased for the three pairs (C1-C2, C4-C5, and C7-C8) and decreased for the other three pairs (C8-C10, C12-C13, and C15-C16).

3.4.3 Peel Test

A representative load-displacement curve illustrating both the first and the second specimen of combination 1 (A-P-13TH-20T/48H-C1) among the tested peel specimens is presented in Figure 3.25. The peel strength (f_{ap}) of the first and second specimens is calculated by evaluating the average load per unit width for the first 127 mm of peeling from the load-displacement curve. This process was repeated to determine the first and second specimens under each combination, and the averages of both the specimens' peel strengths per combination were calculated. The resulting peel strengths for all the combinations are summarized in Table 3.6. From the peel testing data, the average peel strength was found to be 6.63 N/mm with a standard deviation of 2.49 N/mm. The peel testing data were observed to be in harmony with the Lord technical data sheet (LORD Corporation 2020).

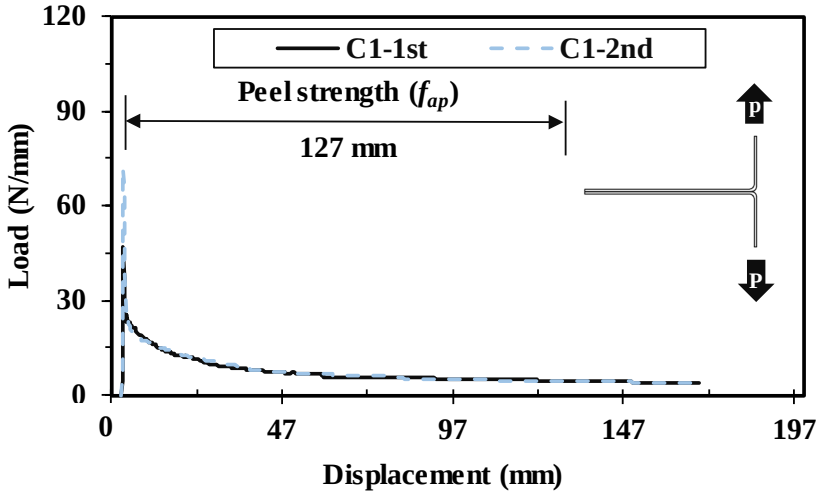

Figure 3.25 Load-displacement curve for peel test of combination 1

Table 3.6 Peel strength from all the combinations

Combination	Specimen	Peel strength, f_{ap}(N/mm)
C1	A-P-13TH-20T/48H-C1	8.10
C2	A-P-38TH-20T/48H-C2	5.82
C3	A-P-25TH-20T/71H-C3	4.41
C4	A-P-13TH-20T/95H-C4	8.28
C5	A-P-38TH-20T/95H-C5	6.55
C6	A-P-25TH-52T/48H-C6	5.77
C7	A-P-13TH-52T/71H-C7	7.73
C8	A-P-25TH-52T/71H-C8	7.51
C9	A-P-25TH-52T/71H-C9	6.54
C10	A-P-38TH-52T/71H-C10	6.10
C11	A-P-25TH-52T/95H-C11	5.03
C12	A-P-13TH-85T/48H-C12	6.79
C13	A-P-38TH-85T/48H-C13	5.84
C14	A-P-25TH-85T/71H-C14	7.63
C15	A-P-13TH-85T/95H-C15	7.75
C16	A-P-38TH-85T/95H-C16	6.16

3.4.3.1 Effect of Conditioning Temperature

To investigate the influence of conditioning temperature on the adhesive's peel strength, specimens conditioned at different conditioning temperatures were compared. Figure 3.26 shows the graphical representation of the conditioning temperature's effect on peel strength. When the conditioning temperature is increased from 20°C to 85°C, the peel strength of 13 mm width specimens is reduced at both 48% and 95% conditioning humidity as depicted in Figure 3.26a. At 71.5% conditioning humidity, when the conditioning temperature of 25-mm width specimens increases from 20°C to 52.5°C, the peel strength also increases. When the conditioning temperature is increased from 52.5°C to 85°C, the peel strength is further slightly increased (see Figure 3.26b). When the conditioning temperature of 38-mm width specimens is increased to 85°C from 20°C, the peel strength slightly increases at 48% conditioning humidity; however, it decreases at 95% conditioning humidity (see Figure 3.26c).

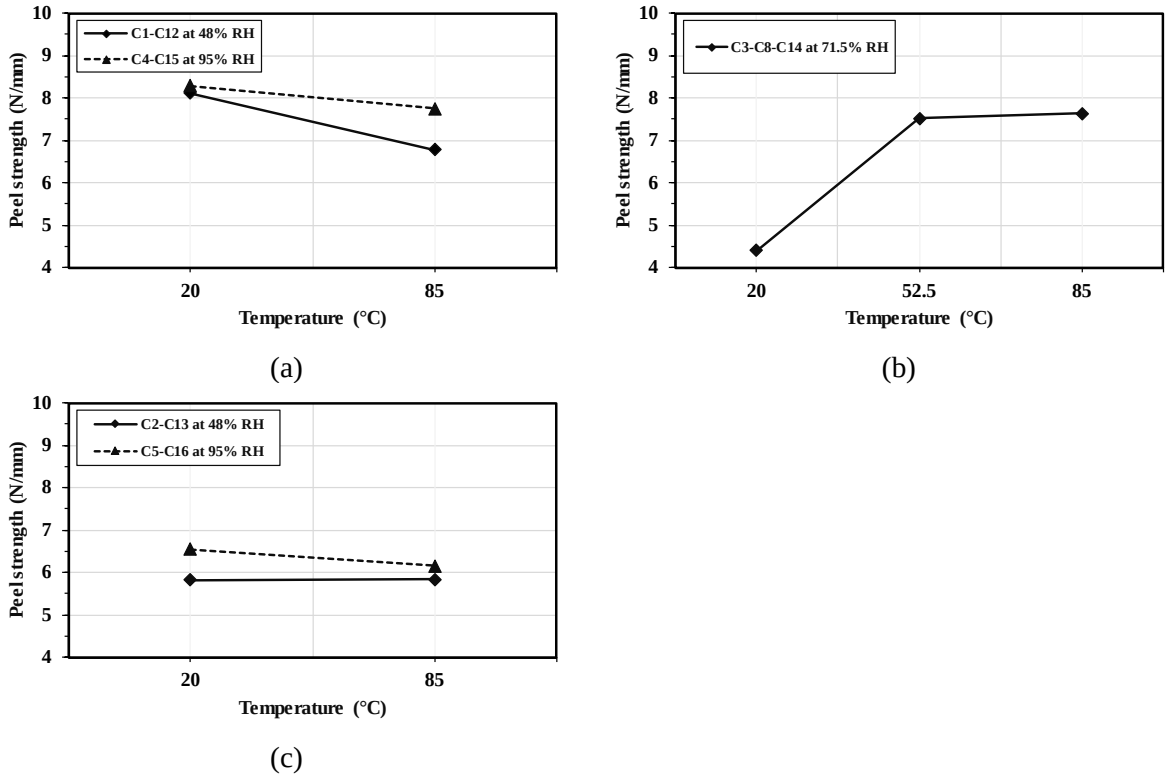

Figure 3.26 Effect of conditioning temperature on the peel strength for the specimens with different widths: (a) 13 mm, (b) 25 mm, and (c) 38 mm

Figure 3.27 shows the effect of conditioning temperature on the peel strength in the bar graph with the percent difference. For specimens of 13-mm width, the peel strength is reduced by 16.3% at 48% conditioning humidity and by 6.4% at 95% conditioning humidity when the conditioning temperature is increased from 20°C to 85°C as illustrated in pairs C1-C12 and C4-C15 in this figure. At 71.5% conditioning humidity, when the conditioning temperature elevates from 20°C to 52.5°C, the peel strength is increased by 70.4% for 25-mm width specimens as depicted in the C3-C8 pair. The peel strength further increases by 1.6% after the elevation of conditioning temperature to 85°C from 52.5°C as shown in the C8-C14 pair. As presented in a pair of C2-C13, the peel strength is increased by 0.4% at 48% conditioning humidity after the elevation of conditioning temperature to 85°C from 20°C; however, it is decreased by 5.9% at 95% conditioning humidity for specimens with 38-mm width from 20°C to 85°C (see C5-C16 in Figure 3.27).

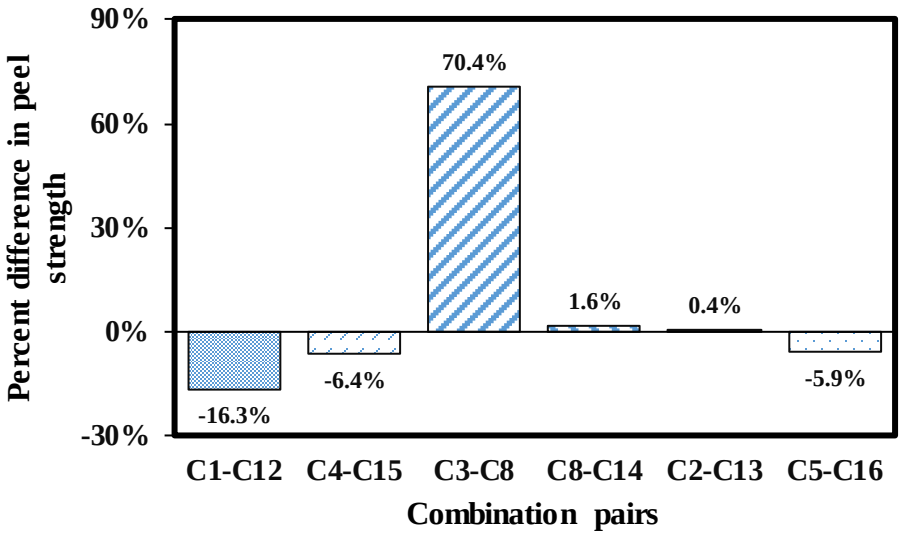

Figure 3.27 Percent difference in peel strength due to the variation in conditioning temperature with a fixed conditioning humidity and width

3.4.3.2 Effect of Conditioning Humidity

The effect of conditioning humidity on peel strength is illustrated in Figure 3.28. When conditioning humidity rises from 48% to 95%, the peel strength of 13-mm width specimens increased at both 20°C and 85°C (see Figure 3.28a). The peel strength of 25-mm width specimens is increased at 52.5°C when conditioning humidity is increased from 48% to 71.5%; however, the strength is decreased after the elevation of conditioning humidity to 95% from 71.5% (see Figure 3.28b). When the conditioning humidity of 38-mm width specimens is increased from 48% to 95%, the peel strength is observed to be improved at both 20°C and 85°C as shown in Figure 3.28c.

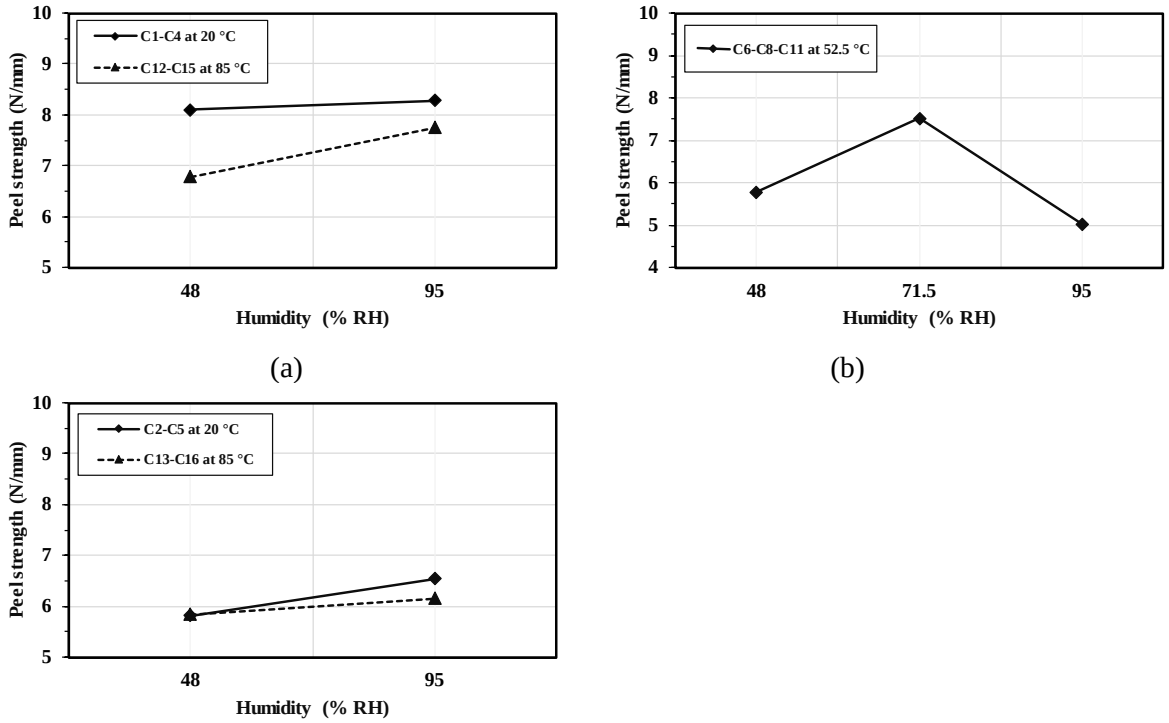

Figure 3.28 Effect of conditioning humidity on peel strength for specimens with different widths (a) 13 mm, (b) 25 mm, and (c) 38 mm

The effect of conditioning humidity on the peel strength in terms of percent difference among different combination pairs is also examined in Figure 3.29. In this figure, for specimens with 13-mm width, the peel strength is raised by 2.2% at 20°C (see a pair of C1-C4) and 14.3% at 85°C (see a pair of C12-C15), respectively, when the conditioning humidity is increased from 48% to 95%. At 52.5°C, when conditioning humidity is elevated from 48% to 71.5%, the peel strength is improved by 30.1% for 25-mm width specimens as shown in the C6-C8 pair. The peel strength is, however, decreased by 33% after the elevation of conditioning humidity to 95% from 71.5% as shown in C8-C11. The peel strength is increased by 12.5% at 20°C as shown in pair C2-C5 and by 5.5% at 85°C as displayed in pair C13-C16 for specimens of 38-mm width after the elevation of conditioning humidity from 48% to 95%.

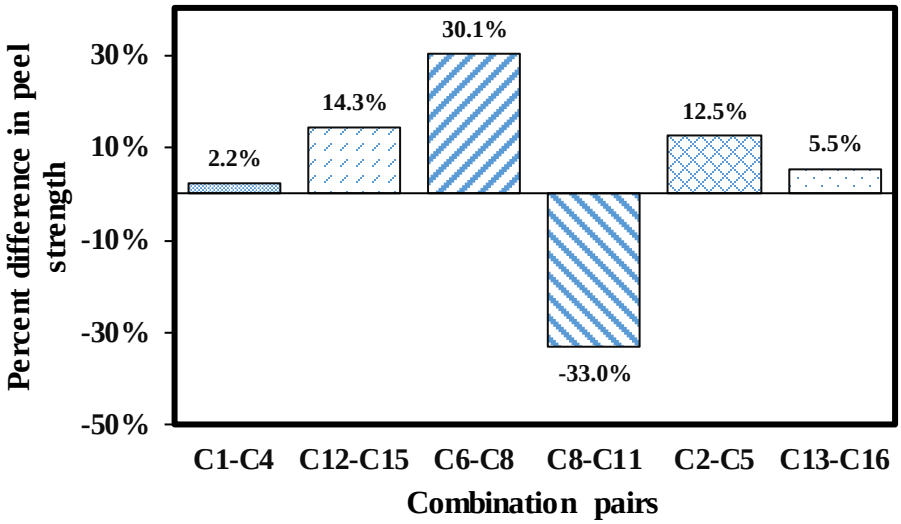

Figure 3.29 Percent difference in peel strength due to the variation in conditioning humidity with a fixed conditioning temperature and width

3.4.3.3 Effect of Width

The effect of width in peel strength can be seen in Figure 3.30. When specimen width increases from 13 mm to 38 mm at 20°C, peel strength reduces at both 48% and 95% conditioning humidity (see Figure 3.30a). The peel strength at 52.5°C is decreased when specimen width is increased from 13 mm to 25 mm, and 25 mm to 38 mm simultaneously for specimens conditioned at 71.5% conditioning humidity (see Figure 3.30b). When the width of the specimens is increased from 13mm to 38mm at 85°C, the peel strength is reduced at both 48% and 95% conditioning humidity as shown in Figure 3.30c.

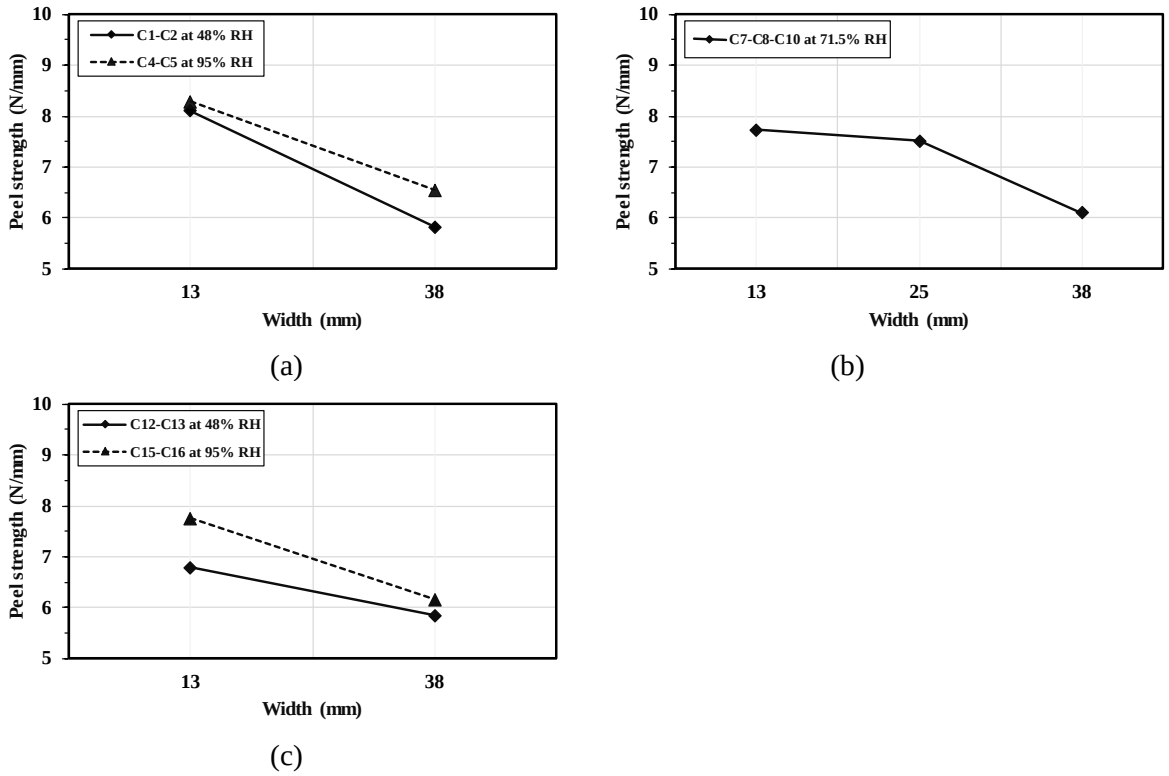

Figure 3.30 Width effect on peel strength for specimens at different conditioning temperatures (a) 20°C (b), 52.5°C, and (c) 85°C

Figure 3.31 portrays the percent difference of peel strength in a bar graph due to the effect of width. For specimens at 20°C, the peel strength is reduced by 28.2% at 48% conditioning humidity (see a pair of C1-C2) and by 20.9% at 95% conditioning humidity (see a pair of C4-C5), when the width of the specimen is increased from 13mm to 38mm. At 52.5°C, when specimen width is increased from 13 mm to 25 mm, peel strength declines by 2.8% at 71.5% conditioning humidity as seen in C7-C8. At the same conditioning humidity as in C7-C8, the peel strength further decreases by 18.8% after the increment of width to 38 mm from 25 mm (refer to C8-C10). The peel strength is dropped by 13.9% at 48% conditioning humidity (see C12-C13) and 20.5% at 95% conditioning humidity (see C15-C16) for the four specimens conditioned at 85°C with the increment of specimen width from 13mm to 38mm.

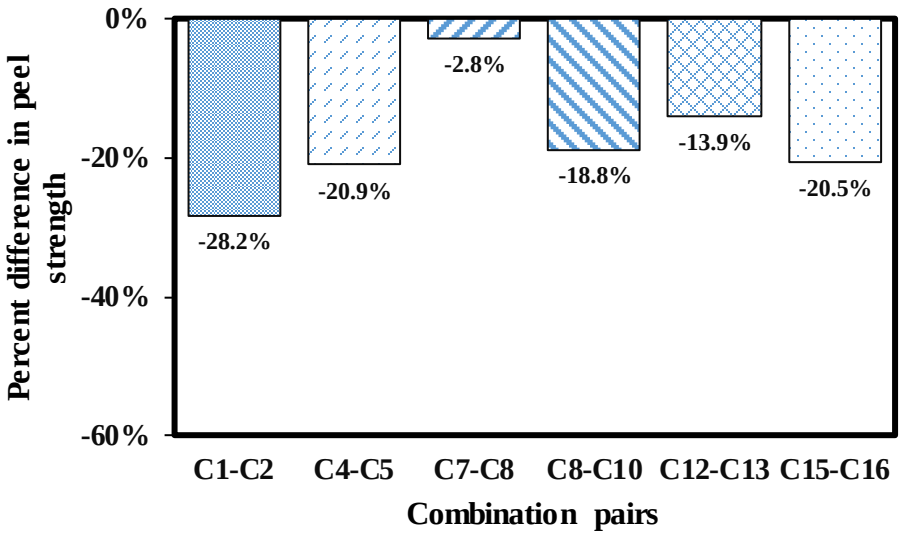

Figure 3.31 Percent difference in peel strength due to the variation in width with a fixed conditioning temperature and conditioning humidity

3.4.3.4 Summary of Peel Testing Results

When the conditioning temperature was increased, the peel strength was reduced for the three combination pairs (C1-C12, C4-C15, and C5-C16), whereas the peel strength increased for the three combination pairs (C3-C8, C8-C14, and C2-C13). The peel strength was improved for all the combination pairs except for combination pair C8-C11 when the conditioning humidity was increased. The peel strength of the specimens was observed to be decreased for all the combination pairs significantly when the width of the specimens was increased.

3.4.4 Cleavage Test

An illustrative load-displacement curve that includes both the first and the second specimen of combination 1 (A-C-13TH-20T/48H-C1) is shown in Figure 3.32. The cleavage strength of the specimens is calculated by taking the maximum load from the load-displacement curve and dividing that load by respective specimen width. The results of the cleavage tests for all the combinations are summarized in Table 3.7. An average cleavage strength of 196.61 N/mm with a standard deviation of 30.14 N/mm is observed from the cleavage testing data.

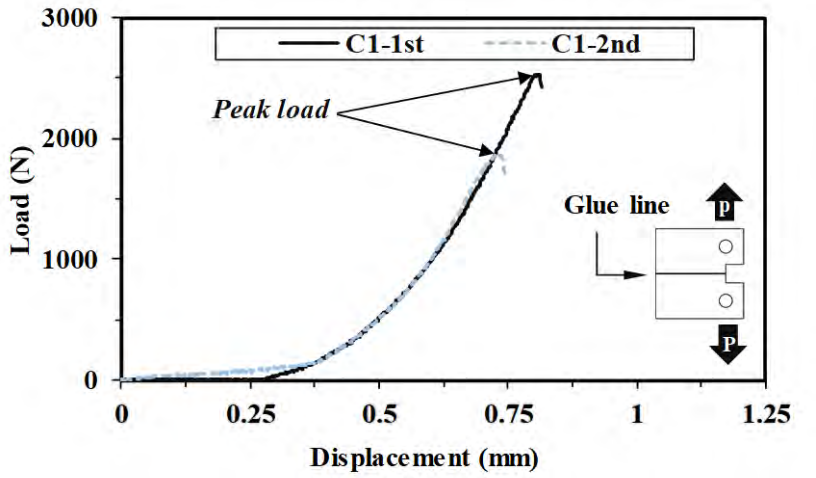

Figure 3.32 Load-displacement curve for cleavage test of combination 1

Table 3.7 Cleavage strength from all the combinations

Combination	Specimen	Cleavage strength, (N/mm)
C1	A-C-13TH-20T/48H-C1	173.52
C2	A-C-38TH-20T/48H-C2	191.19
C3	A-C-25TH-20T/71H-C3	195.01
C4	A-C-13TH-20T/95H-C4	149.75
C5	A-C-38TH-20T/95H-C5	185.77
C6	A-C-25TH-52T/48H-C6	216.15
C7	A-C-13TH-52T/71H-C7	198.32
C8	A-C-25TH-52T/71H-C8	198.11
C9	A-C-25TH-52T/71H-C9	208.16
C10	A-C-38TH-52T/71H-C10	254.55
C11	A-C-25TH-52T/95H-C11	180.67
C12	A-C-13TH-85T/48H-C12	220.62
C13	A-C-38TH-85T/48H-C13	191.54
C14	A-C-25TH-85T/71H-C14	188.74
C15	A-C-13TH-85T/95H-C15	190.76
C16	A-C-38TH-85T/95H-C16	202.82

3.4.4.1 Effect of Conditioning Temperature

The effect of conditioning temperature on cleavage strength is shown in Figure 3.33. The increase in conditioning temperature from 20°C to 85°C improves the cleavage strength of 13-mm width specimens at both 48% and 95% conditioning humidity as displayed in Figure 3.33a. The increase in conditioning temperature from 20°C to 52.5°C increases the cleavage strength of 25-mm width specimens at 71.5%; however, the cleavage strength is declined with a further increment of conditioning temperature from 52.5°C to 85°C (see Figure 3.33b). When the conditioning temperature of 38-mm width cleavage specimens is increased from 20°C to 85°C, the cleavage strength is increased at both 48% and 95% conditioning humidity as shown in Figure 3.33c.

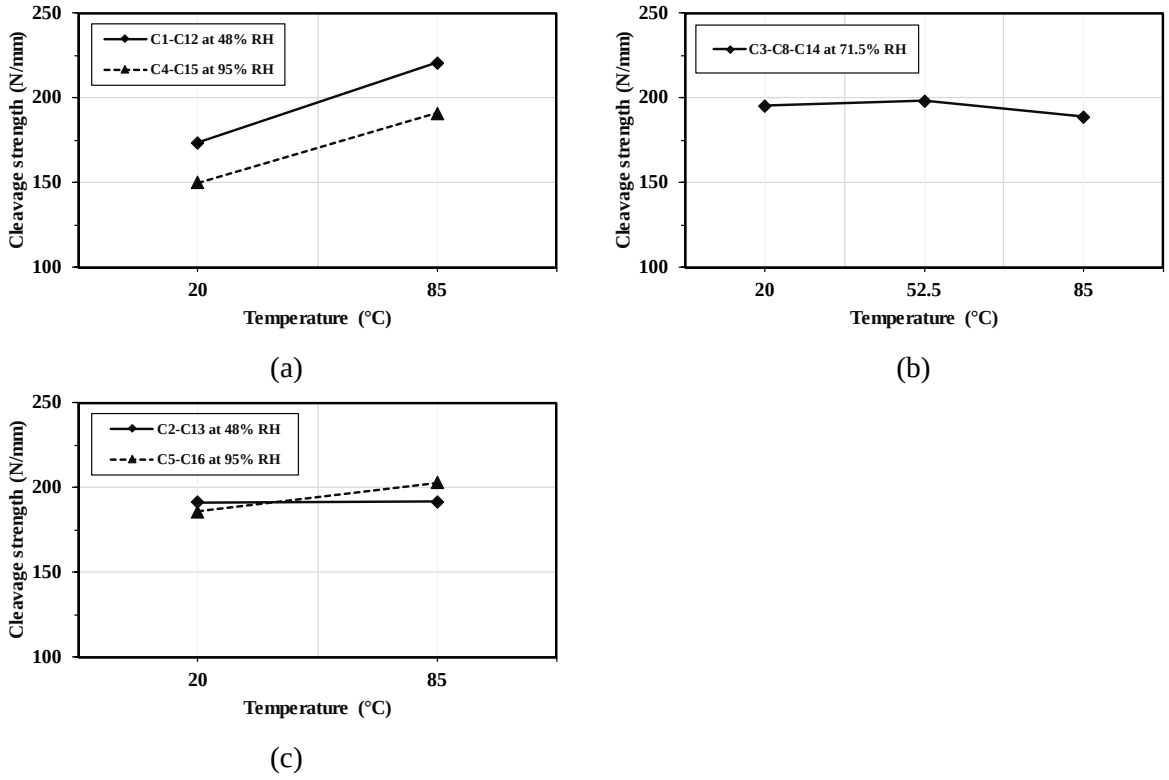

Figure 3.33 Effect of conditioning temperature on cleavage strength for specimens with different widths (a) 13 mm, (b) 25 mm, and (c) 38 mm

Figure 3.34 demonstrates the bar graph depicting the effect of conditioning temperature in cleavage strength. For specimens of 13-mm width, the cleavage strength is increased by 27.1% at 48% conditioning humidity as shown in pairs C1-C12, and by 27.4% at 95% conditioning humidity as shown in pairs C4-C15 when the conditioning temperature is increased from 20°C to 85°C. At 71.5% conditioning humidity, when the conditioning temperature increases from 20°C to 52.5°C, the cleavage strength is improved by 1.6% for 25-mm width specimens (see a pair of C3-C8). The cleavage strength, on the contrary, is decreased by 4.7% after the elevation of conditioning temperature to 85°C from 52.5°C as depicted in pair C8-C14. The cleavage strength is increased by 0.2% at 48% conditioning humidity as depicted in pair C2-C13 and by 9.2% at 95% conditioning humidity as displayed in pair C5-C16 for specimens of 38-mm width after the elevation of conditioning temperature from 20°C to 85°C.

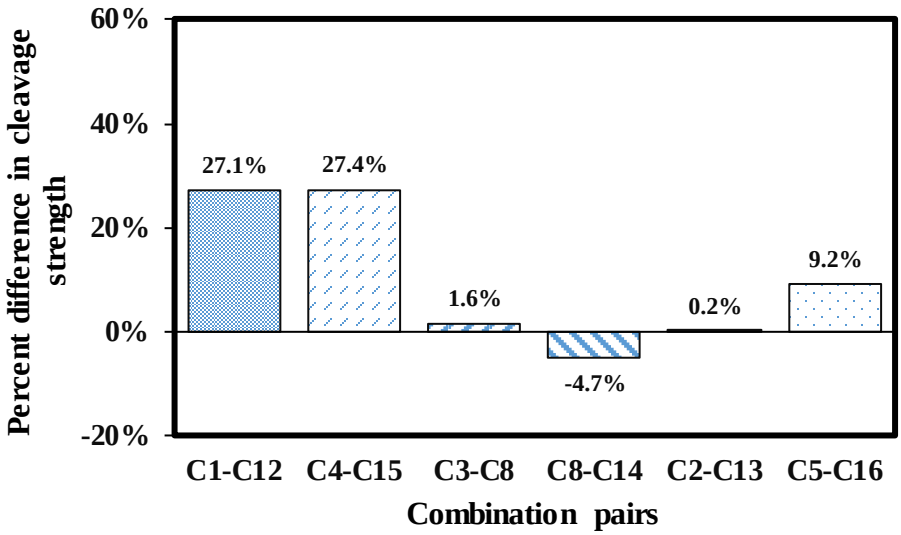

Figure 3.34 Percent difference in cleavage strength due to the variation in conditioning temperature with a fixed conditioning humidity and width

3.4.4.2 Effect of Conditioning Humidity

The effect of conditioning humidity in cleavage strength is shown graphically in Figure 3.35. When the conditioning humidity is increased from 48% to 95%, the cleavage strength of 13-mm width specimens is decreased at both 20°C and 85°C (see Figure 3.35a). With the increment of conditioning humidity of 25-mm width specimens from 48% to 71.5%, the cleavage strength decreases at 52.5°C. The cleavage strength further decreases with the increase of conditioning humidity from 71.5% to 95% as shown in Figure 3.35b. When the conditioning humidity is increased from 48% to 95%, the cleavage strength of 38-mm width specimens decreases at 20°C; however, the cleavage strength minimally increases at 85°C (see Figure 3.35c).

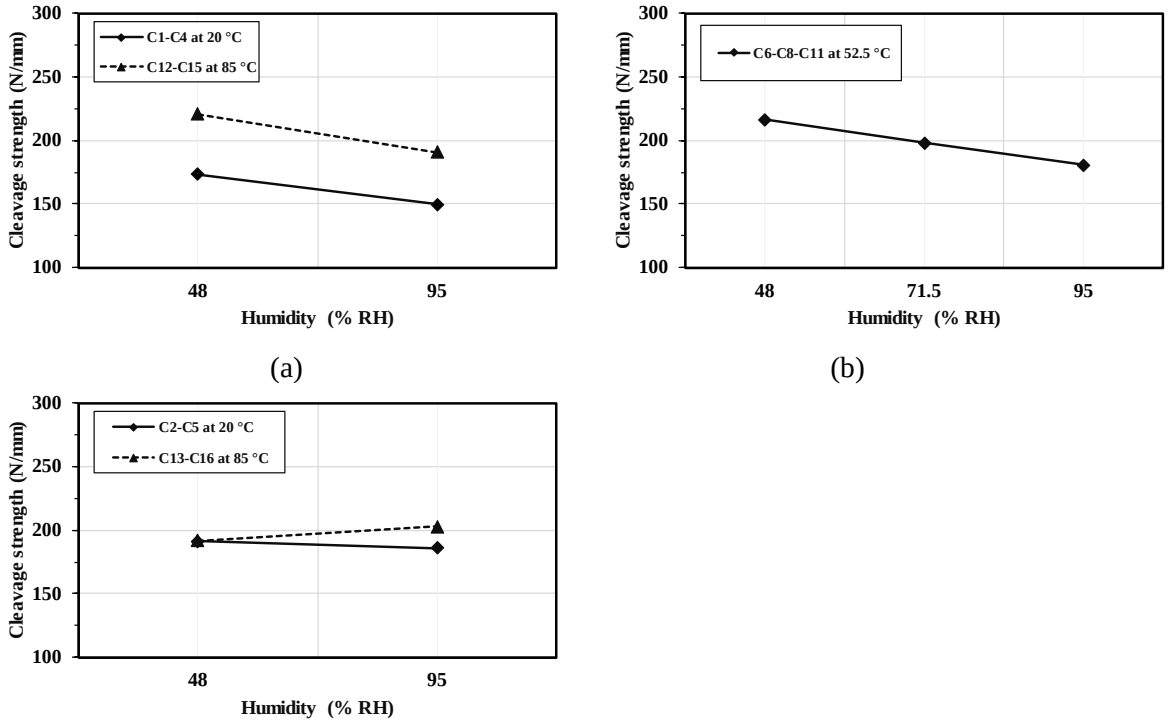

Figure 3.35 Effect of conditioning humidity on cleavage strength for specimens with different widths (a) 13 mm, (b) 25 mm, and (c) 38 mm

Figure 3.36 shows the effect of conditioning humidity on the cleavage strength in terms of percent difference among combination pairs. For specimens of 13-mm width, the strength is reduced by 13.7% at 20°C (see a pair of C1-C4) and by 13.5% at 85°C (see a pair of C12-C15), respectively, when conditioning humidity is increased from 48% to 95%. At 52.5°C, when conditioning humidity is increased from 48% to 71.5%, the strength declines by 8.3% for 25-mm width specimens as displayed in pair C6-C8. The strength of 25-mm width specimens is further decreased by 8.8% after the elevation of conditioning humidity to 95% from 71.5% as depicted in pair C8-C11. The cleavage strength decreases by 2.8% at 20°C (see a pair of C2-C5) but is increased by 5.9% at 85°C for 38-mm specimens after the elevation of conditioning humidity from 48% to 95% as shown in pair C13-C16.

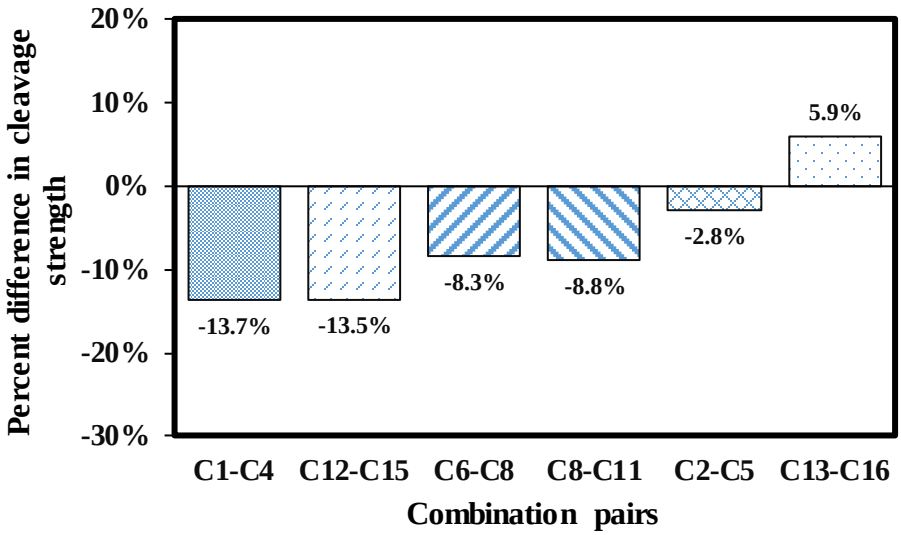

Figure 3.36 Percent difference in cleavage strength due to the variation in conditioning humidity with a fixed conditioning temperature and width

3.4.4.3 Effect of Width

The effect of width in cleavage strength can be seen in Figure 3.37. When the width of the specimens at 20°C is increased from 13 mm to 38 mm, the cleavage strength is increased at both 48% and 95% conditioning humidity as shown in Figure 3.37a. At 52.5°C, when specimen width increases from 13 mm to 25 mm, the cleavage strength very slightly decreases at 71.5% conditioning humidity. The cleavage strength, however, significantly increases after the increment of width to 38 mm from 25 mm (see Figure 3.37b). The cleavage strength decreases at 48% conditioning humidity; however, it increases at 95% conditioning humidity for specimens at 85°C with the increment of specimen width from 13mm to 38mm (see Figure 3.37c).

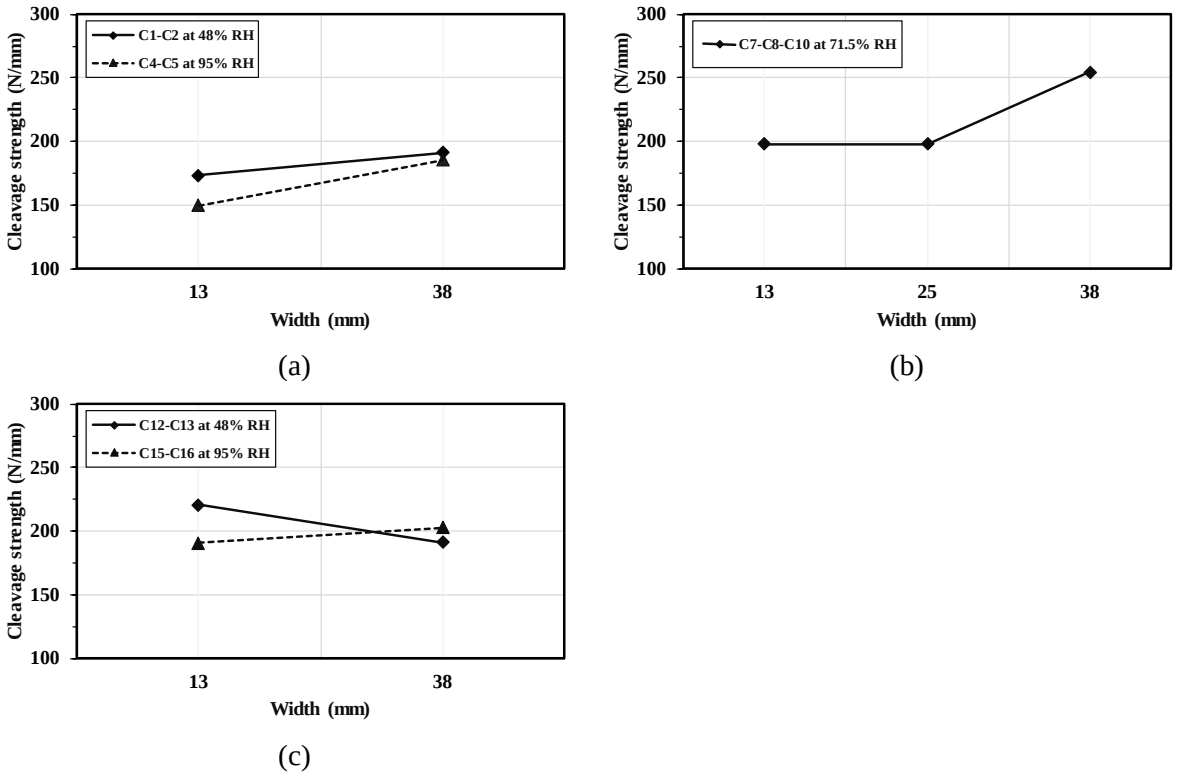

Figure 3.37 Width effect on cleavage strength for specimens at different conditioning temperatures (a) 20°C, (b) 52.5°C, and (c) 85°C

Figure 3.38 illustrates the percent difference of cleavage strength due to the effect of width in a bar graph. For specimens at 20°C, the cleavage strength is increased by 10.2% at 48% conditioning humidity as shown in pair C1-C2, and by 24.1% at 95% conditioning humidity as shown in pair C4-C5 when the width of the specimen increases from 13mm to 38mm. At 52.5°C, when the specimen width increases from 13 mm to 25 mm, the cleavage strength declines by 0.1% at 71.5% conditioning humidity (refer to C8-C10). At the same conditioning temperature and conditioning humidity, the cleavage strength, however, increases by 28.5% after the increment of width to 38 mm from 25 mm as displayed in pair C8-C10. The cleavage strength decreases by 13.2% at 48% conditioning humidity (see a pair of C12-C13); however, the cleavage strength increases by 6.3% at 95% conditioning humidity (refer to C15-C16) for specimens at 85°C with the increment of specimen width from 13mm to 38mm.

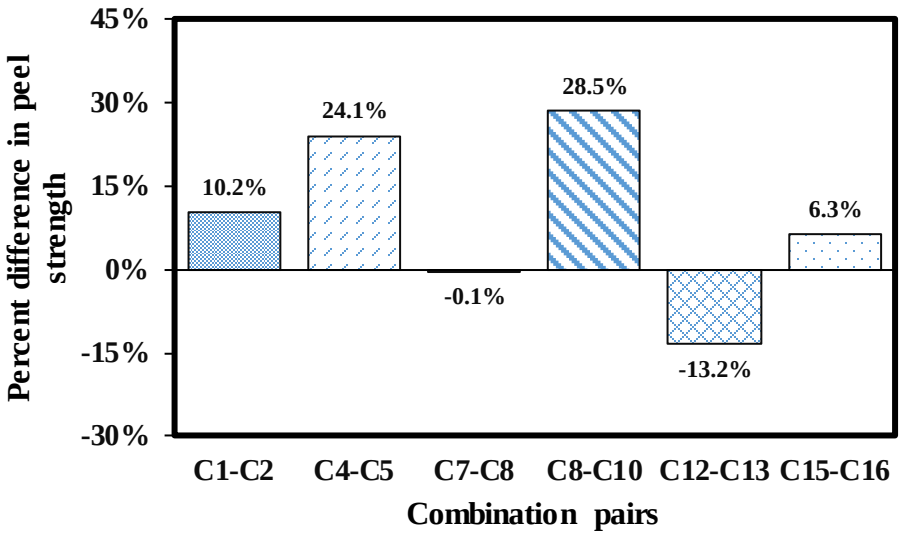

Figure 3.38 Percent difference in cleavage strength due to the variation in width with a fixed conditioning temperature and conditioning humidity

3.4.4.4 Summary of Cleavage Testing Results

When the conditioning temperature was increased, the cleavage strength increased for all the combination pairs (C1-C12, C4-C15, C3-C8, C2-C13, and C5-C16) excluding the pair C8-C14. With the increase in conditioning humidity, the cleavage strength was reduced for all the combination pairs (C1-C4, C12-C15, C6-C8, C8-C11, and C2-C5) except for the pairs C13-C16. When the width of the specimens was increased, the cleavage strength declined for the two combination pairs (C7-C8 and C12-C13) and increased for the other four pairs (C1-C2, C4-C5, C8-C10, and C15-C16).

3.5 Statistical Analysis on Testing Data

This section discusses findings gained through statistical analysis of each of the testing strength datasets. The following subsection deals with the sensitivity analysis necessary for the determination of statistically significant parameters on each of the strengths and statistical model selection required for the prediction of the respective strengths in an efficient manner.

3.5.1 Tensile Strength

3.5.1.1 Regression Model Development

MLR and RSM models were created only for the ultimate tensile stress from the testing, which is the most critical to design the adhesive connection for DMSs. The testing data were modeled to generate both MLR and RSM models using R, a commercially available statistical software. Note, MLR (Seo and Pokhrel 2019, Kokaly and Clark 1999) and RSM (Seo and Linzell 2013, Seo and Linzell 2012, Seo and Linzell 2010) models have been used in previous studies to investigate the effect of different input parameters on outputs such as structural or mechanical behaviors. Three parameters, including conditioning temperature, conditioning humidity, and width of the specimens, were considered for this project in each of the statistical models. The MLR and RSM models for prediction of the ultimate tensile stress are shown in Equations (1) and (2), respectively.

$$f_u(MLR) = 19.4329 - 0.0098T - 0.0263H - 0.0378W \quad (1)$$

$$f_u(\text{RSM}) = 21.104 + 0.004 * T - 0.096 * H + 0.026 * W - 0.0003 * T * H - 0.0002 * T * W + 0.0007 * \text{H} * W + 0.0001 * T^2 + 0.0005 * H^2 - 0.0014 * W^2 \quad (2)$$

where f_u = ultimate tensile stress, T = conditioning temperature, H = conditioning humidity, and W = width of the specimen.

3.5.1.2 Sensitivity Analysis

To determine significant parameters on ultimate tensile stress data, P-values for the developed MLR and RSM models were calculated through statistical analysis. The standard level of significance was set at 5% for the analysis where a P-value less than 0.05 was considered significant. Table 3.8 shows the resulting P-value of each parameter with regard to tensile stress. By analyzing the P-values from the MLR and RSM models, conditioning humidity was found to be the most significant parameter for the tensile stress.

Table 3.8 P-values acquired from the statistical analysis on the tensile stress data

Parameter	MLR	RSM
T	0.09473	0.17736
H	**0.00427**	**0.02529**
W	0.78412	0.82129
T:H	-	0.36704
T:W	-	0.80011
H:W	-	0.41685
T^2	-	0.77909
H^2	-	0.53467
W^2	-	0.59727

3.5.1.3 Comparison between MLR and RSM

To better predict the ultimate tensile stress for the adhesive connection with respect to different parameters taken for this study, the most reliable model between MLR and RSM models was determined by comparing R^2 values acquired from each (see Table 3.9). The R^2 values of the RSM model on the tensile stress are higher than those of the MLR model. It turns out that the predicted ultimate tensile stress from the RSM model was more accurate than the MLR-derived values; thus, the RSM model was chosen for predicting the tensile stress at different conditioning temperature, conditioning humidity, and width. To graphically evaluate the accuracy of RSM and MLR models, the testing data versus the predicted ultimate tensile stress from each are compared as seen in Figure 3.39. Based on the statistical and graphical comparisons with the experimental data, it was proven that the RSM model was the best model.

Table 3.9 Multiple R-squared values for MLR and RSM models

Strength	MLR	RSM
Tensile stress	0.567	0.6949

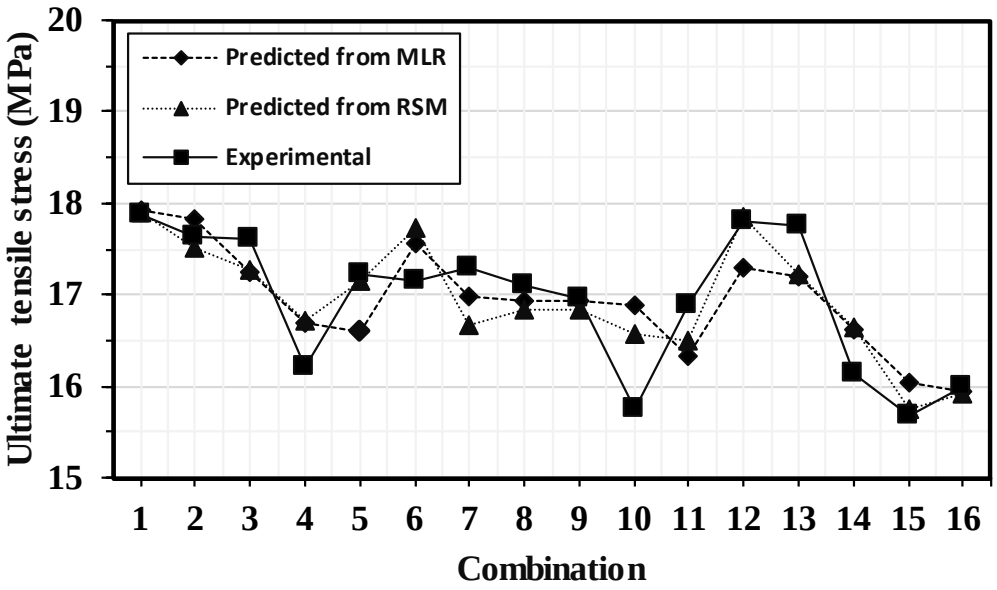

Figure 3.39 Experimental stress versus predicted stress from the MLR and RSM model for tensile data

3.5.1.4 RSM Surfaces for Tensile Strength

The RSM model was used to create 3D surface plots for ultimate tensile stress with respect to different parameters. The tensile stress was plotted against two parameters at a time, while the remaining parameter was considered a fixed value; thus, three separate figures (see Figure 3.40a, b, and c) showing the effects of two parameters were developed. Specifically, an average value of the remaining parameter is taken for developing the plots between the two input parameters deemed as variables. For instance, an average value of width (25 mm) is taken for the RSM model to explore the effect of conditioning temperature and conditioning humidity on tensile stress and to develop the corresponding plot as shown in Figure 3.40a. Figure 3.40b shows the plot for width and conditioning temperature variation with the constant of conditioning humidity, while Figure 3.40c displays the plot regarding different values of width versus conditioning humidity with the fixed value of conditioning temperature.

In Figure 3.40a, at lower conditioning humidity, an increase in conditioning temperature decreased the ultimate tensile stress slightly by 1.12%. At higher conditioning humidity, the tensile stress is reduced by 6.41% when the conditioning temperature is increased. When the ultimate tensile stress is observed at higher conditioning temperatures, there is a significant drop of 9.52% with the increase in conditioning humidity. At lower conditioning temperature, when the conditioning humidity is increased, the tensile stress is dropped by 4.40%. The tensile stress for different width and conditioning temperature is shown in Figure 3.40b. The increase in width is observed to increase the tensile stress with a slight reduction up to 1.39%. The increased conditioning temperature resulted in a significant decrease in tensile stress by 3.00% at smaller width and by 4.45% at larger width specimens. It can be observed in Figure 3.40c that conditioning humidity plays a vital role in tensile stress. The tensile stress is dropped considerably by 9.34% at smaller width and by 4.81% at larger width when the conditioning humidity is increased. Only a slight increase of 1.92% in tensile stress is observed at high conditioning humidity when the width is increased. The tensile stress, however, is reduced by 2.81% at low conditioning humidity when the specimen width is increased.

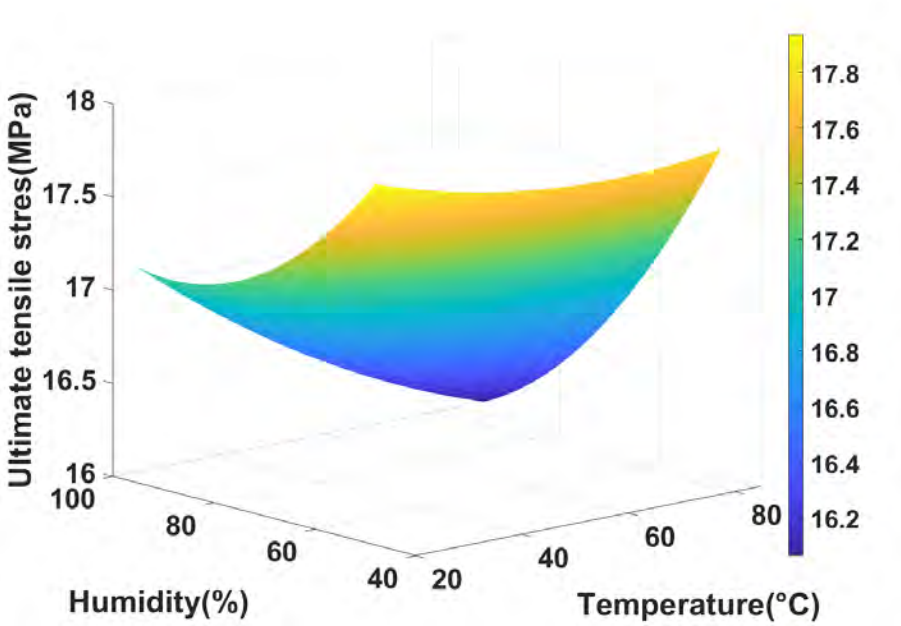
Ultimate tensile stres(MPa)
18
17.5
17
16.5
16
100
80
60
40
Humidity(%)
20
40
60
80
Temperature(°C)
17.8
17.6
17.4
17.2
17
16.8
16.6
16.4
16.2

(a)

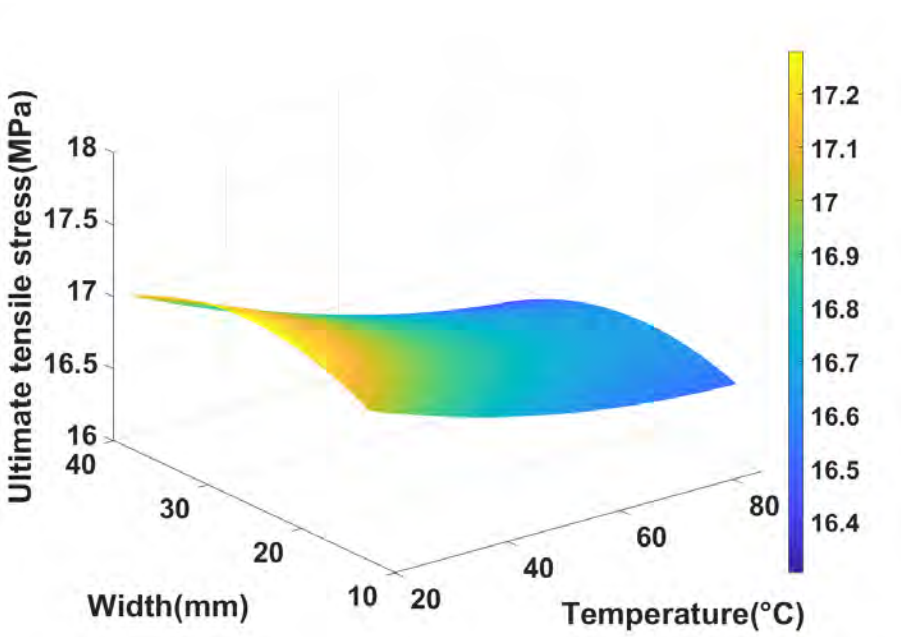
Ultimate tensile stress(MPa)
18
17.5
17
16.5
16
40
30
20
10
Width(mm)
20
40
60
80
Temperature(°C)
17.2
17.1
17
16.9
16.8
16.7
16.6
16.5
16.4

(b)

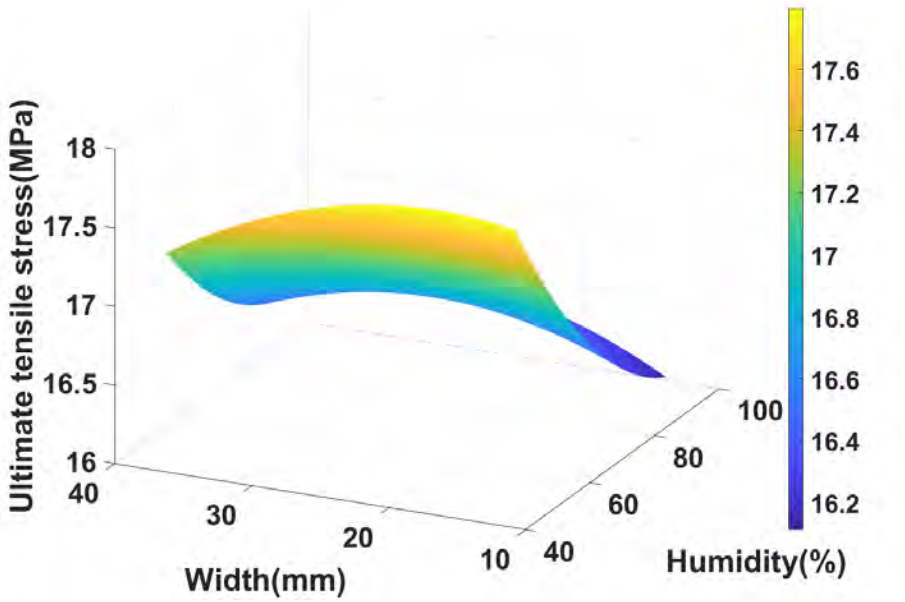

(c)

Figure 3.40 3D RSM surfaces of ultimate tensile stress showing effects of (a) conditioning temperature and conditioning humidity, (b) conditioning temperature and width, and (c) conditioning humidity and width

From the above discussion, it was found that conditioning humidity plays a significant role in determining the ultimate tensile stress in adhesive connection. An increase in conditioning humidity changed the ultimate tensile stress up to 9.52%. A maximum percentage change of 6.41% is observed for the ultimate tensile stress with the increase in conditioning temperature, but the effect of width while predicting ultimate stress cannot be neglected either. The ultimate tensile stress is found to be changed up to 2.81% when the width of the specimens is increased. It should be noted that the developed RSM functions can be used for a certain range of input parameters only to predict the ultimate tensile stress at low uncertainties. The conditioning temperature should be in the range of 20°C to 85°C, conditioning humidity should be limited to 48% to 95%, and the width of the adhesive joints should be within 12.7 to 38.1 mm only. Beyond that range, significant uncertainties can be expected for the outputs from the RSM functions.

3.5.2 Shear Strength

3.5.2.1 Regression Model Development

MLR and RSM models were generated for the ultimate shear stress utilizing the shear test data acquired from all the combinations consisting of each input parameter using the statistical software R. For each of the statistical models, three distinct input parameters, encompassing conditioning temperature, conditioning humidity, and specimen width, were considered. The ultimate shear stress can be predicted according to Equation (3) for the MLR model and Equation (4) for the RSM model.

$$\tau_u(\text{MLR}) = 18.583 - 0.008 * T - 0.029 * H + 0.011 * W \quad (3)$$

$$\tau_u(\text{RSM}) = 21.161 + 0.006 * T - 0.072 * H - 0.122 * W - 0.0004 * T * H + 0.0004 * T * W + 0.0005 * \text{H} * W + 0.00004 * T^2 + 0.0004 * H^2 + 0.0015 * W^2 \quad (4)$$

where τ_u = ultimate shear stress, T = conditioning temperature, H = conditioning humidity, and W = width of the specimen.

3.5.2.2 Sensitivity Analysis

The P-values for MLR and RSM models were determined during the statistical analysis to examine the crucial parameters, which have an influence on the ultimate shear stress. The standard level of significance was considered to be at 5% in this study; thus, a P-value higher than 0.05 was not considered significant. The P-values for each parameter in reference to the shear stress are shown in Table 3.10. The shear stress did not show any parameters to be significant in any of the models.

Table 3.10 P-values acquired from the statistical analysis on the shear stress data

Parameter	MLR	RSM
T	0.435	0.5596
H	0.053	0.1518
W	0.671	0.7503
T:H	-	0.5429
T:W	-	0.7386
H:W	-	0.7685
T^2	-	0.9565
H^2	-	0.8070
W^2	-	0.7655

3.5.2.3 Comparison between MLR and RSM

The R^2 values acquired from MLR and RSM models presented in Table 3.11 were compared to determine the most trustworthy model for the prediction of the ultimate shear stress in adhesive specimens considering different parameters taken in this study. Because the R^2 value from the RSM model for the ultimate shear stress is greater than that from the MLR model, the RSM model was selected for the prediction of the ultimate shear stress. As shown in Figure 3.41, the predicted ultimate shear stress from each model is plotted against the testing data to visually check the accuracy of each. The RSM model was found to be the most reliable model on the basis of statistical and graphical comparisons with the experimental data.

Table 3.11 Multiple R-squared values for MLR and RSM models

Strength	MLR	RSM
Shear stress	0.3123	0.412

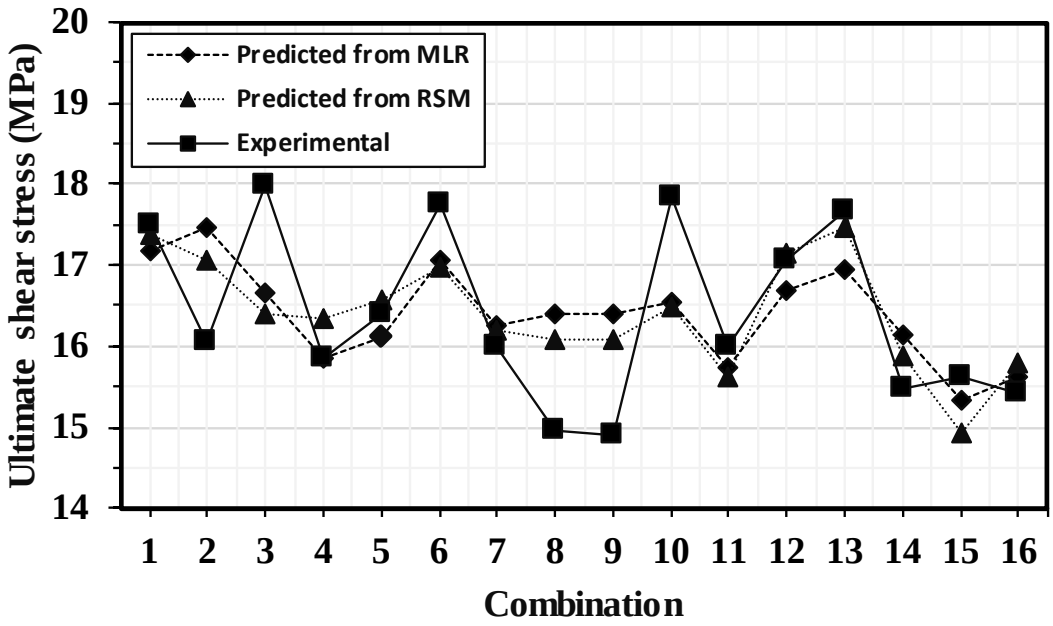

Figure 3.41 Experimental stress versus predicted stress from the MLR and RSM model for shear data

3.5.2.4 RSM Surfaces

3D surface plots for ultimate shear stress were developed using the RSM function presented in equation (4). 3D plots of the ultimate shear stress are shown in Figure 3.42. The plots show the behavior of shear stress with respect to two different parameters. In Figure 3.42a, the increase in conditioning temperature at lower conditioning humidity increased the ultimate shear stress by 0.47%; however, at the higher conditioning humidity, the ultimate shear stress is reduced by 6.72%. The increase in conditioning humidity is observed to decrease the ultimate shear stress by 4.47% at the lower conditioning temperature and by 11.31% at the higher conditioning temperature. When the width is plotted with respect to conditioning temperature in Figure 3.42b, an increase in width decreased the shear stress by 0.30% at a lower conditioning temperature; however, the shear stress is increased by 3.72% at the higher conditioning temperature. When the conditioning temperature is increased, the shear stress is decreased rapidly at smaller widths by 4.98%; however, the effects seem to be minimal at wider specimens with 1.08% reduction in the shear stress. The shear stress for width and conditioning humidity is plotted in Figure 3.42c. At lower conditioning humidity, with the increase in width, the shear stress is reduced only by 0.05%; however, it increased by 3.59% at higher conditioning humidity. The increase in conditioning humidity decreased the shear stress by 9.47% at a smaller width and 6.16% at a larger width.

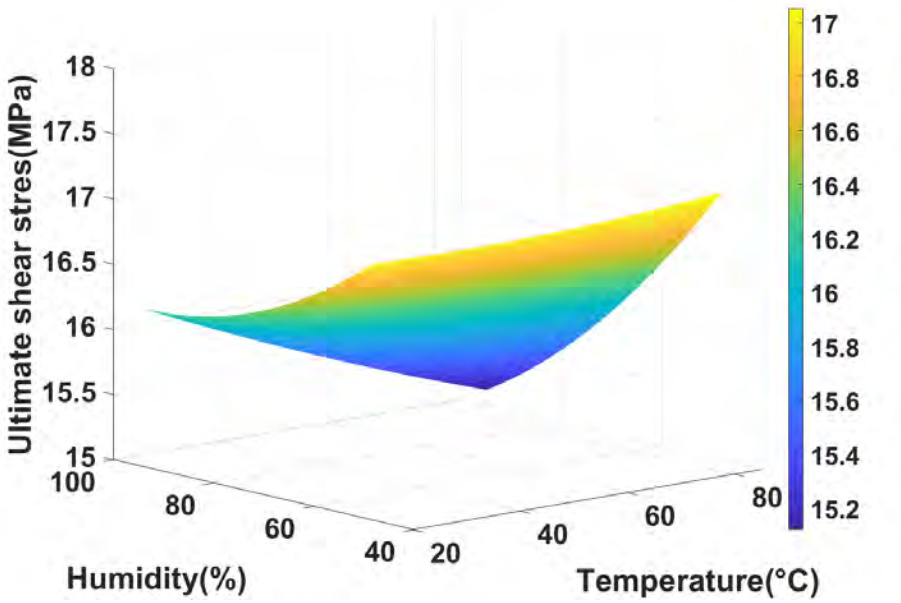
Ultimate shear stres(MPa)
18
17.5
17
16.5
16
15.5
15
100
80
60
40
Humidity(%)
20
40
60
80
Temperature(°C)
17
16.8
16.6
16.4
16.2
16
15.8
15.6
15.4
15.2

(a)

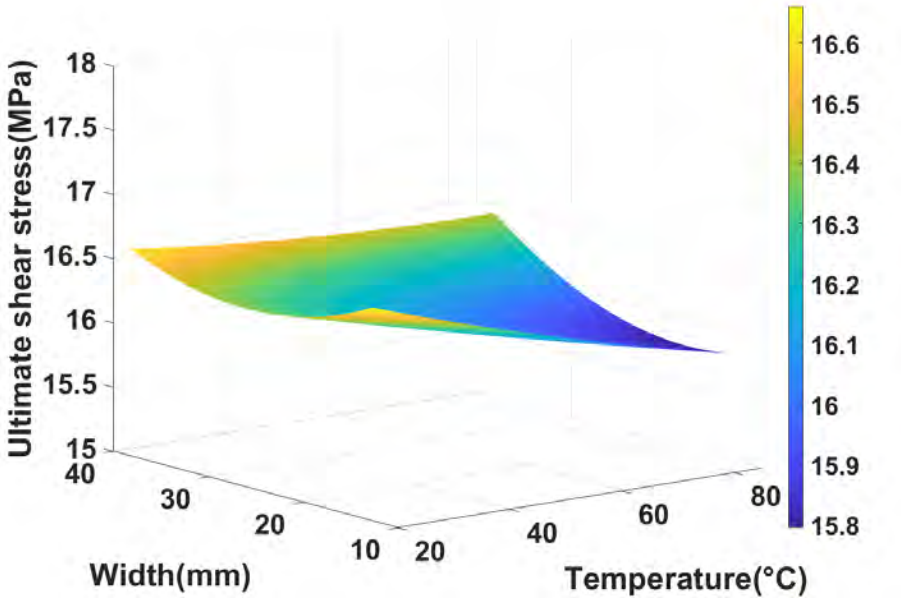
Ultimate shear stress(MPa)
18
17.5
17
16.5
16
15.5
15
40
30
20
10
Width(mm)
20
40
60
80
Temperature(°C)
16.6
16.5
16.4
16.3
16.2
16.1
16
15.9
15.8

(b)

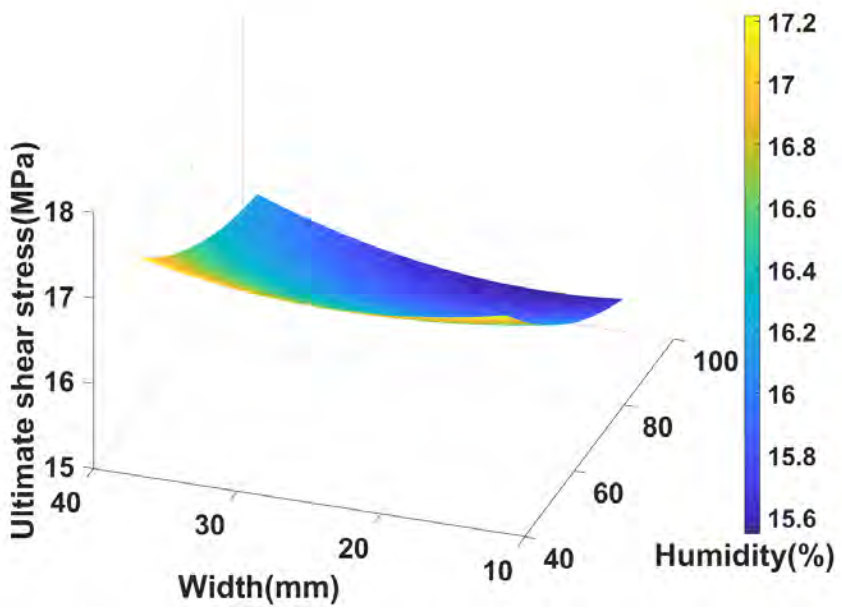

(c)

Figure 3.42 3D RSM surfaces of ultimate shear stress showing effects of (a) conditioning temperature and conditioning humidity, (b) conditioning temperature and width, and (c) conditioning humidity and width

Conditioning humidity was observed to affect the ultimate shear stress of the adhesive connection. When the conditioning humidity was increased, the ultimate shear stress was changed up to 11.31%. The increase in conditioning temperature changed ultimate shear stress to a peak variation of 6.72%, although the effect of width should be also taken into consideration while predicting the ultimate stress. The ultimate shear stress is changed up to 3.72% when the width of the specimens is increased. The RSM model developed should be used for the prediction of the ultimate shear stress between a conditioning temperature range of 20°C to 85°C, a conditioning humidity range of 48% to 95%, and width of the adhesive joints between 12.7 and 38.1 mm only. The ultimate shear stress predicted from the RSM model outside that range might have unexpected results.

3.5.3 Peel Strength

3.5.3.1 Regression Model Development

To explore the significance of each input parameter on the peel strength of specimens in an efficient manner, MLR and RSM models were also developed. Statistical software R was employed to generate both MLR and RSM models using the peel strength data resulting from the experimental program. Three input parameters, including conditioning temperature and conditioning humidity of the conditioning environment and width of the specimens, were considered in the statistical model for the study. Equations (5) and (6) present the MLR and RSM models, respectively, for the prediction of the peel strength.

$$f_{ap}(MLR) = 7.6609 + 0.0031 * T + 0.0061 * H - 0.0644 * W \quad (5)$$

$$f_{ap}(RSM) = 11.4711 - 0.2503 * T + 0.1656 * H - 0.1796 * W + 0.0462 * T * H + 0.0072 * T * W - 0.0004 * H * W + 0.0796 * T^2 - 0.5353 * H^2 + 0.0015 * W^2 \quad (6)$$

where f_{ap} = peel strength, T = conditioning temperature, H = conditioning humidity, and W = width of the specimen

3.5.3.2 Sensitivity Analysis

To examine the key parameters, which have an influence on the peel strength, P-values from both MLR and RSM models were examined. The P-values were acquired from each model during the creation of individual MLR and RSM models. For the analysis, a P-value less than 0.05 was considered significant and the standard level of significance was established at 5%. The P-value for each parameter subjected to the peel strength is presented in Table 3.12. The width was found to be the most significant parameter for the peel strength as the P-value of the MLR model for peel strength is less than 0.05.

Table 3.12 P-values acquired from the statistical analysis to evaluate peel strength

Parameter	MLR	RSM
T	0.75540	0.80105
H	0.65950	0.72175
W	**0.02480**	0.07834
T:H	-	0.91470
T:W	-	0.68182
H:W	-	0.97824
T^2	-	0.91737
H^2	-	0.50150
W^2	-	0.24176

3.5.3.3 Comparison between MLR and RSM

The coefficient of determination (R^2 value) of the models created from RSM for the peel strength is higher than the MLR model as presented in Table 3.13. The higher R^2 value of the model indicates better reliability of the model for the prediction of peel strength. The peel strength predicted from the RSM model was observed to be more precise than the strength values predicted from the MLR model. The RSM model was, therefore, considered for predicting the peel strength for the various environmental and geometrical parameters. A graphical illustration of experimental versus predicted strengths from MLR and RSM models for peel strength is shown in Figure 3.43 to compare the precision of the models diagrammatically. In this figure, the lowest variation of peel strength found between the RSM values and experimental data is only 0.07%; however, the MLR values and experimental data differed by 0.82%. Based on the graphical comparisons, it was confirmed that the RSM model better predicted the peel strength than the MLR model.

Table 3.13 Multiple R-squared values for MLR and RSM models

Strength	MLR	RSM
Peel strength	0.3646	0.5346

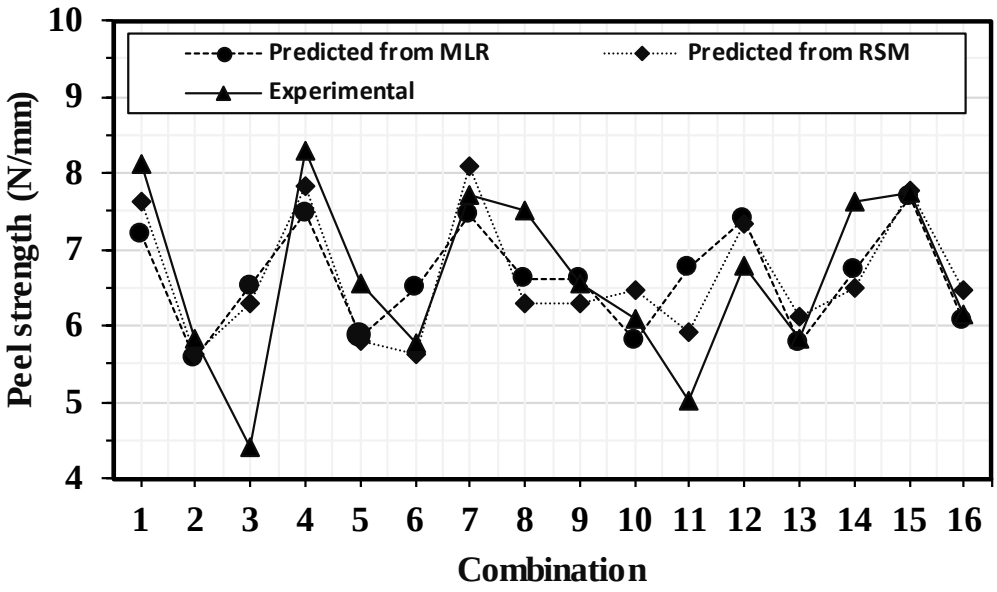

Figure 3.43 Experimental strength versus predicted strength from the MLR and RSM model for peel data

3.5.3.4 RSM Surfaces

This section presents the use of the RSM model to determine the effects of conditioning temperature, conditioning humidity, and width on the peel strength. The RSM model, Equation (6), was used to create a 3D surface for the peel strength to explore the RSM responses with respect to variation in a pair of different considered parameters. Specifically, the peel strength was plotted for two input parameters at a time with a fixed average value for the third parameter as shown in Figure 3.44a through c.

In Figure 3.44a, an increase in conditioning temperature decreased the peel strength by 5.06% at lower conditioning humidity and 1.77% at higher conditioning humidity. The peel strength is observed to increase at first, reaching a maximum and then dropping to a minimum when conditioning humidity is increased without regard to conditioning temperature. The peel strength is ultimately increased by 3.33% at a lower conditioning temperature and 6.91% at a higher conditioning temperature after dropping from the highest value. The peel strength for different width and conditioning temperature is shown in Figure 3.44b. The increase in width is observed to decrease the peel strength with a slight increment at the end. At a lower conditioning temperature, the increase in width decreased the peel strength significantly by 24.29%, and peel strength is reduced by 15.66% at a higher conditioning temperature with the increase in specimen width. At smaller widths, an increase in conditioning temperature resulted in the reduction of peel strength by 2.05%; however, the peel strength is increased by 9.11% at larger widths when the conditioning temperature is increased. Figure 3.44c shows the plot of peel strength against conditioning humidity and width. The increase in width decreased the peel strength considerably by 21.59% at lower conditioning humidity and 21.51% at higher conditioning humidity. The increase in conditioning humidity, but increased the peel strength by 4.44% at a smaller width and by 4.56% at a larger width.

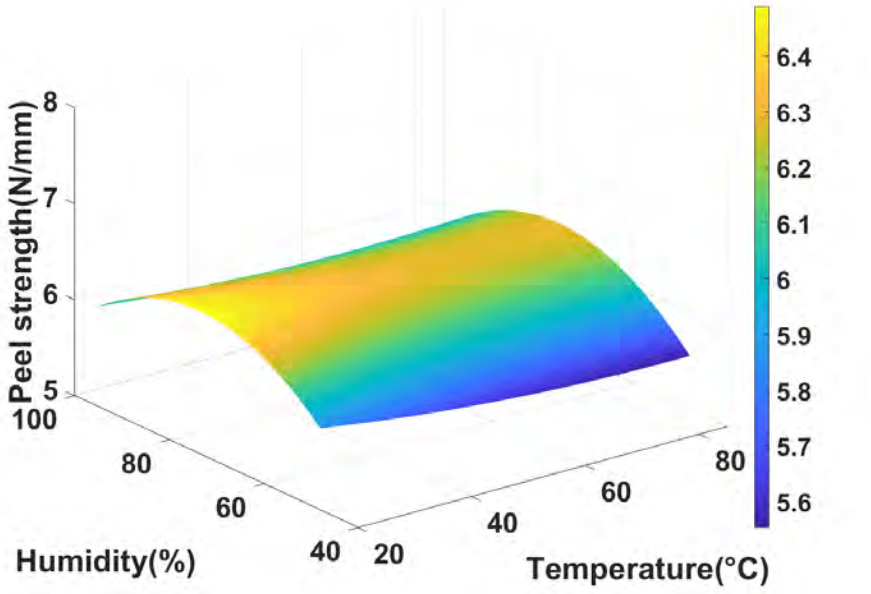
Peel strength(N/mm)
8
7
6
5
100
80
60
40
Humidity(%)
20
40
60
80
Temperature(°C)
6.4
6.3
6.2
6.1
6
5.9
5.8
5.7
5.6

(a)

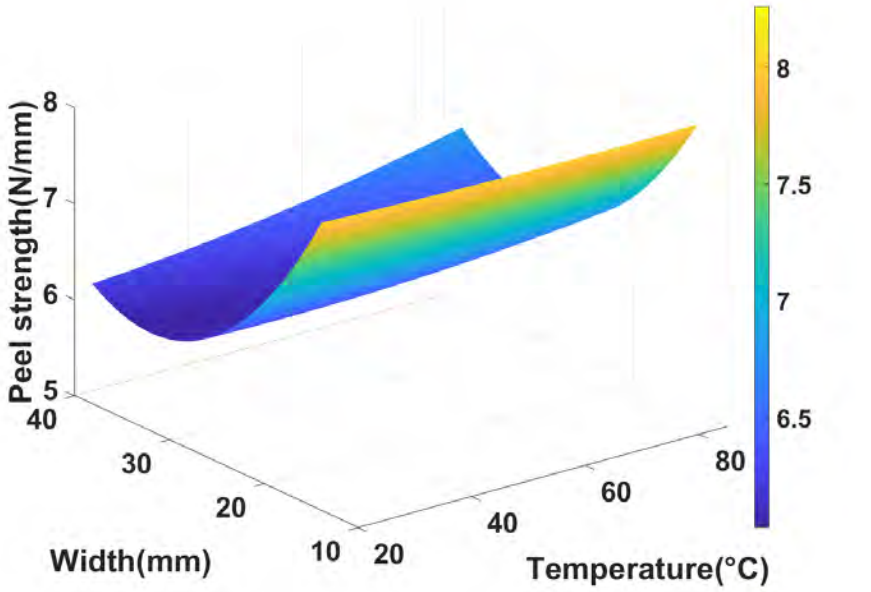
Peel strength(N/mm)
8
7
6
5
40
30
20
10
Width(mm)
20
40
60
80
Temperature(°C)
8
7.5
7
6.5

(b)

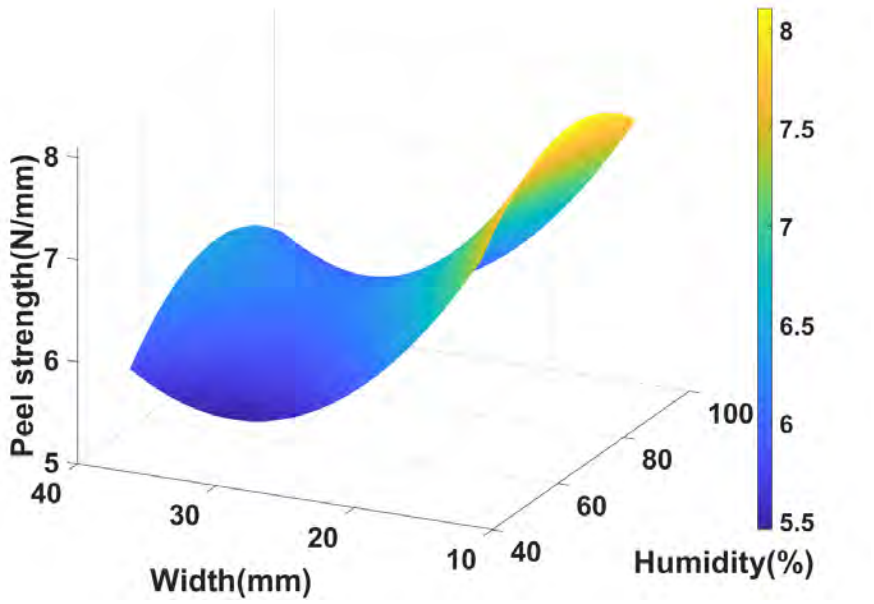

(c)

Figure 3.44 3D surface plots of peel strength showing effects of (a) conditioning temperature and conditioning humidity, (b) conditioning temperature and width, and (c) conditioning humidity and width

It was observed that out of all three parameters, specimen width affects the peel strength significantly. From the above discussion, it was found that an increase in conditioning humidity changed the peel strength up to 6.92%. The increase in conditioning temperature altered the peel strength up to 9.11%. The increase in width, however, decreased the peel strength from 15.66% to 24.29%. The RSM functions presented in this project, however, should be used for a certain range of input parameters only to predict the peel and cleavage strength. The conditioning temperature should be in the range of 20°C to 85°C, conditioning humidity should be within 48% to 95%, and the width of the adhesive joints should be between 12.7 and 38.1 mm only.

3.5.4 Cleavage Strength

3.5.4.1 Regression Model Development

For the prediction of cleavage strength, MLR and RSM models were generated to examine the influence of different parameters in cleavage strength. As for the other strengths, when developing MLR and RSM models, the statistical software R was used. The cleavage strength data acquired from the testing at each input parameter were utilized to create each of the models. The predicted cleavage strength for MLR and RSM models can be obtained from Equations (7) and (8), respectively.

$$f_c(MLR) = 187.3232 + 0.3054 * T - 0.3543 * H + 0.7315 * W \quad (7)$$

$$f_c(RSM) = 243.5033 + 26.9055 * T - 22.6119 * H - 1.7691 * W + 1.3262 * T * H - 0.3479 * T * W + 0.2927 * H * W - 20.4477 * T^2 - 13.9127 * H^2 + 0.0218 * W^2 \quad (8)$$

where f_c = cleavage strength, T = the conditioning temperature, H = the conditioning humidity, and W = the specimen width.

3.5.4.2 Sensitivity Analysis

P-values from each of the MLR and RSM models were assessed during the statistical analysis. As mentioned before, for the statistical analysis, a P-value more than 5% was not considered significant. For the cleavage strength, the P-values of each parameter for both models are listed in Table 3.14. All the input parameters, including conditioning temperature, conditioning humidity, and width, appeared to be statistically insignificant in both MLR and RSM models.

Table 3.14 P-values acquired from the statistical analysis to evaluate cleavage strength

Parameter	MLR	RSM
T	0.1580	0.1188
H	0.2300	0.1778
W	0.1840	0.1394
T:H	-	0.8351
T:W	-	0.1974
H:W	-	0.2685
T^2	-	0.1026
H^2	-	0.2383
W^2	-	0.2324

3.5.4.3 Comparison between MLR and RSM

The R^2 value of both MLR and RSM models created for the prediction of cleavage strength is shown in Table 3.15. The R^2 value of the RSM model is observed to be significantly higher than the MLR model. The experimental versus predicted cleavage strengths from the MLR and RSM models are shown in Figure 3.45. The cleavage strength predicted from the RSM model was also found have higher accuracy than the cleavage strength obtained from the MLR model. RSM model. In this figure, the minimum variations between the predicted values from each of the MLR and RSM models and experimental cleavage strength were calculated. The cleavage strength from the RSM model fluctuates by 0.53% only, while that from the MLR model is changed by 1.51%. The RSM model was observed to be more reliable for the cleavage strength prediction on the basis of visual and statistical comparison. Hence, the RSM model was considered for predicting the cleavage strength with conditioning temperature, conditioning humidity, and width parameters.

Table 3.15 Multiple R-squared values for MLR and RSM models

Strength	MLR	RSM
Cleavage strength	0.328	0.7695

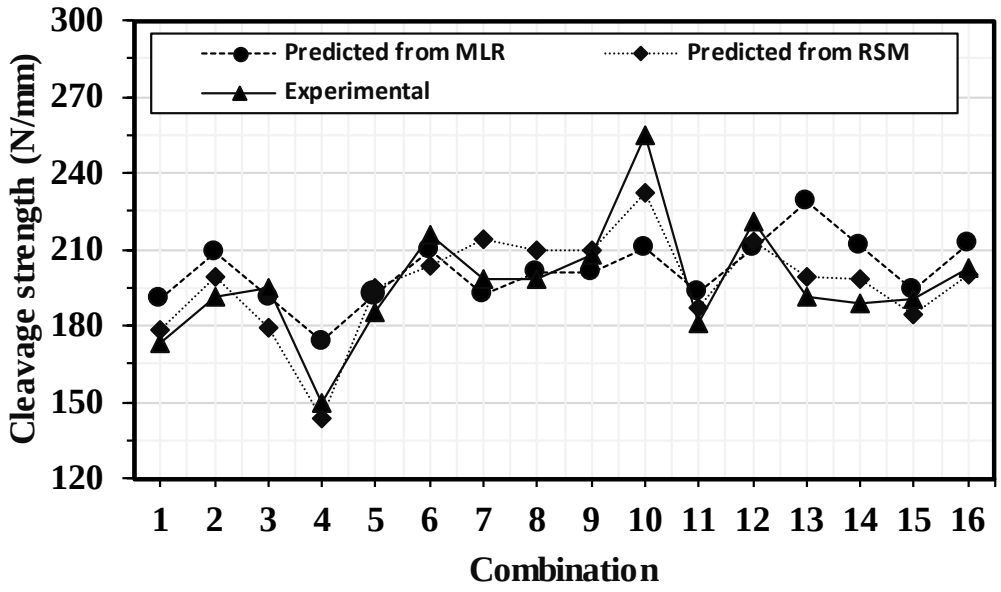

Figure 3.45 Experimental strength vs. predicted strength from the MLR and RSM model for cleavage data

3.5.4.4 RSM Surfaces

The RSM model, Equation (8), was utilized to create 3D surface plots for the cleavage strength. The 3D plots of the cleavage strength are shown in Figure 3.46a through c. In Figure 3.46a, the cleavage strength is increased by 9.85% at lower conditioning humidity and by 14.19% at higher conditioning humidity when the conditioning temperature is increased. The cleavage strength is reduced by 10.82% at a lower conditioning temperature and by 7.30% at a higher conditioning temperature with the increment in conditioning humidity. In Figure 3.46b, at a lower conditioning temperature, an increase in width improved the cleavage strength significantly by 20.70%; and at a higher conditioning temperature, the cleavage strength increased slightly by 0.57%. In Figure 3.46c, at lower conditioning humidity, the cleavage strength is increased by 1.71% with the increase in specimen width. The cleavage strength is raised significantly by 18.17% at higher conditioning humidity when the specimen width is increased. An increase in conditioning humidity decreased the cleavage strength by 14.59% at smaller width specimens and by 0.77% at larger width specimens.

The cleavage strength was found to be affected most by width within all three parameters considered in this study. From the above discussion on the RSM data, it was observed that the cleavage strength changed up to 14.60% with the increment in conditioning humidity, the cleavage strength is varied up to 21.27% when conditioning temperature is increased, and the cleavage strength is changed up to 20.70% with the increase in width. Note that the RSM model for the prediction of cleavage strength should only be utilized for conditioning temperature in the range of 20°C to 85°C, conditioning humidity in the range of 48% to 95%, and width in the range of 12.7 mm to 38.1 mm.

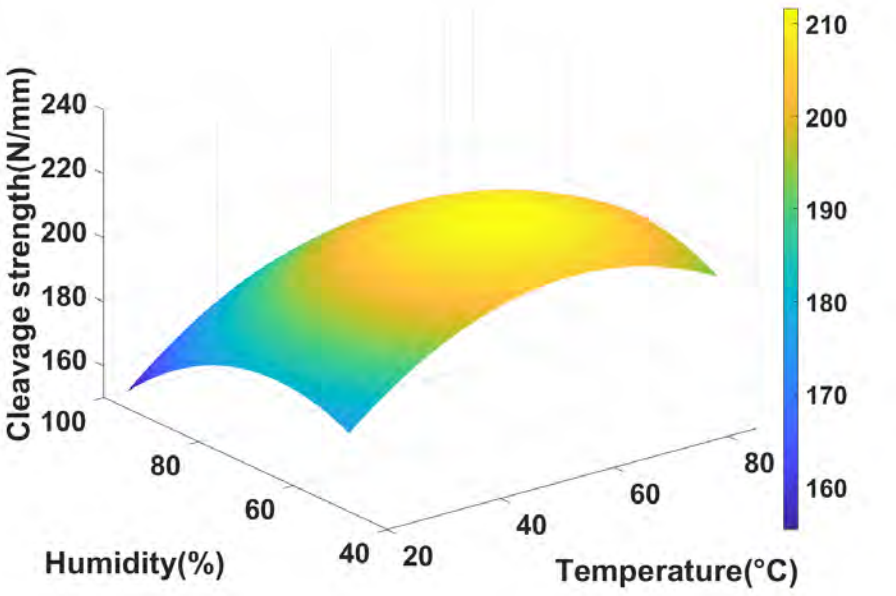
Cleavage strength(N/mm)
240
220
200
180
160
100
80
60
40
Humidity(%)
20
40
60
80
Temperature(°C)
210
200
190
180
170
160

(a)

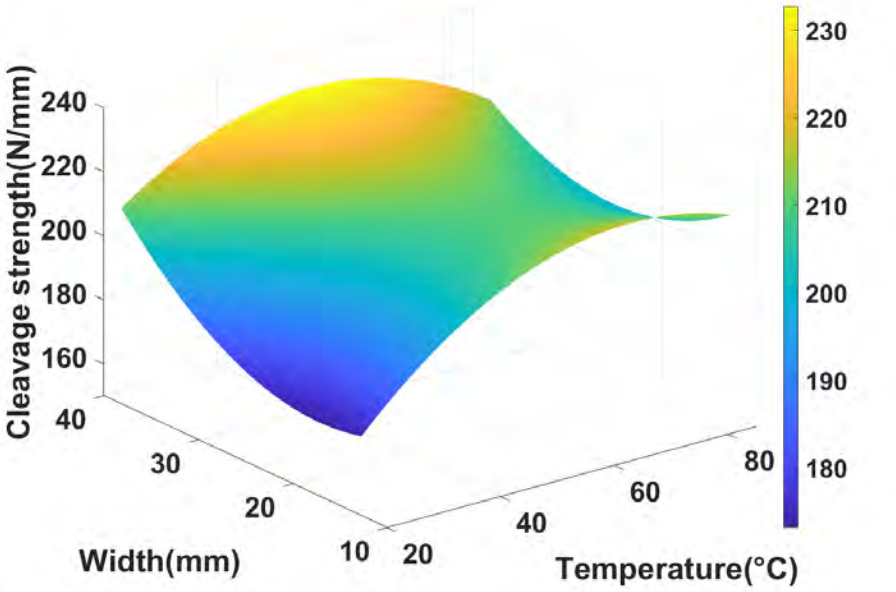
Cleavage strength(N/mm)
240
220
200
180
160
40
30
20
10
Width(mm)
20
40
60
80
Temperature(°C)
230
220
210
200
190
180

(b)

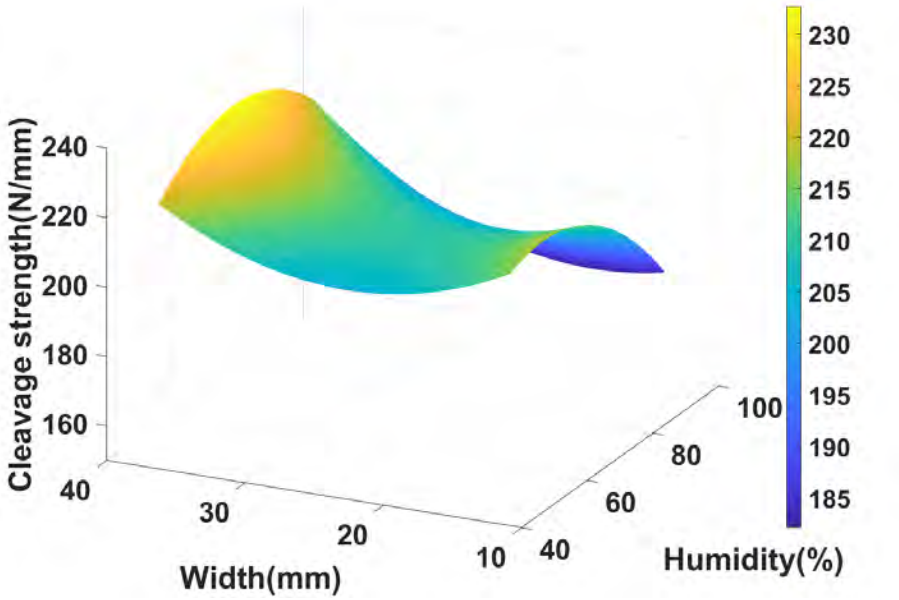

(c)

Figure 3.46 3D surface plots of cleavage strength showing effects of (a) conditioning temperature and conditioning humidity, (b) conditioning temperature and width, and (c) conditioning humidity and width

4. COMPARISON WITH WELDED SPECIMENS

4.1 Testing Combinations

To examine the effect of the extreme conditioning temperatures ranging from -56.67°C to 93.33°C on each strength type, additional adhesive specimens were also tested. A combination table encompassing various conditioning temperatures and widths created for this study is presented in Table 4.1. An individual set of 30 specimen combinations was tested per strength type. Each combination consisted of two specimens for tensile, shear, peel, and cleavage specimens individually. An additional 12 adhesive specimen combinations (A1 through A6) and 18 welded specimen combinations (W1 through W9) were tested for each strength type. All strength data presented for the adhesive specimen combinations C1, C2, C3, C7, C8, C10, C12, C14, and C16 were reused from Section 3.4 to facilitate examination of the effects of conditioning temperature and width over a broader range on each strength. Note that adhesive and welded specimens with the same specimen width were tested after conditioning at the identical temperature to make comparisons between the strength of adhesive and welded specimens for each test type.

Table 4.1 Combinations for the experimental program

Specimen type	Combination	Specimen ID	Conditioning Temperature (°C)	Width (mm)
Adhesive	A1	A-T/S/P/C-13TH-93.3T-A1	93.3	13
	A2	A-T/S/P/C-25TH-93.3T-A2	93.3	25
	A3	A-T/S/P/C-38TH-93.3T-A3	93.3	38
	A4	A-T/S/P/C-13TH-(-56.7)T-A4	-56.7	13
	A5	A-T/S/P/C-25TH-(-56.7)T-A5	-56.7	25
	A6	A-T/S/P/C-38TH-(-56.7)T-A6	-56.7	38
	C1	A-T/S/P/C-13TH-20.0T-C1	20.0	13
	C2	A-T/S/P/C-38TH-20.0T-C2	20.0	38
	C3	A-T/S/P/C-25TH-20.0T-C3	20.0	25
	C7	A-T/S/P/C-13TH-52.5T-C7	52.5	13
	C8	A-T/S/P/C-25TH-52.5T-C8	52.5	25
	C10	A-T/S/P/C-38TH-52.5T-C10	52.5	38
	C12	A-T/S/P/C-13TH-85.0T-C12	85.0	13
	C14	A-T/S/P/C-25TH-85.0T-C14	85.0	25
	C16	A-T/S/P/C-38TH-85.0T-C16	85.0	38
Welded	W1	W-T/S/P/C-13TH-93.3T-W1	93.3	13
	W2	W-T/S/P/C-25TH-93.3T-W2	93.3	25
	W3	W-T/S/P/C-38TH-93.3T-W3	93.3	38
	W4	W-T/S/P/C-13TH-(-56.7)T-W4	-56.7	13
	W5	W-T/S/P/C-25TH-(-56.7)T-W5	-56.7	25
	W6	W-T/S/P/C-38TH-(-56.7)T-W6	-56.7	38
	W7	W-T/S/P/C-13TH-20.0T-W7	20.0	13
	W8	W-T/S/P/C-25TH-52.5T-W8	52.5	25
	W9	W-T/S/P/C-38TH-85.0T-W9	85.0	38

The specimens per combination were conditioned in a temperature and humidity controlled chamber. Each specimen was assigned an ID, e.g., W-T-25TH-93.3T-A2, where the first character is the specimen type (A-adhesive/W-welded), and the following character represents the test type (T-tensile/S-shear/P-peel/C-cleavage). The width of the specimens is denoted by 13TH, 25TH, and 38TH for 13 mm, 25 mm, and 38 mm specimen widths. The temperature of the conditioning chamber is represented by T, and the last character symbolizes the combination number shown in Table 4.1. The specimens having the same conditioning temperatures were placed collectively in the chamber for at least 24 hours to be conditioned before testing them. For instance, the specimens under the combinations A1, A2, A3, W1, W2, and W3, were conditioned in the chamber at 93.3°C together.

4.2 Welded Specimens

This section focuses on the fabrication and geometry of the tensile, shear, peel, and cleavage welded specimens. Note, the adhesive specimens for each of the tensile, shear, peel, and cleavage tests are described in Section 3.2.1.

The welded tensile, shear, peel, and cleavage specimens were designed according to the guidelines of AWS (AWS 2000) and ASTM D638 (2010), ASTM D1002 (2010), ASTM D1876 (2008), and ASTM D1062 (2008), respectively. All the specimens were manufactured by the local DMS producer in South Dakota using weld of 4043 aluminum alloy. The entirety of the dimensions was kept as close as possible to the adhesive specimens as described in Section 3.2.1. The sample welded tensile, shear, peel, and cleavage specimens with a width of 13 mm is shown in Figure 4.1. As in the adhesive specimens, the 5052 aluminum was used to fabricate all types of the specimens. Specifically, the tensile specimens were fabricated by joining two aluminum bars with 3.2 mm square groove welds in dogbone shape. Two 5052 aluminum metal bars with 6.4 mm thickness were overlapped and bonded by transverse fillet welds in the middle to build the shear specimens. To install the extensometer, a small piece of additional aluminum was glued to each of the welded shear specimens. The additional aluminum piece helps measure the shear strain accurately using the extensometer. The peel specimens were fabricated by bending two 5052 aluminum bars 90° up to 76 mm from the tail of the specimen. The bent aluminum bars were joined by 3.2 mm fillet welds up to the length of 229 mm. The cleavage specimens were manufactured by attaching two aluminum blocks with 6.35 mm fillet welds.

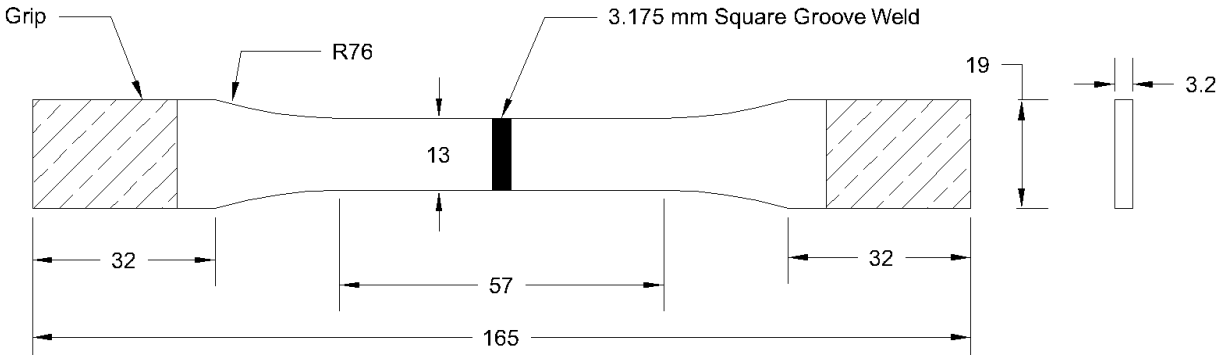

(a) (b)

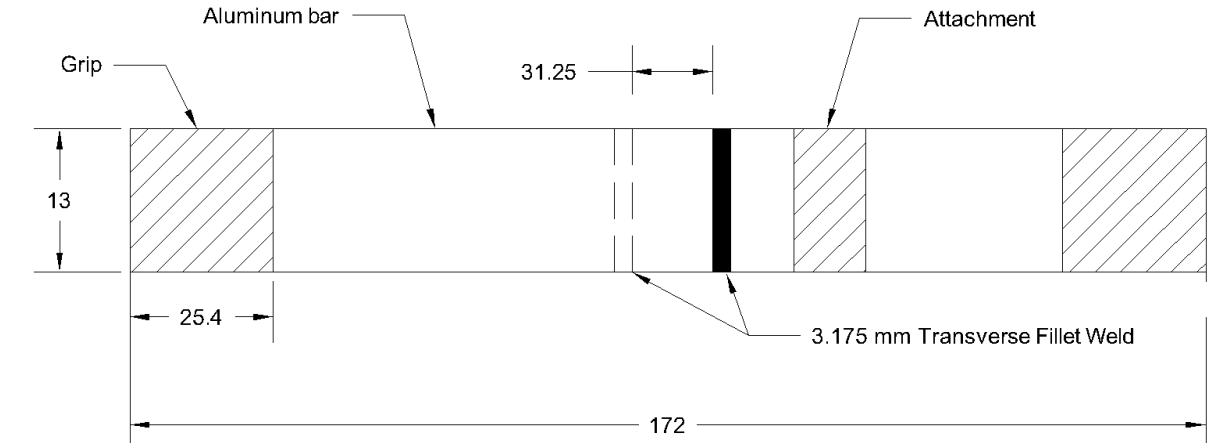
Aluminum bar
Attachment
Grip
31.25
13
25.4
3.175 mm Transverse Fillet Weld
172

(c)

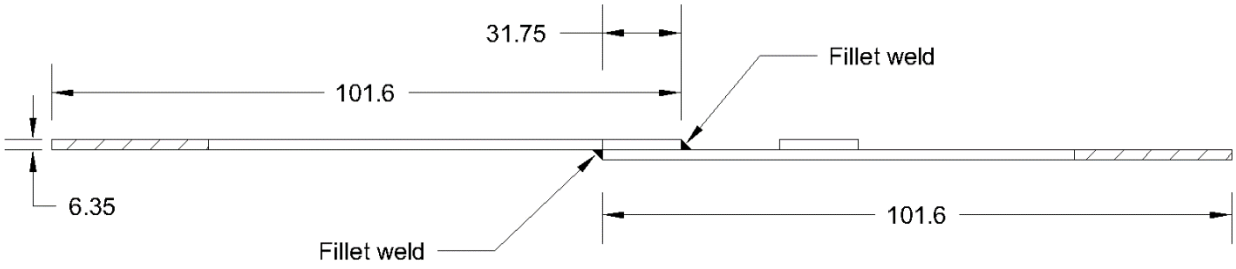
31.75
Fillet weld
101.6
6.35
Fillet weld
101.6

(d)

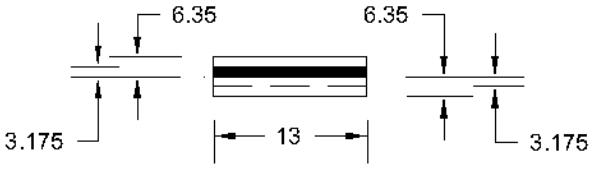
6.35
6.35
3.175
13
3.175

(e)

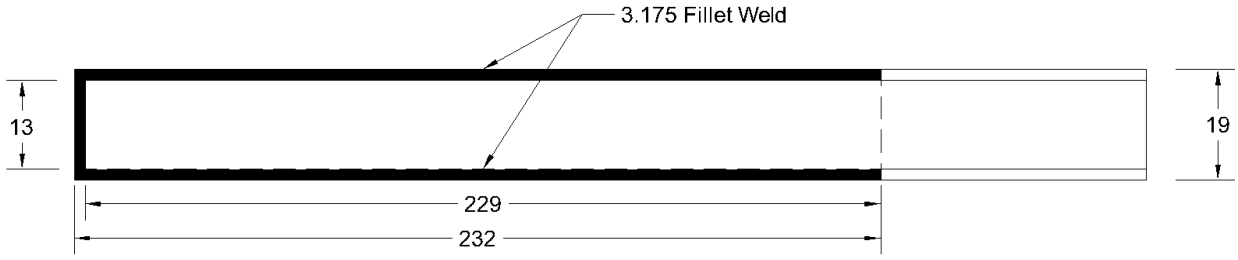
3.175 Fillet Weld
13
19
229
232

(f)

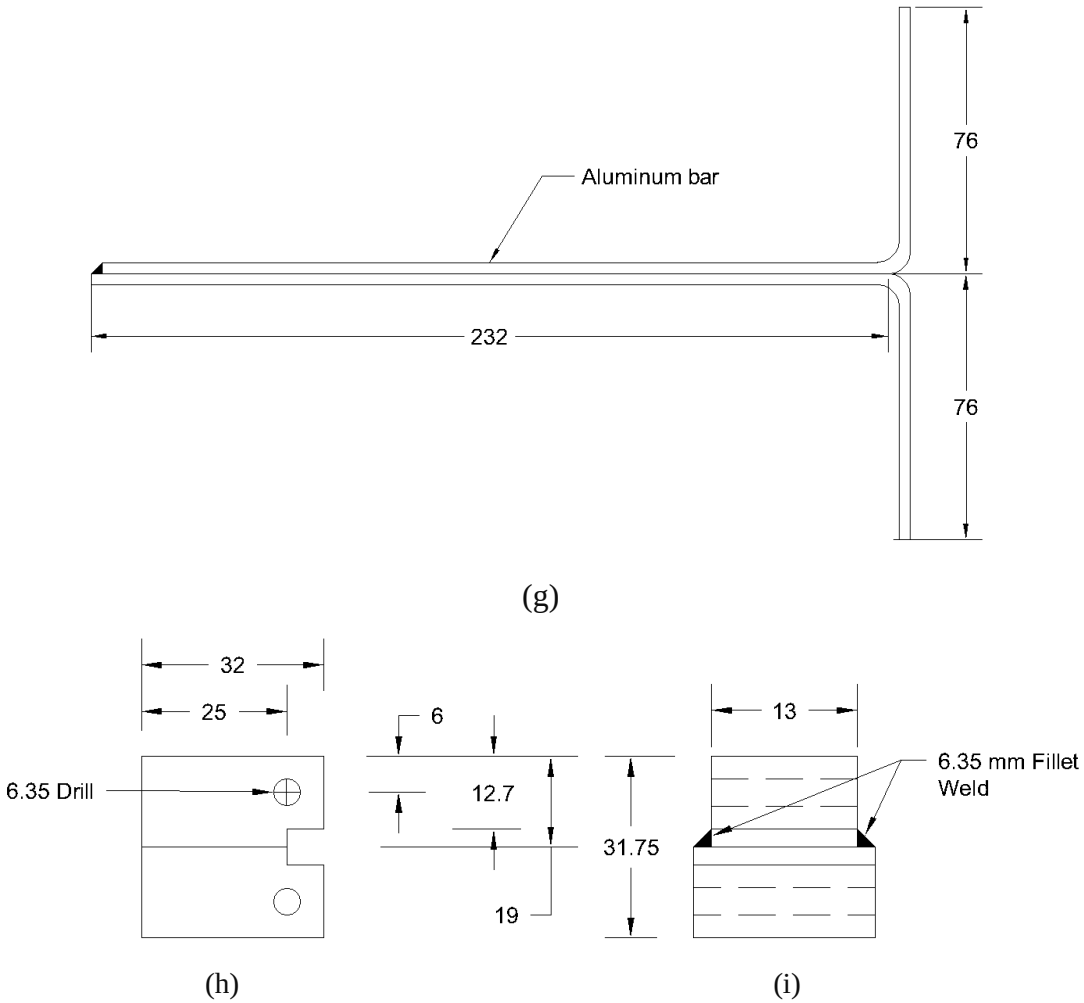

Figure 4.1 Geometry of welded test specimens (a) top view of tensile dogbone, (b) cross-section of tensile dogbone, (c) top view of single-lap shear, (d) side view of single-lap shear, (e) front view of single-lap shear, (f) top view of peel, (g) side view of peel, (h) side view of cleavage, and (i) front view of cleavage (All dimensions are in mm)

4.3 Testing

Two different MTS universal testing systems were utilized for the testing of specimens. This section encompasses the testing setups of tensile, shear, peel, and cleavage specimens with adhesive and welded connections. The welded specimens (W1 through W9) and the additional adhesive specimens (A1 through A6) were conditioned at different temperatures according to the combinations presented in Section 4.1; however, all tests were conducted at room temperature. Each specimen was fitted and supported by the grips of the MTS. The MTS 370 Landmark (MTS Systems Corporation 2018) was employed to perform the tensile, shear, and cleavage specimens. The MTS Insight 5 (MTS Systems Corporation 2019) was used for the peel specimens as displacement of the MTS needed to be higher than MTS 370 Landmark to conduct the peel tests. An extensometer (MTS 634.31F-24) with 20-mm gauge length was installed on each of the shear specimens. The loading for the tensile, shear, peel, and cleavage specimens were approximated with a free crosshead speed of 5 mm/min, 1.3 mm/min, 254 mm/min, and 1.27 mm/min, respectively. The tensile, shear, peel, and cleavage tests were performed following the specifications and testing procedures presented in ASTM D638 (2010), ASTM D1002 (2010), ASTM D1876 (2008), and

ASTM D1062 (2008), respectively. Figure 4.2 presents the testing arrangement for the tensile, shear, peel, and cleavage specimens.

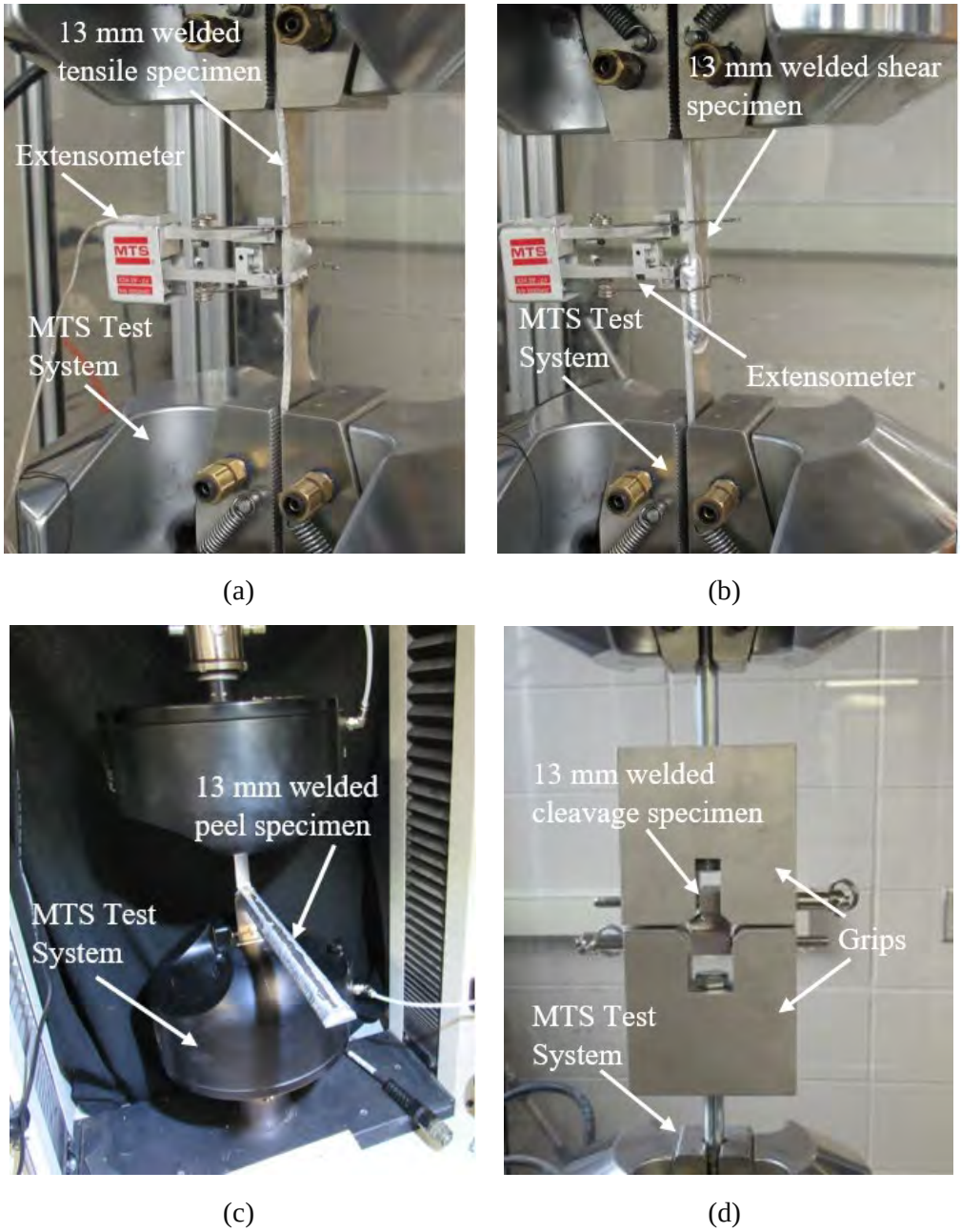

Figure 4.2 Installation of the welded specimens in the testing machine (a) tensile, (b) shear, (c) peel, and (d) cleavage

4.4 Results and Discussion

Results from the tensile, shear, peel, and cleavage tests are presented and discussed in this section. Stress-strain curves were plotted for each of the tests to calculate the strengths, and the influence of conditioning temperature and width on each of the strengths of both adhesive and welded specimens is graphically explained.

4.4.1 Tensile Test

Representative stress-strain curves for the adhesive and welded tensile specimens of 13-mm width at a conditioning temperature of -56.67°C are presented in Figure 4.3a and b, respectively. Ultimate tensile stresses were determined from the stress-strain curves for both adhesive and welded specimens. All the calculated ultimate tensile stresses at varying conditioning temperature and width are summarized in Table 4.2.

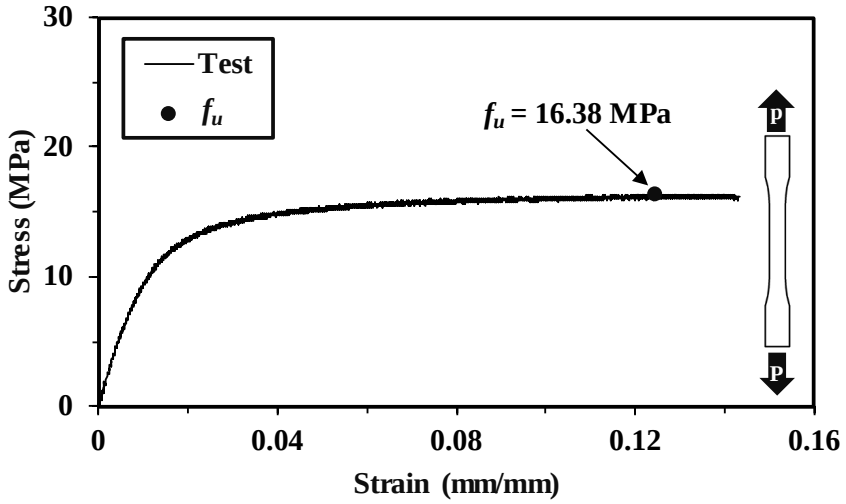

(a)

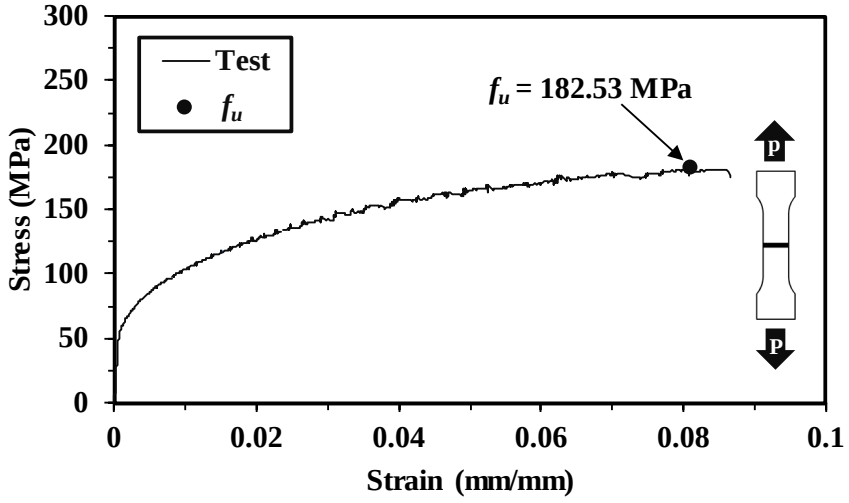

(b)

Figure 4.3 Representative stress-strain curves for tensile specimens (a) adhesive and (b) weld

Table 4.2 Ultimate tensile strength from the tensile test

Specimen type	Combination	Specimen ID	Ultimate tensile stress, f_u(MPa)
Adhesive	A1	A-T-13TH-93.3T-A1	20.76
	A2	A-T-25TH-93.3T-A2	21.28
	A3	A-T-38TH-93.3T-A3	20.40
	A4	A-T-13TH-(-56.7)T-A4	19.37
	A5	A-T-25TH-(-56.7)T-A5	19.62
	A6	A-T-38TH-(-56.7)T-A6	19.80
	C1	A-T-13TH-20.0T-C1	17.87
	C2	A-T-38TH-20.0T-C2	17.63
	C3	A-T-25TH-20.0T-C3	17.61
	C7	A-T-13TH-52.5T-C7	17.30
	C8	A-T-25TH-52.5T-C8	17.10
	C10	A-T-38TH-52.5T-C10	15.75
	C12	A-T-13TH-85.0T-C12	17.80
	C14	A-T-25TH-85.0T-C14	16.13
	C16	A-T-38TH-85.0T-C16	16.00
Welded	W1	W-T-13TH-93.3T-W1	117.74
	W2	W-T-25TH-93.3T-W2	110.84
	W3	W-T-38TH-93.3T-W3	122.77
	W4	W-T-13TH-(-56.7)T-W4	170.99
	W5	W-T-25TH-(-56.7)T-W5	116.45
	W6	W-T-38TH-(-56.7)T-W6	107.78
	W7	W-T-13TH-20.0T-W7	103.05
	W8	W-T-25TH-52.5T-W8	81.36
	W9	W-T-38TH-85.0T-W9	121.23

4.4.1.1 Effect of Conditioning Temperature

The effect of conditioning temperature on the ultimate tensile stress at different conditioning temperatures is shown in Figure 4.4. In Figure 4.4a, the ultimate stress for the adhesive tensile specimens with different widths is plotted against conditioning temperature. For 13-mm specimens, the ultimate stress decreases by 7.7% and 3.2% when the conditioning temperature increases from -56.67°C to 20°C and 20°C to 52.5°C, respectively. The ultimate stress, however, is increased by 2.9% and 16.7% when the conditioning temperature elevates from 52.5°C to 85°C and 85°C to 93.33°C as shown in A4-C1-C7-C12-A1. For 25-mm specimens, the ultimate stress declines by 10.3% and 2.9% when the conditioning temperature rises from -56.67°C to 20°C and 20°C to 52.5 °C. The ultimate stress of the 25-mm specimens is further reduced by 5.7% when the conditioning temperature increases from 52.5°C to 85°C. When the conditioning temperature was increased from 85°C to 93.33°C, the ultimate stress is increased significantly by 31.9% as displayed in A5-C3-C8-C14-A2. The ultimate stress of 38-mm specimens is decreased by 11% and 10.7% with an increment of conditioning temperature from -56.67°C to 20°C and 20°C to 52.5°C, simultaneously. The ultimate stress is increased by 1.6% and 27.5% when the

conditioning temperature was elevated from 52.5°C to 85°C and 85°C to 93.33°C, respectively as illustrated in A6-C2-C10-C16-A3.

In Figure 4.4b, the effect of conditioning temperature on the ultimate tensile stress for the welded tensile specimens with different widths is presented. The ultimate stress of 13-mm specimens is decreased by 39.7% when the conditioning temperature is raised from -56.67°C to 20°C; whereas, the ultimate stress is increased by 14.3% with a further elevation of conditioning temperature from 20°C to 93.33°C (see W4-W7-W1). The rise in conditioning temperature from -56.67°C to 52.5°C declined the ultimate stress of 25-mm specimens by 30.1%. The ultimate stress, however, increases by 36.2% when conditioning temperature is further elevated to 93.33°C from 52.5°C as shown in W5-W8-W2. For 38-mm specimens, the ultimate stress rises slightly by 12.5% when conditioning temperature is increased from -56.67°C to 85°C. The increment of conditioning temperature from 85°C to 93.33°C increased the ultimate stress by 1.3% as portrayed in W6-W9-W3. In this figure, the design tensile strength of the 4043 aluminum filler weld (165 MPa) acquired from the Aluminum Design Manual (Aluminum Association 2010) is observed to be higher for all the welded tensile specimens tested, except for 13 mm welded specimens conditioned at -56.67°C from combination W4. It was found that among the two specimens tested for combination W4, tensile stress of only one specimen was found to be higher than the design tensile strength (165 MPa) of the weld. Figure 4.5 shows the top view of welded tensile specimens from combination W4 fabricated with weld at the middle of the specimens. High ultimate tensile stress in the welded tensile specimens of combination W4 can be attributed to a residual weld at the top while welding the specimens. Further, the ultimate tensile stress of welded specimens for combination W8 was observed to be significantly low. The tested tensile specimens from combination W8 were carefully examined to determine the possible reason for this low tensile stress. The cross-section of the welded section after failure of the specimens is shown in Figure 4.6. The weld was not found to have penetrated well over the whole area of cross-section in the tensile specimens from combination W8. Because of this, the strength of the welded section was decreased due to inadequate penetration of the weld.

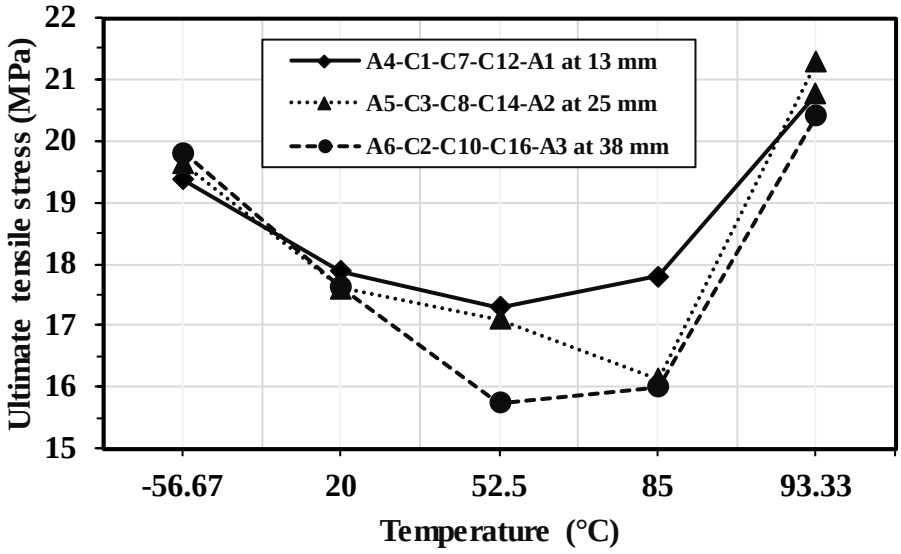

(a)

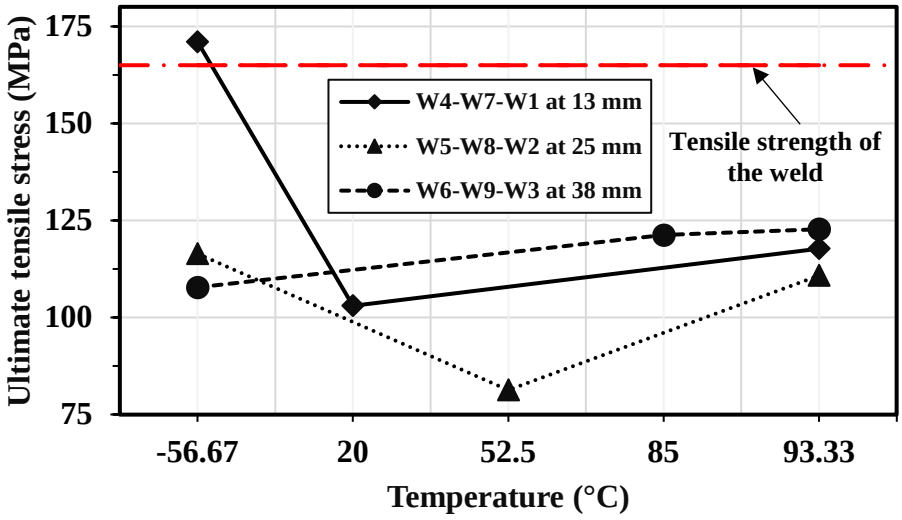

(b)

Figure 4.4 Effect conditioning temperature on ultimate stress for tensile specimens (a) adhesive and (b) weld

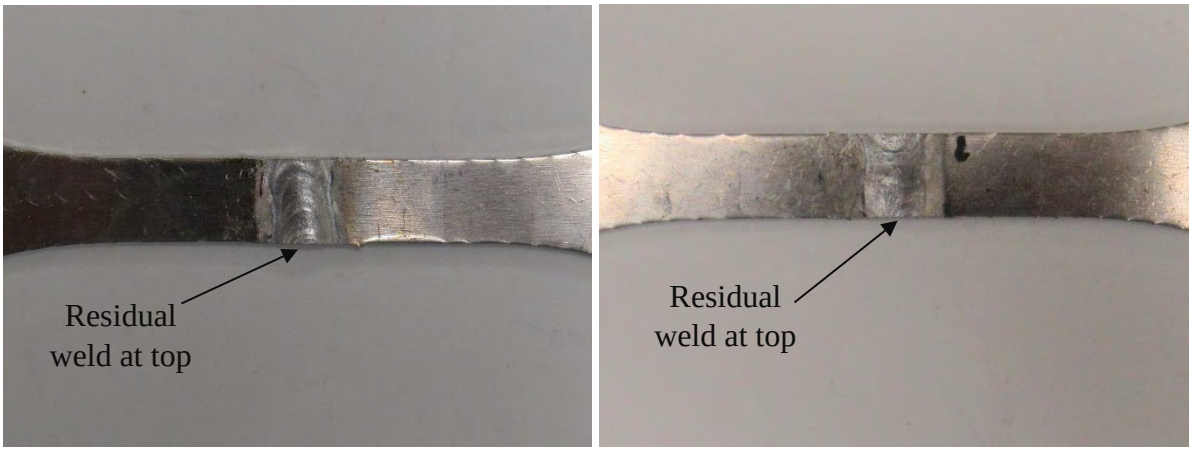

(a) (b)

Figure 4.5 Top view of welded tensile specimens from combination W4: (a) 1st specimen and (b) 2nd specimen

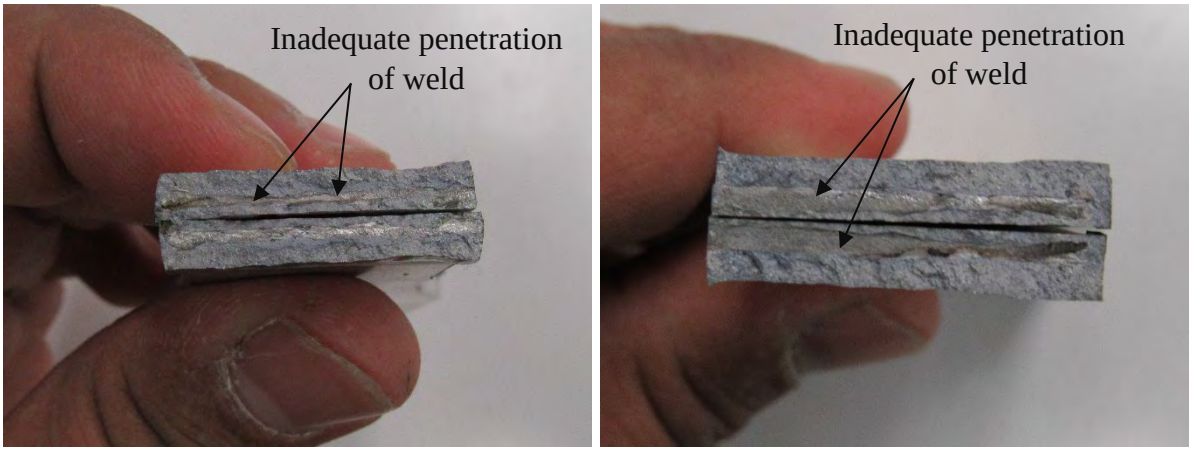

(a) (b)

Figure 4.6 Cross-section view of welded tensile specimens from combination W8: (a) 1st specimen and (b) 2nd specimen

4.4.1.2 Effect of Width

The effect of the specimen width on the ultimate tensile stress is shown in Figure 4.7. The ultimate stress for the adhesive tensile specimens having different widths at various conditioning temperatures is plotted in a bar chart in Figure 4.7a. At -56.67°C, the ultimate stress is increased by 1.3% and 0.9% when the specimen width increases from 13 mm to 25 mm and 25 mm to 38 mm, respectively, as shown in A4-A5-A6. The ultimate stress is decreased by 1.5% and increased by 0.1% with increment of specimen width from 13 mm to 25 mm and 25 mm to 38 mm at 20°C as shown in C1-C3-C2. For specimens at 52.5°C, the ultimate stress declines by 1.2% and 7.9% when width of the specimen increases from 13 mm to 25 mm and 25 mm to 38 mm as displayed in C7-C8-C10. The ultimate stress of specimens at 85°C is reduced by 9.4% and 0.8% as depicted in C12-C14-C16 with increment of specimen width from 13 mm to 25 mm and 25 mm to 38 mm. When the width of the specimens at 93.33°C is increased from 13 mm to

25 mm, the ultimate stress is increased by 2.5%; whereas, the ultimate stress decreases by 4.1% when the specimen width is increased from 25 mm to 38 mm as displayed in A1-A2-A3.

In Figure 4.7b, the effect of width on the ultimate stress for the welded tensile specimens at different conditioning temperatures is shown. The ultimate stress at -56.67°C is decreased by 31.9% and 7.4% with an increment of specimen width from 13 mm to 25 mm and 25 mm to 38 mm as displayed in W4-W5-W6. As shown in W1-W2-W3 at 93.33°C, the ultimate stress is decreased by 5.9% with increment of specimen width from 13 mm to 25 mm; however, the ultimate stress is increased by 10.8% with further increment of specimen width from 25 mm to 38 mm. The ultimate stress is decreased by 21.1% when the stress of 25-mm specimens at 52.5°C is compared with that of 13-mm specimens at 20°C (see W7 and W8). The comparison between 38-mm specimens at 85°C and 25-mm specimens at 52.5°C shows 49% increment in ultimate tensile stress (see W8 and W9). As shown in the figure, the design tensile strength of the welded specimens (165 MPa) is observed to be significantly higher than the tensile strength obtained from the testing, excluding 13-mm welded specimens conditioned at -56.67°C (combination W4). As mentioned previously, this can be attributed to a residual weld at the joint during the manufacturing process.

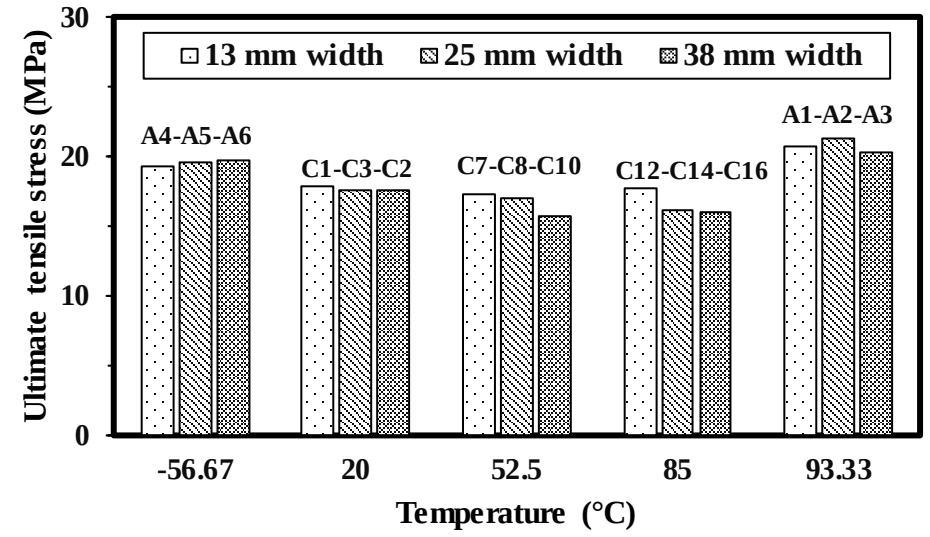

(a)

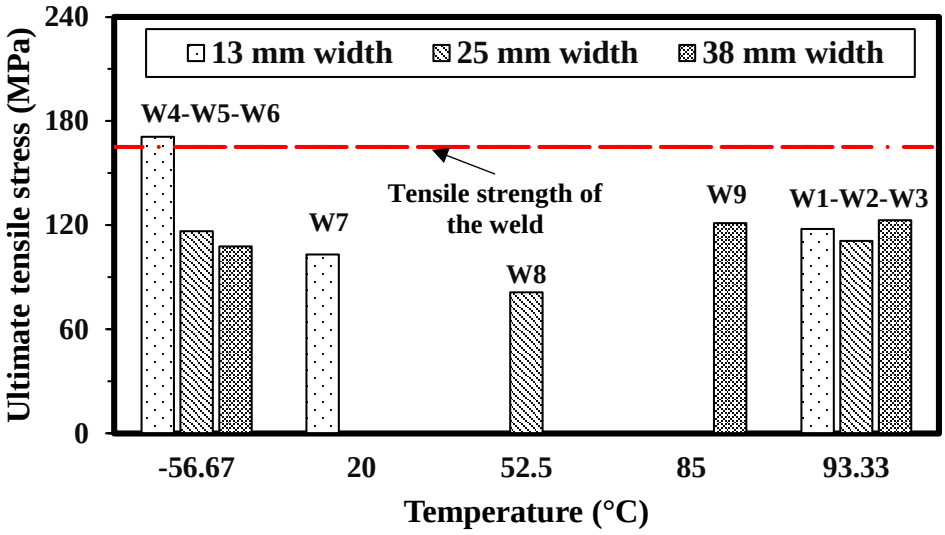

(b)

Figure 4.7 Width effect on ultimate stress for tensile specimens (a) adhesive and (b) weld

4.4.1.3 Comparison in Tensile Strength between Adhesive and Weld Specimens

Figure 4.8 shows a comparative representation of ultimate tensile stress between the adhesive and welded specimens. For 13-mm specimens, the welded specimens have significantly more ultimate stress than the adhesive specimens by 467%, 783%, and 477% at 93.33°C, -56.67°C, and 20°C, respectively, as displayed in pairs A1-W1, A4-W4, and C1-W7. The welded specimens with 25-mm width at 93.33°C, -56.67°C, and 52.5°C are observed to have 421%, 493%, and 376% higher ultimate tensile stress compared with the adhesive specimens as shown in pairs A2-W2, A5-W5, and C8-W8. For specimens at 93.33°C, -56.67°C, and 85°C, the welded specimens are found to have 502%, 444%, and 658% higher ultimate tensile stress relative to the adhesive specimens (see pairs A3-W3, A6-W6, and C16-W9).

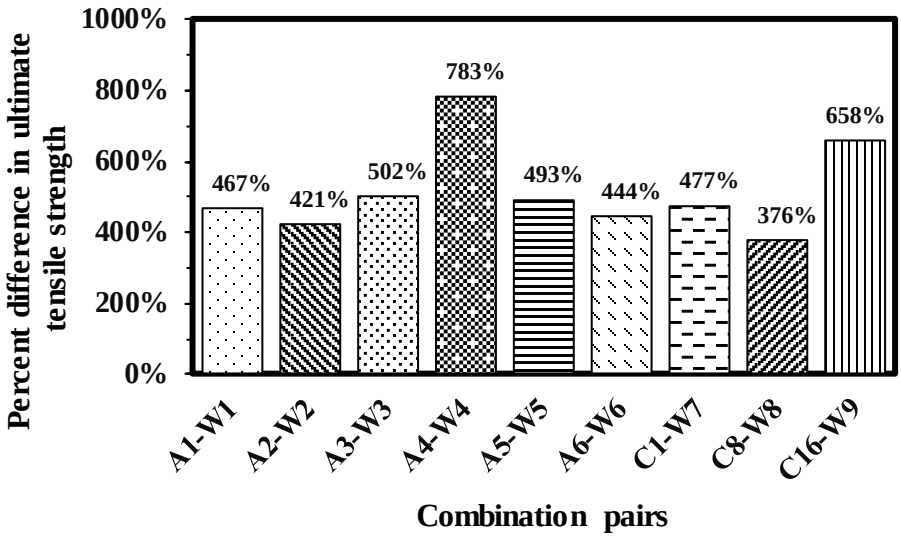

Figure 4.8 Percent difference in ultimate tensile stress between adhesive and welded specimens

4.4.2 Shear Test

Figure 4.9a and Figure 4.9b depict representative stress-strain curves for the shear adhesive and welded specimens of 13-mm width at a conditioning temperature of -56.67°C. The ultimate shear stress is determined from the stress-strain curve. The ultimate shear stresses at different conditioning temperatures and widths are listed in Table 4.3.

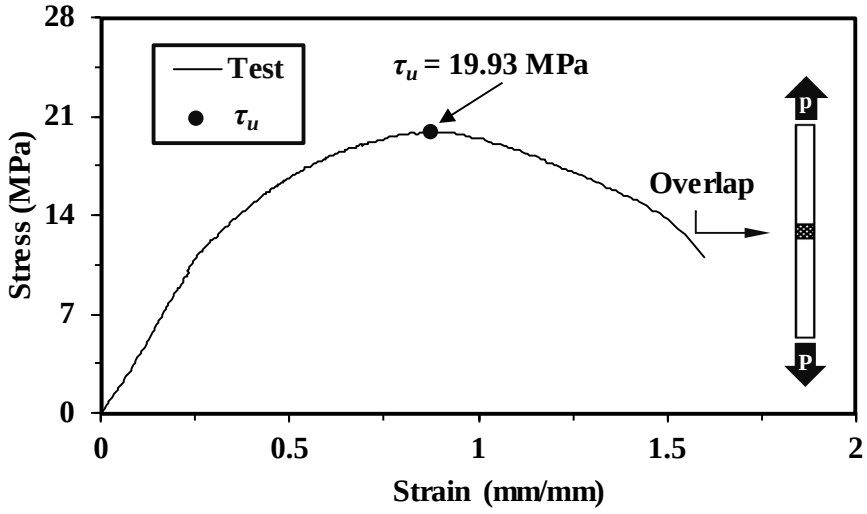

(a)

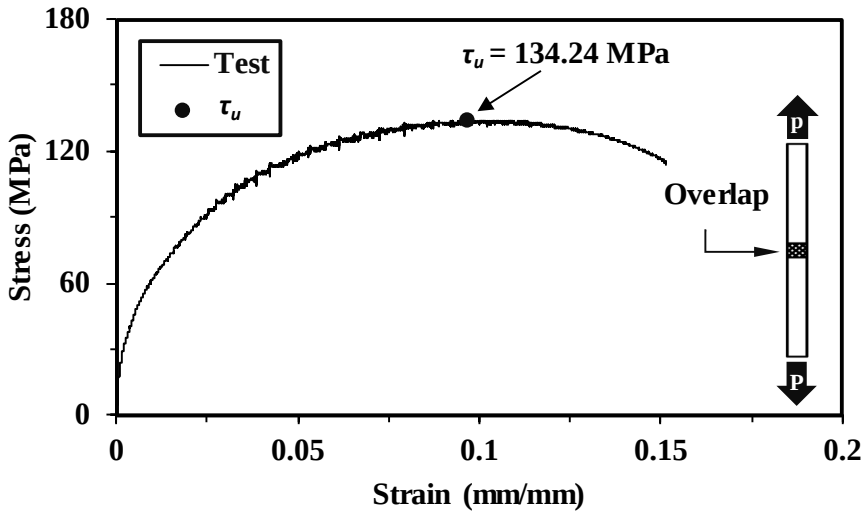

(b)

Figure 4.9 Representative stress-strain curves for shear specimens (a) adhesive and (b) welded

Table 4.3 Ultimate shear strength from the shear test

Specimen type	Combination	Specimen ID	Ultimate shear stress, τ_u (MPa)
Adhesive	A1	A-S-13TH-93.3T-A1	19.38
	A2	A-S-25TH-93.3T-A2	20.17
	A3	A-S-38TH-93.3T-A3	19.18
	A4	A-S-13TH-(-56.7)T-A4	18.68
	A5	A-S-25TH-(-56.7)T-A5	18.10
	A6	A-S-38TH-(-56.7)T-A6	18.39
	C1	A-S-13TH-20.0T-C1	17.48
	C2	A-S-38TH-20.0T-C2	16.06
	C3	A-S-25TH-20.0T-C3	17.97
	C7	A-S-13TH-52.5T-C7	16.00
	C8	A-S-25TH-52.5T-C8	14.96
	C10	A-S-38TH-52.5T-C10	17.84
	C12	A-S-13TH-85.0T-C12	17.05
	C14	A-S-25TH-85.0T-C14	15.47
	C16	A-S-38TH-85.0T-C16	15.41
Welded	W1	W-S-13TH-93.3T-W1	150.86
	W2	W-S-25TH-93.3T-W2	149.07
	W3	W-S-38TH-93.3T-W3	171.21
	W4	W-S-13TH-(-56.7)T-W4	134.16
	W5	W-S-25TH-(-56.7)T-W5	135.72
	W6	W-S-38TH-(-56.7)T-W6	134.79
	W7	W-S-13TH-20.0T-W7	147.21
	W8	W-S-25TH-52.5T-W8	150.76
	W9	W-S-38TH-85.0T-W9	144.56

4.4.2.1 Effect of Conditioning Temperature

Figure 4.10 illustrates the effect of conditioning temperature on the ultimate shear stress at several conditioning temperature conditions considered. The effect of conditioning temperature on the ultimate stress of the adhesive shear specimens is shown in Figure 4.10a. The ultimate stress of 13-mm shear specimens is decreased by 6.4% and 8.5% when the conditioning temperature is increased from -56.67°C to 20°C and 20°C to 52.5°C, subsequently. When the conditioning temperature increases from 52.5°C to 85°C and 85°C to 93.3 °C, successively, the ultimate stress is increased by 6.5% and 13.7%, as shown in A4-C1-C7-C12-A1. For 25-mm specimens, the ultimate stress is decreased by 0.7% and 16.8% with an increment of conditioning temperature from -56.67°C to 20°C and 20°C to 52.5°C. The ultimate stress of the 25-mm specimens increases by 3.4% and 30.4% when the conditioning temperature is increased from 52.5°C to 85°C and 85°C to 93.33°C (see A5-C3-C8-C14-A2). For 38-mm shear specimens, the ultimate stress reduces by 12.7% and increases by 11.1% when the conditioning temperature increases from -56.67°C to 20°C and 20°C to 52.5°C. The ultimate stress is reduced by 13.6% when the conditioning

temperature further increases from 52.5°C to 85°C; whereas, the ultimate stress is increased by 24.5% with an increment of conditioning temperature from 85°C to 93.33°C as shown in A6-C2-C10-C16-A3.

Figure 4.10b presents the conditioning temperature effect on the ultimate shear stress for the welded shear specimens. As shown in W4-W7-W1, the ultimate stress of 13-mm specimens is increased by 9.7% and 2.5% with the increment of conditioning temperature from -56.67°C to 20°C and 20°C to 93.33°C, successively. The ultimate stress of 25-mm specimens increases by 11.1% when conditioning temperature is increased from -56.67°C to 52.5°C but decreases by 1.1% with further increment in conditioning temperature from 52.5°C to 93.33°C (see W5-W8-W2). For 38-mm specimens, when the conditioning temperature was increased from -56.67°C to 85°C, the ultimate stress surged by 7.3%. The ultimate stress is increased by 18.4% when the conditioning temperature further increased from 85°C to 93.33°C as displayed in W6-W9-W3. Observing the general trend of tested welded shear specimens, an increase in conditioning temperature was found to have positive effects on the ultimate shear stress. Further, the shear stress of the welded shear specimens was found to be substantially higher than the design shear stress of the 4043 aluminum filler weld (80 MPa) calculated according to the Aluminum Design Manual (Aluminum Association 2010). It should be noted that the ultimate shear stress of welded shear specimens for combination W3 is observed to be noticeably high as depicted in Figure 4.10b. This can be explained from the fracture surface of weld analysis in shear specimens of W3 as shown in Figure 4.11. In this figure, weld in the shear specimens of combination W3 was not uniform throughout the weld length. One edge of the specimen consisted of uniform weld size; whereas, the other edge of the specimen had thicker weld size. Therefore, the shear specimens from combination W3 observed higher ultimate shear stress compared with specimens from the other combinations.

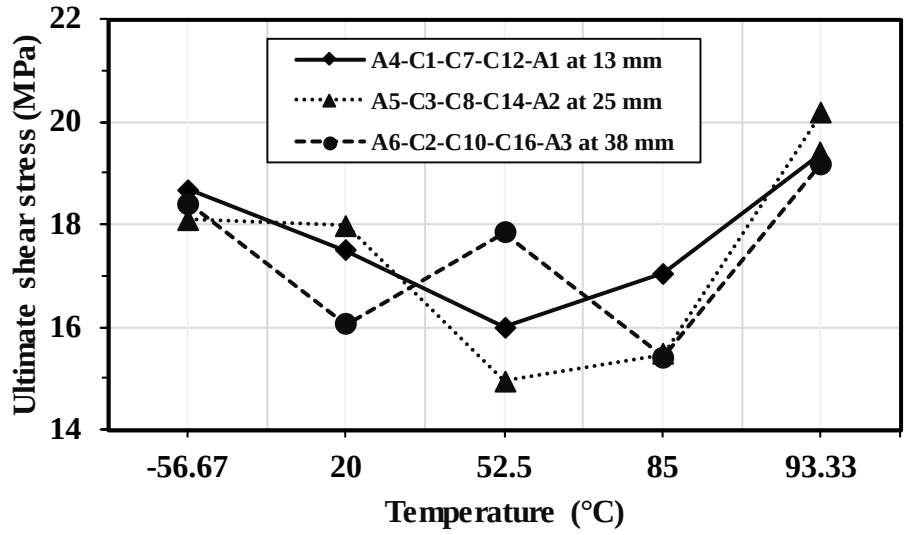

(a)

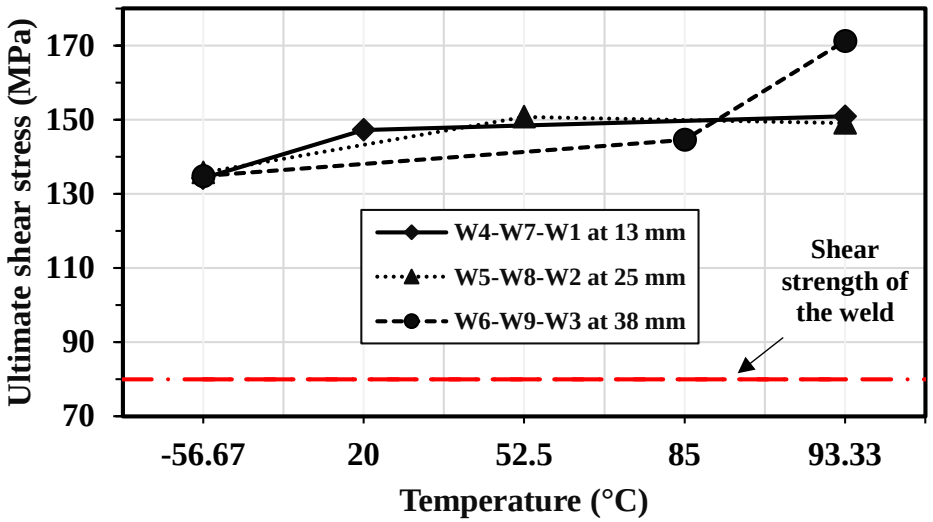

(b)

Figure 4.10 Effect of conditioning temperature on ultimate stress for shear specimens (a) adhesive and (b) weld

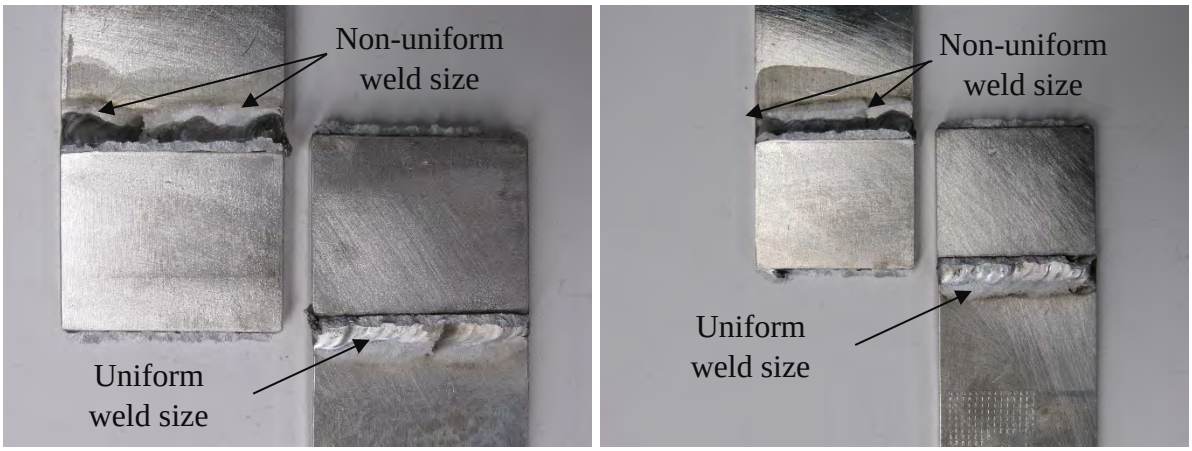

(a) (b)

Figure 4.11 Failure mode of welded shear specimens from combination W3: (a) 1st specimen and (b) 2nd specimen

4.4.2.2 Effect of Width

The effect of a specimen's width on the ultimate shear stress is shown in Figure 4.12 in a bar graph. Figure 4.12a shows the effect of width on the ultimate stress of the adhesive specimens at five distinct conditioning temperatures. The ultimate stress at -56.67°C reduces by 3.1% with an increment of specimen width from 13 mm to 25 mm. When the specimen width is increased from 25 mm to 38 mm, the ultimate stress is increased by 1.6% at -56.67°C as presented in A4-A5-A6. At 20°C, the ultimate stress is improved by 2.8% and decreased by 10.6% with the increment of specimen width from 13 mm to 25 mm and 25 mm to 38 mm as shown in C1-C3-C2. The ultimate stress of the specimens at 52.5°C is decreased by 6.5% and increased by 19.3% with the increment of specimen width from 13 mm to 25 mm and 25 mm to 38 mm as depicted in C7-C8-C10. At 85°C, when the specimen width is increased from 13 mm to 25 mm and 25 mm to 38 mm, the ultimate stress is decreased by 9.3% and 0.3%, respectively (see C12-C14-C16). The ultimate stress of specimens at 93.33°C increases by 4% when the specimen width is increased from 13 mm to 25 mm. The ultimate stress, however, decreases by 4.9% when the width of the specimen is increased from 25 mm to 38 mm as shown in A1-A2-A3.

In Figure 4.12b, the effect of width on the ultimate shear stress for the welded shear specimens at different conditioning temperatures is illustrated. The ultimate stress at -56.67°C is increased by 1.2% when the width of welded shear specimen is increased from 13 mm to 25 mm and is decreased by 0.7% with an increase of specimen width from 25 mm to 38 mm as shown in W4-W5-W6. At 93.33°C, the ultimate stress of welded specimens is decreased by 1.2% with the increment of specimen width from 13 mm to 25 mm; however, the ultimate stress increases by 14.9% with a further increase of specimen width from 25 mm to 38 mm as shown in W1-W2-W3. The 25-mm welded shear specimens at 52.5°C are observed to have 2.4% higher ultimate stress than 13-mm welded shear specimens at 20°C (see W7 and W8). The 38-mm welded shear specimens at 85°C are observed to have 4.1% lower ultimate stress than the 25-mm specimens at 52.5°C (see W8 and W9).

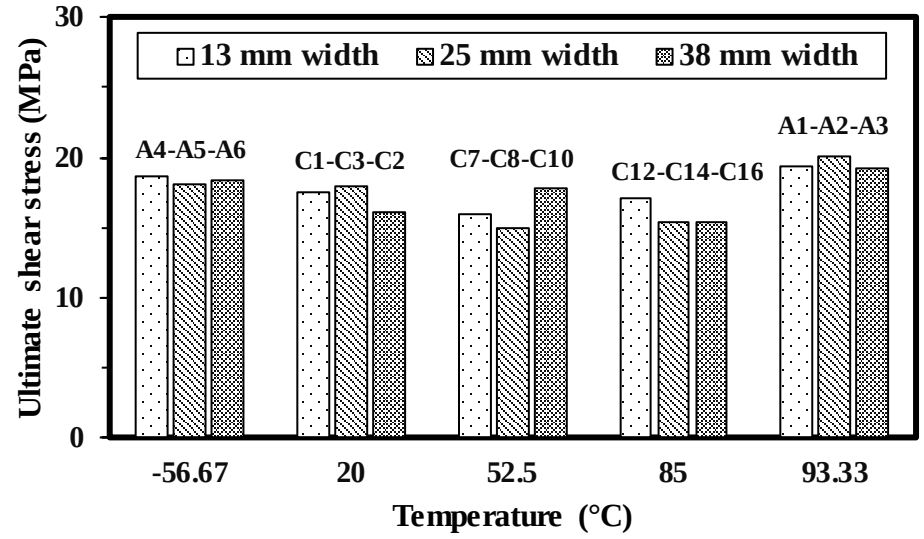

(a)

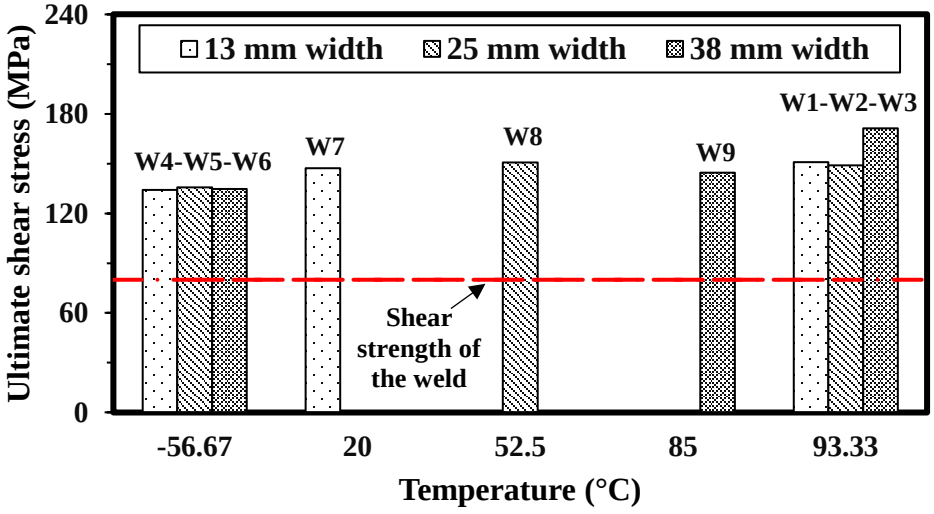

(b)

Figure 4.12 Width effect on ultimate stress for shear specimens (a) adhesive and (b) weld

4.4.2.3 Comparison in Shear Strength between Adhesive and Welded Specimens

A graphical comparison of the ultimate shear stress between the adhesive and welded shear specimens is shown in Figure 4.13. The 13-mm welded shear specimens are observed to have 678% higher shear stress than the adhesive specimens at 93.33°C as shown in pair A1-W1. At -56.67°C and 20°C, the 13 mm welded specimens are found to be stronger than the adhesive specimens by 618% and 742%, respectively, as shown in pairs A4-W4 and C1-W7. The 25 mm welded specimens at 93.33°C, -56.67°C, and 52.5°C observed 639%, 650%, and 908% higher ultimate shear stress in comparison to the adhesive specimens as displayed in pairs A2-W2, A5-W5, and C8-W8. For 38-mm specimens at 93.33°C, -56.67°C, and 85°C, the welded specimens are found to have, respectively, 792%, 633%, and 838% higher ultimate shear stress compared with the adhesive specimens (see pairs A3-W3, A6-W6, and C16-W9).

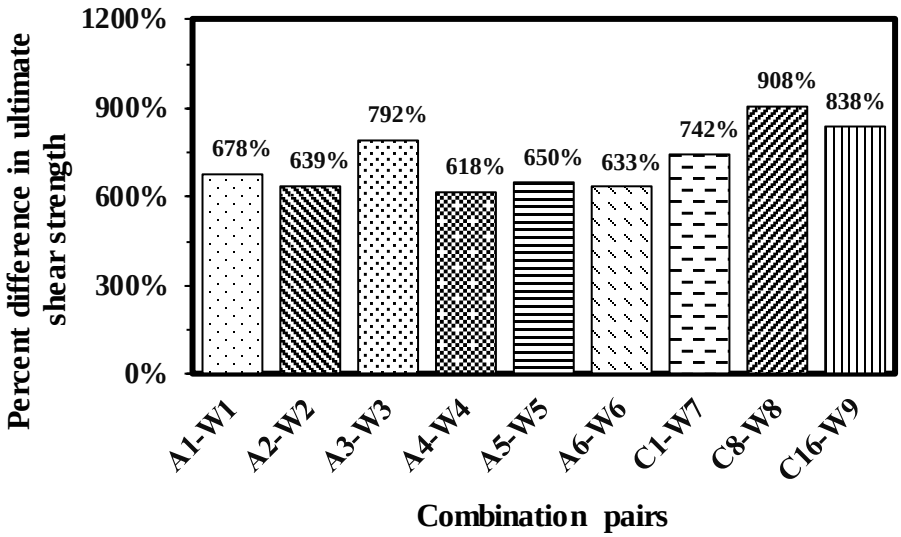

Figure 4.13 Percent difference in ultimate shear stress between adhesive and welded specimens

4.4.3 Peel Test

Figure 4.14 presents representative load-displacement curves for the peel specimens of 13-mm width at a conditioning temperature of -56.67°C. The peel strengths of the adhesive and welded peel specimens tested for all the combinations are tabulated in Table 4.4. A discussion on the effect of conditioning temperature and width on the peel strength of both the adhesive and welded peel specimens, and its comparison, is provided in the following subsections.

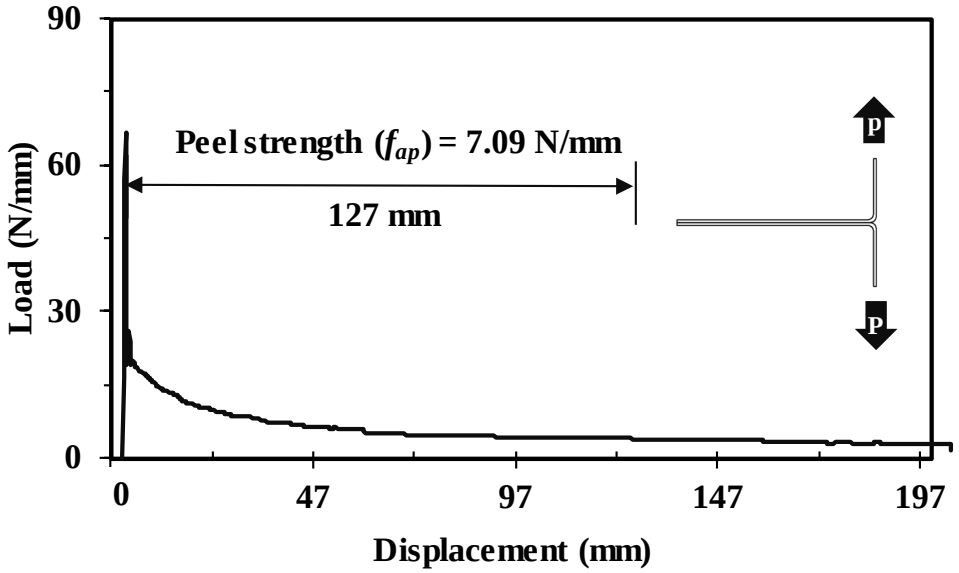

(a)

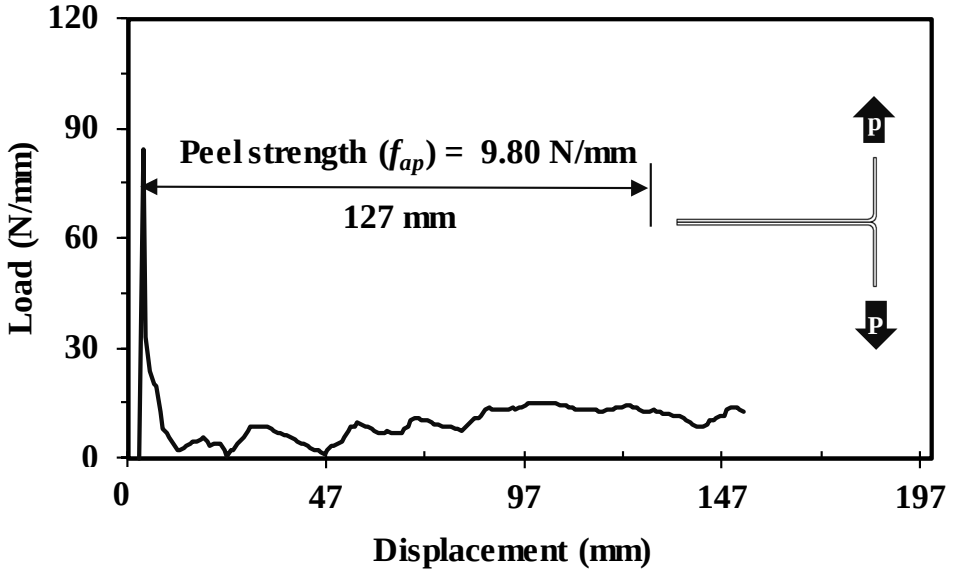

(b)

Figure 4.14 Representative load-displacement curve for peel specimens (a) adhesive and (b) welded

Table 4.4 Peel strength from the peel test

Specimen type	Combination	Specimen ID	Peel strength, f_{ap} (N/mm)
Adhesive	A1	A-P-13TH-93.3T-A1	5.06
	A2	A-P-25TH-93.3T-A2	5.26
	A3	A-P-38TH-93.3T-A3	3.47
	A4	A-P-13TH-(-56.7)T-A4	5.42
	A5	A-P-25TH-(-56.7)T-A5	6.61
	A6	A-P-38TH-(-56.7)T-A6	5.34
	C1	A-P-13TH-20.0T-C1	8.10
	C2	A-P-38TH-20.0T-C2	5.82
	C3	A-P-25TH-20.0T-C3	4.41
	C7	A-P-13TH-52.5T-C7	7.73
	C8	A-P-25TH-52.5T-C8	7.51
	C10	A-P-38TH-52.5T-C10	6.10
	C12	A-P-13TH-85.0T-C12	6.79
	C14	A-P-25TH-85.0T-C14	7.63
	C16	A-P-38TH-85.0T-C16	6.16
Welded	W1	W-P-13TH-93.3T-W1	40.42
	W2	W-P-25TH-93.3T-W2	14.67
	W3	W-P-38TH-93.3T-W3	4.52
	W4	W-P-13TH-(-56.7)T-W4	16.06
	W5	W-P-25TH-(-56.7)T-W5	19.98
	W6	W-P-38TH-(-56.7)T-W6	10.74
	W7	W-P-13TH-20.0T-W7	65.88
	W8	W-P-25TH-52.5T-W8	35.80
	W9	W-P-38TH-85.0T-W9	14.81

4.4.3.1 Effect of Conditioning Temperature

The effect of conditioning temperature on the peel strength of both the adhesive and welded specimens is shown in Figure 4.15. The behavior of adhesive specimens on the peel strength due to the effect of conditioning temperature is depicted in Figure 4.15a. The peel strength of 13-mm specimens is increased by 49.7% with the increment of conditioning temperature from -56.67°C to 20°C. When the conditioning temperature is further increased from 20°C to 52.5°C, 52.5°C to 85°C, and 85°C to 93.33°C, the peel strength declines by 4.7%, 12.2%, and 25.5%, respectively, as shown in A4-C1-C7-C12-A1. For 25-mm specimens, the decrement in the peel strength is 33.3% when the conditioning temperature elevates from -56.67°C to 20°C. The peel strength is increased by 70.4% and 1.6% with an additional increment of conditioning temperature from 20°C to 52.5°C and 52.5°C to 85°C, respectively. However, the peel strength decreases significantly by 31.1% when the conditioning temperature increases by 85°C to 93.33°C as depicted in A5-C3-C8-C14-A2. The peel strength of 38-mm specimens improved by 8.9%, 4.8%, and 1.0% with an elevation of conditioning temperature from -56.67°C to 20°C, 20°C to 52.5°C,

and 52.5°C to 85°C. The peel strength decreases by 43.7% when the conditioning temperature increases from 85°C to 93.33°C (see A6-C2-C10-C16-A3).

The influence of conditioning temperature on the peel strength of the welded specimens is presented in Figure 4.15b. Note, the design peel strength of the 4043 aluminum filler weld was not incorporated in this figure as no such information has been provided in the Aluminum Design Manual (Aluminum Association 2010). For the 13-mm specimens, the peel strength is raised substantially by 310.3% with the increment of conditioning temperature from -56.67°C to 20°C; however, it is decreased by 38.7% when conditioning temperature is increased from 20°C to 93.33°C as shown in W4-W7-W1. The peel strength of 25-mm welded specimens is increased by 79.1% when conditioning temperature is increased from -56.67°C to 52.5°C; whereas, the peel strength is decreased by 59.0% with a further elevation of conditioning temperature from 52.5°C to 93.33°C as shown in W5-W8-W2. As shown in W6-W9-W3, the peel strength of 38-mm welded specimens is increased by 37.9% with the increase of conditioning temperature from -56.67°C to 85°C. The increment of conditioning temperature from 85°C to 93.33°C decreased the peel strength by 69.5%.

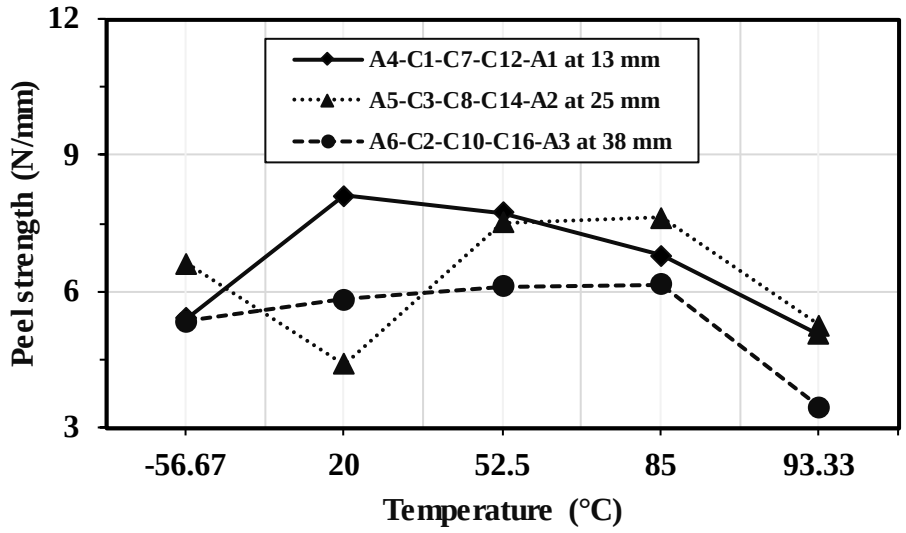

(a)

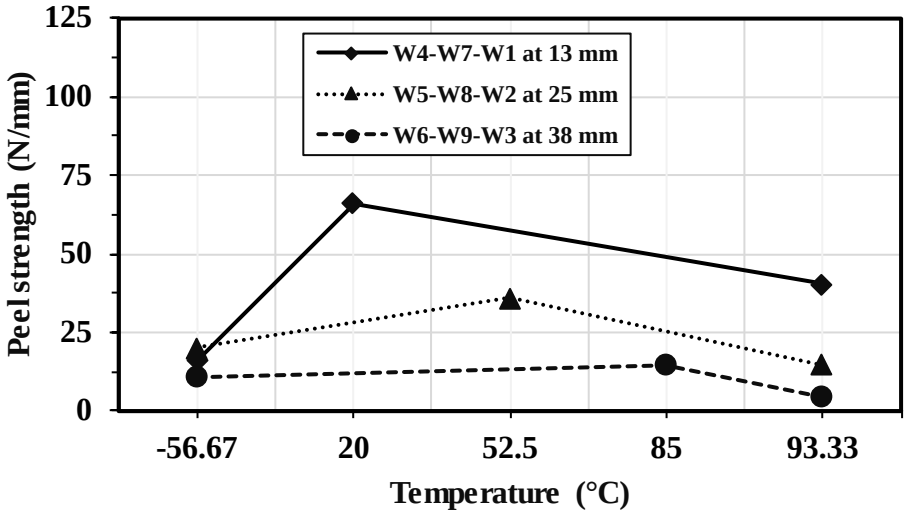

(b)

Figure 4.15 Effect of conditioning temperature on peel strength (a) adhesive and (b) weld

4.4.3.2 Effect of Width

The effect of width on the peel strength of the adhesive and welded specimens is shown in Figure 4.16. The peel strength for the adhesive peel specimens of different widths at various conditioning temperatures is plotted in a bar chart in Figure 4.16a. At -56.67°C, the peel strength is increased by 22.1% and decreased by 19.2% when the specimen width increases from 13 mm to 25 mm and 25 mm to 38 mm, respectively, as shown in A4-A5-A6. The peel strength is decreased by 45.6% and increased by 32% with an increment of specimen width from 13 mm to 25 mm and 25 mm to 38 mm at 20 °C as shown in C1-C3-C2. For the specimens at 52.5 °C, the peel strength declines by 2.8% and 18.8% when width of specimen increases from 13 mm to 25 mm and 25 mm to 38 mm as displayed in C7-C8-C10. The peel strength of specimens at 85°C is improved by 12.5% but reduced by 19.2%, as depicted in C12-C14-C16, with an increment of specimen width from 13 mm to 25 mm and 25 mm to 38 mm. When the width of the specimen at 93.33°C is increased from 13 mm to 25 mm, the peel strength is increased by 4.1% only;

whereas, the peel strength decreases by 34.1% when the specimen width is increased from 25 mm to 38 mm as displayed in A1-A2-A3.

In Figure 4.16b, the effect of width on the peel strength for the welded peel specimens at different conditioning temperatures is shown. The peel strength at -56.67°C is increased by 24.4% and decreased by 46.2% with an increment of specimen width from 13 mm to 25 mm and 25 mm to 38 mm, respectively, as displayed in W4-W5-W6. As shown in W1-W2-W3, at 93.33°C, the peel strength is decreased by 63.7% with an increment of specimen width from 13 mm to 25 mm and is further decreased by 69.2% with an increment of specimen width from 25 mm to 38 mm. The peel strength is decreased by 45.7% when the peel strength of the 25-mm welded specimens at 52.5°C is compared with that of the 13-mm welded specimens at 20°C (see W7 and W8). The comparison between the 38-mm specimens at 85°C and 25-mm specimens at 52.5°C shows a 58.6% decrement in peel strength (see W8-W9).

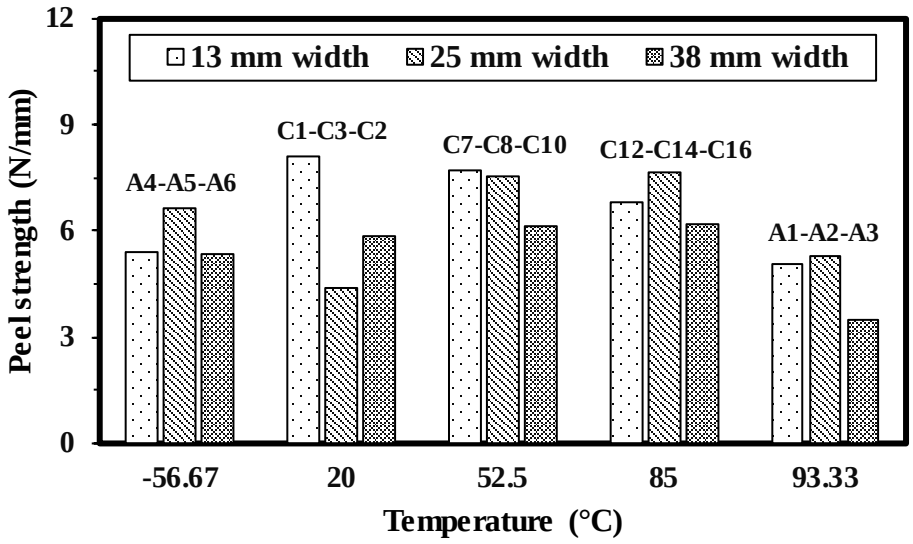

(a)

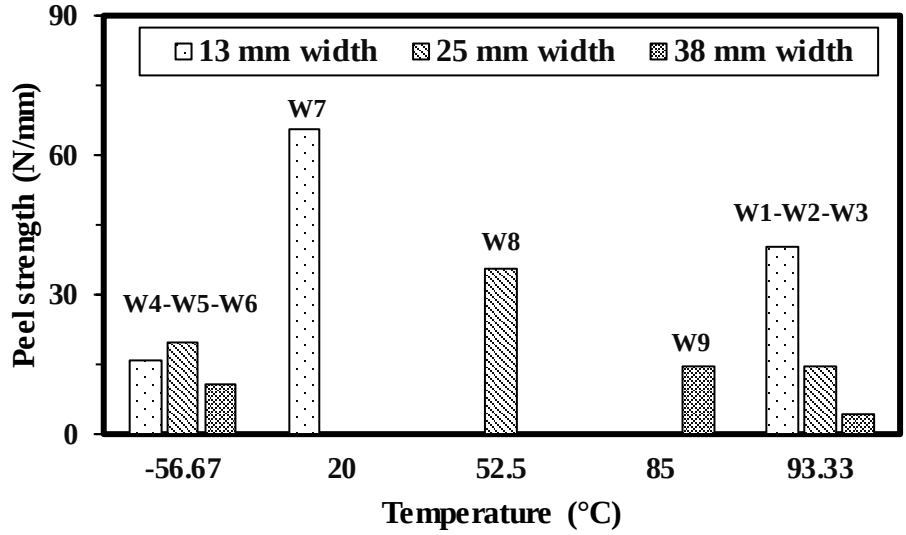

(b)

Figure 4.16 Width effect on peel strength for peel specimens (a) adhesive and (b) weld

4.4.3.3 Comparison in Peel Strength between Adhesive and Welded Specimens

Figure 4.17 shows a comparative representation of peel strength between the adhesive and welded peel specimens. For the 13-mm specimens, the welded specimens are more resilient than the adhesive specimens by 699%, 197%, and 713% at 93.33°C, -56.67°C, and 20°C, individually, as displayed in pairs A1-W1, A4-W4, and C1-W7. The 25-mm welded specimens at 93.33°C, -56.67°C, and 52.5°C were found to have 179%, 202%, and 376% higher peel strength compared with the adhesive specimens as shown in pairs A2-W2, A5-W5, and C8-W8. For the 38-mm specimens at 93.33°C, -56.67°C, and 85°C, the welded specimens are observed to have 30%, 101%, and 140% higher peel strength compared with the adhesive specimens (see pairs A3-W3, A6-W6, and C16-W9).

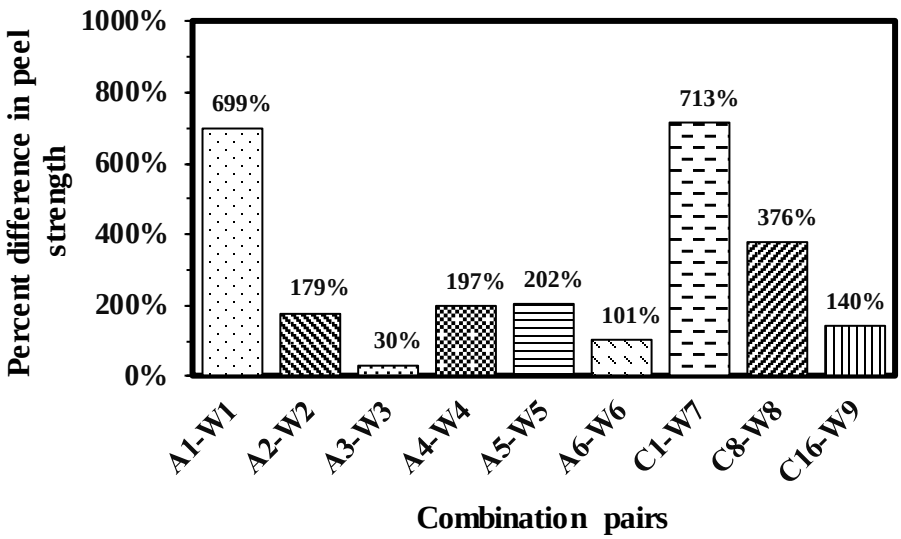

Figure 4.17 Percent difference in peel strength between adhesive and welded specimens

4.4.4 Cleavage Test

Load-displacement curves for each of the cleavage specimens tested were drawn from the testing data. Figure 4.18 shows representative load-displacement curves for the adhesive and welded cleavage specimens of 13-mm width at -56.67°C. The cleavage strengths at a variety of conditioning temperatures and widths for adhesive and welded cleavage specimens are presented in Table 4.5.

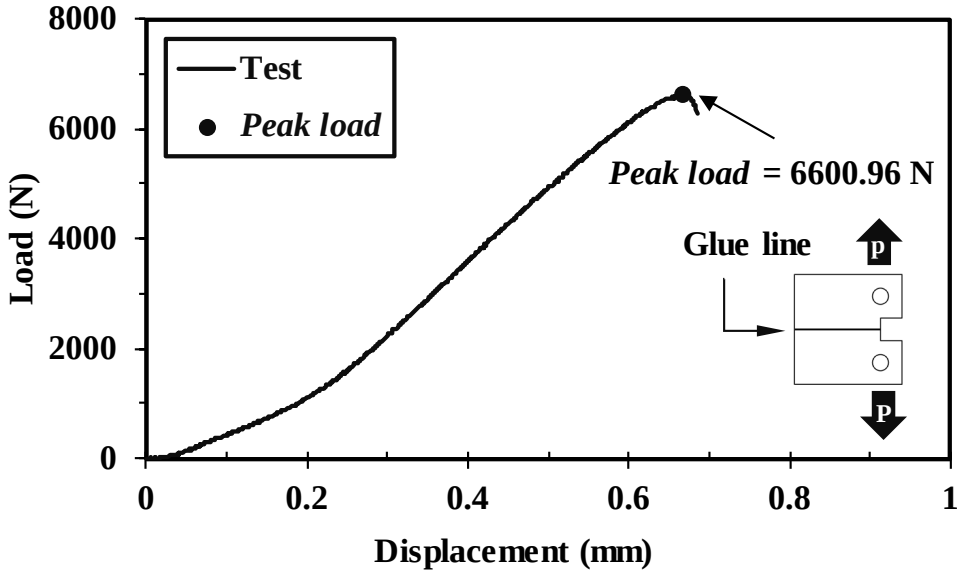

(a)

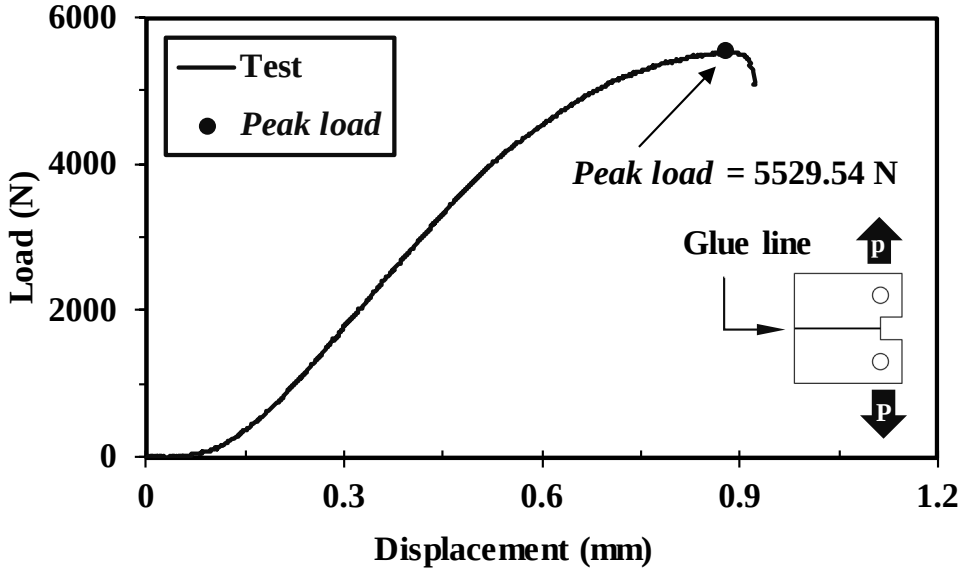

(b)

Figure 4.18 Load-displacement curve for cleavage specimens (a) adhesive and (b) welded

Table 4.5 Cleavage strength from the cleavage test

Specimen type	Combination	Specimen ID	Cleavage strength (N/mm)
Adhesive	A1	A-C-13TH-93.3T-A1	261.19
	A2	A-C-25TH-93.3T-A2	260.17
	A3	A-C-38TH-93.3T-A3	236.44
	A4	A-C-13TH-(-56.7)T-A4	242.24
	A5	A-C-25TH-(-56.7)T-A5	201.12
	A6	A-C-38TH-(-56.7)T-A6	215.30
	C1	A-C-13TH-20.0T-C1	173.52
	C2	A-C-38TH-20.0T-C2	191.19
	C3	A-C-25TH-20.0T-C3	195.01
	C7	A-C-13TH-52.5T-C7	198.32
	C8	A-C-25TH-52.5T-C8	198.11
	C10	A-C-38TH-52.5T-C10	254.55
	C12	A-C-13TH-85.0T-C12	220.62
	C14	A-C-25TH-85.0T-C14	188.74
	C16	A-C-38TH-85.0T-C16	202.82
Welded	W1	W-C-13TH-93.3T-W1	453.77
	W2	W-C-25TH-93.3T-W2	217.07
	W3	W-C-38TH-93.3T-W3	162.76
	W4	W-C-13TH-(-56.7)T-W4	499.92
	W5	W-C-25TH-(-56.7)T-W5	253.82
	W6	W-C-38TH-(-56.7)T-W6	148.23
	W7	W-C-13TH-20.0T-W7	449.88
	W8	W-C-25TH-52.5T-W8	216.42
	W9	W-C-38TH-85.0T-W9	191.13

4.4.4.1 Effect of Conditioning Temperature

The influence of conditioning temperature on cleavage strength is illustrated in Figure 4.19. In Figure 4.19a, the effect of conditioning temperature on cleavage strength of adhesively bonded cleavage specimens is presented. The cleavage strength of 13-mm specimens is observed to be decreased by 28.4% with the increase in conditioning temperature from -56.67 °C to 20 °C. The cleavage strength is elevated by 14.3% when the conditioning temperature increases beyond 20°C to 52.5°C. With further increment of conditioning temperature from 52.5°C to 85°C and 85°C to 93.33°C, the cleavage strength of adhesive specimens is increased by 11.2% and 18.4%, respectively, as depicted in A4-C1-C7-C12-A1. The cleavage strength of 25-mm specimens is decreased by 3% when conditioning temperature of the specimens is increased from -56.67°C to 20°C and increased by 1.6% with further increment of conditioning temperature from 20°C to 52.5°C. The cleavage strength is decreased by 4.7% and increased by 37.8% when conditioning temperature increases from 52.5°C to 85°C and 85°C to 93.33°C (see A5-C3-C8-C14-A2). For the 38-mm cleavage specimens, the strength is decreased by 11.2% when conditioning temperature is raised from -56.67°C to 20°C; however, it is increased by 33.1% when

conditioning temperature rises from 20°C to 52.5°C. The cleavage strength is observed to be decreased by 20.3% and increased by 16.6% with the increment of conditioning temperature from 52.5°C to 85°C and 85°C to 93.33°C (see A6-C2-C10-C16-A3).

The effect of conditioning temperature for welded specimens on cleavage strength is displayed in Figure 4.19b. Note, the design cleavage strength of the 4043 aluminum filler weld was not incorporated in this figure as no such information has been provided in the Aluminum Design Manual (Aluminum Association 2010). When the conditioning temperature is increased from -56.67°C to 20°C, the strength for 13-mm welded specimens is declined by 10%; whereas, additional increment of conditioning temperature from 20°C to 93.33°C raised the cleavage strength only by 0.9% as shown in W4-W7-W1. With the elevation of conditioning temperature from -56.67°C to 52.5°C for the 25-mm specimens, the strength is decreased by 14.7%; however, the strength is slightly increased by 0.3% when conditioning temperature increases from 52.5°C to 93.33°C as portrayed in W5-W8-W2. In W6-W9-W3 for 38-mm specimens, it is observed that the strength is increased by 28.9% with the increment of conditioning temperature from -56.67°C to 85°C; whereas, it is decreased by 14.8% when conditioning temperature increases from 85°C to 93.33°C.

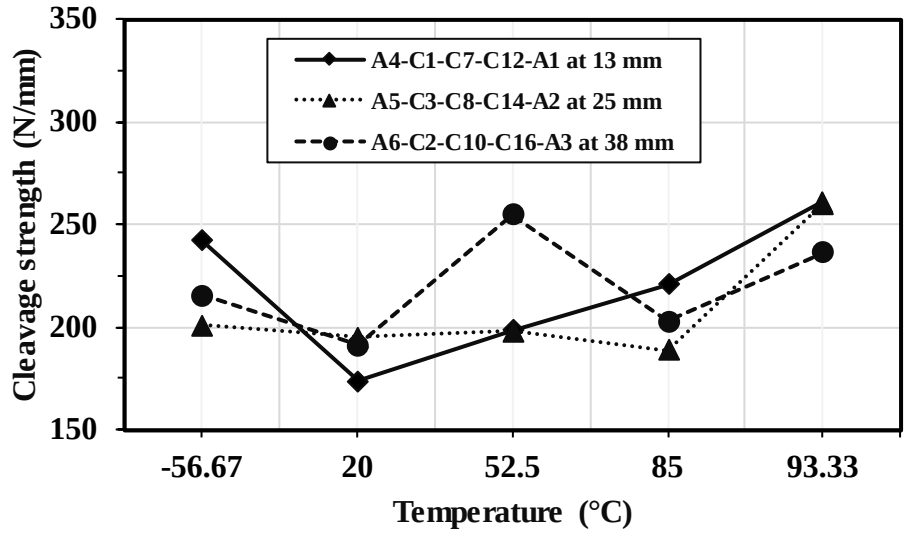

(a)

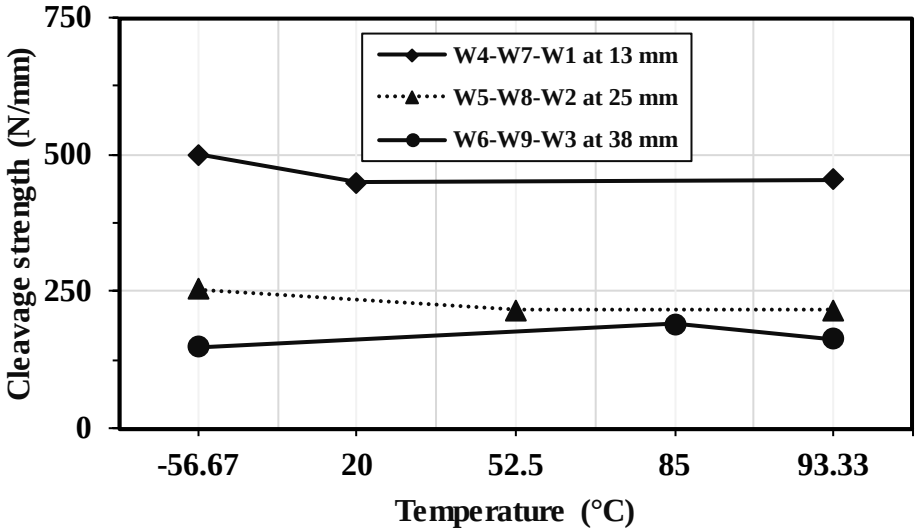

(b)

Figure 4.19 Effect of conditioning temperature on cleavage strength (a) adhesive and (b) weld

4.4.4.2 Effect of Width

The effect of specimen width on cleavage strength is shown in Figure 4.20 in the form of a bar chart. Figure 4.20a shows the effect of width in the strength of adhesive specimens at different conditioning temperatures taken for study. The cleavage strength at -56.67°C reduces by 17% with an increment of specimen width from 13 mm to 25 mm, but the strength is increased by 7.1% at -56.67°C with the increment from 25 mm to 38 mm width as presented in A4-A5-A6. At 20°C, the strength is improved by 12.4% and decreased by 2% with the increment of specimen width from 13 mm to 25 mm and 25 mm to 38 mm as shown in C1-C3-C2. The strength of the specimens at 52.5°C is only decreased by 0.1%, but increased by 28.5% with the increment of specimen width from 13 mm to 25 mm and 25 mm to 38 mm (see C7-C8-C10). At 85°C, when the specimen width is increased from 13 mm to 25 mm, the strength is decreased by 14.4% and increased by 7.5% when the specimen width is increased from 25 mm to 38 mm

(refer to C12-C14-C16). The strength at 93.33°C decreases by 0.4% and 9.1% when the specimen width is increased from 13 mm to 25 mm and 25 mm to 38 mm as shown in A1-A2-A3.

In Figure 4.20b, the effect of width on cleavage strength for welded cleavage specimens is presented. The strength at -56.67°C is decreased by 49.2% and 41.6% when the width of welded cleavage specimen is increased from 13 mm to 25 mm and 25 mm to 38 mm as shown in W4-W5-W6. At 93.33°C, the strength of welded specimens is decreased by 52.2% and by 25.0% with the increment of specimen width from 13 mm to 25 mm and from 25 mm to 38 mm as illustrated in W1-W2-W3. The 25-mm specimens at 52.5°C are observed to have 51.9% less strength than 13-mm welded cleavage specimens at 20°C (see W7 and W8). The 38-mm specimens at 85°C exhibit 11.7% reduction in the cleavage strength compared with the 25-mm specimens at 52.5°C as shown in W8 and W9.

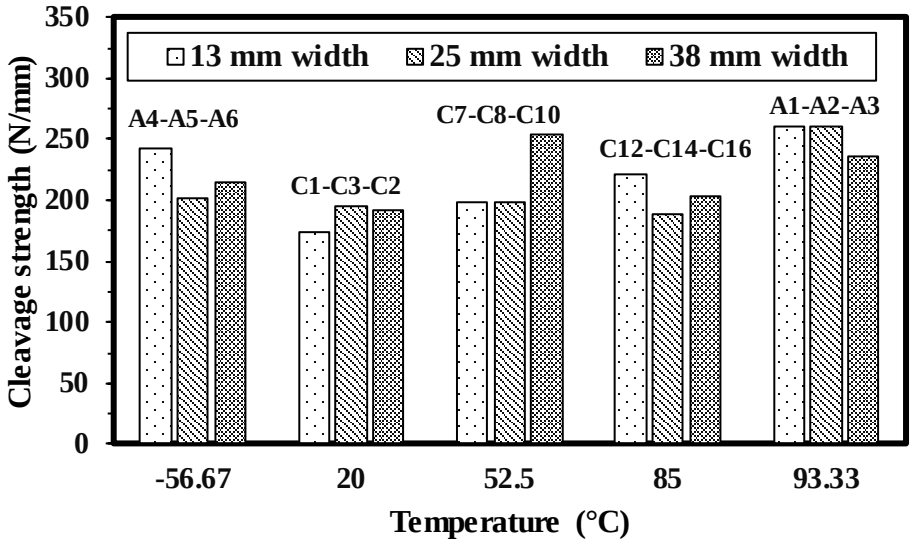

(a)

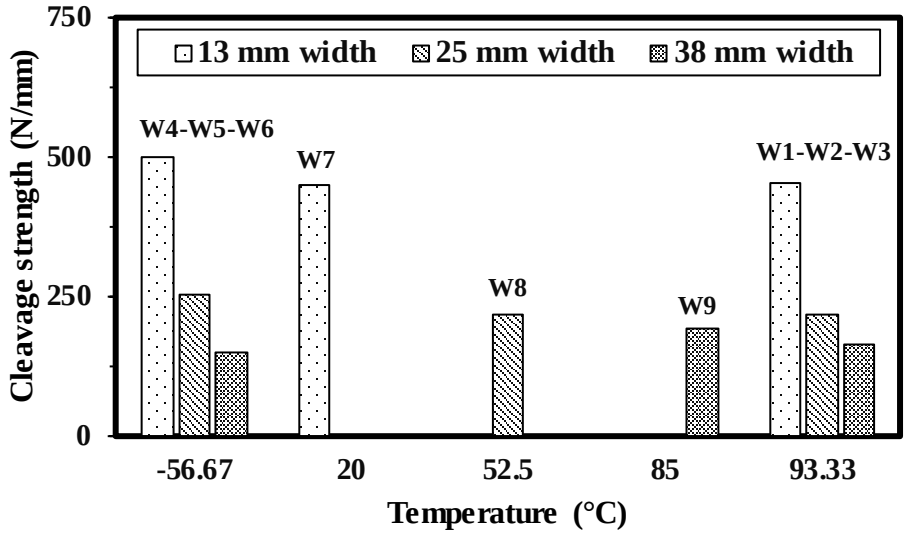

(b)

Figure 4.20 Width effect on cleavage strength for cleavage specimens (a) adhesive and (b) weld

4.4.4.3 Comparison between Adhesive and Welded Specimens

A comparative demonstration of cleavage strength between each combination of adhesive and welded cleavage specimens is shown in Figure 4.21. The 13-mm welded specimens are observed to have higher cleavage strength than the adhesive specimens by 74% at 93.33°C, 106% at -56.67°C, and 159% at 20°C as shown in pairs A1-W1, A4-W4, and C1-W7. At 93.33°C, the 25-mm welded specimens are found to have 17% less cleavage strength than the adhesive specimens as shown in pair A2-W2. The 25-mm welded specimens at -56.67°C and 52.5°C observed 26% and 9% higher cleavage strength in comparison with the adhesive specimens as displayed in pairs A5-W5 and C8-W8. For the 38-mm width at 93.33 °C, -56.67 °C, and 85 °C, the welded specimens are shown to have 31%, 31%, and 6% lower cleavage strength compared with the adhesive specimens (see pairs A3-W3, A6-W6, and C16-W9).

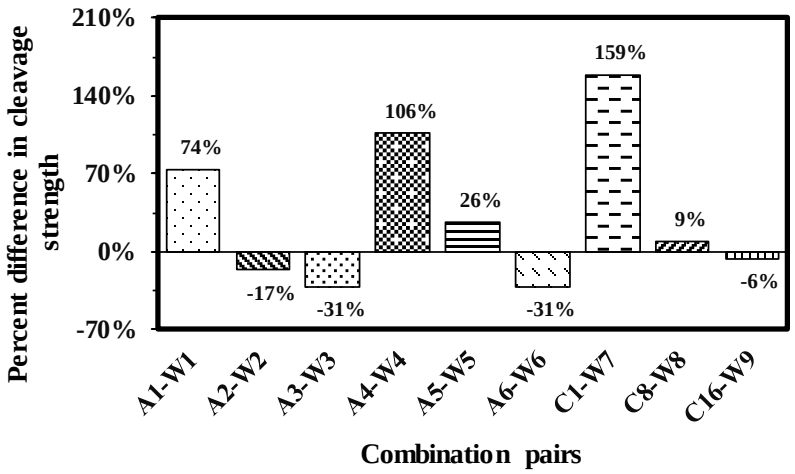

Figure 4.21 Percent difference in cleavage strength between adhesive and welded specimens

5. ULTIMATE STRENGTH AND FATIGUE LOAD TESTING

The full-scale testing was aimed to study the ultimate strength and fatigue behavior of the DMS with adhesive connections and the DMS with welded connections. Strain and displacement gauges were installed on individual DMS specimens to record two fundamental sets of physical parameters, strains and displacements, when loaded to failure and under fatigue load conditions. This section further discusses the DMS specimens and the testing setup of the ultimate strength test and fatigue load test along with the testing results and discussion.

5.1 Full-Sized DMS Specimens

In the ultimate strength testing, two full-sized aluminum DMS specimens, which encompass one DMS specimen with adhesive connections and one DMS with welded connections, were utilized. Each DMS specimen mainly consists of aluminum back skin, aluminum internal frame structure, and channels to properly function with the support structure. The back skin was fabricated with 5052-H32 aluminum alloy (Aluminum Association 2010), whereas the internal frame structure and channels were made of 6061-T6 aluminum alloy (Aluminum Association 2010). As shown in Figure 5.1, the dimensions of each of the DMSs were 1.52 m in length, 1.43 m in width, and 0.28 m in depth. Each was connected with two 1.27-m-long channels on the top and bottom end. The channels were connected to the frame with a bolt connection. The DMS specimen with adhesive connections was bonded with 6.47-cm-wide LORD 406-19GB (LORD 2018) acrylic adhesive on the north and south end of the DMS for the connection between the back skin and the frame. Meanwhile, an adhesive connection of 5.91-cm width was applied on the east and west end of the DMS for connecting the back skin and the frame. The geometry of the adhesive DMS with the top and the side view is also shown in Figure 5.1a and b, respectively. On the other hand, the DMS specimen with weld connections was connected with a 3.18-mm fillet weld to connect the back skin and the frame on the outer edge. The geometry of the welded DMS with the top view and the side view is shown in Figure 5.1c and d, respectively. For the fatigue load testing, two additional full-sized DMS specimens, including one adhesively bonded DMS specimen and one welded DMS specimen, were used. It should be noted that the fatigue testing adhesive and welded specimens are identical to the ultimate testing adhesive and welded specimens, respectively.

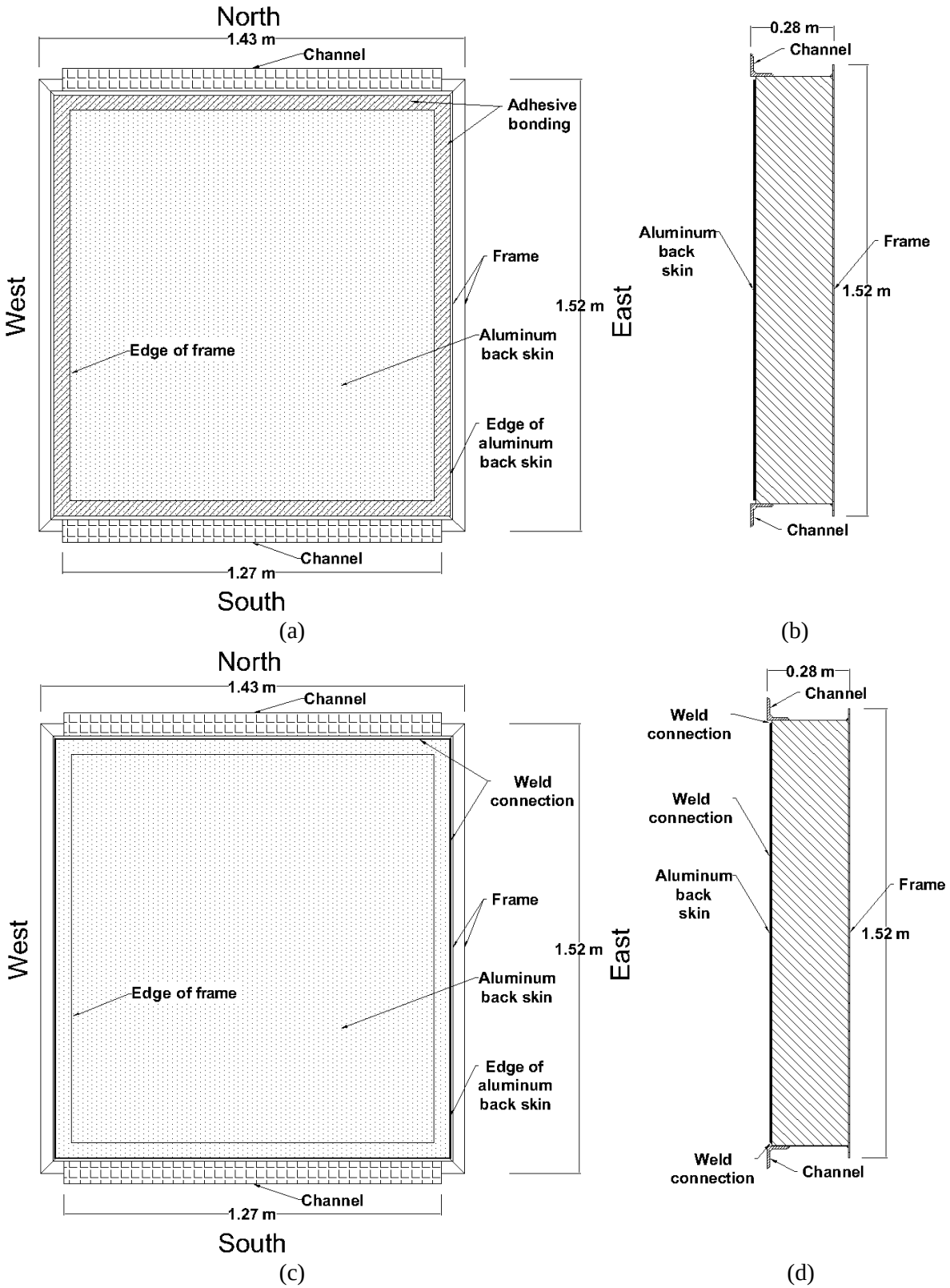

Figure 5.1 Geometry of DMS specimens for ultimate strength and fatigue load testing: (a) top view of adhesive DMS, (b) side view of adhesive DMS, (c) top view of welded DMS, and (d) side view of welded DMS

5.2 Testing Setup

Both the ultimate strength and fatigue load tests followed an identical instrumentation plan. The instrumentation plan is made up of 24 strain-gauges installed on the surface of the aluminum skin inside the DMS near the corners, edges, and perimeter of the loaded region near the center. There were 15 displacement gauges installed at the bottom inside the DMS to record displacement data, including 14 linear variable differential transformers (LVDTs) and one string potentiometer. Strictly speaking, the LVDTs were installed near the corners, edges, and perimeter of the loaded region near the center, and the string potentiometer was attached to the center. The strain and displacement data were obtained using a 128-channel data acquisition system. Figure 5.2 shows the details of the instrumentation plan. Figure 5.2a shows the bottom view of the instrumentation plan, while Figure 5.2b and c display the elevation views of section A-A and section B-B of the tested DMS.

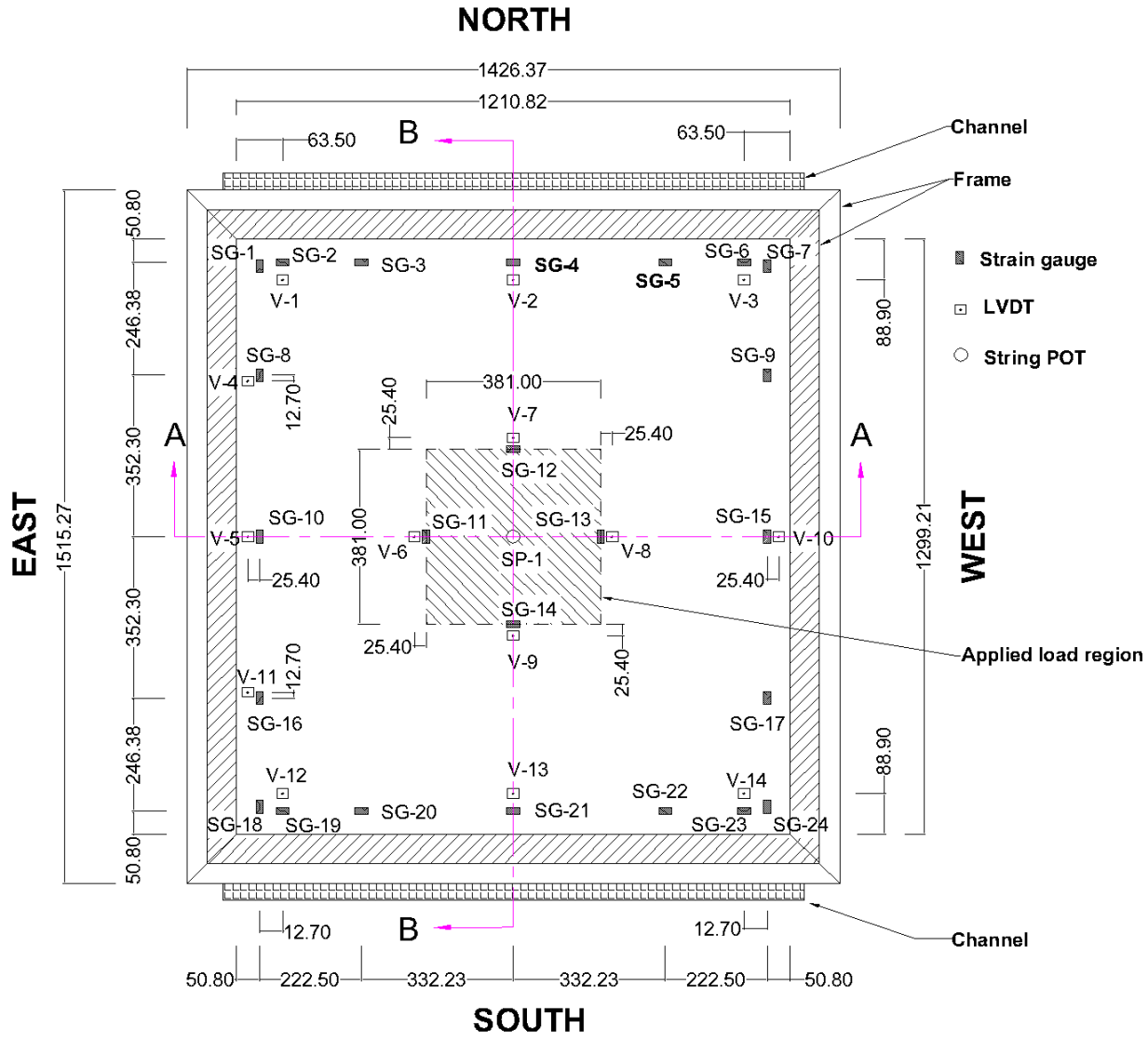

(a)

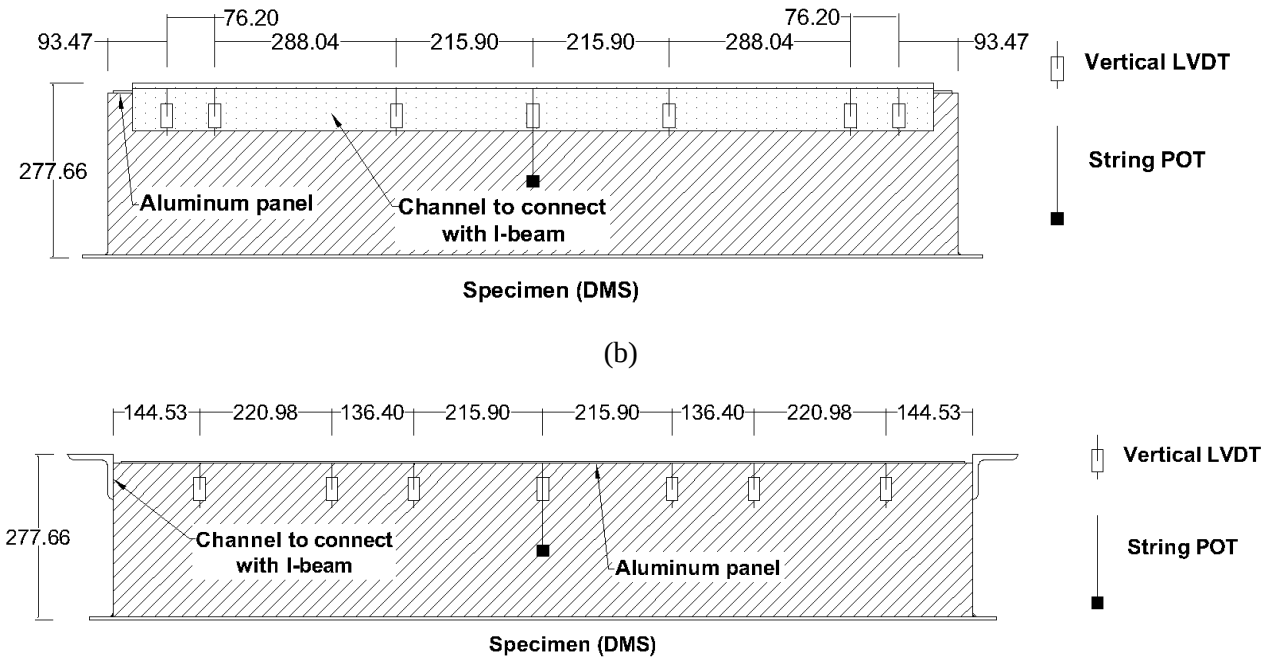

Figure 5.2 Instrumentation plan for strain and displacement gauges: (a) Bottom view, (b) Elevation view of section A-A, and (c) Elevation view of section B-B (All dimensions are in mm).

The testing setup for the ultimate strength tests and fatigue load tests is shown in Figure 5.3. An actuator of 649.44 kN capacity with 38.1 cm stroke length was used to load each of the DMS specimens at the center of the panel as shown in Figure 5.3a. Two W6X12 steel I-shaped beams were connected to the channels on the rear of the DMS. The DMS attached with the I-beams was placed on two abutments located at the north and south end of the test lab during each of the tests. Four 444.8 kN load cells (LC) were installed under the I-beams at each corner to measure the reaction forces. Rubber pads were also placed at the center of the DMS panel followed by a 38.1 cm x 38.1 cm steel plate on the aluminum back skin to facilitate uniform load transfer from the actuator as shown in Figure 5.3b.

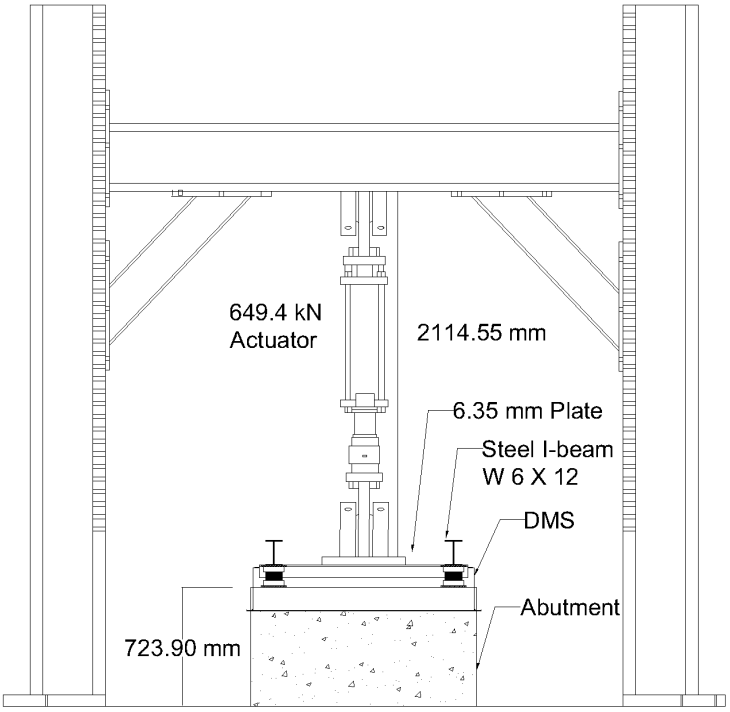

(a)

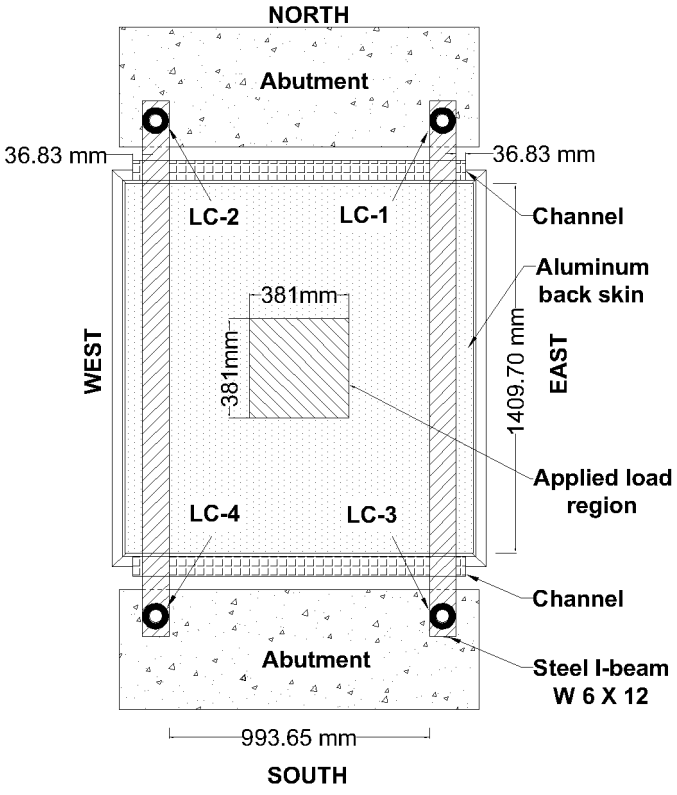

(b)

Figure 5.3 Test setup: (a) cross-section view and (b) top view.

5.2.1.1 Ultimate Strength Test

As stated before, the ultimate strength of one adhesive DMS and one welded DMS were examined in this project. The ultimate strength tests were performed under displacement control by applying a monotonic load to the back-skin of the aluminum panel with a displacement rate of 0.178 mm/sec until failure. Strain, displacement, and load data were recorded until failure. A regular inspection of the DMS was conducted to check the damage on the structure during the test. The testing setup of the adhesive DMS for the ultimate strength test is shown in Figure 5.4.

(a)

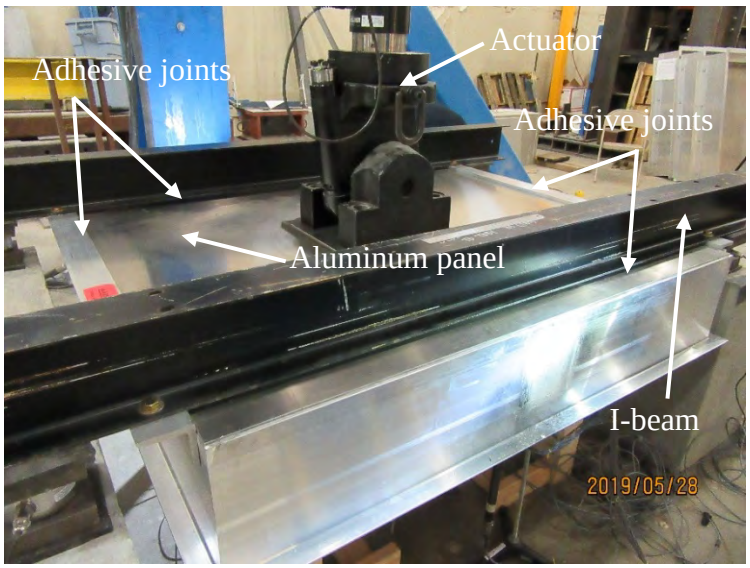

(b)

Figure 5.4 Ultimate strength test of adhesive DMS: (a) isometric view and (b) close-up view.

5.2.1.2 Fatigue Load Test

One adhesive DMS and one welded DMS were tested under a fatigue design load of 0.818kN for 500,000 cycles. The load was calculated from the AASHTO Specifications (2015) simulating the wind load exerted by natural wind gust pressure based on a yearly mean speed of 18.02 km/hr. The actuator was operated at a frequency of 1 Hz in a displacement control manner. Strain, displacement, and load responses were logged every hour during the test. Each of the DMSs was inspected for the existence of any damage every four hours initially up to 100,800 cycles and every two hours between 100,800 and 302,400 cycles, which was later truncated to an hourly observation. The fatigue testing setup of the welded DMS is shown in Figure 5.5.

(a)

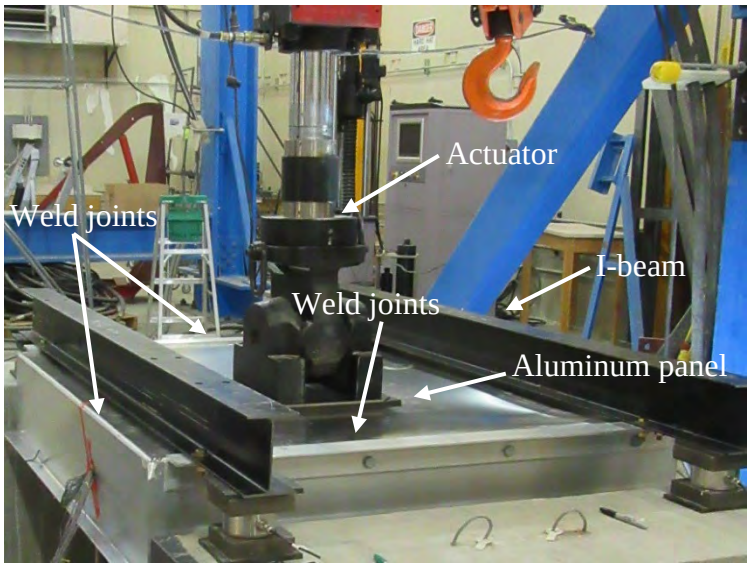

(b)

Figure 5.5 Fatigue load test of welded DMS: (a) isometric view and (b) close-up view.

5.3 Results and Discussion

Results from the ultimate strength and fatigue load tests are summarized and discussed in this section. Details on the results with a focus on load-displacement curves and strain profiles are presented in the following subsections.

5.3.1 Ultimate Strength Data Investigation

5.3.1.1 Adhesive DMS Strength

A load-displacement curve for the ultimate strength test of the adhesive DMS is presented in Figure 5.6. The adhesive DMS was loaded at the center of the back-skin aluminum of the DMS. The adhesive DMS failed at 123.41 kN when center-line deflection was 133.35mm. An abrupt drop in the actuator load from 102.57 kN to 70.74 kN was observed as shown in this figure. The actuator was pulled up for the removal of the LVDTs that were installed at the bottom of the DMS to avoid any damage on the LVDTs, which explains the unusual behavior of the load-displacement curve. The failure modes of the adhesive DMS are presented in Figure 5.7. Specifically, distortion of the aluminum back skin, along with adhesive debonding, was observed at northeast and northwest corners as shown in Figure 5.7a and Figure 5.7c, respectively. Adhesive debonding was not observed in southeast (see Figure 5.7b) and southwest (see Figure 5.7d) corners; however, distortion of the aluminum back skin can be clearly detected in both the corners. Figure 5.7e presents the overall failure of the adhesive DMS after the completion of the test.

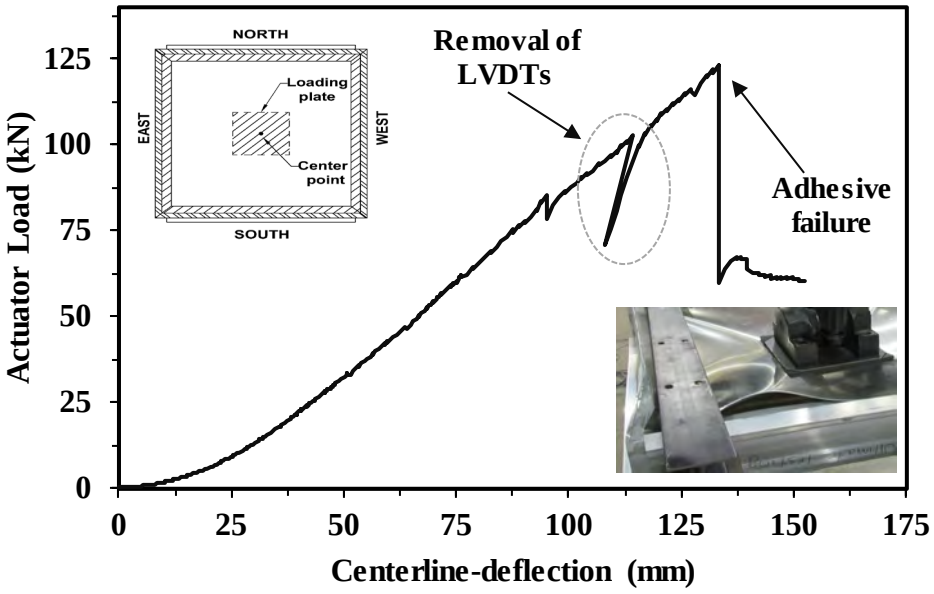

Figure 5.6 Load-displacement curve for tested adhesive DMS.

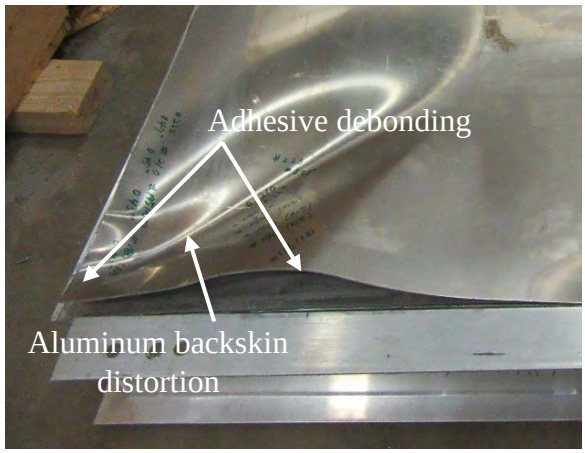

(a)

(b)

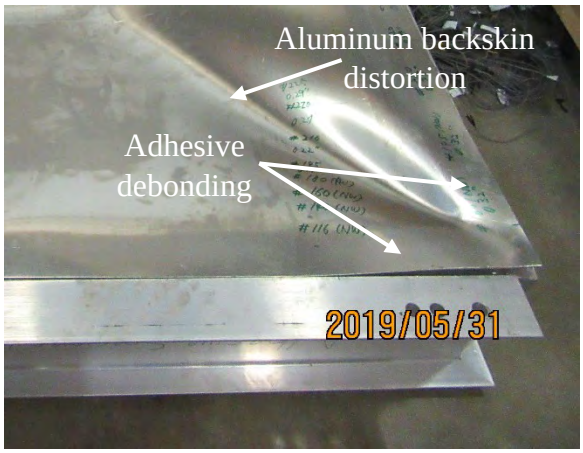

(c)

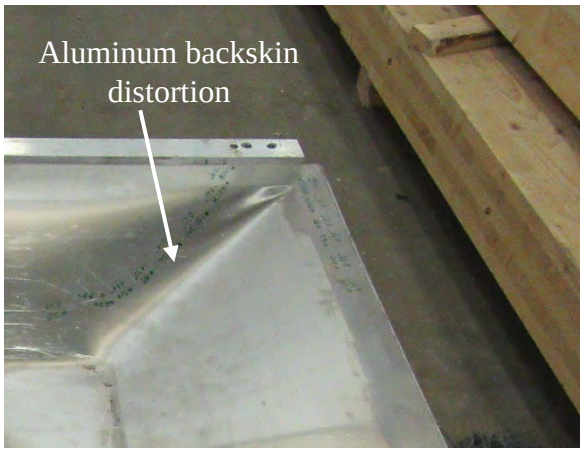

(d)

(e)

Figure 5.7 Failure mode of adhesive DMS at: (a) northeast end, (b) southeast end, (c) northwest end, (d) southwest end, and (e) overall failure.

Figure 5.8 shows a representative actuator load versus strains of the adhesive DMS. The representative strain profiles of the strain gauges installed on the north, south, east, and west end of the adhesive DMS are presented in Figure 5.8a through Figure 5.8d, respectively. It should be noted that tensile strains observed are well below the yield strains of the aluminum on the north, south, east, and west end of the adhesive DMS. The aluminum panel in all four edges experienced compression at the beginning of the test. Figure 5.8e and Figure 5.8f illustrate the strain profiles at the corners in the longitudinal and transverse directions, respectively. Strains at the corners of the adhesive DMS were found to be substantially higher than the yield values of the aluminum, as expected. Each corner of the aluminum panel was on compression at the beginning of the test; however, it was observed that there were extreme strains experienced near the failure of the DMS. Strain profiles of the four strain gauges installed around the perimeter of the applied loading area at the center are also shown in Figure 5.8g. The aluminum panel was found to be in tension throughout the test until failure. The highest tensile strains were observed for the strain gauges installed at the corners in the transverse direction followed by the longitudinally installed strain gauge group. It was found that the corner sections of the aluminum panel in the DMS play a more critical role as strain gauges installed in the corners observed the highest strains than the other locations.

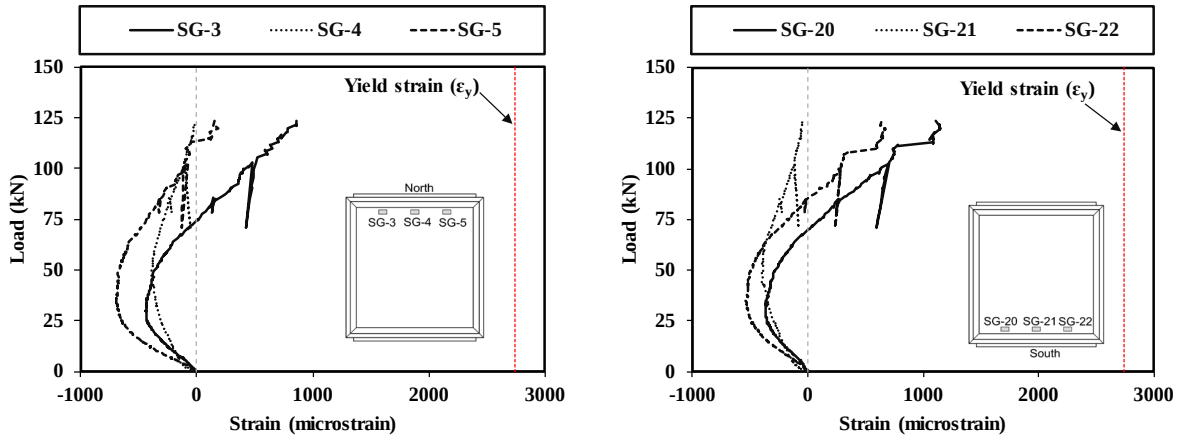

(a)

(b)

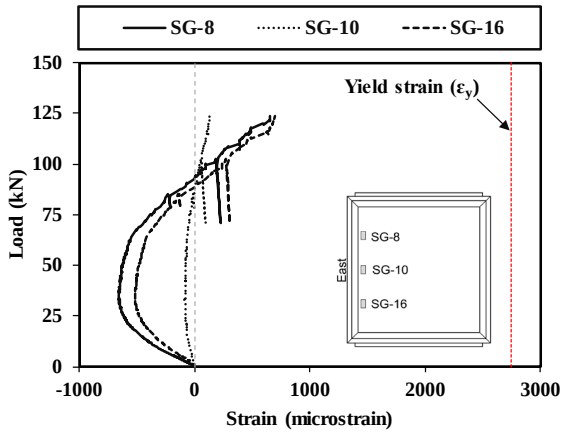

(c)

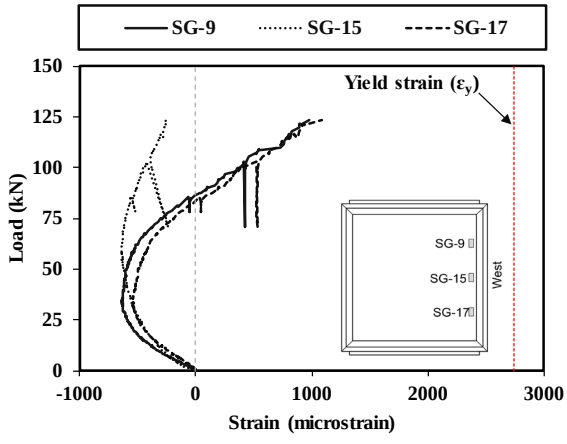

(d)

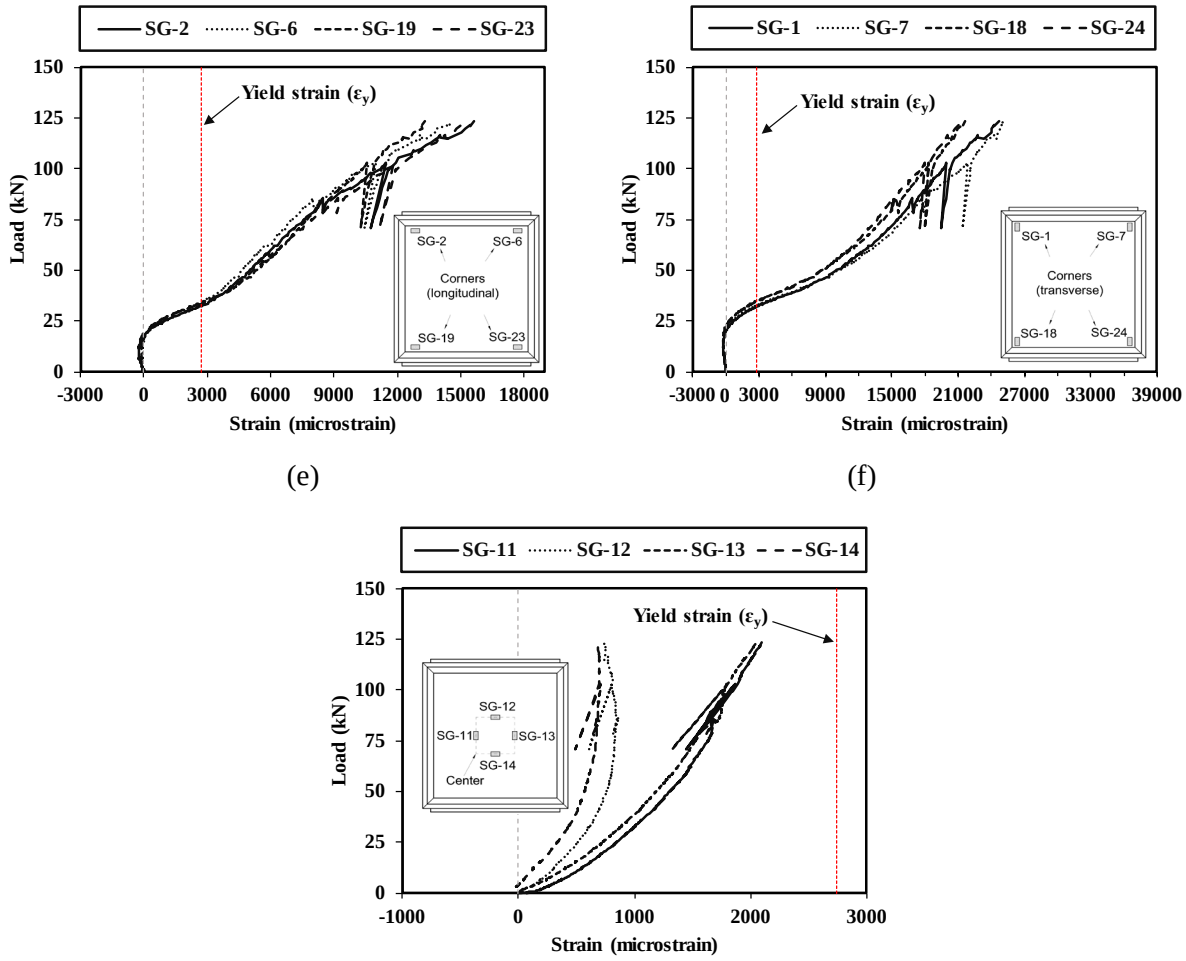

Figure 5.8 Strain profiles for adhesive DMS at (a) north end, (b) south end, (c) east end, (d) west end, (e) corners in the longitudinal direction, (f) corners in the transverse direction, and (g) center

Figure 5.9 shows the load versus deflection responses at all LVDT locations in the panel. All deflection profiles are nearly linear. The LVDTs installed near the center of the adhesive DMS (V-6, V-7, V-8, and V-9) were removed at 83.04 kN; whereas, the rest of the LVDTs were removed at 102.57 kN to prevent any damage to the LVDTs. The LVDTs installed near the center of the DMS (V-6, V-7, V-8, and V-9) recorded maximum deflections, followed by the LVDTs installed at the corners of the DMS (V-1, V-3, V-12, and V-14). The peak deflection was observed near the center of the DMS for V-7 with 91.49 mm.

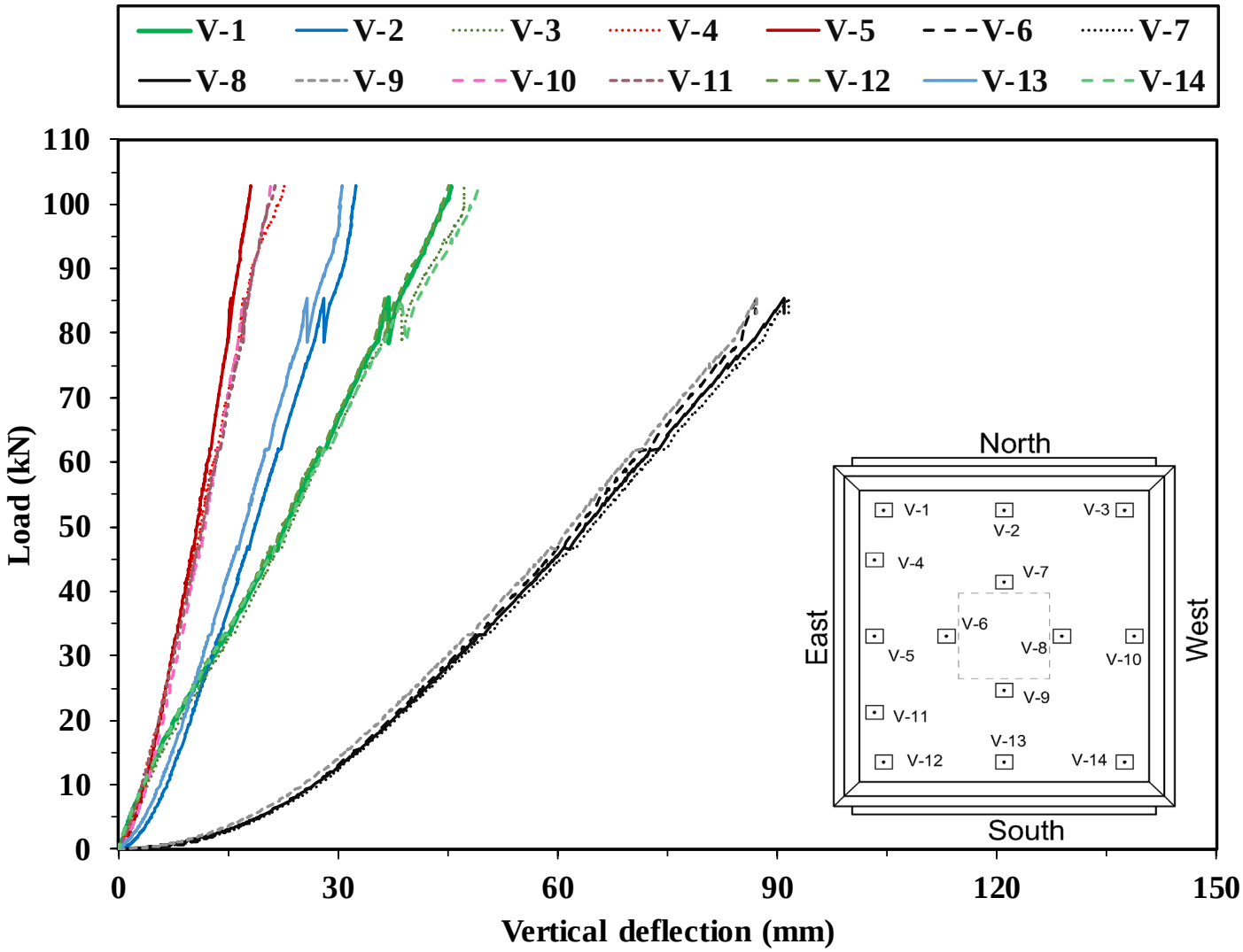

Figure 5.9 LVDT profile for adhesive DMS

Figure 5.10 shows the reaction force from the load cells installed at four ends of the adhesive DMS. The load cells were installed at each corner of the DMS. The progression of the reaction force with respect to time is shown in Figure 5.10a. The reaction force is observed to be increasing with the increment in the actuator load during the test. A bar chart for the reaction force in the four load cells when reaching the yield strength of the aluminum panel is shown in Figure 5.10b. It appears that LC-3 observed the maximum reaction force of 11.92 kN; whereas, LC-4 experienced the lowest reaction force of 6.27 kN up to the yield strength. Figure 5.10c presents another bar chart of the reaction force recorded at the failure of the adhesive DMS. It turned out that the adhesive DMS experienced the maximum reaction force of 35.74 kN in LC-3 and minimum reaction force of 25.06 kN in LC-4.

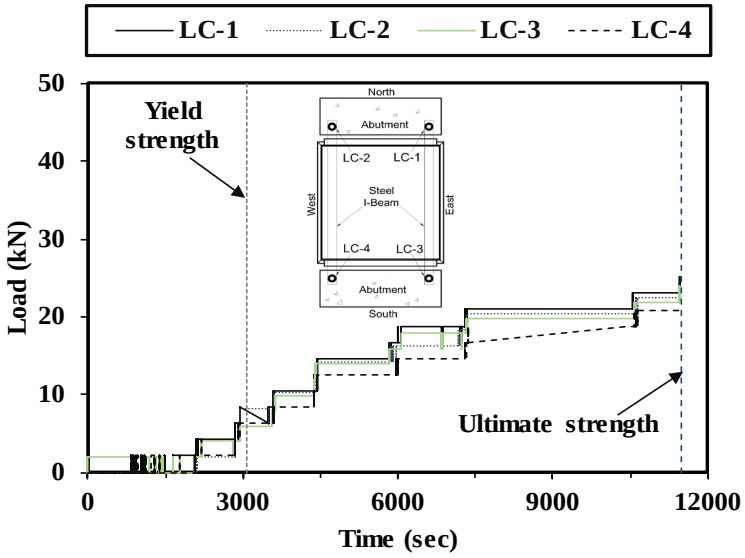

(a)

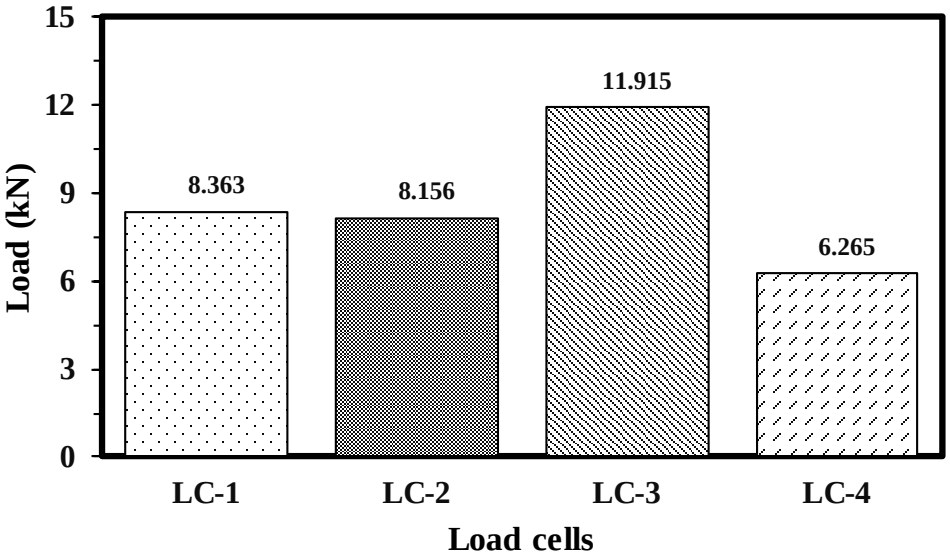

(b)

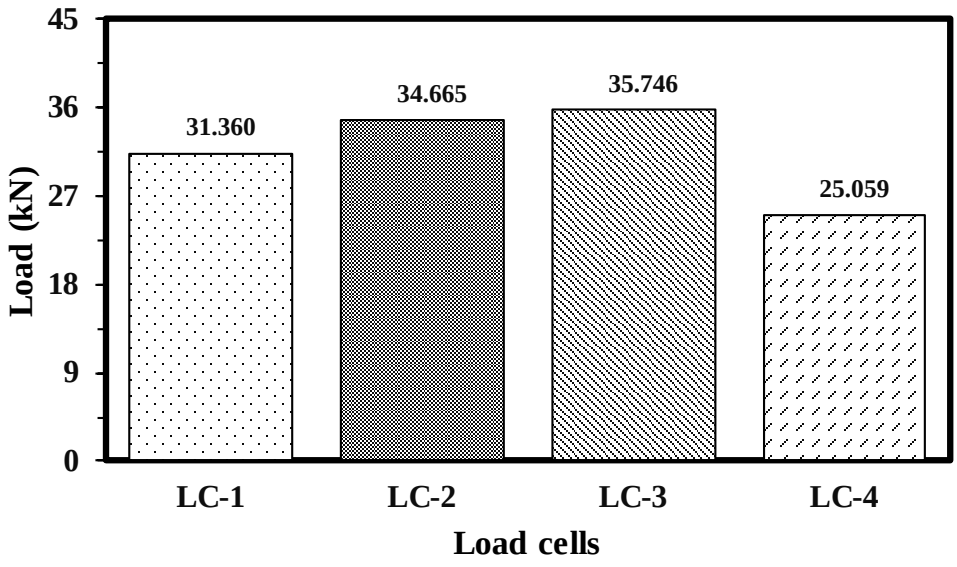

(c)

Figure 5.10 Reaction force from load cells for adhesive DMS: (a) load vs time, (b) at yield strength, and (c) at ultimate strength

5.3.1.2 Welded DMS Strength

Figure 5.11 shows the load-displacement curve for the ultimate strength testing of the welded DMS. The welded DMS was loaded at the center of the back-skin aluminum of the DMS. Two different failure modes were observed during the testing. The first failure was observed at 153.46 kN at 158.57 mm deflection due to the failure of the interior welds connecting back-skin and the frame inside the DMS. The load was decreased up to 113.38 kN after the first failure. The second failure was observed at 145.18 kN at 175.95 mm deflection caused by the rupture of the frame at the location of the bolt connecting the frame and channel on the southwest edge of the DMS.

Detailed images for the first failure of the welded DMS are presented in Figure 5.12. As shown in Figure 5.12a, b, and c, two welds were observed to have failed at the northeast corner, at the southeast corner, and at the northwest corner; whereas, the failure of only one weld was found at the southeast corner as displayed in Figure 5.12d. It should be noted that the welds closest to the corners of the DMS were failed due to the high stress concentration at the corners.

The second failure of the welded DMS is depicted in Figure 5.13. Figure 5.13a shows the rupture of the frame due to the detachment of the bolt connecting the channel and frame of the DMS at the southwest end. The channel connecting the DMS and I-beam was also bent along with the distortion of aluminum back skin. The overall failure of the welded DMS after accomplishing the test is shown in Figure 5.13b.

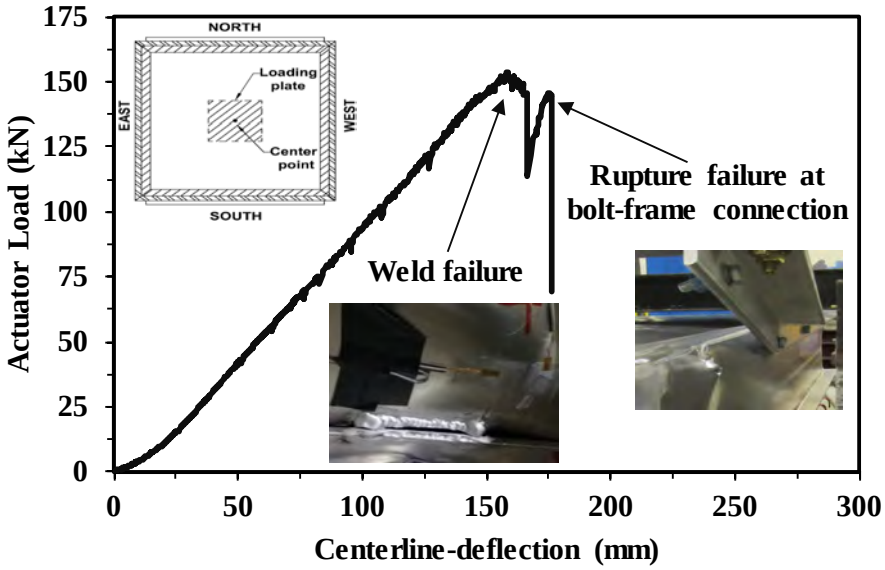

Figure 5.11 Load-displacement curve for welded DMS

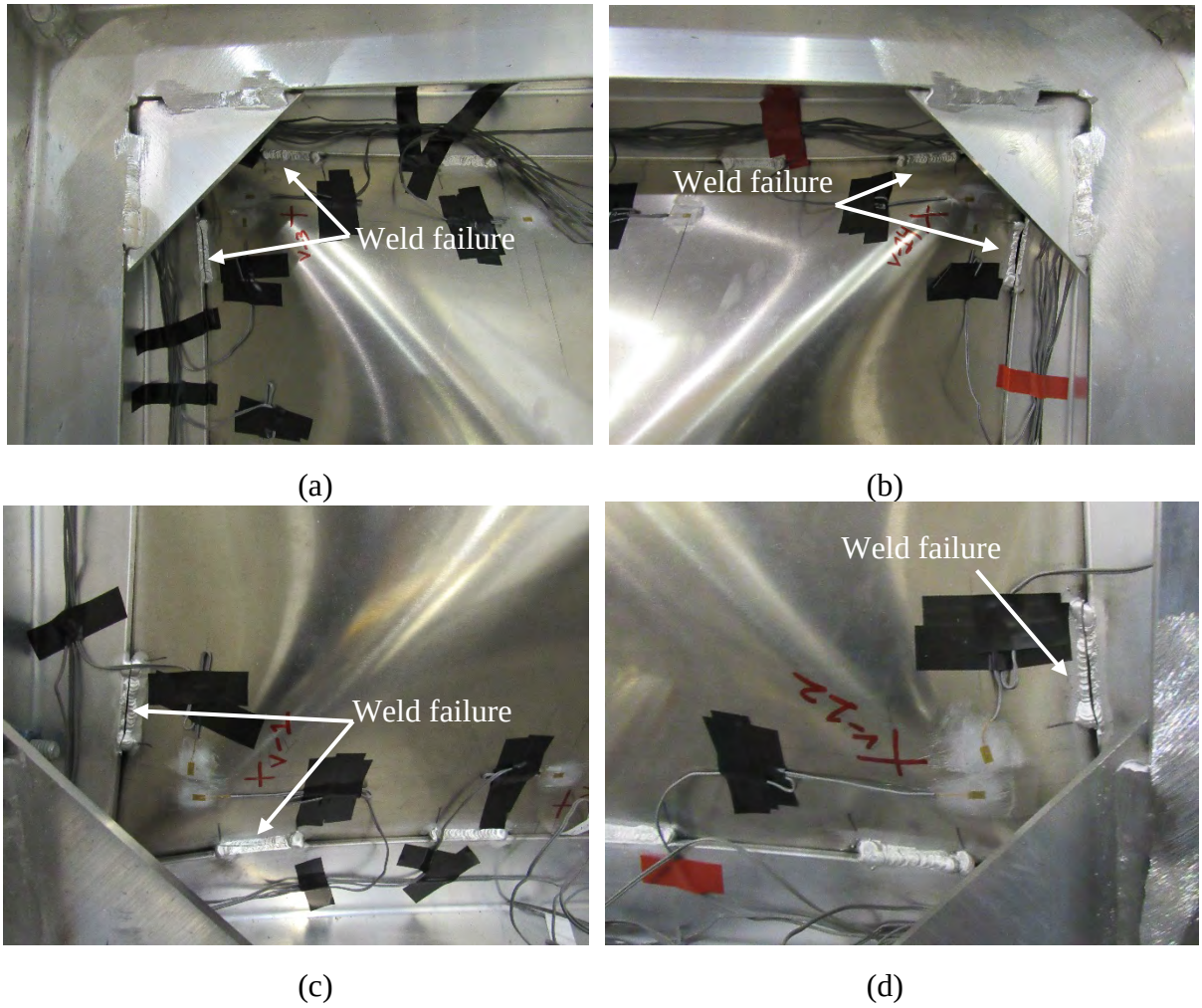

Figure 5.12 First failure mode of welded DMS at: (a) northeast end, (b) southeast end, (c) northwest end, and (d) southwest end.

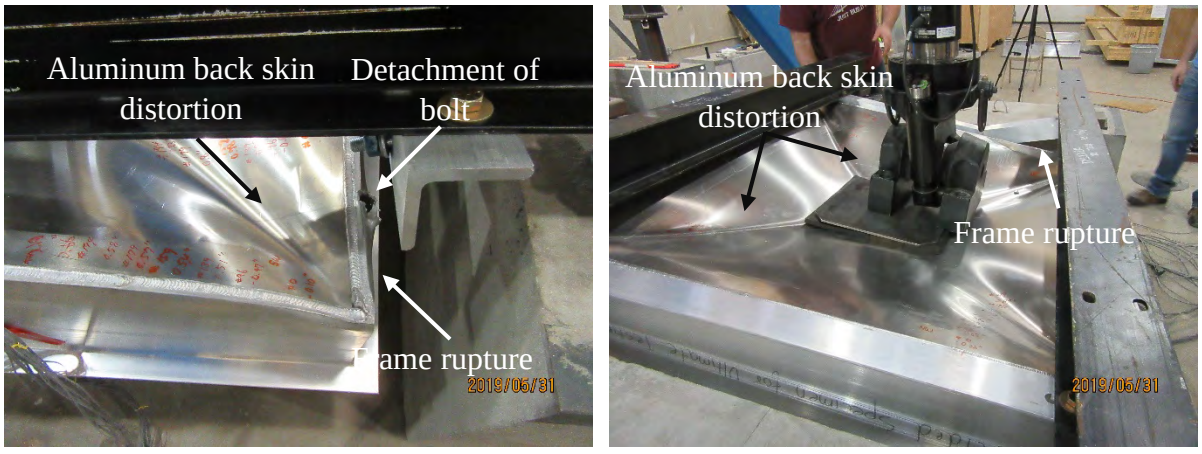

Figure 5.13 Second failure mode of welded DMS at: (a) southwest end, and (b) overall failure.

The representative plots of the actuator load against strains observed in the aluminum panel of the welded DMS are presented in Figure 5.14. Similar to the strain profiles of the adhesive DMS, the overall tensile strains observed are less than the yield strains of the aluminum on the north, south, east, and west end of the DMS. The strain profiles of the gauges installed on the north, south, east, and west end of the DMS are presented in Figure 5.14a through Figure 5.14d, respectively. The aluminum panel in all four edges experienced compression at the beginning of the test. Figure 5.14e and Figure 5.14f illustrate the strain profiles at the corners in longitudinal and transverse directions, respectively. Strains at the corners of the DMS were found to be considerably higher than the yield values of the aluminum. Each corner of the aluminum panel was on compression at the beginning of the test; however, it was observed that the panel experienced extreme tension at the end of the test when it failed. Strain profiles of the four strain gauges installed around the perimeter of the loading plate at the center are shown in Figure 5.14g. For the strain gauges installed near the center, the aluminum panel was found to be in tension throughout the test until failure. All four strain gauges located near the center observed strains below yield strain, excluding SG-11. The highest tensile strains were observed for the strain gauges installed at the corners in the transverse direction followed by the longitudinally installed strain gauge group. The general strain behavior of the welded DMS is found to be analogous to that of the adhesive DMS, although the strain values are different between welded and adhesive DMSs on each test and location.

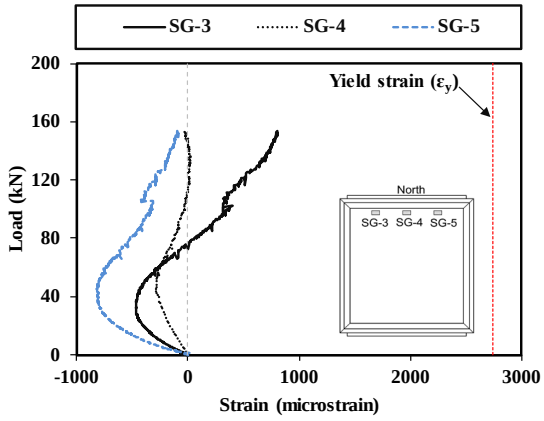

(a)

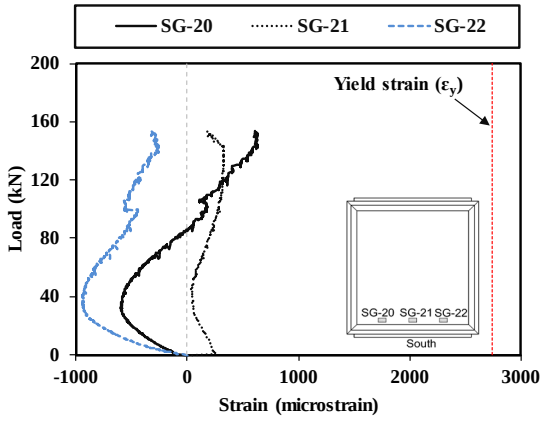

(b)

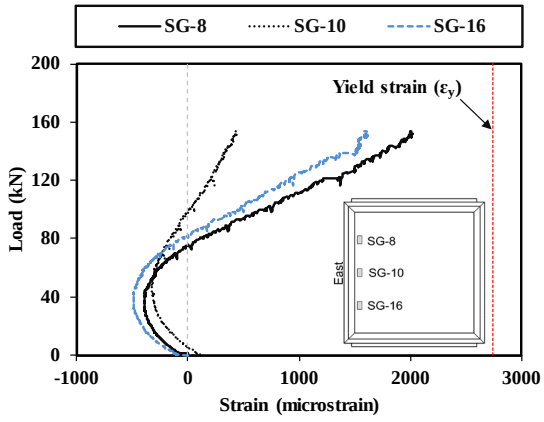

(c)

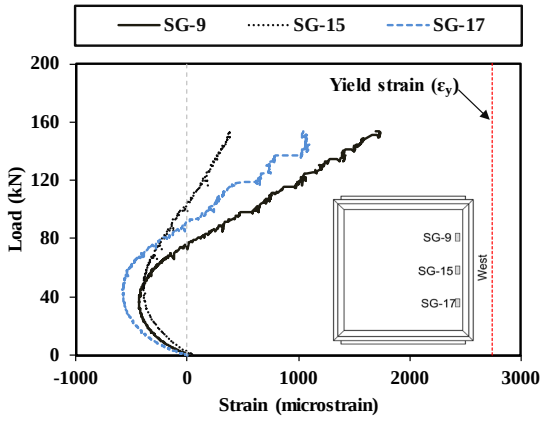

(d)

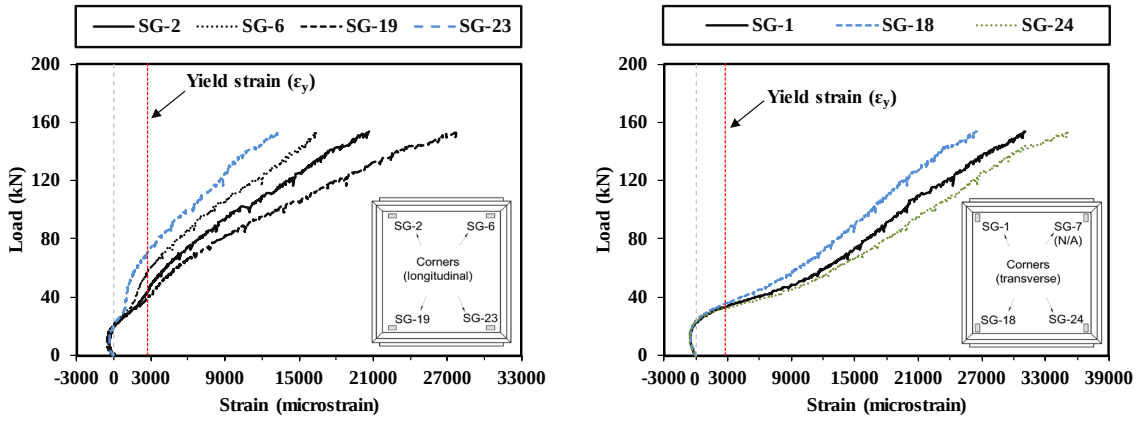

(e) (f)

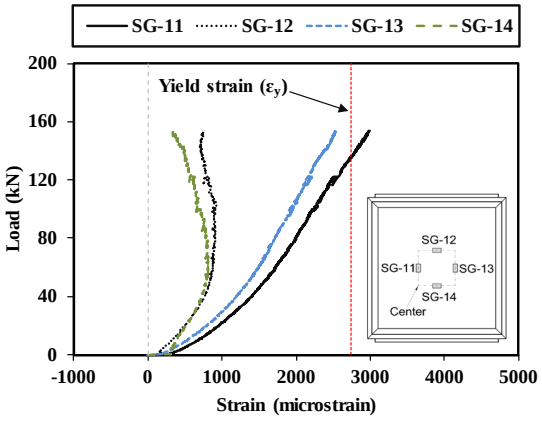

(g)

Figure 5.14 Strain profiles for welded DMS at: (a) north end, (b) south end, (c) east end, (d) west end, (e) corners in the longitudinal direction, (f) corners in the transverse direction, and (g) center

For the welded DMS, the plot of the deflection responses of the aluminum panel at all LVDT locations and actuator load is shown in Figure 5.15. The deflection responses from all the LVDTs exhibited a linear behavior. The LVDTs installed near the center of the welded DMS (V-6, V-7, V-8, and V-9) were removed at 69.48 kN; whereas, the rest of the LVDTs were removed at 74.65 kN to prevent any damage to the LVDTs. The center LVDTs recorded maximum deflections, followed by the LVDTs installed at the corners of the DMS (V-1, V-3, V-12, and V-14). The peak deflection was observed near the center of the welded DMS for V-7 with 96.14 mm. The deflection behavior of the aluminum panel in the welded DMS is similar to that of the adhesive DMS.

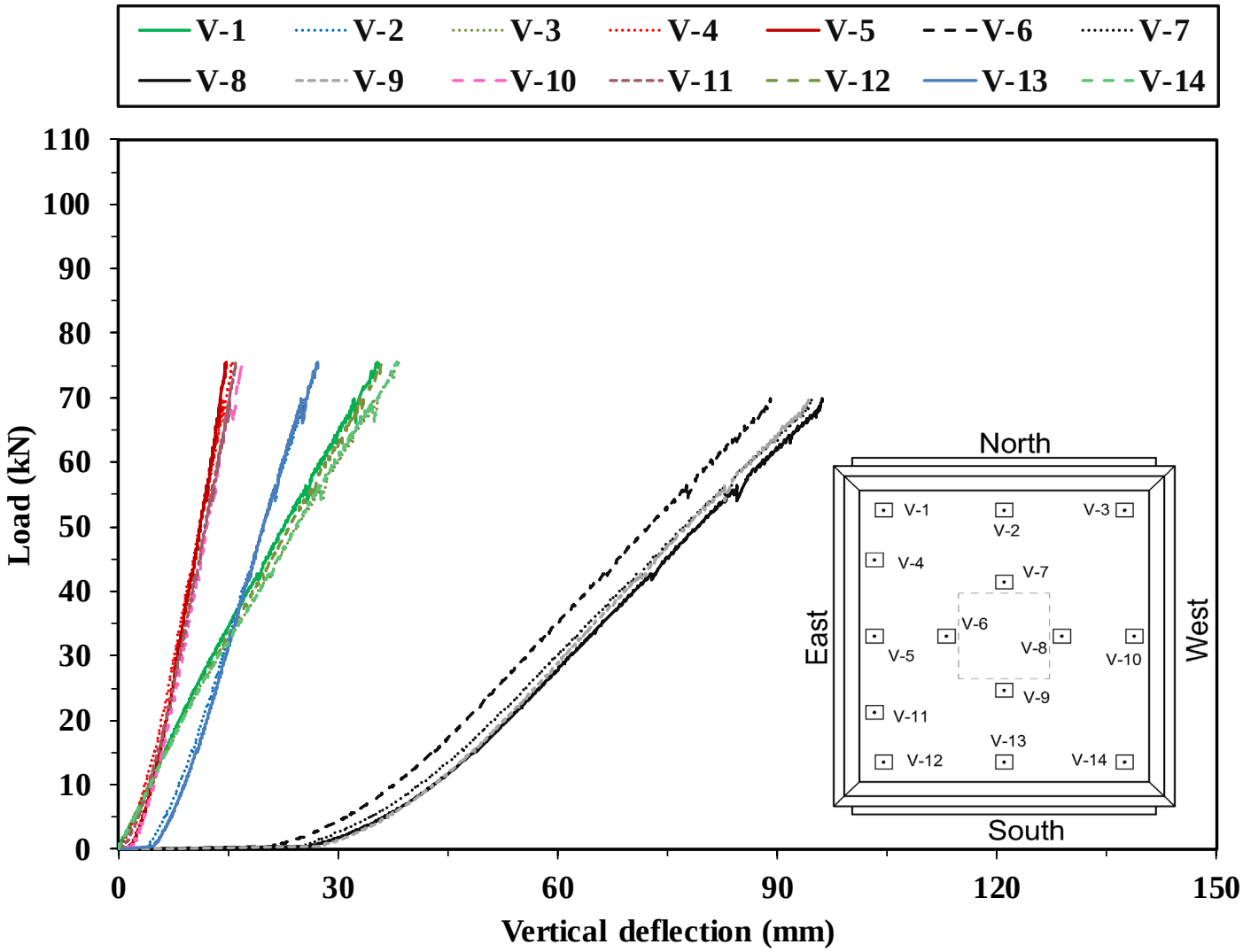

Figure 5.15 LVDT profile for welded DMS

The reaction force from the load cells installed at all the corners of the welded DMS is shown in Figure 5.16. Figure 5.16a displays the plot of the reaction force versus time during the test. The reaction force is observed to be increasing with the increase in the actuator load throughout the test. A bar chart for the reaction force in each load cell during the first yield of the aluminum panel is shown in Figure 5.16b. At the first yield of the aluminum panel, the highest reaction force of 8.36 kN is detected in LC-1, and the lowest reaction force of 5.96 kN is noted in LC-3. Figure 5.16c illustrates an additional bar chart of the reaction force at the failure of the welded DMS with the maximum reaction force of 39.72 kN in LC-1 and the minimum reaction force of 35.50 kN in LC-4.

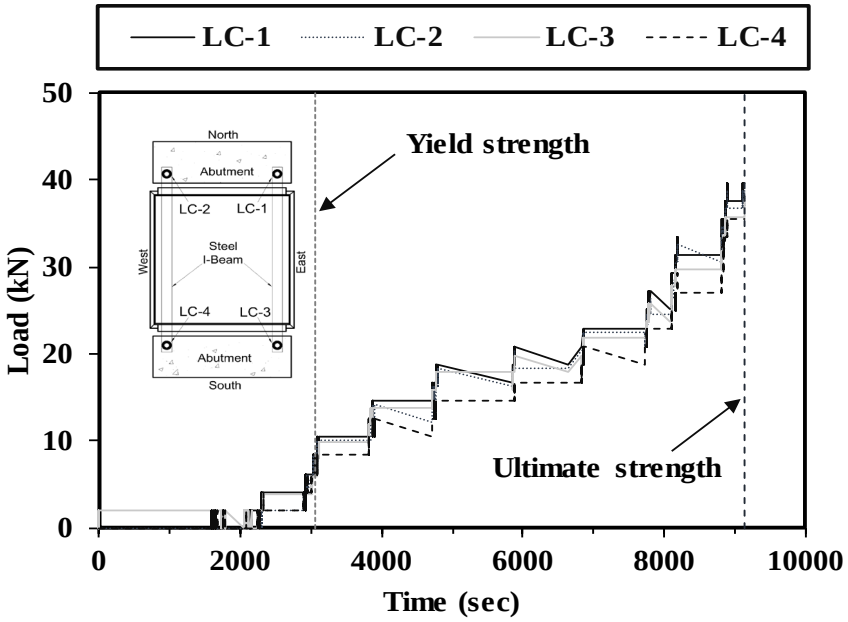

(a)

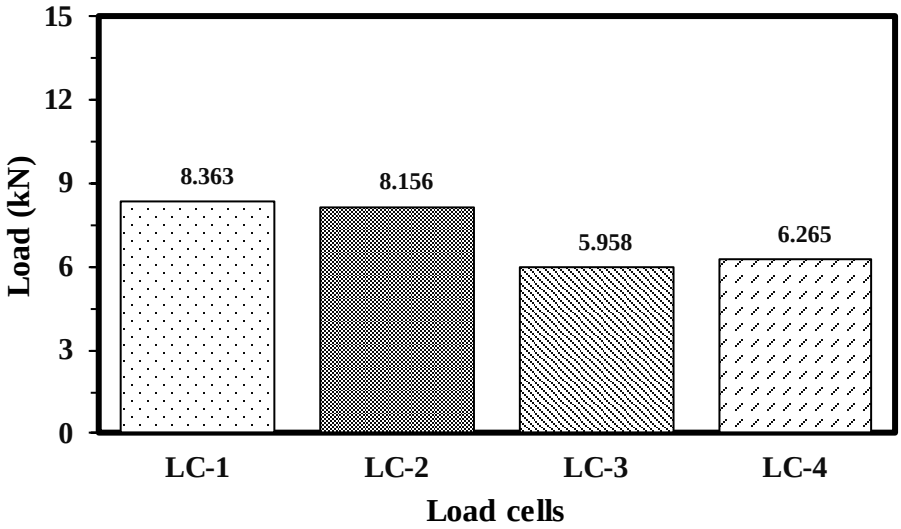

(b)

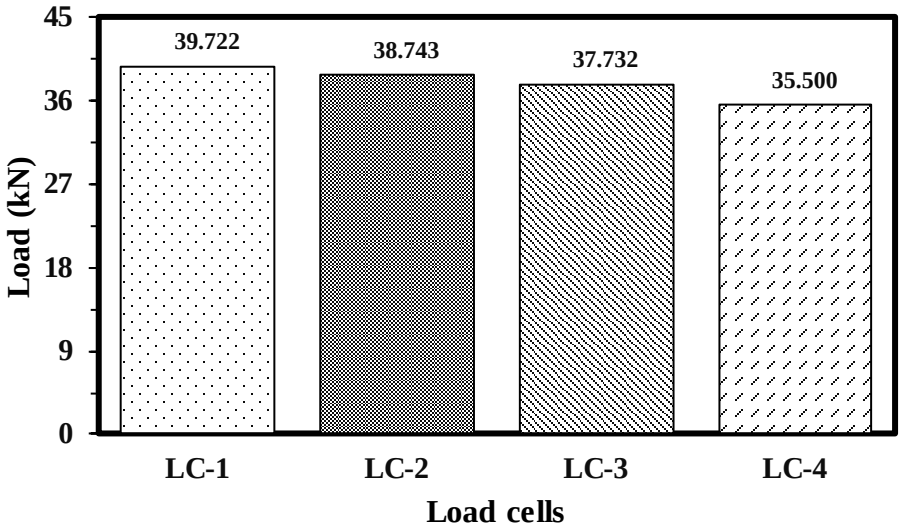

(c)

Figure 5.16 Reaction force from load cells for welded DMS: (a) load vs time, (b) at 1st yield, and (c) at ultimate strength

5.3.1.3 Comparison in Strength between Adhesive and Weld DMSs

The maximum deflections recorded by LVDTs at different locations during the ultimate strength test of adhesive and welded DMSs are compared and tabulated in Table 5.1. The comparison of the vertical deflection is further depicted in a bar chart showing the percent difference in Figure 5.17. It is observed that the deflections near the center of the adhesive DMS are higher up to 8% for V-9 compared with those for the welded DMS. All other LVDTs, excluding the center LVDTs, observed lower deflections in the welded DMS than the adhesive DMS. The percent difference was found to be the most for V-4 with a 31% lower deflection in the welded DMS than the adhesive DMS.

The maximum strains in both tension and compression are compared, along with the percent difference, and tabulated in Table 5.2. The comparison of peak strains in tension between the adhesive and welded DMSs is also presented in Figure 5.18. The welded DMS observed higher strain values in 15 strain gauge locations with a maximum percent difference of 240% for SG-10 located on the east side of the DMS. Six strain gauges observed lower value of strains in the welded DMS than the adhesive DMS with a peak decrement of 100% for SG-7 installed at the northwest corner and SG-22 installed at the south end of the DMS. Figure 5.19 displays the comparison of peak strains in compression between the adhesive and welded DMSs. The welded DMS observed higher strain values in 13 strain gauge locations with the maximum percent difference of 454% for SG-6 installed at the northwest corner in the longitudinal direction. Eight strain gauges in the welded DMS observed lower strain values compared with that of the adhesive DMS with the percent difference of 100%, which is observed in SG-7 installed at the northwest corner and SG-21 located at the south end of the DMS.

Table 5.1 LVDT maximum deflection

LVDT-ID	Adhesive DMS (mm)	Weld DMS (mm)	Percent difference (%)
V-1	45.49	35.43	-22%
V-2	32.33	27.18	-16%
V-3	47.24	38.23	-19%
V-4	22.58	15.47	-31%
V-5	17.96	14.61	-19%
V-6	87.20	89.08	2%
V-7	91.49	94.69	3%
V-8	90.81	96.14	6%
V-9	87.20	94.23	8%
V-10	20.73	16.81	-19%
V-11	21.36	15.98	-25%
V-12	45.03	36.14	-20%
V-13	30.45	27.10	-11%
V-14	49.28	38.13	-23%

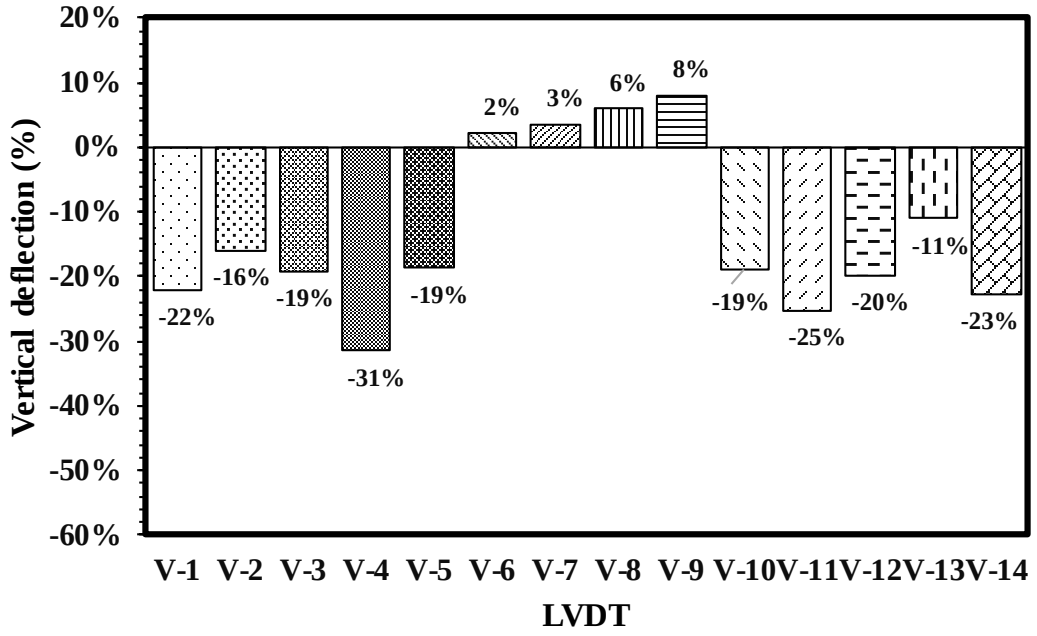

Figure 5.17 Percent difference in vertical deflection between adhesive and welded DMS

Table 5.2 Peak strains recorded during the ultimate strength test

Strain gauge-ID	Maximum strain in tension (microstrain)			Maximum strain in compression (microstrain)		
	Adhesive DMS	Weld DMS	Percent difference (%)	Adhesive DMS	Weld DMS	Percent difference (%)
SG-1	24703.73	31088.54	26%	-223.75	-506.76	126%
SG-2	15639.28	20618.09	32%	-235.11	-320.25	36%
SG-3	863.45	808.22	-6%	-438.18	-469.13	7%
SG-4	0	20.8	-	-388.2	-289.17	-26%
SG-5	182.57	8.24	-95%	-697.62	-821.94	18%
SG-6	14565.98	16653.58	14%	-76.83	-425.89	454%
SG-7	25103.37	0	-100%	-230.84	0	-100%
SG-8	656.22	2015.54	207%	-663.1	-391.41	-41%
SG-9	980.61	1733.33	77%	-638.35	-431.44	-32%
SG-10	128.05	434.92	240%	-85.2	-328.36	285%
SG-11	2100.5	2985.87	42%	0	-0.48	-
SG-12	855.04	925.79	8%	0	-0.97	-
SG-13	2052.66	2529.56	23%	0	-0.97	-
SG-14	704.05	816.82	16%	-16.42	-0.97	-94%
SG-15	0	385.39	-	-640.99	-397.22	-38%
SG-16	701.53	1617.94	131%	-521.88	-490.08	-6%
SG-17	1085.32	1096.51	1%	-543.23	-587.13	8%
SG-18	21620.11	26518.36	23%	-199.38	-494.05	148%
SG-19	13322.57	27801.33	109%	-131.61	-537.9	309%
SG-20	1148.04	633.36	-45%	-366.31	-593.85	62%
SG-21	0	331.16	-	-397.79	-0.96	-100%
SG-22	669.29	0	-100%	-535.66	-941.69	76%
SG-23	15214.75	13370.91	-12%	-263.24	-339.57	29%
SG-24	21127.7	35290.54	67%	-230.4	-588.38	155%

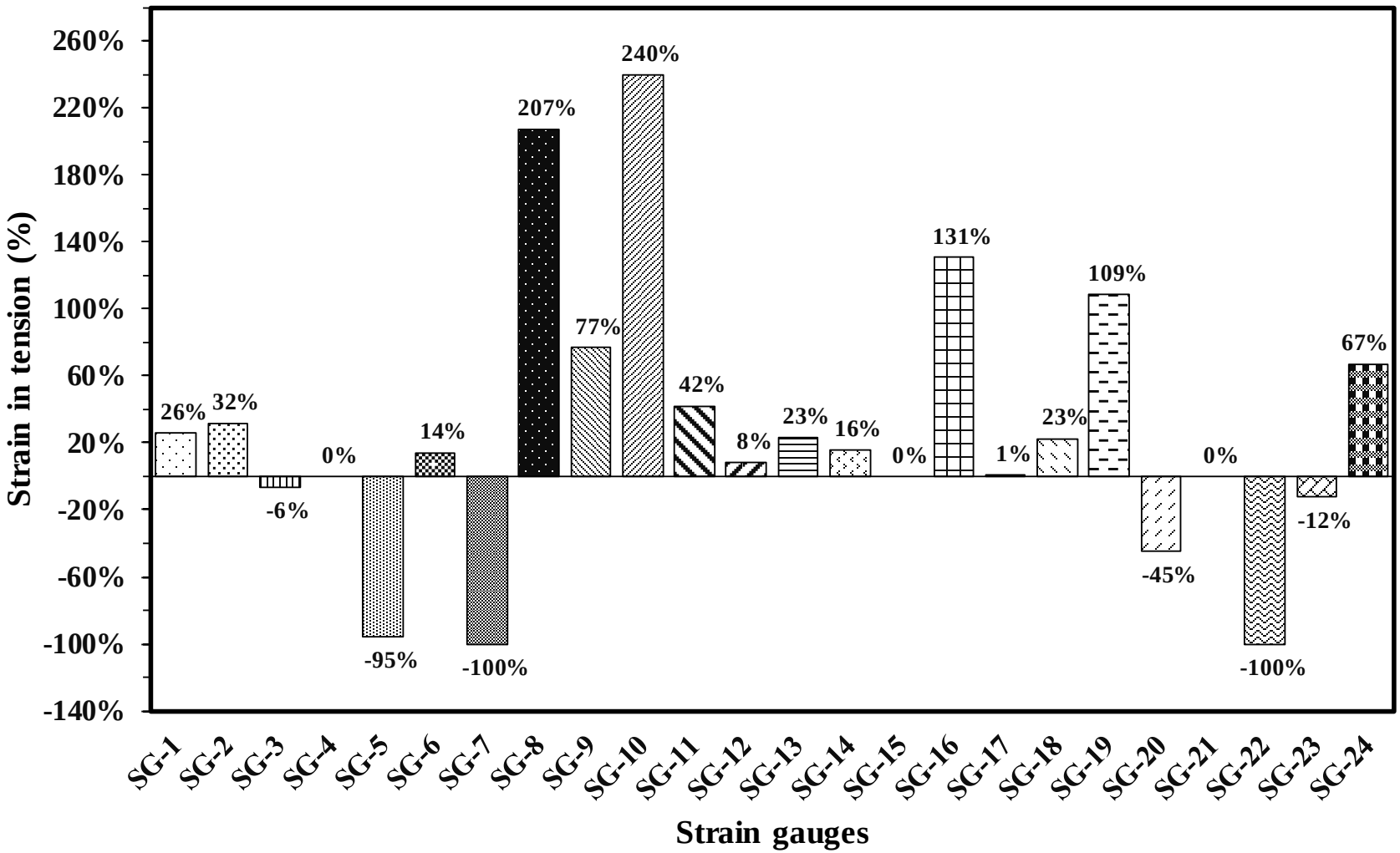

Figure 5.18 Percent difference between adhesive and weld DMS for peak strains in tension

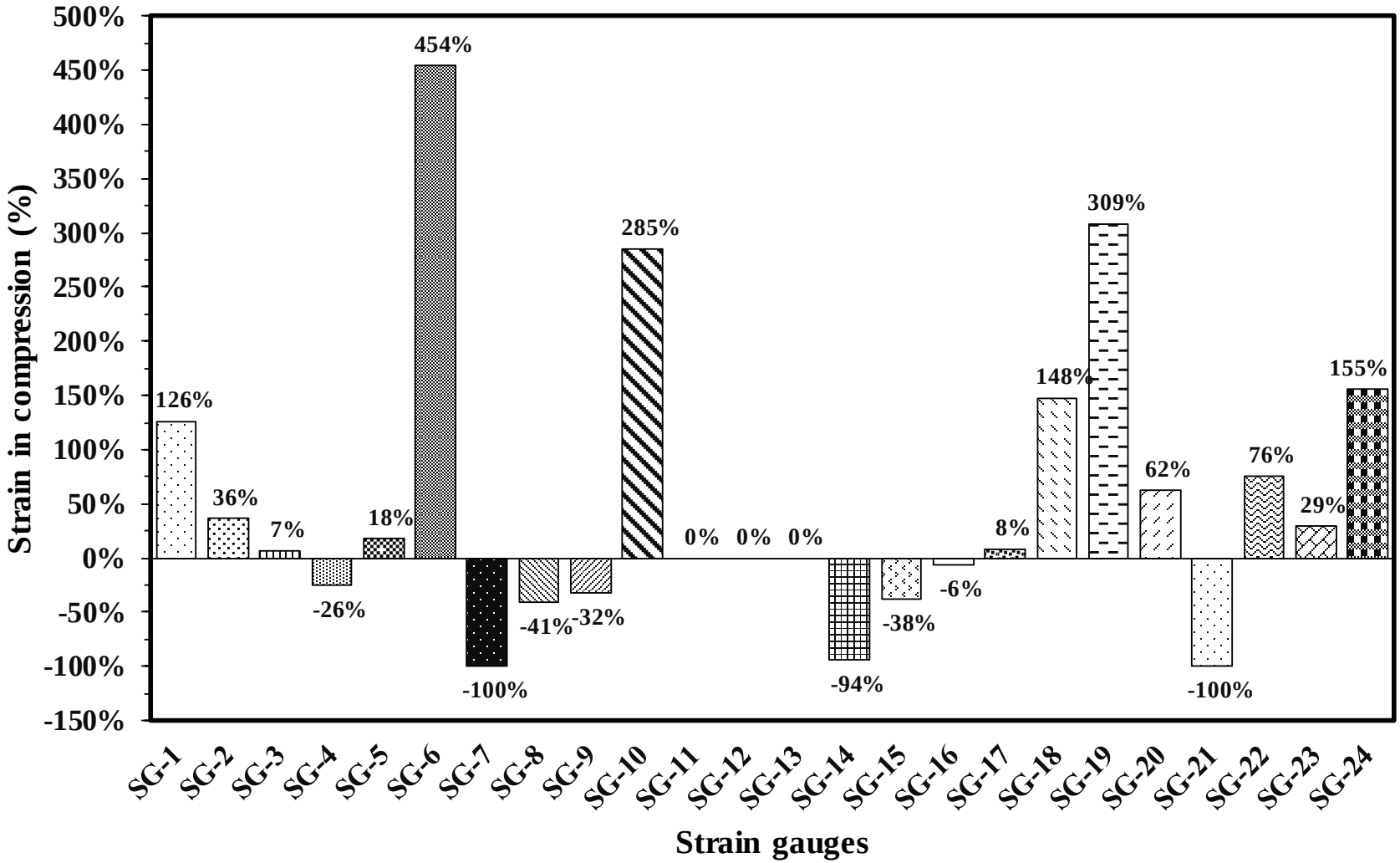

Figure 5.19 Percent difference between adhesive and weld DMS for peak strains in compression

5.3.2 Fatigue Testing Data Investigation

5.3.2.1 Adhesive DMS

Figure 5.20 shows representative strain profiles for the fatigue load test of the adhesive DMS plotted against the number of cycles. The strain profile of strain gauges installed on the north, south, east, and west end of the adhesive DMS is presented in Figure 5.20a through Figure 5.20d, respectively. The strains observed in all gauge locations in the DMS during the cyclic loading is significantly less than the aluminum yield strain of 2745.4 με. At the north end of the adhesive DMS, SG-3 is observed to be under tensile strain; whereas, SG-4 and SG-5 are observed under tensile and compression cycles of strains (see Figure 5.20a). Two strain gauges (SG-9 and SG-17) installed near the west end of the DMS are under tensile and compression cycles of strains with the other strain gauge (SG-15) being completely in compression.

The strain profiles of the strain gauges installed at the corners in the longitudinal and transverse directions are presented in Figure 5.20e and Figure 5.20f, respectively. In the longitudinal direction, all the strain gauges experienced both tensile and compression strains except for SG-2, which is under tension during the test (see Figure 5.20e). In the transverse direction, two strain gauges are found to be under tension (SG-18 and SG-24) with the other two strain gauges under compression (SG-1 and SG-7).

Strains recorded from the gauges installed near the center are plotted against the number of fatigue load cycles, which is shown in Figure 5.20g. SG-11 and SG-14 observed both tensile and compression strains while SG 13 experienced tensile strain only; finally, SG-12 was under compression throughout the fatigue test. The results from the strain profiles suggest that the adhesive DMS subjected to the design fatigue load from the AASHTO Specifications (AASHTO 2015) be adequate up to the applied 500,000 cycles because the strains observed in the aluminum panel are substantially less than the yield strain of the aluminum.

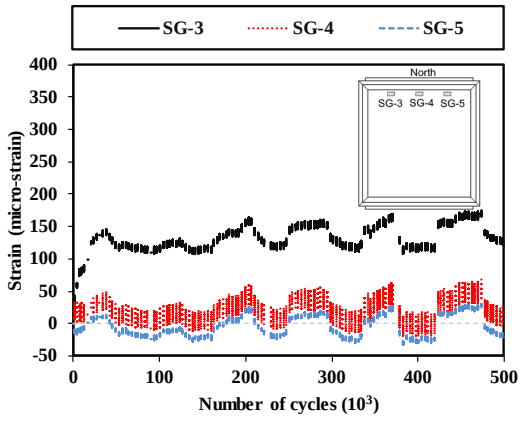

(a)

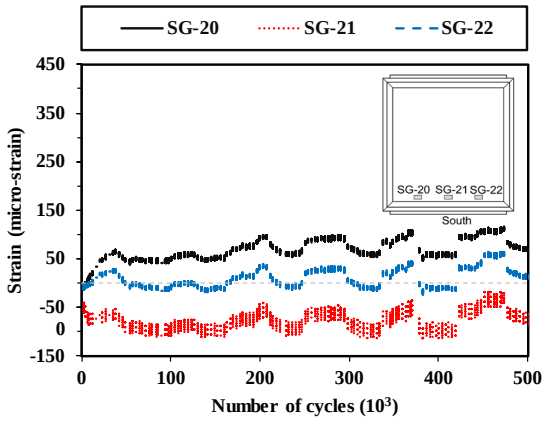

(b)

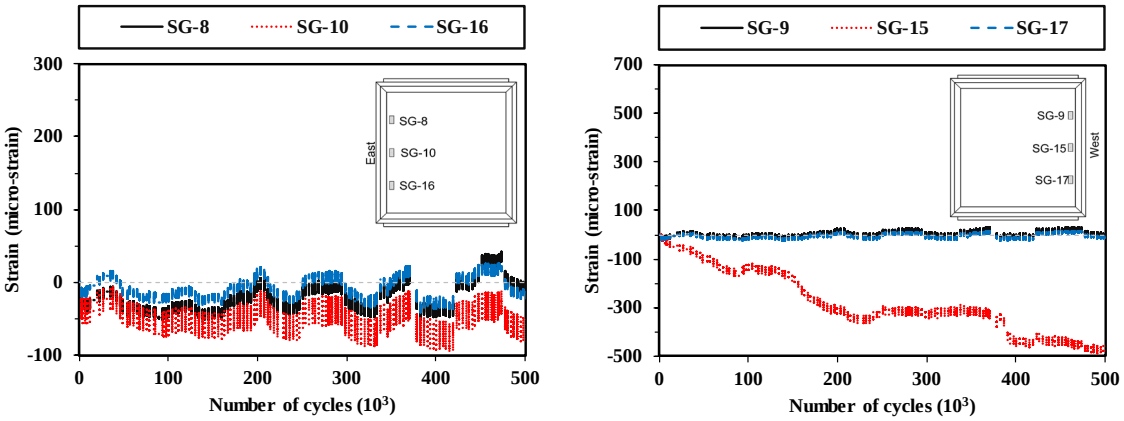

(c)

(d)

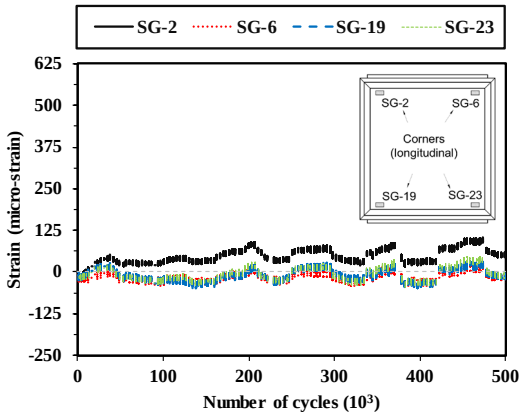

(e)

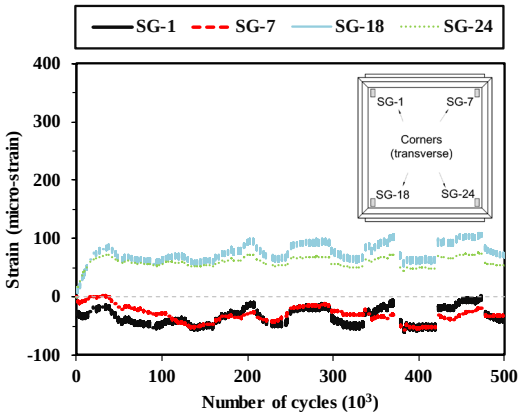

(f)

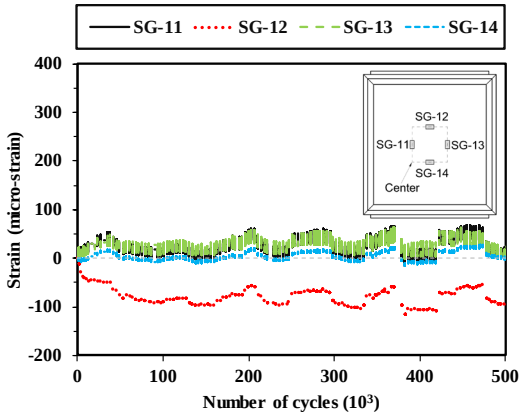

(g)

Figure 5.20 Strain profile for adhesive DMS from fatigue load test at: (a) north end, (b) west end, (c) corners in the longitudinal direction, (d) corners in the transverse direction, and (e) center

Figure 5.21 presents the plot of the maximum stress range (observed in each strain gauge locations) with an S-N curve of 5052-H32 aluminum. The highest maximum stress range is observed for SG-10 (located at the east end) at around 316,000 cycles of fatigue load; whereas, the maximum stress range is the least for SG-7 (located at northeast corner) at around 323,500 cycles of fatigue load. The stress ranges observed during the test of the adhesive DMS are not over the fatigue threshold of the aluminum panel. It can be also concluded that the adhesive DMS is adequate for 500,000 cycles of the considered design fatigue load.

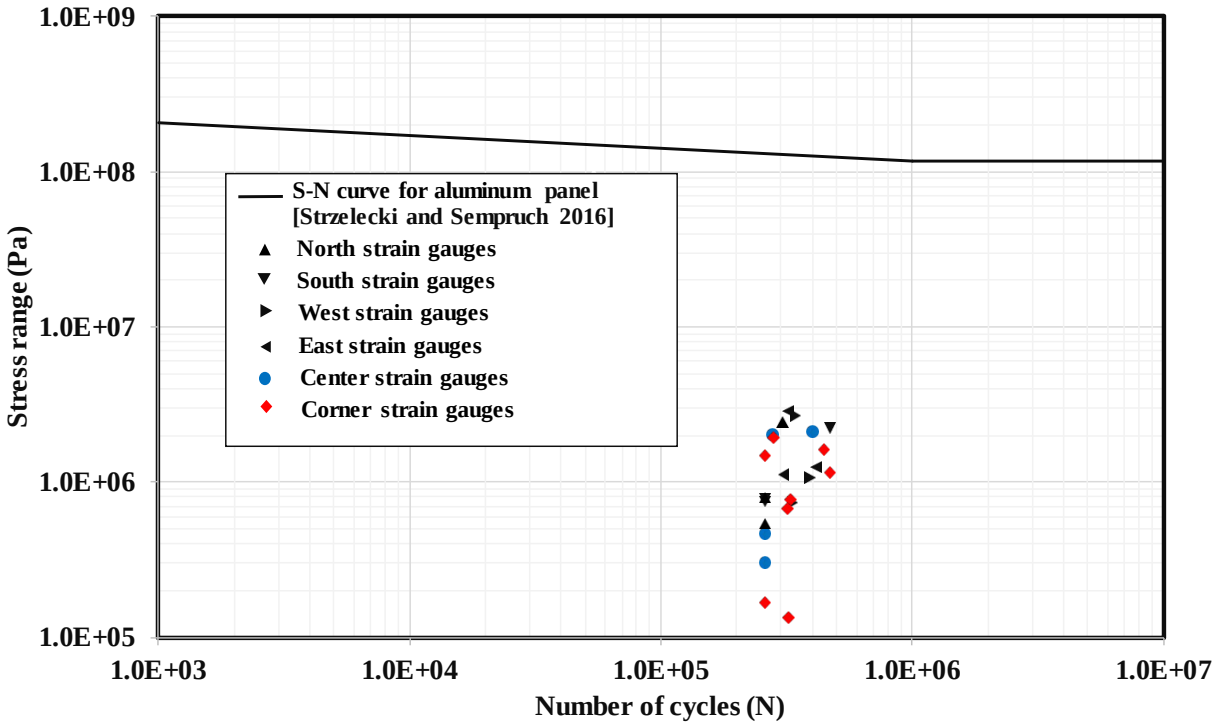

Figure 5.21 Fatigue performance of adhesive DMS with maximum stress range

The performance of the adhesive DMS during the test with respect to deflection is shown in Figure 5.22. The deflection ranges for the LVDTs located near the center of the DMS are observed to be significantly higher than the deflection ranges observed in the other locations. The maximum deflection range is the highest for LVDT V-8 (center) at around 469,500 cycles and is the lowest for LVDT V-12 (south end) at around 418,700 cycles of fatigue load. This indicates that the DMS is subjected to higher vibrations near the center than the other locations when encountered with cyclic wind loads. Note, no sign of damage was observed in the adhesively bonded region of the DMS as well as in all other parts of the DMS. Each corner of the adhesively bonded DMS before the test and after its test completion is shown in Figure 5.23. The adhesive was intact, suggesting the DMS with an adhesive bond to be reliable in terms of wind-induced fatigue loading.

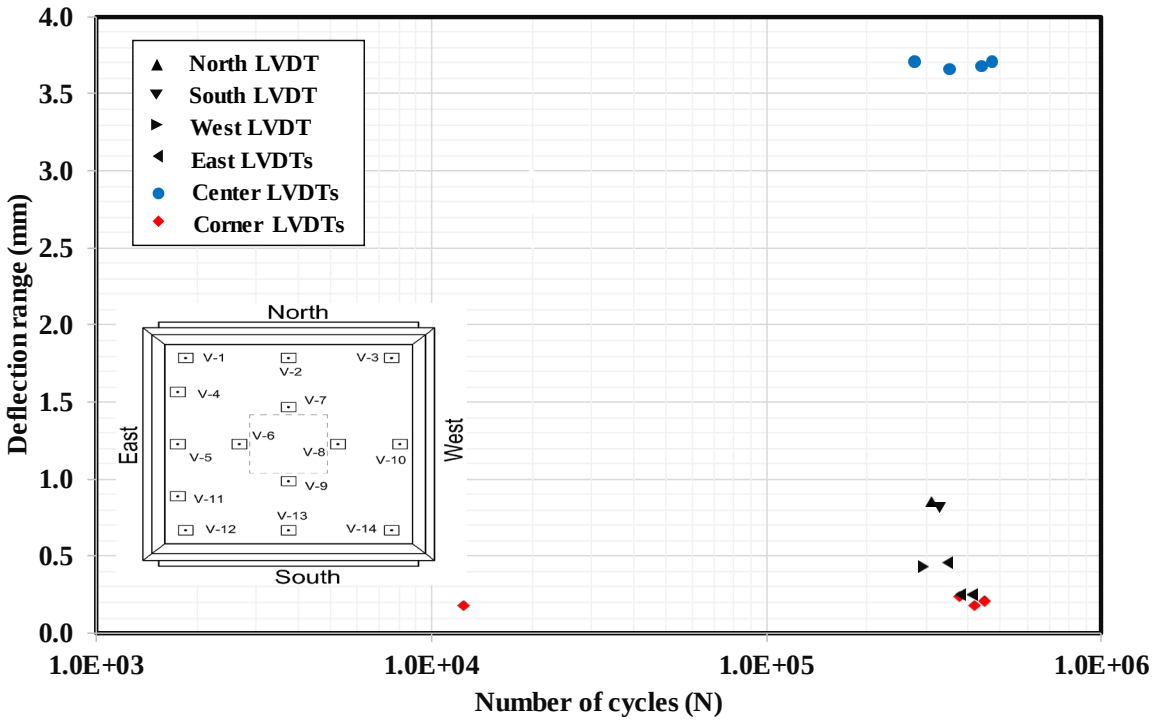

Figure 5.22 Fatigue performance of adhesive DMS with maximum deflection range at LVDT locations

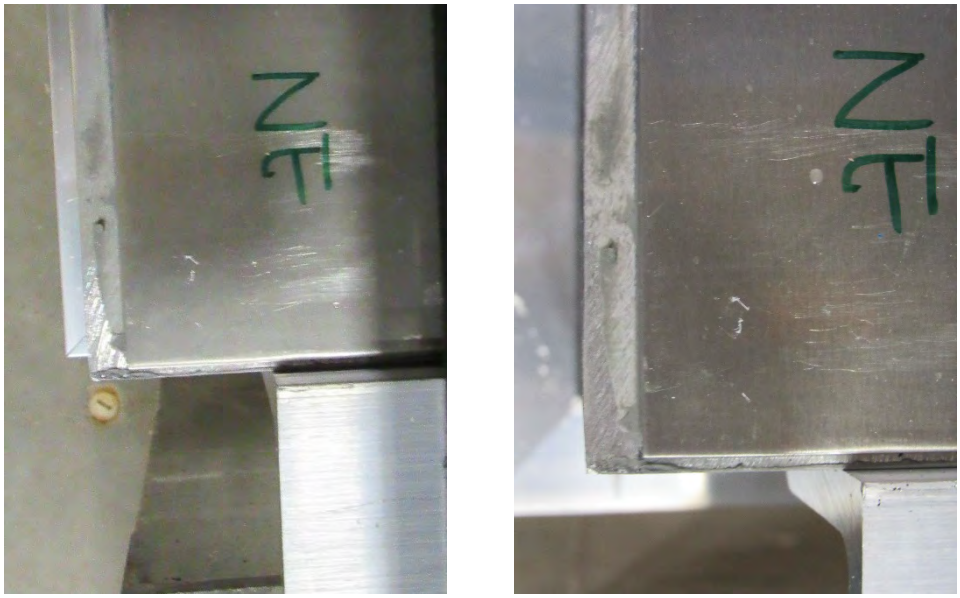

(a) (b)

(c)

(d)

(e)

(f)

(g) (h)

Figure 5.23 Adhesively bonded DMS in fatigue test at: (a) northeast end in beginning, (b) northeast end after the test, (c) southeast end in beginning, (d) southeast end after the test, (e) northwest end in beginning, (f) northwest end after the test, (g) southwest end in beginning, and (h) southwest end after the test.

5.3.2.2 Welded DMS

Figure 5.24 shows representative strain profiles for the fatigue load test of the welded DMS plotted against the number of cycles. The strain profiles of the gauges installed on the north, south, east, and west end of the welded DMS are presented in Figure 5.24a through Figure 5.24d, respectively. Similar to the adhesive DMS results, the strains observed in all gauge locations in the DMS during the cyclic loading is substantially less than the aluminum yield strain of 2745.4 με. At the north end of the welded DMS, SG-3 and SG-5 are observed to be the strains in compression; whereas, SG-4 is observed to be under tensile and compression cycles of strains (see Figure 5.24a). Two strain gauges (SG-9 and SG-15) installed near the west end of the DMS are completely under compression strains with the other strain gauge (SG-17) being under tensile and compression cycles. The strain profile of the strain gauges installed at the corners in the longitudinal and transverse directions is presented in Figure 5.24e and Figure 5.24f, respectively. In the longitudinal direction, all the strain gauges are observed to be under compression except for SG-2, which is under compression initially; however, SG-2 is found to be under tension at the end of the test (see Figure 5.24e). In the transverse direction, all the strain gauges are found to be under compression (SG-1, SG-7, and SG-18) excluding SG-24, which is observed to be under both tension and compression. Strains recorded from the center gauges are plotted against the number of fatigue load cycles and shown in Figure 5.24g. SG-12 and SG-13 observed both tensile and compression strains; whereas, SG 11 and SG-14 were under compression only throughout the fatigue test. It appears that the weld connected DMS is adequate for the design fatigue load from AASHTO (2015) up to 500,000 cyclic loads.

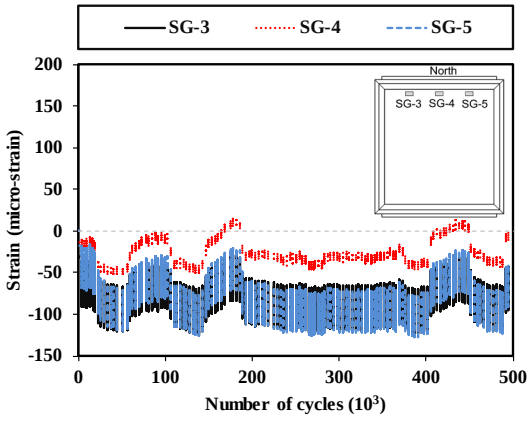
SG-3
SG-4
SG-5
Strain (micro-strain)
Number of cycles (10^3)
North
SG-3 SG-4 SG-5

(a)

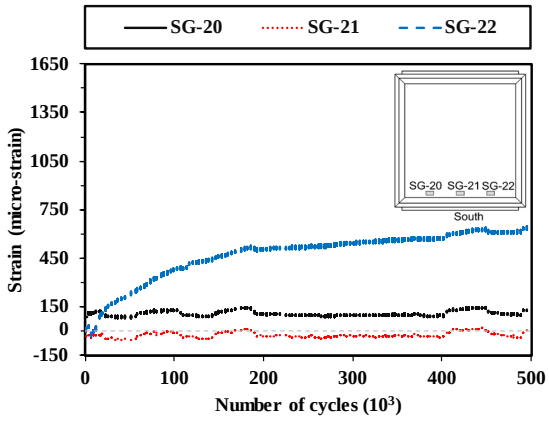
SG-20
SG-21
SG-22
Strain (micro-strain)
Number of cycles (10^3)
SG-20 SG-21 SG-22
South

(b)

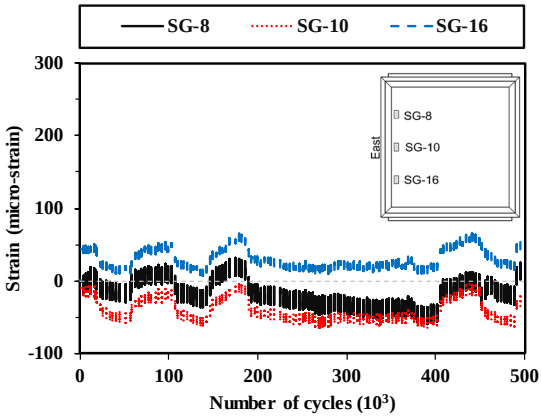
SG-8
SG-10
SG-16
Strain (micro-strain)
Number of cycles (10^3)
East
SG-8
SG-10
SG-16

(c)

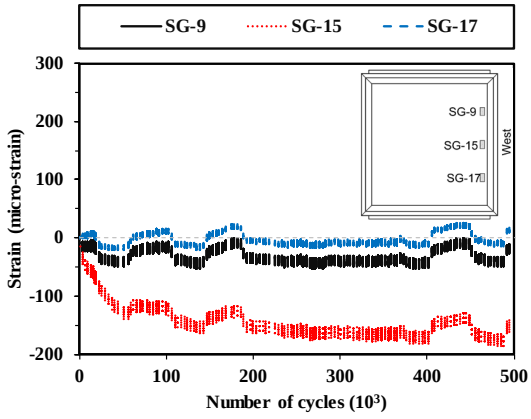
SG-9
SG-15
SG-17
Strain (micro-strain)
Number of cycles (10^3)
SG-9
SG-15
SG-17
West

(d)

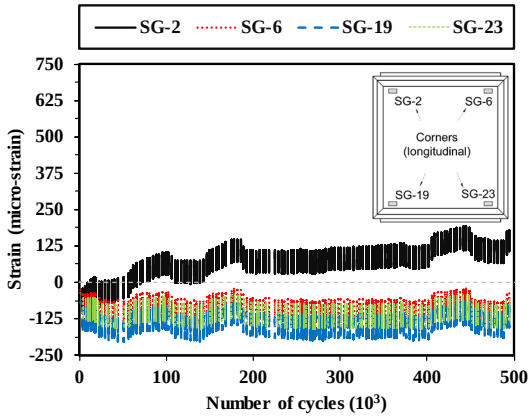
SG-2
SG-6
SG-19
SG-23
Strain (micro-strain)
Number of cycles (10^3)
SG-2
SG-6
Corners
(longitudinal)
SG-19
SG-23

(e)

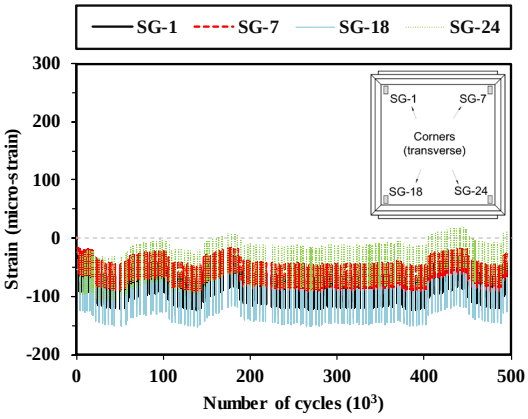
SG-1
SG-7
SG-18
SG-24
Strain (micro-strain)
Number of cycles (10^3)
SG-1
SG-7
Corners
(transverse)
SG-18
SG-24

(f)

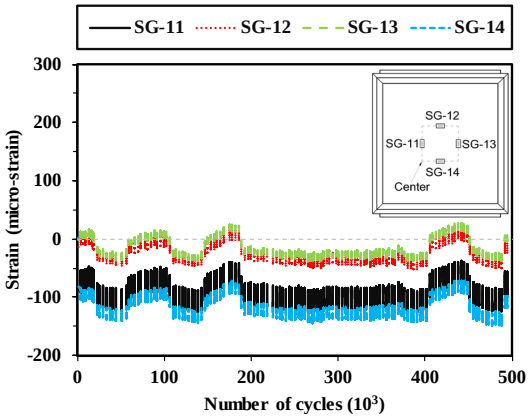

(g)

Figure 5.24 Strain profile for welded DMS from fatigue load test at: (a) north end, (b) west end, (c) corners in the longitudinal direction, (d) corners in the transverse direction, and (e) center

The plot of maximum stress range observed in each of the strain gauge locations in the welded DMS with the S-N curve of 5052-H32 aluminum is shown in Figure 5.25. The highest maximum stress range is observed for SG-23 (located at the southwest corner) at around 444,600 cycles of fatigue load; whereas, the maximum stress range is the least for SG-17 (located at the west end) at around 17,700 cycles of fatigue load. The stress ranges observed during the fatigue test of welded DMS are also below the fatigue threshold of the aluminum panel. The results from the plot indicate the welded DMS is also adequate for 500,000 cycles of the wind-induced fatigue load.

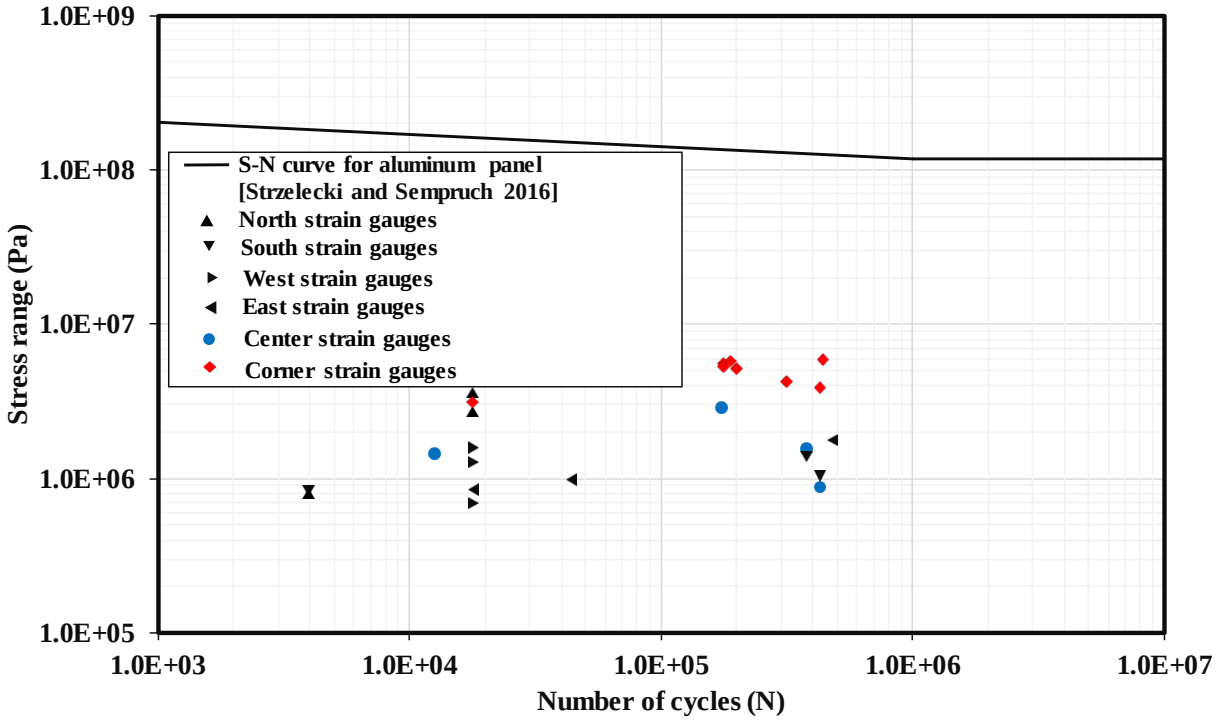

Figure 5.25 Fatigue performance of welded DMS with maximum stress range

The fatigue performance of the welded DMS for deflection criteria is shown in Figure 5.26. A higher range of deflection for the LVDTs located near the center of the DMS is observed when compared with the deflection ranges observed in the other locations. The maximum deflection range is the highest for LVDT V-6 (center) at around 22,300 cycles and is the least for LVDT V-13 (south end) at around 217,900 cycles of fatigue load. Based on the results of the deflection range, a higher vibration of DMS aluminum panel with welded connections is expected near the center than in the other locations as found in the fatigue testing of the adhesively bonded DMS.

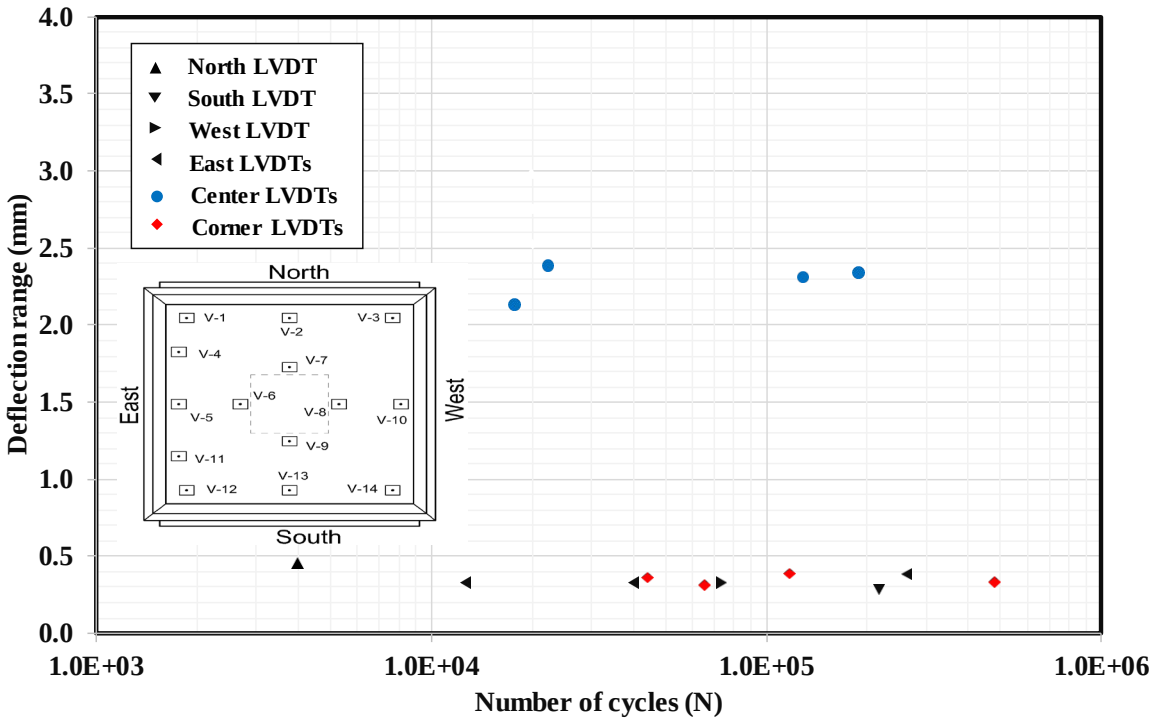

Figure 5.26 Fatigue performance of welded DMS with maximum deflection range at LVDT locations

Figure 5.27 presents each corner of the welded DMS before the test and after the end of the test. The tested welded DMS did not show any damage in the weld and other parts. The results indicate that the weld connection in DMS is also appropriate with respect to the applied fatigue load up to 500,000 cycles.

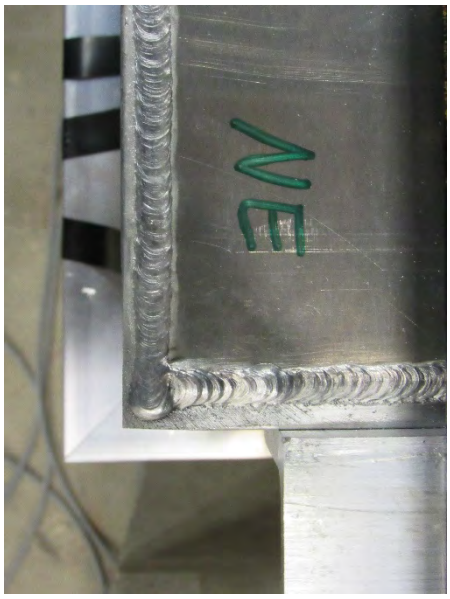

(a)

(b)

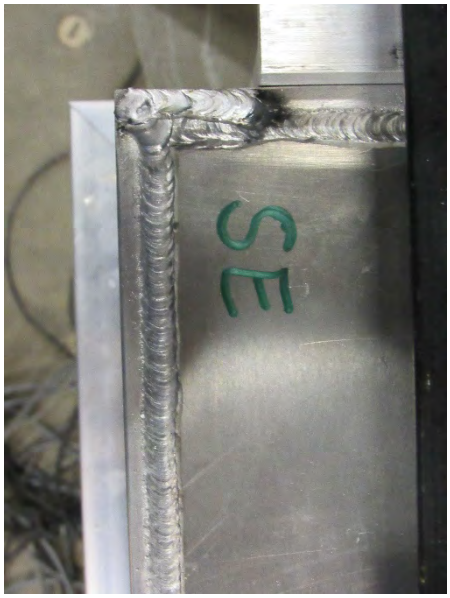

(c)

(d)

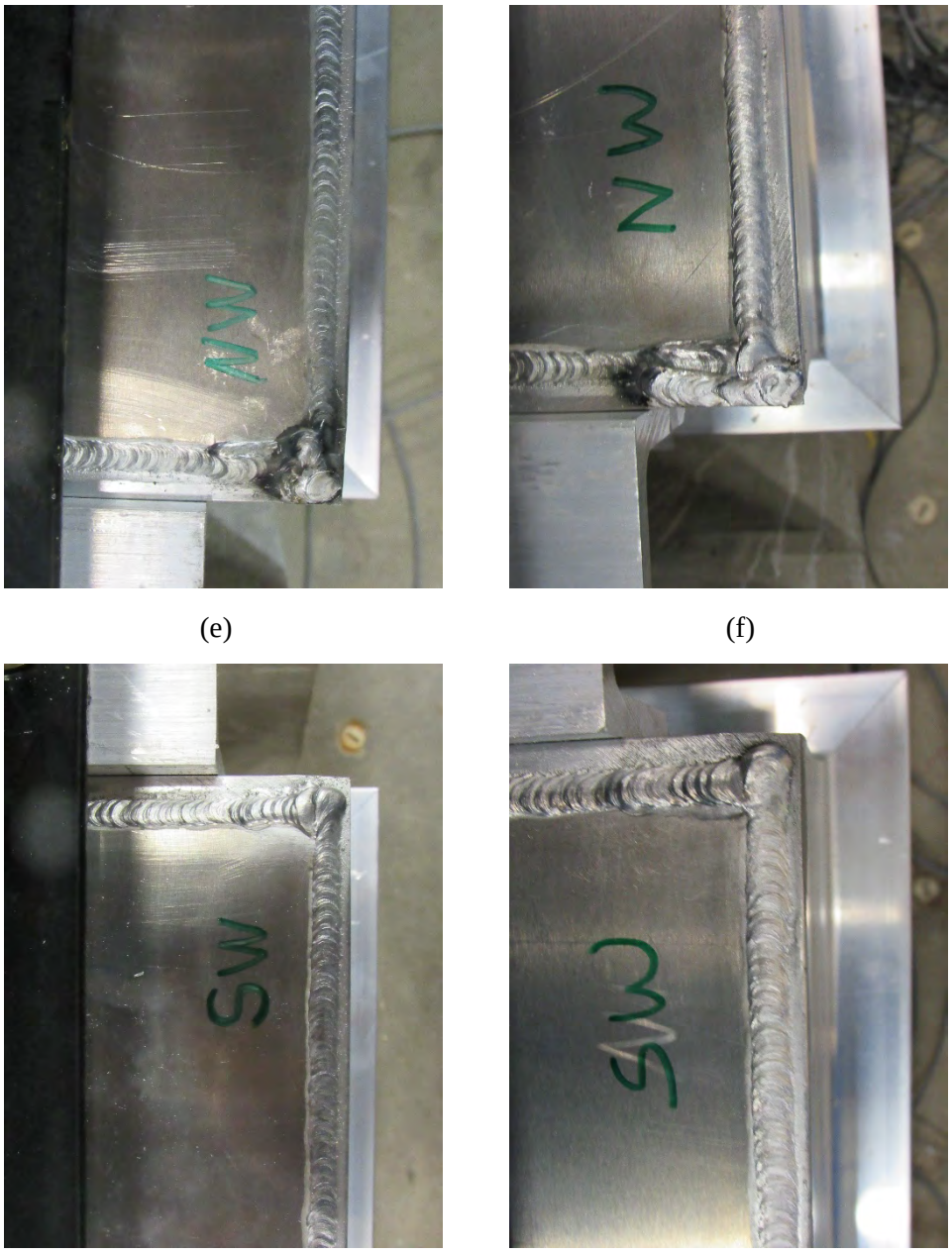

(e) (f)

(g) (h)

Figure 5.27 Welded DMS in fatigue test at: (a) northeast end in beginning, (b) northeast end after the test, (c) southeast end in beginning, (d) southeast end after the test, (e) northwest end in beginning, (f) northwest end after the test, (g) southwest end in beginning, and (h) southwest end after the test.

6. CONCLUSIONS AND FUTURE WORK

This project provides knowledge of mechanical behavior of adhesive specimens loaded with tensile, shear, peel, and cleavage loads and structural behavior of dynamic message signs (DMSs) with adhesive bonding subjected to ultimate and fatigue loads. This section includes key findings obtained from the small-scale and full-scale testings and future work necessary for promoting the use of adhesively bonded DMSs.

6.1 Small-Scale Testing

6.1.1 Tensile Test

The mechanical properties of tensile adhesive specimens that serve as the basis to examine structural behavior of main connections in DMSs were determined through small-scale testing. The effects of conditioning temperature, conditioning humidity, and specimen width on the tensile strength were graphically and statistically investigated. The following conclusions can be derived from the graphical and statistical investigation:

1) The average ultimate tensile stress of 16.94 MPa with a standard deviation of 0.87 MPa was found from the tensile testing data. The ultimate tensile stress data were found to be in agreement with the Lord technical data sheet (LORD Corporation 2020).

2) In the tensile test, when the conditioning temperature was increased, the ultimate tensile stress was reduced for all the combination pairs, with the highest reduction of 5.7% in the pair C8-C14 except for the pair C2-C13. Ductility was also reduced for all the combination pairs, with the maximum reduction of 31.2 % for the pair C8-C14 except for the pair C3-C8.

3) For the tensile test, with the increase in conditioning humidity, the ultimate tensile stress showed a decreasing trend for all the combination pairs, with a peak reduction of 11.9% for the pair C12-C15. Ductility increased for four combination pairs, with the highest increment (34.8%) for the pair C2-C5, and decreased for the other two combination pairs, with decrement up to 12.5% for the pair C6-C8.

4) When the width of the specimens was increased in the tensile test, ultimate tensile stress was reduced for four combination pairs, with the highest reduction of 7.9% in the pair C8-C10 excluding the other two pairs with the highest increment (6.3%) in the pair C4-C5. Ductility was reduced for four combination pairs, with the highest reduction (16.5%) in the pair C15-C16; however, ductility increased for the other two combination pairs, with the highest increment of 3.8% in the pair C8-C10.

5) Two statistical models, multiple linear regression (MLR) and response surface metamodels (RSM), were created for the prediction of ultimate tensile stress. It was found that the RSM model was more accurate than MLR with a comparison of the coefficient of determination (R^2) and visual inspection values.

6) A significant effect of conditioning humidity was identified for the ultimate tensile stress from the statistical analysis. P-values obtained from the statistical analysis indicate that conditioning humidity is the decisive parameter causing the most significant effect on ultimate tensile stress. P-values of 0.427% and 2.529% were observed for MLR and RSM models of ultimate tensile stress.

6.1.2 Shear Test

The effects of conditioning temperature, conditioning humidity, and specimen width on the mechanical properties of adhesive specimens loaded with shear loads were examined through small-scale tests. Major results from the shear testing include the following:

1) The average ultimate shear stress of 16.40 MPa with a standard deviation of 1.37 MPa was observed from the shear tests, which was consistent with the Lord technical data sheet (LORD Corporation 2020).

2) In the shear test, when the conditioning temperature was increased, the ultimate shear stress decreased for four combination pairs, with the highest reduction of 16.8% for the pair C3-C8 except for the other two pairs with the highest increment of 10.0% in the pair C2-C13. Ductility decreased for four combination pairs, with the highest reduction of 28.1% in the pair C2-C13, and increased slightly for the other two pairs.

3) With the increase in the conditioning humidity during the shear tests, the ultimate shear stress dropped for four combination pairs, with the maximum reduction of 15.7% for the pair C8-C11, and increased for two combination pairs with the highest increment of 7.0% in the pair C8-C11. Ductility reduced for four combination pairs, with a peak reduction of 21.5% in the pair C2-C5, and increased for two combination pairs, with peak increment of 8.6% in pair C13-C16.

4) In the shear test, with the increment in width, the ultimate shear stress reduced for three combination pairs, with highest reduction of 8.1% in the pair C1-C2, and increased for three combination pairs, with the highest increment of 19.3% in the pair C8-C10. Three combination pairs had a decreasing trend for ductility, with the highest decrement of 9.5% in the pair C12-C13; whereas, other combination pairs had an increasing trend with the highest increment of 6.7% in pair C1-C2.

5) Two statistical models, containing MLR and RSM, were created for the prediction of ultimate tensile and shear stress. It was found that the RSM model was more accurate than MLR with a comparison of R^2 and visual inspection values.

6) None of the parameters were found to have a significant effect on the ultimate shear stress from the statistical analysis.

6.1.3 Peel Test

The peel strength of the adhesive specimens was experimentally studied and the resulting experimental data indicated the following:

1) From the peel testing data, the average peel strength was found to be 6.63 N/mm with a standard deviation of 2.49 N/mm. The peel testing data were observed to be compatible with the Lord technical data sheet (LORD Corporation 2020).

2) No significant effects of conditioning temperature were found in the peel strength. The increment in conditioning humidity showed improvement in the peel strength. Peel strength was found to decrease significantly with the increase in width of specimens.

3) When the conditioning temperature was increased, the peel strength decreased for three combination pairs, with the highest reduction of 16.3% for the pair C1-C12; whereas, peel strength increased for three combination pairs, with the peak increment of 70.4% for the pair C3-C8. With the increase in conditioning humidity, the peel strength increased for all the combination pairs except for pair C8-C11, with the highest increment of 30.1% in the pair C6-C8. When the specimen width was

increased, the peel strength reduced for all the combination pairs significantly, with the maximum reduction of 28.2% for the pair C1-C2.

4) The RSM model was found to be more reliable for the prediction of the peel strength than the MLR model by evaluating R^2 of the models and comparison of peel strength predicted from the model with experimental data.

5) The MLR-based statistical analysis indicated that the specimen width was the most significant parameter for the peel strength as the P-value of 0.00248 was less than 0.05. This was in agreement with the observations from the 3-D surface plots created using the RSM models.

6.1.4 Cleavage Test

The cleavage tests of the adhesive specimens were performed to study the effect of conditioning temperature, conditioning humidity, and specimen width on the cleavage strength. The following conclusions can be drawn from the cleavage tests:

1) The average cleavage strength of 196.61 N/mm with a standard deviation of 30.14 N/mm was observed from the cleavage testing data.

2) The increment in conditioning temperature and specimen's width was observed to have a progressive effect in the cleavage strength; whereas, the increment in the conditioning humidity was found to have a negative effect on the cleavage strength.

3) With the increase in the conditioning temperature, the cleavage strength improved for all the combination pairs (excluding the pair C8-C14), with the peak increment of 27.1% for the pair C4-C15. The increase in conditioning humidity lowered the cleavage strength for all the combination pairs (eliminating the pair C13-C16), with the peak reduction of 13.7% for the pair C1-C4. When the width of the specimens was increased, the cleavage strength decreased for two combination pairs, with the highest reduction of 13.2% for the pair C12-C13; however, cleavage strength increased for the other four pairs, with the maximum increment of 28.5% for the pair C8-C10.

4) The RSM model was found to be more reliable for the prediction of the cleavage strength than the MLR model by evaluating R^2 of the models and comparison of cleavage strength predicted from the model with experimental data.

5) The RSM surface plots found the cleavage strength was substantially affected by specimen width.

6.1.5 Comparison with Welded Specimens

The tensile, shear, peel, and cleavage strength of the adhesive and weld specimens conditioned at different conditioning temperatures, including extreme conditioning temperatures, were examined to study the effect of conditioning temperature and width on each strength. The adhesive specimens conditioned at temperature (from -56.67°C to 93.33°C) and conditioning humidity (48% to 95%) performed well. Based on these results, adhesive joints are safe to operate within the temperature range of -56.67°C to 93.33°C and humidity range of 48% to 95%. As the testing was limited to these ranges of temperature and humidity, we cannot make any conclusions beyond these ranges; however, the Lord technical data sheet (LORD Corporation 2020) has reported that the Lord 400 series acrylic adhesive used for this project is resistant up to 149°C. Each strength of the adhesive specimens was also compared with that of the welded specimens. The results from these studies indicated the following:

1) For the adhesive tensile specimens, the tensile stress was observed to be decreasing when the conditioning temperature was increased below glass transition temperature of the adhesive; whereas, the tensile stress was increased with the increment of conditioning temperature above the adhesive's glass transition temperature.

2) Due to the effect of conditioning temperature, in the tensile strength test of adhesive specimens, the highest increment and decrement in the tensile stress were 31.9% when conditioning temperature increased from 85°C to 93.33°C for 25-mm width and 11% when conditioning temperature increased from -56.67°C to 20°C for 38-mm width. For the welded specimens, the highest increment and decrement were 36.2% when conditioning temperature increased from 52.5°C to 93.33°C for 25-mm width and 39.7% when conditioning temperature increased from -56.67°C to 20°C for 13-mm width.

3) Owing to the effect of width, for the tensile adhesive strength testing, the peak increment and decrement in the tensile stress were 2.5% when width increased from 13 mm to 25 mm at 93.33°C and 9.4% when width increased from 13 mm to 25 mm at 85°C. With the welded specimens, the peak increment and decrement in the tensile stress were 49% when width increased from 25 mm at 52.5°C to 38 mm at 85°C and 31.9% when width increased from 13 mm to 25 mm at -56.67°C.

4) The tensile stress of welded specimens was found to be higher than the adhesive specimen with the maximum difference of 783% for 13-mm width at -56.67°C.

5) For adhesive shear specimens, the increment of conditioning temperature below adhesive's glass transition temperature observed a decreasing trend in the shear stress, while the increment of conditioning temperature beyond the adhesive's glass transition temperature followed an increasing trend in the shear stress.

6) Due to the effect of conditioning temperature, in the shear strength test of adhesive specimens, the maximum increment and decrement in the shear stress were 30.4% as conditioning temperature increased from 85°C to 93.33°C for 25-mm width and 16.8% as conditioning temperature increased from 20°C to 52.5°C for 25-mm width. For the welded specimens, the maximum increment and decrement were 18.4% as conditioning temperature increased from 85°C to 93.33°C for 38-mm width and 1.1% as conditioning temperature increased from 52.5°C to 93.33°C for 25-mm width.

7) As a result of the effect of width, in the shear strength test of adhesive specimens, the highest increment and decrement in the shear stress were 19.3% when width increased from 25 mm to 38 mm at 52.5°C and 10.6% when width increased from 25 mm to 38 mm at 20°C. For the welded specimens, the highest increment and decrement were 14.9% when width increased from 25 mm to 38 mm at 93.33°C and 4.1% when width increased from 25 mm at 52.5°C to 38 mm at 85°C.

8) In the shear test, each of the welded specimens was observed to be stronger than adhesive specimens in terms of shear stress, with the peak difference of 908% for 25-mm width at 52.5°C.

9) On account of the effect of conditioning temperature, in the peel strength test of adhesive specimens, the peak increment and decrement in the peel strength were 70.4% as conditioning temperature increased from 20°C to 52.5°C for 25-mm width and 43.7% as conditioning temperature increased from 85°C to 93.33°C for 38-mm width. For the welded specimens, the peak increment and decrement were 310.3% as conditioning temperature increased from -56.67°C to 20°C for 13 mm-width and 69.5% as conditioning temperature increased from 85°C to 93.33°C for 38-mm width.

10) Attributable to the effect of width, in the peel strength test of adhesive specimens, the maximum increment and decrement in the peel strength were 32% when width increased from 25 mm to 38 mm at 20°C and 45.6% when width increased from 13 mm to 25 mm at 20°C. For the welded specimens,

the maximum increment and decrement were 24.4% when width increased from 13 mm to 25 mm at -56.67°C and 69.2% when width increased from 25 mm to 38 mm at 93.33°C.

11) In the peel test, the welded specimens were observed to have higher peel strength than adhesive specimens, with the highest difference of 713% for 13-mm width at 20°C.

12) Owing to the effect of conditioning temperature, in the cleavage strength test of adhesive specimens, the highest increment and decrement in the cleavage strength were 37.8% as conditioning temperature increased from 85°C to 93.33°C for 25-mm width and 28.4% as conditioning temperature increased from -56.67°C to 20°C for 13-mm width. For the welded specimens, the highest increment and decrement were 28.9% as conditioning temperature increased from -56.67°C to 85°C for 38-mm width and 14.8% as conditioning temperature increased from 85°C to 93.33°C for 38-mm width.

13) On account of the effect of width, in the cleavage strength test of adhesive specimens, the peak increment and decrement in the cleavage strength were 28.5% when width increased from 25 mm to 38 mm at 52.5°C and 17% when width increased from 13 mm to 25 mm at -56.67°C. For welded specimens, the peak decrement was 52.2% when width increased from 13 mm to 25 mm at 93.33°C. The cleavage strength was not found to have increased when width of the specimens was increased.

14) In the cleavage test, the welded specimens were observed to have higher cleavage strength than adhesive specimens for five pairs with the maximum difference 159% for 130mm width at 20°C. Four other pairs, however, possessed lower cleavage strength than adhesive specimens, with the maximum difference of 31% for 38-mm width at 93.33°C and -56.67°C. These results suggested that the adhesive joints can perform better than the welded joints in terms of cleavage strength at certain environmental and geometrical conditions.

6.2 Full-Scale Testing

6.2.1 Ultimate Strength Testing

The ultimate strength testing was performed on one DMS with adhesive joints and one with typical welded connections. The ultimate strength testings were performed with a monotonic load until failure Load, deflection, and strain responses were recorded for each test and analyzed in depth. Based on the results from the ultimate tests, the following conclusions can be drawn:

1) In the ultimate strength testing, the strains at the corner location of the adhesive DMS and the welded DMS were found to surpass the yield strain of the aluminum DMS panel, indicating high tensile strength at its corners.

2) For the ultimate strength testing, the maximum deflection near the center of the welded DMS (V-6, V7, V8, and V9) was higher up to 8% than the adhesive DMS. The maximum deflection in the boundary and corner locations of the welded DMS (V-1 through V-5 and V-10 through V-14), however, was lower up to 31% than the adhesive DMS. This result indicated that the adhesive DMS was capable of resisting higher deflection at the corner and boundary locations.

3) The ultimate strength testing demonstrated that the maximum strain in the tension of the welded DMS was up to 240% higher than that of the adhesive DMS, and the maximum strain in compression of the welded DMS was up to 454% higher compared with the adhesive DMS.

6.2.2 Fatigue Load Testing

The fatigue testing was performed on one DMS with adhesive joints and one with welded connections. The fatigue load testings were carried out with the application of wind-gust-based design fatigue load from the American Association of State Highway and Transportation Officials (AASHTO) (AASHTO 2015) for 500,000 cycles. Numerous fatigue responses were measured for each of the full-scale tests and examined in detail. The results demonstrated the following:

1) In the fatigue strength testing, the maximum stress ranges observed in both the adhesive and welded DMSs were below the fatigue threshold of the aluminum panel for 500,000 cycles according to the S-N curves.

2) For the fatigue strength testing, the maximum deflection range was found to be highest near the center for both adhesive (V-8) and welded (V-6) DMSs. The results indicated that the DMSs were exposed to higher vibrations near the center than the corner or boundary locations when encountered with the fatigue loads.

3) During the fatigue strength testing, damage was not observed in both adhesive and welded DMSs, and the structural behavior of the adhesive DMS was found to be analogous to the welded DMS in terms of maximum stress ranges and deflection ranges. These results indicated that the strength of adhesive DMS was equivalent to the welded DMS in terms of fatigue loading.

6.3 Future Work

In the future, work presented in this project can be further extended in the following areas:

- Performing finite element analysis of the tested DMS to improve its structural performance through parametric study with variation in adhesive properties and types along with new bonding alternatives.
- Conducting the full-scale tests for DMSs subjected to truck-induced wind loads to examine their fatigue performance.
- Establishing a comprehensive extreme load-based DMS design guideline by conducting representative full-sized DMS tests with seismic loadings.
- Field monitoring, data collection, and analysis from the adhesive bonded DMS installed in highways to investigate the effect of natural wind gust and truck-induced wind load with variation in temperature and moisture.

7. REFERENCES

AASHTO. (2015). LRFD Specifications for Structural Supports for Highway Signs, Luminaires, and Traffic Signals.

Agarwal, A., Foster, S. J., Hamed, E., & Ng, T. S. (2014). “Influence of freeze–thaw cycling on the bond strength of steel–FRP lap joints.” *Composites Part B: Engineering*, *60*, 178-185.

Aluminum Association. (2010). *Aluminum Design Manual*. Washington, D.C.

Arabi, S., Shafei, B., & Phares, B. M. (2018). “Fatigue analysis of sign-support structures during transportation under road-induced excitations.” *Engineering Structures*, *164*, 305-315.

ASTM Committee D-20 on Plastics. (2010). *Standard test method for tensile properties of plastics*. ASTM International.

ASTM D1062-08. (2008). “Standard test method for cleavage strength of metal-to-metal adhesive bonds.” West Conshohocken: American Society of Testing and Materials.

ASTM D1876-08. (2008). “Standard test method for peel resistance of adhesives (T-peel test).” West Conshohocken: American Society of Testing and Materials.

ASTM International. (2010). *Standard test method for apparent shear strength of single-lap-joint adhesively bonded metal specimens by tension loading (metal-to-metal)*. ASTM international.

Broughton, W. R., Mera, R. D., & Hinopoulos, G. “Project PAJ3—Combined Cyclic Loading and Hostile Environments 1996-1999: Report No. 13—Creeping Testing of Adhesive Joints T-Peel Test, Oct. 1999.” *NPL Report CMMT (A)*, *193*, 4-5.

Chandorkar, A. N., Mande, S., & Iwai, H. (2008). “Estimation of process variation impact on DG-FinFET device performance using Plackett-Burman design of experiment method.” In *2008 9th International Conference on Solid-State and Integrated-Circuit Technology* (pp. 215-218). IEEE.

Chang, B., Phares, B. M., Zou, H., & Couch, T. (2014). “Thermal analysis of highway overhead support structures.” *Transportation Research Record*, *2406*(1), 32-41.

Çolak, A., Çoşgun, T., & Bakırcı, A. E. (2009). “Effects of environmental factors on the adhesion and durability characteristics of epoxy-bonded concrete prisms.” *Construction and Building Materials*, *23*(2), 758-767.

Connor, R. J., & Altstadt, S. (2013). “After-Fracture Reserve Strength of Two Four-Chord Aluminum Sign Trusses.” *Journal of Structural Engineering*, *140*(1), 04013030.

Constantinescu, G., Bhatti, A., & Tokyay, T. (2007). *Improved Method for Determining Wind Loads on Highway Sign and Traffic-signal Structures* (No. TR-559).

Da Silva, L. F., Carbas, R. J. C., Critchlow, G. W., Figueiredo, M. A. V., & Brown, K. (2009). “Effect of material, geometry, surface treatment and environment on the shear strength of single lap joints.” *International Journal of Adhesion and Adhesives*, *29*(6), 621-632.

De Freitas, S. T., & Sinke, J. (2014). “Adhesion properties of bonded composite-to-aluminium joints using peel tests.” *The Journal of Adhesion*, *90*(5-6), 511-525.

Ferreira, J. A. M., Reis, P. N., Costa, J. D. M., & Richardson, M. O. W. (2002). "Fatigue behaviour of composite adhesive lap joints." *Composites Science and Technology*, *62*(10-11), 1373-1379.

Goglio, L., & Rezaei, M. (2014). "Variations in mechanical properties of an epoxy adhesive on exposure to warm moisture." *Journal of Adhesion Science and Technology*, *28*(14-15), 1394-1404.

Hu, P., Han, X., Li, L., Shao, Q., & Li, W. D. (2012). "Effect of temperature on shear strength of adhesively bonded joints for automobile industry." In *Advanced Materials Research* (Vol. 418, pp. 1259-1265). Trans Tech Publications Ltd.

Huckelbridge Jr, A. A., & Metzger, A. T. (2009). "Investigation of the Dayton, Ohio, IR 75 sign truss failure of September 11, 2006." *Journal of Performance of Constructed Facilities*, *23*(5), 372-378.

Kim, K. S., & Aravas, N. (1988). "Elastoplastic analysis of the peel test." *International Journal of Solids and Structures*, *24*(4), 417-435.

Kim, Y. J., Hossain, M., & Yoshitake, I. (2012). "Cold region durability of a two-part epoxy adhesive in double-lap shear joints: Experiment and model development." *Construction and Building Materials*, *36*, 295-304.

Kokaly, R. F., & Clark, R. N. (1999). "Spectroscopic determination of leaf biochemistry using band-depth analysis of absorption features and stepwise multiple linear regression." *Remote Sensing of Environment*, *67*(3), 267-287.

LORD Corporation. (2018). LORD® 406 Acrylic Adhesive. Retrieved November 29, 2018, from https://www.lord.com/products-and-solutions/adhesives/lord-406-acrylic-adhesive

LORD Corporation. (2020). LORD TECHNICAL DATA. Retrieved July 15, 2020, from https://files.lord.com/pdf/44/DS3882_LORD400Series.pdf

Lettieri, M., & Frigione, M. (2011). "Natural and artificial weathering effects on cold-cured epoxy resins." *Journal of Applied Polymer Science*, *119*(3), 1635-1645.

McLean, T. W., Park, J. S., & Stallings, J. M. (2004). *Fatigue Evaluation of Two Variable Message Sign Structures*. Highway Research Center, Auburn University.

Mocibob, D., & Crisinel, M. (2008). *Linear connection system for structural application of glass panels in fully-transparent pavilions* (No. CONF, pp. 253-261). IOS Press BV.

Moussa, O., Vassilopoulos, A. P., de Castro, J., & Keller, T. (2012). "Time–temperature dependence of thermomechanical recovery of cold-curing structural adhesives." *International Journal of Adhesion and Adhesives*, *35*, 94-101.

MTS Systems Corporation. (2018). MTS Landmark® Servohydraulic Test Systems. Retrieved November 29, 2018, from http://www.mts.com/en/products/producttype/test-systems/load-frames-uniaxial/servohydraulic/standard/index.htm

MTS Systems Corporation. (2019). A complete family of quality, affordable electromechanical test systems. Retrieved March 03, 2019, from http://www.mts.com/en/forceandmotion/materialstesting/MTS_002886?article=3

Neto, J. A. B. P., Campilho, R. D., & Da Silva, L. F. M. (2012). "Parametric study of adhesive joints with composites." *International Journal of Adhesion and Adhesives*, *37*, 96-101.

Noori, H., Jain, M., Nielsen, K., & Brandys, F. (2016). “Effect of Deformation-induced Residual Stress on Peel Strength of Polymer Laminated Sheet Metal.” *The Journal of Adhesion*, *92*(10), 862-876.

Park, J. S., & Stallings, J. M. (2006). “Fatigue evaluations of variable message sign structures based on AASHTO specifications.” *KSCE Journal of Civil Engineering*, *10*(3), 207-217.

Puckett, J. A., Erikson, R. G., & Peiffer, J. P. (2010). “Fatigue testing of stiffened traffic signal structures.” *Journal of Structural Engineering*, *136*(10), 1205-1214.

SAS Institute Inc. (2008). *JMP Statistics and Graphics Guide, version 5.1.2*, Cary, NC

Savvilotidou, M., Vassilopoulos, A. P., Frigione, M., & Keller, T. (2017). “Development of physical and mechanical properties of a cold-curing structural adhesive in a wet bridge environment.” *Construction and Building Materials*, *144*, 115-124.

Seo, J. (2013). “Statistical determination of significant curved I-girder bridge seismic response parameters.” *Earthquake Engineering and Engineering Vibration*, *12*(2), 251-260.

Seo, J., & Linzell, D. G. (2010). “Probabilistic Vulnerability Scenarios for Horizontally Curved Steel I-Girder Bridges under Earthquake Loads.” *Transportation Research Record*, *2202*(1), 206-211.

Seo, J., & Linzell, D. G. (2012). “Horizontally curved steel bridge seismic vulnerability assessment.” *Engineering Structures*, *34*, 21-32.

Seo, J., & Linzell, D. G. (2013a). “Influential Curved Steel Bridge Fragility Analysis Parameters.” In *Forensic Engineering 2012: Gateway to a Safer Tomorrow* (pp. 84-92).

Seo, J., & Linzell, D. G. (2013b). “Use of response surface metamodels to generate system level fragilities for existing curved steel bridges.” *Engineering Structures*, *52*, 642-653.

Seo, J., & Pokhrel, J. (2019). “Surrogate Modeling for Self-Consolidating Concrete Characteristics Estimation for Efficient Prestressed Bridge Construction.” *American Concrete Institute Special Publication.*

Shahid, M., & Hashim, S. A. (2000). “Cleavage strength of steel/composite joints.” *The Journal of Adhesion*, *73*(4), 365-384.

Shahid, M., & Hashim, S. A. (2002). “Effect of surface roughness on the strength of cleavage joints.” *International Journal of Adhesion and Adhesives*, *22*(3), 235-244.

Silva, P., Fernandes, P., Sena-Cruz, J., Xavier, J., Castro, F., Soares, D., & Carneiro, V. (2016). “Effects of different environmental conditions on the mechanical characteristics of a structural epoxy.” *Composites Part B: Engineering*, *88*, 55-63.

Sousa, J. M., Correia, J. R., & Cabral-Fonseca, S. (2018). “Durability of an epoxy adhesive used in civil structural applications.” *Construction and Building Materials*, *161*, 618-633.

Strzelecki, P., & Sempruch, J. (2016). “Experimental method for plotting SN curve with a small number of specimens.” *Polish Maritime Research*, *23*(4), 129-137.

Sugiman, S., Crocombe, A. D., & Aschroft, I. A. (2013a). “The fatigue response of environmentally degraded adhesively bonded aluminium structures.” *International Journal of Adhesion and Adhesives*, *41*, 80-91.

Sugiman, S., Crocombe, A. D., & Aschroft, I. A. (2013b). “Experimental and numerical investigation of the static response of environmentally aged adhesively bonded joints.” *International Journal of Adhesion and Adhesives, 40*, 224-237.

Tsai, C. L., Park, S. C., & Cheng, W. T. (1999). “Welding distortion of a thin-plate panel structure.” *Welding Journal-New York, 78*, 156-s.

Zheng, X. L., Zhang, M. S., You, M., Yu, H. Z., & Li, Z. (2007). “A Study on Normal Stress Distribution and Failure of Adhesively Bonded Joint under Cleavage Loading.” In *Key Engineering Materials* (Vol. 348, pp. 949-952). Trans Tech Publications.

APPENDIX A

Summary of Tensile Testing Results

Mechanical properties from the tensile test of adhesive specimens

Combination	Specimen ID	Young's modulus, E (MPa)	Stiffness, k (KN/m)	Ultimate tensile stress, f_u(Mpa)	Ultimate tensile load, P_u(N)	Strain at ultimate load, (mm/mm)	Yield stress, f_y (MPa)	Load at yield point, P_y (N)	Strain at yield point, (mm/mm)	Ductility, e (%)
C1	A-T-13TH-20T/48H-C1-1	1390.69	651.84	18.12	870.96	0.11900	10.63	511.15	0.00947	14.28
	A-T-13TH-20T/48H-C1-2	1288.29	690.86	17.63	976.34	0.12800	10.09	558.79	0.00927	15.34
C2	A-T-38TH-20T/48H-C2-1	1298.21	2142.50	17.68	3033.60	0.12260	10.15	1741.17	0.00964	12.60
	A-T-38TH-20T/48H-C2-2	1307.91	1946.71	17.57	2725.78	0.12923	9.57	1485.22	0.00874	13.43
C3	A-T-25TH-20T/71H-C3-1	1318.53	1401.17	17.61	1854.77	0.07985	10.64	1120.77	0.01000	8.38
	A-T-25TH-20T/71H-C3-2	1261.22	1301.33	17.62	1784.36	0.17623	10.31	1044.13	0.01017	21.33
C4	A-T-13TH-20T-95H-C4-1	1240.42	425.77	16.35	638.19	0.21417	9.15	357.26	0.00908	21.42
	A-T-13TH-20T-95H-C4-2	1215.04	454.21	16.07	648.12	0.12743	8.95	360.82	0.00937	15.27
C5	A-T-38TH-20T-95H-C5-1	1166.27	1903.45	17.10	2917.90	0.21155	9.07	1546.67	0.00949	21.15
	A-T-38TH-20T-95H-C5-2	1287.76	1832.35	17.37	2752.02	0.12953	9.50	1504.83	0.00898	13.94
C6	A-T-25TH-52T/48H-C6-1	1115.95	1172.37	17.43	1866.16	0.15752	9.02	966.38	0.00983	16.45
	A-T-25TH-52T/48H-C6-2	935.99	951.24	16.86	1702.42	0.20701	7.85	792.94	0.01047	21.13
C7	A-T-13TH-52T/71H-C7-1	935.09	472.33	17.29	752.86	0.19269	9.36	407.77	0.01177	20.52
	A-T-13TH-52T/71H-C7-2	1008.14	421.67	17.31	675.68	0.14376	9.47	369.74	0.01156	14.95
C8	A-T-25TH-52T/71H-C8-1	1044.76	1123.61	17.03	1802.33	0.14060	9.23	976.65	0.01070	14.83
	A-T-25TH-52T/71H-C8-2	1106.73	1175.24	17.16	1807.94	0.17687	9.30	984.35	0.01038	18.07
C9	A-T-25TH-52T/71H-C9-1	1064.03	1185.63	17.08	1865.50	0.14372	9.12	996.49	0.01018	15.09
	A-T-25TH-52T/71H-C9-2	1099.46	1112.93	16.82	1723.55	0.13973	9.22	944.89	0.01020	14.73
C10	A-T-38TH-52T/71H-C10-1	937.53	1653.70	16.62	2712.57	0.21150	7.95	1297.10	0.01043	21.15
	A-T-38TH-52T/71H-C10-2	840.20	1526.30	14.88	2469.43	0.12544	7.36	1222.33	0.01063	13.00
C11	A-T-25TH-52T-95H-C11-1	1335.47	1234.08	17.18	1728.86	0.15190	9.98	1004.92	0.00939	16.03
	A-T-25TH-52T-95H-C11-2	1222.69	999.94	16.60	1521.22	0.15610	9.18	840.74	0.00964	16.56
C12	A-T-13TH-85T/48H-C12-1	858.94	511.07	17.06	945.56	0.13170	8.05	446.16	0.01142	13.28
	A-T-13TH-85T/48H-C12-2	933.52	581.16	18.53	1002.45	0.10057	9.37	507.10	0.01182	10.21
C13	A-T-38TH-85T/48H-C13-1	1211.68	1623.58	17.69	2838.77	0.12915	8.37	1342.92	0.00867	12.98
	A-T-38TH-85T/48H-C13-2	1311.10	1614.63	17.83	2709.14	0.10624	8.94	1357.69	0.00860	10.88
C14	A-T-25TH-85T/71H-C14-1	925.49	1135.12	17.33	2001.30	0.14291	8.73	1008.28	0.01133	14.39
	A-T-25TH-85T/71H-C14-2	940.04	892.60	14.92	1384.64	0.08080	7.78	721.41	0.01008	8.23
C15	A-T-13TH-85T-95H-C15-1	954.83	421.62	15.02	665.44	0.17589	7.39	327.25	0.00937	18.29
	A-T-13TH-85T-95H-C15-2	1103.58	415.51	16.35	647.48	0.12731	8.77	347.52	0.00993	13.30
C16	A-T-38TH-85T-95H-C16-1	1046.33	1674.26	15.57	2659.33	0.11712	8.23	1405.72	0.00985	11.93
	A-T-38TH-85T-95H-C16-2	975.50	1652.72	16.44	2716.69	0.14338	8.88	1467.40	0.01115	14.45

Mechanical properties from the tensile test of adhesive specimens for extreme temperature conditions

Combination	Specimen ID	Young's modulus, E (MPa)	Stiffness, k (KN/m)	Ultimate tensile stress, f_u(Mpa)	Ultimate tensile load, P_u(N)	Strain at ultimate load, (mm/mm)	Yield stress, f_y (MPa)	Load at yield point, P_y (N)	Strain at yield point, (mm/mm)	Ductility, e (%)
A1	A-T-13TH-93T-A1-1	1140.51	600.35	20.33	898.36	0.10100	11.71	517.28	0.01200	10.85
	A-T-13TH-93T-A1-2	1317.06	571.04	21.20	902.77	0.09400	11.78	501.54	0.01100	9.87
A2	A-T-25TH-93T-A2-1	1185.33	1197.08	21.48	1891.92	0.07300	12.81	1128.20	0.01200	7.65
	A-T-25TH-93T-A2-2	1367.55	1224.03	21.07	1835.43	0.06900	11.97	1042.71	0.01000	7.15
A3	A-T-38TH-93T-A3-1	1330.75	1854.77	21.11	2901.13	0.08900	11.62	1596.51	0.01000	9.17
	A-T-38TH-93T-A3-2	1449.42	2013.78	19.70	2735.08	0.05400	11.64	1616.80	0.00900	7.00
A4	A-T-13TH-(-56.67)T-A4-1	1281.14	560.91	19.03	787.48	0.12411	11.14	460.99	0.01037	14.32
	A-T-13TH-(-56.67)T-A4-2	1369.15	491.98	19.71	755.33	0.21205	10.99	421.16	0.00950	21.39
A5	A-T-25TH-(-56.67)T-A5-1	1574.27	1241.07	19.93	1797.52	0.11429	12.28	1107.57	0.00961	12.02
	A-T-25TH-(-56.67)T-A5-2	1388.22	1355.99	19.32	1710.13	0.16274	11.27	997.50	0.01003	17.28
A6	A-T-38TH-(-56.67)T-A6-1	1475.22	2210.63	20.76	3224.87	0.12385	12.45	1934.23	0.01032	13.78
	A-T-38TH-(-56.67)T-A6-2	1316.66	1997.67	18.84	3017.47	0.12438	10.79	1728.21	0.01019	12.59

Mechanical properties from the tensile test of welded specimens

Combination	Specimen ID	Young's modulus, E (MPa)	Stiffness, k (KN/m)	Ultimate tensile stress, f_u(Mpa)	Ultimate tensile load, P_u(N)	Strain at ultimate load, (mm/mm)	Yield stress, f_y (MPa)	Load at yield point, P_y (N)	Strain at yield point, (mm/mm)	Ductility, e (%)
W1	W-T-13TH-93.33T-W1-1	49470.08	22194.52	129.83	5235.20	0.02674	69.75	2812.44	0.00319	3.87
	W-T-13TH-93.33T-W1-2	59727.89	21964.58	105.64	4259.57	0.01449	68.05	2743.84	0.00337	1.47
W2	W-T-25TH-93.33T-W2-1	52398.93	39692.31	109.52	8832.26	0.01326	71.25	5745.68	0.00287	1.34
	W-T-25TH-93.33T-W2-2	75100.00	38668.17	112.17	9045.74	0.01860	71.05	5729.80	0.00299	2.27
W3	W-T-38TH-93.33T-W3-1	85321.10	50508.67	155.01	18750.65	0.04249	71.91	8698.51	0.00301	4.28
	W-T-38TH-93.33T-W3-2	80800.26	47873.54	90.53	10950.79	0.00830	70.72	8555.08	0.00288	0.86
W4	W-T-13TH-(-56.67)T-W4-1	61823.78	22562.99	182.53	7360.14	0.08087	75.34	3037.87	0.00304	8.67
	W-T-13TH-(-56.67)T-W4-2	47511.30	22282.78	159.44	6429.17	0.03879	78.97	3184.31	0.00312	3.88
W5	W-T-25TH-(-56.67)T-W5-1	80289.77	38003.39	125.67	10134.88	0.02865	68.44	5519.38	0.00306	3.36
	W-T-25TH-(-56.67)T-W5-2	75568.25	37496.40	107.24	8648.04	0.01309	70.74	5704.60	0.00288	1.31
W6	W-T-38TH-(-56.67)T-W6-1	81098.26	49082.79	106.51	12884.06	0.01203	73.29	8865.18	0.00292	1.74
	W-T-38TH-(-56.67)T-W6-2	85879.90	47962.15	109.05	13191.84	0.01368	71.56	8656.50	0.00282	1.41
W7	W-T-13TH-20T-W7-1	87322.12	22165.80	95.26	3841.00	0.01228	65.87	2656.05	0.00335	2.67
	W-T-13TH-20T-W7-2	67024.75	23418.13	110.84	4469.41	0.01173	82.50	3326.54	0.00331	2.01
W8	W-T-25TH-52.5T-W8-1	74686.48	38437.18	86.33	6962.43	0.00872	71.75	5786.25	0.00337	2.32
	W-T-25TH-52.5T-W8-2	77224.47	40350.26	76.38	6159.39	0.00423	69.28	5586.81	0.00296	2.06
W9	W-T-38TH-85T-W9-1	75533.17	47651.65	117.49	14211.97	0.01625	75.48	9130.28	0.00295	1.89
	W-T-38TH-85T-W9-2	82631.26	47823.97	124.97	15117.24	0.02230	73.49	8889.68	0.00297	2.40

APPENDIX B

Summary of Shear Testing Results

Mechanical properties from the shear test of adhesive specimens

Combination	Specimen ID	Shear modulus, G (MPa)	Stiffness, k (KN/m)	Ultimate shear stress, τ_u (Mpa)	Ultimate shear load, V_u (N)	Strain at ultimate load, (mm/mm)	Yield stress, τ_y (MPa)	Load at yield point, V_y (N)	Strain at yield point, (mm/mm)	Ductility, e (%)
C1	A-S-13TH-20T/48H-C1-1	31.85	8125.53	17.89	2885.38	1.25992	10.54	1699.89	0.33505	3.74
	A-S-13TH-20T/48H-C1-2	20.38	7862.14	17.08	2754.16	1.98534	11.69	1886.13	0.58858	4.59
C2	A-S-38TH-20T/48H-C2-1	33.47	20864.26	17.19	8317.02	1.68660	4.58	2215.84	0.14074	3.43
	A-S-38TH-20T/48H-C2-2	53.43	17949.45	14.93	7224.94	0.84252	9.24	4470.69	0.17871	5.46
C3	A-S-25TH-20T/71H-C3-1	39.41	13937.47	19.02	6134.10	1.04596	10.57	3410.14	0.27560	5.12
	A-S-25TH-20T/71H-C3-2	32.03	14231.68	16.93	5459.75	1.25083	11.60	3742.07	0.36751	4.20
C4	A-S-13TH-20T-95H-C4-1	42.15	8022.56	16.07	2592.27	0.83314	11.48	1851.71	0.27202	3.34
	A-S-13TH-20T-95H-C4-2	27.64	7881.93	15.62	2520.02	1.32835	8.66	1396.13	0.31682	3.47
C5	A-S-38TH-20T-95H-C5-1	31.92	19848.87	16.17	7823.56	1.11222	10.30	4986.07	0.32724	3.62
	A-S-38TH-20T-95H-C5-2	22.73	18269.05	16.61	8037.29	1.52415	11.68	5652.17	0.51979	3.36
C6	A-S-25TH-52T/48H-C6-1	27.76	15270.01	18.71	6036.15	1.56014	11.03	3558.60	0.40650	3.32
	A-S-25TH-52T/48H-C6-2	-	13770.39	16.79	5416.24	0.97961	-	-	-	4.68
C7	A-S-13TH-52T/71H-C7-1	32.94	7849.53	16.70	2692.91	1.26080	6.24	1007.26	0.19171	3.88
	A-S-13TH-52T/71H-C7-2	31.53	8038.67	15.30	2468.01	1.03720	9.68	1561.55	0.31785	3.40
C8	A-S-25TH-52T/71H-C8-1	31.28	14317.84	15.05	4853.37	1.24560	9.50	3065.98	0.31028	4.15
	A-S-25TH-52T/71H-C8-2	43.17	15243.04	14.87	4795.41	0.82539	8.18	2638.60	0.19342	3.16
C9	A-S-25TH-52T/71H-C9-1	24.28	14946.72	17.12	5521.04	1.57680	9.23	2978.44	0.39307	3.40
	A-S-25TH-52T/71H-C9-2	30.28	14174.41	12.67	4087.25	1.10664	9.30	2999.93	0.31508	3.00
C10	A-S-38TH-52T/71H-C10-1	37.99	21337.10	18.57	8983.67	1.37138	8.29	4008.87	0.22302	3.35
	A-S-38TH-52T/71H-C10-2	28.98	20692.81	17.12	8285.61	1.39245	10.79	5222.48	0.37769	3.49
C11	A-S-25TH-52T-95H-C11-1	26.67	12254.67	15.03	4846.83	1.30605	9.84	3174.07	0.37684	3.76
	A-S-25TH-52T-95H-C11-2	26.22	12615.26	16.98	5477.15	1.43404	9.75	3144.27	0.37860	3.65
C12	A-S-13TH-85T/48H-C12-1	33.19	8153.55	16.09	2594.47	1.13195	10.58	1706.83	0.33630	3.47
	A-S-13TH-85T/48H-C12-2	25.98	8509.24	18.01	2904.51	1.52084	8.82	1422.41	0.34353	3.59
C13	A-S-38TH-85T/48H-C13-1	36.71	21209.96	17.69	8560.25	1.24520	8.83	4273.05	0.24706	3.11
	A-S-38TH-85T/48H-C13-2	28.74	21330.79	17.64	8534.58	1.78198	8.25	3994.28	0.29934	3.28
C14	A-S-25TH-85T/71H-C14-1	23.64	12063.78	15.09	4867.20	1.40980	9.32	3005.00	0.39973	4.02
	A-S-25TH-85T/71H-C14-2	34.58	12928.56	15.84	5111.10	1.00550	10.21	3294.18	0.29697	3.49
C15	A-S-13TH-85T-95H-C15-1	27.72	6557.62	16.00	2580.72	1.30314	9.05	1459.34	0.32732	3.47
	A-S-13TH-85T-95H-C15-2	41.46	6001.95	15.26	2461.82	0.92771	8.73	1407.81	0.21425	3.53
C16	A-S-38TH-85T-95H-C16-1	34.73	17062.25	14.21	6876.33	0.90468	10.23	4950.90	0.30077	3.71
	A-S-38TH-85T-95H-C16-2	22.96	17901.29	16.62	8039.75	1.48137	11.33	5482.66	0.49799	3.23

Note: "-" indicates unavailability of the properties due to multiple slippage of extensometer.

Mechanical properties from the shear test of adhesive specimens for extreme temperature conditions

Combination	Specimen ID	Shear modulus, G (MPa)	Stiffness, k (KN/m)	Ultimate shear stress, τ_u (Mpa)	Ultimate shear load, V_u (N)	Strain at ultimate load, (mm/mm)	Yield stress, τ_y (MPa)	Load at yield point, V_y (N)	Strain at yield point, (mm/mm)	Ductility, e (%)
A1	A-S-13TH-93T-A1-1	19.21	8185.25	19.10	3079.95	2.28000	8.15	1314.44	0.43720	4.76
	A-S-13TH-93T-A1-2	19.93	8412.04	19.67	3173.18	2.11000	8.18	1319.11	0.41604	3.96
A2	A-S-25TH-93T-A2-1	27.51	15397.85	20.16	6503.30	2.07000	7.46	2405.64	0.27726	3.86
	A-S-25TH-93T-A2-2	21.49	14488.24	20.17	6507.04	2.35000	8.29	2673.87	0.40023	4.10
A3	A-S-38TH-93T-A3-1	21.47	20054.47	19.18	9279.30	2.16000	8.08	3911.59	0.39004	4.15
	A-S-38TH-93T-A3-2	20.00	19541.70	19.19	9285.22	2.13740	7.95	3846.55	0.40353	4.47
A4	A-S-13TH-(-56.67)T-A4-1	43.26	7849.18	19.93	3214.01	0.87204	11.94	1925.21	0.32732	4.57
	A-S-13TH-(-56.67)T-A4-2	39.27	7359.18	17.42	2810.41	1.33534	8.00	1290.52	0.21122	3.41
A5	A-S-25TH-(-56.67)T-A5-1	25.06	12997.39	19.27	6215.79	1.60170	11.79	3803.19	0.47504	3.67
	A-S-25TH-(-56.67)T-A5-2	45.84	12257.30	16.93	5461.92	1.15363	9.56	3084.60	0.21582	4.27
A6	A-S-38TH-(-56.67)T-A6-1	23.58	19041.89	18.17	8793.22	1.49256	12.41	6002.53	0.30077	3.70
	A-S-38TH-(-56.67)T-A6-2	25.98	18946.79	18.62	9007.24	1.53958	12.26	5930.87	0.48244	3.49

Mechanical properties from the shear test of welded specimens

Combination	Specimen ID	Shear modulus, G (MPa)	Stiffness, k (KN/m)	Ultimate shear stress, τ_u (Mpa)	Ultimate shear load, V_u (N)	Strain at ultimate load, (mm/mm)	Yield stress, τ_y (MPa)	Load at yield point, V_y (N)	Strain at yield point, (mm/mm)	Ductility, e (%)
W1	W-S-13TH-93.33T-W1-1	53170.45	28509.07	135.92	7750.64	0.03347	69.78	3979.42	0.00326	3.85
	W-S-13TH-93.33T-W1-2	101768.51	26547.30	165.81	9455.23	0.04989	75.27	4292.30	0.00280	5.92
W2	W-S-25TH-93.33T-W2-1	37384.09	51064.17	126.42	14418.24	0.01884	85.12	9707.89	0.00442	2.55
	W-S-25TH-93.33T-W2-2	50315.75	47347.45	171.72	19584.84	0.03658	110.58	12611.92	0.00430	3.99
W3	W-S-38TH-93.33T-W3-1	41041.89	62686.63	177.76	30410.61	0.04175	80.31	13738.71	0.00407	4.68
	W-S-38TH-93.33T-W3-2	33543.16	63723.91	164.66	28168.62	0.03119	117.87	20163.70	0.00543	3.49
W4	W-S-13TH-(-56.67)T-W4-1	23820.52	18258.89	134.24	7655.15	0.09671	40.58	2314.20	0.00386	15.14
	W-S-13TH-(-56.67)T-W4-2	17389.27	18531.04	134.08	7645.84	0.10221	41.34	2357.47	0.00458	15.67
W5	W-S-25TH-(-56.67)T-W5-1	16210.95	30922.31	135.66	15472.32	0.07014	33.12	3777.03	0.00413	15.89
	W-S-25TH-(-56.67)T-W5-2	19788.67	31822.99	135.77	15484.61	0.08710	41.78	4764.49	0.00428	16.06
W6	W-S-38TH-(-56.67)T-W6-1	19191.67	43213.59	133.99	22921.90	0.07960	38.95	6662.60	0.00420	12.55
	W-S-38TH-(-56.67)T-W6-2	13603.14	43443.70	135.58	23194.67	0.12108	28.44	4864.70	0.00401	20.60
W7	W-S-13TH-20T-W7-1	49945.46	32850.11	148.13	8446.85	0.02163	85.68	4885.88	0.00368	2.87
	W-S-13TH-20T-W7-2	42917.63	32770.08	146.30	8342.57	0.03883	67.70	3860.73	0.00356	4.52
W8	W-S-25TH-52.5T-W8-1	35058.57	49978.38	155.54	17739.43	0.03683	82.51	9409.89	0.00446	3.84
	W-S-25TH-52.5T-W8-2	107355.34	50662.78	145.98	16649.38	0.03859	93.49	10662.22	0.00307	4.41
W9	W-S-38TH-85T-W9-1	32563.43	70449.66	137.59	23537.55	0.02563	69.46	11883.25	0.00411	2.87
	W-S-38TH-85T-W9-2	32746.29	72505.99	151.54	25924.72	0.04983	66.34	11349.13	0.00427	5.66

APPENDIX C

Summary of Peel Testing Results

Peel strength from the peel test of adhesive specimens

Combination	Specimen ID	Peel strength, f_{ap}(N/mm)
C1	A-P-13TH-20T/48H-C1-1	8.01
	A-P-13TH-20T/48H-C1-2	8.20
C2	A-P-38TH-20T/48H-C2-1	3.69
	A-P-38TH-20T/48H-C2-2	7.95
C3	A-P-25TH-20T/71H-C3-1	5.03
	A-P-25TH-20T/71H-C3-2	3.79
C4	A-P-13TH-20T-95H-C4-1	7.48
	A-P-13TH-20T-95H-C4-2	9.08
C5	A-P-38TH-20T-95H-C5-1	9.01
	A-P-38TH-20T-95H-C5-2	4.08
C6	A-P-25TH-52T/48H-C6-1	8.13
	A-P-25TH-52T/48H-C6-2	3.42
C7	A-P-13TH-52T/71H-C7-1	6.95
	A-P-13TH-52T/71H-C7-2	8.50
C8	A-P-25TH-52T/71H-C8-1	9.79
	A-P-25TH-52T/71H-C8-2	5.24
C9	A-P-25TH-52T/71H-C9-1	9.87
	A-P-25TH-52T/71H-C9-2	3.21
C10	A-P-38TH-52T/71H-C10-1	3.16
	A-P-38TH-52T/71H-C10-2	9.05
C11	A-P-25TH-52T-95H-C11-1	5.99
	A-P-25TH-52T-95H-C11-2	4.07
C12	A-P-13TH-85T/48H-C12-1	5.70
	A-P-13TH-85T/48H-C12-2	7.87
C13	A-P-38TH-85T/48H-C13-1	3.89
	A-P-38TH-85T/48H-C13-2	7.80
C14	A-P-25TH-85T/71H-C14-1	7.07
	A-P-25TH-85T/71H-C14-2	8.19
C15	A-P-13TH-85T-95H-C15-1	12.81
	A-P-13TH-85T-95H-C15-2	2.70
C16	A-P-38TH-85T-95H-C16-1	3.78
	A-P-38TH-85T-95H-C16-2	8.54

Peel strength from the peel test of adhesive specimens for extreme temperature conditions

Combination	Specimen ID	Peel strength, f_{ap}(N/mm)
A1	A-P-13TH-93T-A1-1	30.19
	A-P-13TH-93T-A1-2	27.55
A2	A-P-25TH-93T-A2-1	36.05
	A-P-25TH-93T-A2-2	24.03
A3	A-P-38TH-93T-A3-1	21.17
	A-P-38TH-93T-A3-2	18.42
A4	A-P-13TH-(-56.67)T-A4-1	40.48
	A-P-13TH-(-56.67)T-A4-2	21.36
A5	A-P-25TH-(-56.67)T-A5-1	29.48
	A-P-25TH-(-56.67)T-A5-2	46.01
A6	A-P-38TH-(-56.67)T-A6-1	40.56
	A-P-38TH-(-56.67)T-A6-2	20.48

Peel strength from the peel test of welded specimens

Combination	Specimen ID	Peel strength, f_{ap} (N/mm)
W1	W-P-13TH-93.33T-W1-1	38.03
	W-P-13TH-93.33T-W1-2	42.80
W2	W-P-25TH-93.33T-W2-1	5.17
	W-P-25TH-93.33T-W2-2	24.16
W3	W-P-38TH-93.33T-W3-1	5.86
	W-P-38TH-93.33T-W3-2	3.18
W4	W-P-13TH-(-56.67)T-W4-1	22.31
	W-P-13TH-(-56.67)T-W4-2	9.80
W5	W-P-25TH-(-56.67)T-W5-1	30.63
	W-P-25TH-(-56.67)T-W5-2	9.33
W6	W-P-38TH-(-56.67)T-W6-1	7.39
	W-P-38TH-(-56.67)T-W6-2	14.09
W7	W-P-13TH-20T-W7-1	62.46
	W-P-13TH-20T-W7-2	69.30
W8	W-P-25TH-52.5T-W8-1	44.02
	W-P-25TH-52.5T-W8-2	27.57
W9	W-P-38TH-85T-W9-1	10.40
	W-P-38TH-85T-W9-2	19.23

APPENDIX D

Summary of Cleavage Testing Results

Cleavage strength from the cleavage test of adhesive specimens

Combination	Specimen	Cleavage strength, (N/mm)
C1	A-C-13TH-20T/48H-C1-1	199.43
	A-C-13TH-20T/48H-C1-2	147.62
C2	A-C-38TH-20T/48H-C2-1	203.86
	A-C-38TH-20T/48H-C2-2	178.52
C3	A-C-25TH-20T/71H-C3-1	217.88
	A-C-25TH-20T/71H-C3-2	172.15
C4	A-C-13TH-20T-95H-C4-1	118.61
	A-C-13TH-20T-95H-C4-2	180.90
C5	A-C-38TH-20T-95H-C5-1	184.05
	A-C-38TH-20T-95H-C5-2	187.50
C6	A-C-25TH-52T/48H-C6-1	210.05
	A-C-25TH-52T/48H-C6-2	222.25
C7	A-C-13TH-52T/71H-C7-1	236.73
	A-C-13TH-52T/71H-C7-2	159.91
C8	A-C-25TH-52T/71H-C8-1	206.83
	A-C-25TH-52T/71H-C8-2	189.38
C9	A-C-25TH-52T/71H-C9-1	198.17
	A-C-25TH-52T/71H-C9-2	218.16
C10	A-C-38TH-52T/71H-C10-1	205.17
	A-C-38TH-52T/71H-C10-2	303.92
C11	A-C-25TH-52T-95H-C11-1	193.10
	A-C-25TH-52T-95H-C11-2	168.25
C12	A-C-13TH-85T/48H-C12-1	217.77
	A-C-13TH-85T/48H-C12-2	223.47
C13	A-C-38TH-85T/48H-C13-1	188.90
	A-C-38TH-85T/48H-C13-2	194.19
C14	A-C-25TH-85T/71H-C14-1	188.63
	A-C-25TH-85T/71H-C14-2	188.85
C15	A-C-13TH-85T-95H-C15-1	193.46
	A-C-13TH-85T-95H-C15-2	188.06
C16	A-C-38TH-85T-95H-C16-1	190.36
	A-C-38TH-85T-95H-C16-2	215.28

Cleavage strength from the cleavage test of adhesive specimens for extreme temperature conditions

Combination	Specimen	Cleavage strength, (N/mm)
A1	A-C-13TH-93T-A1-1	1534.90
	A-C-13TH-93T-A1-2	1447.93
A2	A-C-25TH-93T-A2-1	1483.96
	A-C-25TH-93T-A2-2	1487.21
A3	A-C-38TH-93T-A3-1	1430.08
	A-C-38TH-93T-A3-2	1270.14
A4	A-C-13TH-(-56.67)T-A4-1	1458.83
	A-C-13TH-(-56.67)T-A4-2	1307.62
A5	A-C-25TH-(-56.67)T-A5-1	1167.12
	A-C-25TH-(-56.67)T-A5-2	1129.70
A6	A-C-38TH-(-56.67)T-A6-1	1366.55
	A-C-38TH-(-56.67)T-A6-2	1092.23

Cleavage strength from the cleavage test of welded specimens

Combination	Specimen ID	Cleavage strength (N/mm)
W1	W-C-13TH-93.33T-W1-1	436.34
	W-C-13TH-93.33T-W1-2	471.20
W2	W-C-25TH-93.33T-W2-1	217.70
	W-C-25TH-93.33T-W2-2	216.44
W3	W-C-38TH-93.33T-W3-1	166.40
	W-C-38TH-93.33T-W3-2	159.12
W4	W-C-13TH-(-56.67)T-W4-1	501.02
	W-C-13TH-(-56.67)T-W4-2	498.82
W5	W-C-25TH-(-56.67)T-W5-1	246.56
	W-C-25TH-(-56.67)T-W5-2	261.07
W6	W-C-38TH-(-56.67)T-W6-1	153.77
	W-C-38TH-(-56.67)T-W6-2	142.70
W7	W-C-13TH-20T-W7-1	449.37
	W-C-13TH-20T-W7-2	450.39
W8	W-C-25TH-52.5T-W8-1	219.34
	W-C-25TH-52.5T-W8-2	213.51
W9	W-C-38TH-85T-W9-1	176.04
	W-C-38TH-85T-W9-2	206.22